Amphiphilic Linear-Dendritic Block Copolymers For Drug Delivery

by

Phuong Nguyen

B.S., University of California San Diego (2001)
M.S.CEP, Massachusetts Institute of Technology (2004)

Submitted to the Department of Chemical Engineering in Partial Fulfillment of the Requirements for the Degree of

Doctor of Philosophy in Chemical Engineering

at the

MASSACHUSETTS INSTITUTE OF TECHNOLOGY

JUNE 2007
[September 2007]

Author: _____
Department of Chemical Engineering
June 27, 2007

Certified by: _____
Paula T. Hammond, Professor
Thesis Supervisor

Certified by: _____
Robert Langer, Institute Professor
Thesis Supervisor

Accepted by: _____
William Deen, Professor
Chairman, Departmental Committee on Graduate Studies

Amphiphilic Linear-Dendritic Block Copolymers For Drug Delivery

by

Phuong Nguyen

B.S., University of California San Diego (2001)
M.S.CEP, Massachusetts Institute of Technology (2004)

Submitted to the Department of Chemical Engineering on
June 27, 2007 in Partial Fulfillment of the Requirements for the Degree of

Doctor of Philosophy in Chemical Engineering

ABSTRACT

Polymeric drug delivery systems have been widely used in the pharmaceutical industry. Such systems can solubilize and sequester hydrophobic drugs from degradation, thereby increasing circulation half-life and efficacy. However, there are still challenges in the design of drug delivery vehicles to achieve efficient drug delivery in a site-specific manner. In this thesis, an amphiphilic linear-dendritic block copolymer was designed, synthesized, and applied as a new polymeric drug delivery platform.

First, to develop the drug delivery vehicle, an ABA dendritic-linear-dendritic block copolymer consisting of poly(amidoamine) (PAMAM) and poly(propylene oxide) (PPO) was synthesized. In order to determine the viability of the linear-dendritic block copolymer as a drug delivery vehicle, the solution-phase self-assembly behavior and the self-assembled structures were characterized experimentally and through molecular dynamics simulations. The triblock self-assembles in aqueous media to form stable micelles with low CMC values. Dynamic light scattering results and TEM indicate the formation of particles ranging from 9 to 18 nm in diameter, with smaller diameters exhibited at higher generations. Static light scattering also confirmed the trend where the aggregation number decreased with higher generations. The experimental characterization results indicated that the physical characteristics of the PPO-PAMAM micelles were desirable and within the design specifications necessary for drug delivery.

The experimental results were utilized to set up simulations where further knowledge of the microstructure of the micelles formed could be gained. It was found that the block copolymers simulated formed micelles in the same size range that was seen experimentally. However, the simulations indicated that the micelles displayed greater asphericity than dendrimers. Backfolding of the terminal amine ends was encountered, which would have implications for the configuration and spacing of any additional

targeting ligand attached to the dendritic ends. Further analysis revealed that with increasing generation, the porosity of the micelles increased, which could affect the diffusion rate of drugs released out of the system. Another important finding detailed the preferential localization of a model hydrophobid drug, triclosan, in an equilibrated micelle structure.

Additional experiments were performed to assess the feasibility of the nanoparticles for drug delivery applications. Drug loading studies were performed with a model hydrophobic drug, triclosan, resulting in high loading efficiencies. In comparison, linear block copolymers were half as efficient in loading triclosan. It was determined that the dendritic block synergistically increased the drug loading due to either acting as an additional block capable of encapsulating drug or sterically favoring the seclusion of the drug in the core. The linear-dendritic block copolymer synthesized was found to be a promising candidate for drug delivery due to its relative stability in aqueous solution and its drug encapsulation and release properties.

Overall, the linear-dendritic block copolymer displayed physical characteristics and self-assembly behavior that satisfied the design criteria for a viable drug delivery vehicle. As a further step, the potential benefits of the novel linear-dendritic architecture were explored in two different drug delivery applications. First, PPO-PAMAM was explored as a circulating nanoparticle with the capability of multivalently targeting to specific cells, due to the presence of the dense functional groups on the dendritic block forming the corona of the micelles. PPO-PAMAM was functionalized with galactose and targeted to hepatocellular carcinoma cells. It was found that the polymer was not cytotoxic and could bind to the asialoglycoprotein receptor. The galactose-functionalized micelles were loaded with a chemotherapeutic, doxorubicin, and delivered to the carcinoma cells more efficiently than non-functionalized micelles and bare doxorubicin. The results from *in vitro* testing showed that PPO-PAMAM micelles with targeting capability are promising circulating drug delivery vehicles.

In order to ensure success of subsequent testing *in vivo* of the targeted linear-dendritic block copolymer system, some improvements to the system were explored. First, PPO-PAMAM micelles were stabilized by physical entrapment of the hydrophobic core. An emulsion polymerization of hydrophobic methacrylate monomers created an interpenetrating polymer keeping the micelles intact at concentrations below the CMC and in a solubilizing solvent, methanol. This improvement would ensure that once injected into the bloodstream, the micelles would not destabilize and release high concentrations of drug. Another improvement that was explored was the synthesis of a new linear-dendritic block copolymer composed of a hydrophobic poly(amino acid) and a polyester dendron. Additionally, poly(ethyleneglycol) (PEG) groups were attached to the outer surface of the polyester dendron. The new system synthesized has a low CMC and is thermodynamically slow to break apart in the bloodstream. Furthermore, the micelles formed would be able to circulate for longer times with PEG aiding in evading the reticuloendothelial system.

The second drug delivery application explored, which advantageously utilized the dendritic blocks on the outer surface of the block copolymer micelles was as a localized drug delivery coating created by the layer-by-layer (LbL) assembly approach. The electrostatic LbL assembly approach offers large potential in the area of drug delivery from thin films and surfaces; however, because the processing technique is aqueous-based, there have been few strategies proposed to incorporate hydrophobic molecules into these films. Here we created an LbL film that is capable of incorporating hydrophobic drug at high loadings via encapsulation with linear-dendritic block copolymer micelles and demonstrate for the first time release times of a hydrophobic antibacterial agent over a period of several weeks--a significant improvement over reports of other micelle-encapsulated thin films with release times of several minutes. The PAMAM block, which is polycationic, enabled LbL deposition with negatively charged poly(acrylic acid) (PAA). The stable PPO-PAMAM micelles incorporated into the LbL films encapsulated a hydrophobic bactericide, triclosan. Film thickness and UV-vis measurements confirm the formation of the LbL film and incorporation of triclosan into the film. Fluorescence measurements of PPO-PAMAM/PAA films with pyrene indicated the presence of hydrophobic domains in the film. GISAXS revealed regular spacing of approximately 10.5 nm in the direction parallel to the film substrate, which is approximately the same size as the PPO-PAMAM micelles in aqueous solution. Volume fraction measurements based on elemental analysis and TGA confirm the GISAXS data. An *in vitro* release study revealed long release times of triclosan on the order of weeks, and a Kirby Bauer test was performed on *Staphylococcus Aureus* demonstrating that the drug released was still active to inhibit the growth of bacteria.

Linear-dendritic block copolymer micelles were successfully used in two different drug delivery applications where the dendritic block could be fully utilized. It is hoped that with the research and results presented in this thesis further development of this drug delivery platform can result in a product successfully treating a serious disease.

Thesis Supervisor: Paula T. Hammond
Title: Bayer Chair Professor of Chemical Engineering

Thesis Supervisor: Robert Langer
Title: Institute Professor

Acknowledgements

Many individuals have contributed to the success and completion of the research presented in this thesis. I would first like to thank my family for their continued support over my formative educational years. My parents have contributed in many ways to the completion of my thesis including encouraging and supporting my educational goals and helping me through the ups and downs of research. Additionally, my brother and sister, Peter and Kathy, have helped to remind me that there is life outside of graduate school.

I would also like to extend my appreciation to my thesis committee who has contributed greatly to the work in this thesis. Foremost, my advisor, Professor Paula Hammond has introduced me to the world of polymer chemistry and has helped me towards becoming a resourceful and independent scientist. The rest of my thesis committee members, Professor Bob Langer, Professor Daniel Blankschtein, and Professor Bruce Zetter have given me much encouragement in my thesis research and my career development.

Each of the collaborators I have worked with has contributed greatly to my thesis work, and I would sincerely express gratitude to each of them. Dr. Nicole Zacharia and Eric Verploegen added to and rounded out the layer-by-layer work. Dr. Brian Stephenson played a large role in the simulations work, performing most of the simulations and supplying a great deal of expertise.

I would also like to thank the past and present members of the Hammond group, who provided an enjoyful and collaborative work environment. I am most grateful to Dr. Kris Stokes and Dr. Lu Tian for always being available for valuable discussions and great insights.

Last, I am grateful for the NSF Graduate Research Fellowship, the Robert T. Haslem Presidential Fellowship, and the MIT Chemical Engineering department for financial support for this thesis work.

Table of Contents

List of Figures

List of Tables

CHAPTER 1: INTRODUCTION

1.1 Motivation

Systemic drug delivery is a nonspecific treatment that can cause harmful side effects. For example, chemotherapy kills cancer cells but also causes unwanted side effects by destroying other healthy rapidly growing cells within the body. New developments in localized or targeted drug delivery methods can be a promising alternative. Currently, colloidal particles such as liposomes or block copolymers have been designed and studied for use as drug carriers for delivering drugs to localized sites. These colloidal particles can encapsulate a wide variety of drugs and isolate them from the physiological environment where degradation can occur. Furthermore, they can solubilize hydrophobic drugs at concentrations above the solubility limit of the drug in aqueous solution. As a result of employing a nanoparticle, the half-life of the drug is increased as it is sequestered from degradation reactions within the body, and the distribution of drug within the body can be altered.[1] Primarily, drug delivery nanoparticles are delivered parenterally, and the circulation times of these nanoparticles can be increased by the use of polyethylene glycol (PEG) grafted to the exterior of the nanoparticles. PEG creates a hydrodynamic barrier that prevents recognition, uptake, and removal by the reticuloendothelial system (RES).[2-4] Increased circulation times allow for greater passive targeting to targeted sites through the enhanced permeability and retention (EPR) effect.[5] The EPR effect occurs in tumor tissue that have increased permeability of blood vessels in tumor tissue and decreased lymphatic drainage.[6]

Although these studies have contributed to the development of promising drug delivery vehicles targeting drugs to solid tumors, there are still challenges in the use of colloidal particles for site-specific drug delivery. The first challenge is to develop a nanoparticle that is stable in aqueous solution and does not break apart when it is administered into the body.[7] The second challenge is to control the biodistribution of the drug delivery vehicle and have effective extravasation of the nanoparticles from the vascular system into the treatment site.[8] Once the particle enters the tumor, it must then be taken up by the cancer cells and undergo endocytosis. The next challenge is to effectively release the drug in a controlled manner while within the endosome or after escaping the endosome.[9] Other challenges include the ability to increase drug-loading capacity, to vary the size of the particle while maintaining stability, to prevent the aggregation of particles, to introduce cell-specific targeting capability through the addition of targeting ligand, and to vary ligand valency on the surface of the particle.

To address these issues, the scope of this thesis includes the design and creation of a novel amphiphilic linear-dendritic block copolymer. As shown in Figure 1-1, the linear-dendritic block copolymer consists of a hydrophobic linear block attached to a hydrophilic dendron. These copolymers will undergo self-assembly in solution due to thermodynamic driving forces that strive to isolate the hydrophobic linear block from the surrounding media and to expose the hydrophilic dendron. In addition to synthesizing the polymer, the aqueous phase self-assembly behavior of the linear-dendritic block copolymer has also been studied to determine its feasibility as a drug delivery vehicle. Molecular dynamics simulations of some of the linear-dendritic block copolymer micelle systems also provided insight into the microstructure of the self-assembled micelles.

The linear-dendritic block copolymer micelles were then used in two different drug delivery applications. The main application that was studied was exploring the use of the linear-dendritic block copolymers as circulating nanoparticles for drug delivery. *In vitro* studies were undertaken to evaluate the role of multivalency and the effectiveness of the targeting ligand to deliver the drug-encapsulated colloidal particles to carcinoma cells. Additional improvements were investigated including stabilizing the linear-dendritic block copolymers through physical entrapment of the hydrophobic cores and also developing a different linear-dendritic block copolymer system for future use.

The other application that was explored with the linear-dendritic block copolymer micelles was to incorporate these micelles into a thin film as a coating for biomedical implants. The block copolymer micelles were used to provide a hydrophobic environment available as a hydrophobic drug depot in a film formed through the layer-by-layer dipping process.

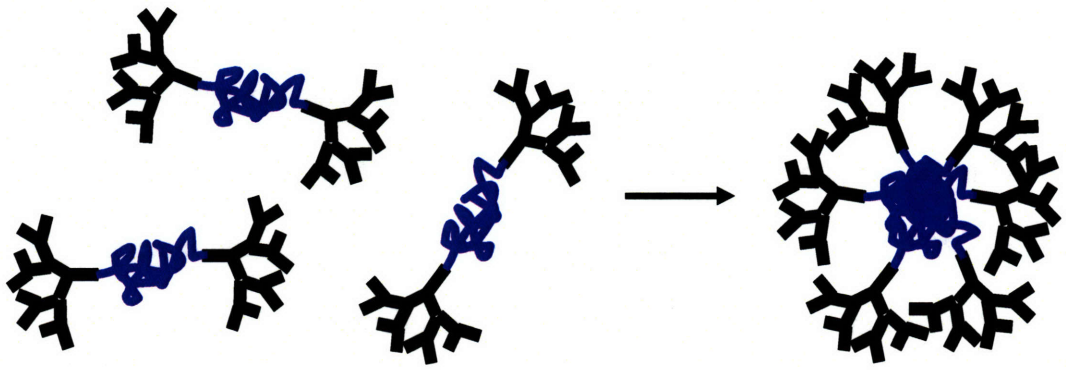

Figure 1-1. Linear-dendritic block copolymers self-assembling into a micelle.

1.2 Background: Colloidal Drug Delivery Systems

Colloidal drug delivery systems have shown a lot of promise in the effective targeting of cytotoxic drugs to cancer tumors and areas of infarction by protecting the drugs from degradation and prolonging circulation within the body. By encapsulating drugs in a nanoparticle, the distribution of the drug is less determined by the properties of the drug and more dependent on the size and surface properties of the drug carrier. There are two different mechanisms that can be exploited to alter the biodistribution of the nanoparticles circulating in the body. First, the size of the nanoparticles can be manipulated to affect their passive accumulation at sites with arterial damage. Specific targeting of the drug-encapsulating nanoparticles can be introduced through the attachment of cell-specific targeting ligand to the outer surface of the particles.

1.2.1 Factors for Passive Targeting

The size of the circulating nanoparticles is a critical factor in controlling the biodistribution of the drug. First, there are size restrictions that have to be met in order for the nanoparticles to avoid removal from circulation. The nanoparticle must be larger than 2-3 nm to avoid being filtered out by the kidney but smaller than 150 nm in order to avoid the RES.[10] The RES is mainly composed of monocytes and macrophages in the liver and spleen that have the ability to recognize microparticulate systems and remove them from circulation. Recognition by the RES is aided by the adsorption of proteins, called opsonins, onto the surface of the nanoparticles which promote phagocytosis.[11, 12] With an increase in size of the drug delivery vehicle, there is an increased rate of uptake by the RES.[13]

The size of the nanoparticle is important as it will determine the rate of extravasation and uptake into the cells. Although macroparticles have a tendency to accumulate in tumor tissue through the EPR effect, it has been found that as the size of the particle increases, the time for extravasation exponentially increases.[14, 15] Once in the tumor tissue, the size of the particle may also impede transport of the particle through the solid tumor. There is high interstitial fluid pressure that is often present in tumor masses which can decrease the ability of particles to penetrate the tumor as its size gets larger.[16] Another consideration is that it is more difficult to internalize bulky particles by nonphagocytic cells.[17] Typically, endocytosis can only occur for particles that are smaller than 150 nm in diameter. Overall, an intermediate sized particle is necessary in order to avoid the RES and facilitate extravasation and transport through the tumor.

The surface properties of the drug carrier are also crucial in determining the biocompatibility, biodistribution, and retention within the circulatory system. It has been found that neutrally charged liposomes have a lower tendency to be cleared by the RES in comparison to positively or negatively charged liposomes. However, they have a higher tendency to aggregate, which could also induce uptake by the RES.[18] Cationic particles are quickly removed from systemic circulation due to electrostatic interactions with negatively charged cell membranes and the extracellular matrix.[1] Because of this interaction, it has been found that particles with primary amine groups exposed can cause haemolysis[19] and are cytotoxic.[20] Receptors found on macrophages can recognize negative surface charges; thus, anionic particles are rapidly cleared from the body.[2]

To improve retention times and reduce immunogenecity, the surfaces of the drug carriers can be modified with hydrophilic moieties that confer a hydration barrier around

the particle. The most common modification is the conjugation of short chains of PEG. PEG has been well-characterized for biological use and parenteral applications.[18] Other polymers that have been used to form steric barriers include poly(acryloyl morpholine), poly(acrylamide), poly(vinyl pyrrolidone), and polyvinyl alcohol.[9, 18] PEG is usually the polymer of choice due to its high water solubility, low toxicity, low immunogenicity, and high chain mobility.[21] With the addition of PEG, the drug carriers have a reduced rate of uptake by the RES, thus prolonging the circulation half-life.[4, 22] Water molecules form a sheath around the PEG chains, creating a particle with a large hydrodynamic radius that prevents the adsorption of opsonins to the surface.[23] The addition of the PEG palisade also reduces the toxicity of the nanoparticle by decreasing interactions with the physiological environment[20, 24] and alters the distribution of nanoparticles within the body. For example, after conjugation of PEG to a cationic liposome, accumulation dramatically decreased in the lung.[25]

By designing the drug delivery vehicle with an optimal size and the correct surface properties, the blood circulation time of the drug can be dramatically improved. With the increased circulation half-life and the EPR effect, more of the nanoparticles can passively accumulate within leaky vasculature seen in tumors, inflammations, and infarcted areas.

1.2.2 Active Targeting

To increase the retention of drug delivery nanoparticles in the affected sites beyond what is offered by passive targeting, the attachment of various cell-specific targeting ligands has been explored. In order for active targeting to be effective, there are three key issues that have to be addressed. First, the drug delivery vehicle must circulate

within the system long enough for localization to the site of the tumor and for interaction with the targeted cells. This is ensured through designing the nanoparticle with the ability to passively accumulate at the tumor site in high concentrations as discussed previously. The next consideration is that the ligand or the receptor to the targeted cells should be highly specific. For example, rapidly growing tumor cells upregulate certain receptors to allow for greater uptake of nutrients; therefore, tumor cells have a greater density of specific receptors in comparison to healthy cells. The last consideration is that the targeting molecule on the surface of the drug carrier should be stable *in vivo* and its potential for opsonization is minimal.[18]

There are several classes of targeting ligands that have been used for drug targeting. This includes antibodies, carbohydrates, peptides, cell surface receptor ligands, and oligonucleotide aptamers.[26] For the treatment of tumor cells, ligands that are recognized by cell surface receptors have been the most popular, including transferrin and Apo E/Apo B.[18] Transferrin receptors are overexpressed on the surface of many tumor cells, and transferrin has been attached to liposomes to deliver drug to tumors and into tumor cells.[27, 28]

1.2.2.1 Carbohydrates

Binding between carbohydrates and sugar binding proteins called lectins can be as specific as enzyme-substrate or antigen-antibody interactions. Lectins have multiple binding domains that bind to specific carbohydrate moieties.[29] Through multivalent interactions, the strength of binding is increased dramatically from a K_d in the 10^{-3} M range for monovalent interactions down to a K_d of 10^{-6} M and 10^{-9} M for divalent and trivalent oligosaccharides, respectively.[29] There are two broad classes of lectins.[30] C-

type lectins require calcium for binding, and this includes the hepatic asialoglycoprotein receptor. S-type lectins, also known as galectins, are calcium independent. It has been found that galectins-1 and -3 are overexpressed on the surface of colon cancer cells.[30]

Targeting of carbohydrates to lectins have been applied in multiple applications including gene therapy[31] and drug delivery.[32] Drug delivery systems containing asialofetuin, galactose, or N-acetyl-galactosamine have been able to bind and be endocytosed by the asialoglycoprotein receptor present on hepatocytes.[33] Derivatives of N-(2-hydroxypropyl)methacrylamide covalently bound to sugar ligands have been able to deliver doxorubicin to colon adenocarcinoma and hepatic carcinoma cells.[34, 35] The higher the sugar content in the HPMA polymer, there was a higher extent of cell binding due to the multivalent binding required with lectins.[34]

1.2.2.2 Folate

Another popular targeting ligand is folate, a vitamin required in several metabolic pathways and is essential for the biosynthesis of nucleotide bases. It is consumed in elevated quantities by proliferating cancer cells. Folate is transported across the cell by either of two membrane-associated proteins, a reduced folate carrier or the folate receptor (FR). The reduced folate carrier is the primary pathway for uptake of folate while the folate receptor is found mainly on polarized epithelial cells and activated macrophages. FR has been found to be overexpressed in cancer cells. Furthermore, FR is only accessible after the cells have been transformed into malignant cells. Normally, FR is selectively expressed on the apical membrane surface (surface facing the body cavity) of epithelial cells. After transformation into a malignant cell, the polarity is lost and FR on the cells is accessible to drugs in circulation.[36] Because of these mechanisms for tumor

specificity, folic acid is a natural choice to be used as a molecule for targeting drugs to cancer cells. The advantages to using folic acid is that it is nonimmunogenic, has a high binding affinity (K_d ~.1 nM), has good stability, has simple and defined conjugation chemistry, is available in large quantities, and is compatible with the use of organic solvents.[37]

Folic acid is taken into cells by a process called potocytosis. Folate receptors occur in dense clusters on the cell surface associated to caveolae, which are invaginated pits that have a diameter of approximately 50 nm. Each cluster is composed of 700 receptor molecules. Once the caveolae are closed, the pH decreases to approximately 5.0 and the folate is released from the receptor.[38] Due to the mechanism of folate uptake, it has been found that folate binding is multivalent. The presence of multiple folates on a single dendrimer decreases the Kd dramatically from about 2500 to 170,000-fold.[39]

1.2.2.3 Targeting Challenges

Although there are several promising ligands that are being explored to target to specific cells for drug treatment, extravasation to the tumor site has been found to be the rate-limiting step for liposomes. For example, folate targeting has not increased the concentration of liposomes in subcutaneously growing tumor implants.[40] However, targeting could be used for improved delivery and retention of therapeutics within tumor tissue. Retrograde movement of drug-carrying nanoparticles may be hindered due to binding of the nanoparticles to target cells, and retention of the drug is enhanced through receptor-mediated endocytosis or potocytosis. The therapeutic index of the drug could increase as the drug distribution shifts from the extracellular space of the tumor into the intracellular compartments of the tumor cells—although, the relative contributions of

drug released in the extraceullular space and the intracellular space are unknown. In a study of HER2-targeted immunoliposomes containing doxorubicin (DOX), there was better tumor penetration, tumor cell uptake, and therapeutic efficacy.[41]

In several studies, the role of multivalency has shown to be dramatic. Conjugation of a large number of ligand on the surface of the drug particle has increased the avidity of the particle to the target cells. For polymeric systems, as the ligand density on the surface of the particle was increased, binding increased exponentially.[34] Similarly, the addition of 1000-fold greater concentration in free folate was necessary in order to compete with the binding of folate-targeted liposomes to a folate receptor.[42] Therefore another advantage for creating a targeted nanoparticle is that with greater affinity and efficacy dosage could be lowered.

Although the use of a ligand may confer a greater affinity to targeted cell types, the improved avidity and affinity may also negatively impact tumor penetration. It has been demonstrated that antibody-free vesicles more readily permeate tumors than immunoliposomes. This may be due to the high affinity of the antibody to the antigen where the rate of transport into the tumor is smaller than the rate of binding to tumor cells, thus retarding penetration into the tumor and binding occurs only at the periphery.[43] Modeling of antibodies percolating through solid tumors shows that lower affinity antibodies are able to penetrate into tumors more than higher affinity antibodies.[44] Thus, in the creation of a targeted nanoparticle, there is an optimal ligand density that will balance the need for affinity to target cells and greater penetration into solid tumors.

1.2.3 Nanoparticles for Drug Delivery: Liposomes

Liposomes are phospholipid bilayer vesicles which can entrap hydrophilic drug molecules in its aqueous interior or can incorporate hydrophobic molecules into its bilayer as shown in Figure 1-2. The most common formulation of liposomes utilizes phosphatidylcholine, which is neutrally charged, with fatty acyl chains of varying length and degree of saturation. Cholesterol can also be added to modulate the rigidity and stability of the liposome. In the mid-1990s, liposomes were approved by the FDA for use as therapeutics in humans. Liposomal drug delivery systems have mainly been developed for antifungal and anticancer therapies.[18]

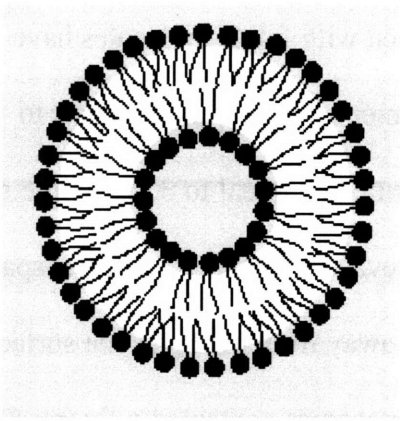

Figure 1-2. Liposomes are composed of lipid bilayers that are able to encapsulate hydrophilic drug in its aqueous core and hydrophobic drug in the lipid region.

Liposomes are characterized with long systemic circulation times in comparison to the free drug. However, they are also characterized by efficient uptake by the RES. In order to evade the RES and increase circulation times, liposomes have been modified by adding PEG to their outer surface.[45, 46] Liposomes modified with PEG have also been approved by the FDA.

As an advancement, targeted liposomes have been developed. A lot of research has been done to couple antibodies to liposomes primarily for cancer targeting. For example, anti-HER2 liposomes to target HER2-overexpressing tumors[47] and CC52 liposomes to target rat colon adenocarcinomas[48] have been efficacious. Liposomes have also been developed with carbohydrates conjugated to the surface. For example, mannosylated liposomes were developed to target macrophages[49] and the brain.[50] Asialofetuin, a protein that presents multiple galactose on its surface, has been conjugated to liposomes for drug delivery and gene delivery to hepatocytes. Increased liver uptake was seen in one study,[51] while the addition of asialofetuin specifically delivered to HepG2 cells and increased transfection in another study.[52]

Liposomes attached with folate molecules have been successfully targeted to cells *in vitro*. In one experiment, folate was attached to a liposome via a PEG spacer of molecular weight approximately equal to 3350, while smaller PEGs were attached to act as the polymer brush to evade the RES. The PEG spacer was long enough to allow the attached folate to extend away from the liposome surface and to avoid steric hindrance by the PEG brush. These liposomes contained a fluorescent dye, calcein, as their cargo and were incubated with KB cell monolayers, which are known to overexpress FR. It was found that approximately 2.5×10^5 liposomes were bound by each KB cell at saturation. The authors also found that the folate-PEG liposomes displayed a much higher affinity for the cells than free folate. Most likely, due to the length of the PEG spacer, more than one folate on a liposome could bind to the cell.[46]

In another study, folate-PEG liposomes with doxorubicin as cargo were incubated with cultured KB cells. It was found that cellular doxorubicin uptake with folate-

conjugated liposomes was 45-fold higher than that of non-targeted liposomes and 1.6 times higher than free doxorubicin. Furthermore, the cytotoxicity of these liposomes was 86 times and 2.7 times higher, respectively.[53] These results indicate that the folate-PEG liposomes are more effective towards targeting cells that overexpress FR than non-targeted liposomes or free doxorubicin.

Liposomes conjugated to PEG-folate have also been tested *in vivo*. Biodistribution studies have indicated that folate-targeted liposomes showed similar patterns of distribution to non-targeted liposomes and did not improve uptake in tumors.[41] Although in an ascitic tumor model, where the distribution between the tumor cell compartment and extracellular fluid could be discerned, liposome levels that were associated to the cells were significantly higher for folate-targeted liposomes.[40] Other *in vivo* studies examining the efficacy of folate-targeted liposomes have shown mixed results. Studies were done in various tumor models, including M109-HiFR, M109R-HiFR, and J6456-HiFR cells, indicating that active targeting improved treatment. In a KB carcinoma model, folate-targeted liposomes showed significantly greater tumor inhibition.[54]

Although there are promising results for ligand-targeted liposomes, there are still some challenges associated with the use of liposomes. If hydrophobic drug is encapsulated in the bilayer region, the liposome could become destabilized.[55] Furthermore, as seen in the previous examples, liposomes need to be modified with PEG in order to be stable in the circulation system. However, with the modifications there is a trade-off. Receptor-ligand interactions can be blocked by the attached PEG. Lee was able to avoid this problem by adding a PEG spacer, but other problems exist due to

stabilizing PEG modifications. The largest difficulty is liposome unloading efficiency following endocytosis by a target cell.[9, 36] Because of the need to balance stability and solubility of the liposome, the density of PEG on liposomes is not closely packed. This could lead to liposome aggregation or protein adsorption causing instability and cargo release or elimination by the RES. Furthermore, high levels of PEG-liposomes can often be found in the liver and the spleen or in tissues that are not the desired targets.[56]

Another disadvantage of liposomes is their size. Smaller liposomes have been found to be more unstable, allowing more leakage of drug,[13] while larger liposomes can not be internalized well.[40] It has also been found that the permeation rates of liposomes (which are approximately 100 nm up to 500 nm in diameter) into the targeted cellular areas are lower than those of smaller nanoparticles due to the liposomes' large size.[57] Finally, liposomes are not a flexible system. For example, modifications to improve interactions, such as hydrophobic, hydrogen bonding, and electrostatic interactions of the drug molecules to the interior of the liposome can not be easily altered.

1.2.4 Nanoparticles for Drug Delivery: Dendrimers

Another class of nanoparticles that are being explored for targeted drug delivery is dendrimers.[56] Dendrimers have an architecture that is globular and highly branched, with regular molecular repeats created from stepwise synthesis as shown in Figure 1-3. They have a dense exterior with porous interior regions that have the potential to store drug molecules. Some of the advantages that dendrimers may have over linear polymers are that dendrimers are monodisperse with respect to molecular weight, their size and structure are highly controllable, and they have a high degree of functionality due to their branched architecture.[15] A variety of dendrimers have been created for drug delivery

applications, including polyamidoamine, poly(propyleneimine),[58] polyether,[59] and polyester[1] dendrimers.

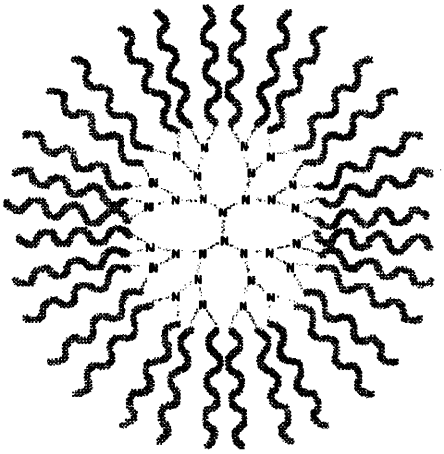

Figure 1-3. A PAMAM dendrimer with conjugated PEG.[20]

The most widely studied and characterized dendrimer is the polyamidoamine (PAMAM) dendrimer. However, in a toxicity study of dendrimers, it was found that PAMAM dendrimers with terminal primary amine groups were quite cytotoxic and were cleared rapidly from the circulation when administered intravenously.[58] In order to remediate this problem, PAMAM dendrimers are synthesized with PEG attached to the outer surface to reduce the adsorption of proteins and to increase circulation times. Additionally, with PEGylation, there is an increase in drug-loading capacity and a decrease in hemolytic toxicity and drug release rate.[24] In work done by Kojima, PAMAM dendrimers with PEG grafted on were shown to be capable of encapsulating two types of anticancer drugs, methotrexate and adriamycin. It was found that the amount that could be encapsulated increased with dendrimer generation and PEG chain

length. The maximum amount of molecules encapsulated was 6.5 adriamycin molecules or 26 methotrexate molecules per dendrimer. In drug release studies, the methotrexate loaded dendrimers released the drug slowly in an aqueous solution of low ionic strength. However, in isotonic solutions, the methotrexate and adriamycin were readily released, indicating the need for more control in the drug release mechanism.[20]

Dendrimers conjugated to targeting ligand have been synthesized and tested. Extensive studies have been performed with carbohydrate ligands. For example, one group has added lactose and maltose to the outer surface of PAMAM generation 2-4 dendrimers and have observed binding of a lectin, concavalin A, to the dendrimers. Binding was reversible with the addition of excess glucose.[60] Another group studied the multivalent binding behavior of mannose-conjugated PAMAM dendrimers with concavalin A. With the increase in the number of mannose ligand attached to the PAMAM dendrimer, binding strength increased due to multivalent interactions. However, a maximum was reached at 50% functionalization. Higher functionalization values resulted in less binding strength due to greater steric hindrance of excess mannose on the PAMAM dendrimer surface.[61, 62]

Folate-targeted dendrimers have also been designed. One group has been able to produce ester terminated polyether dendrimers, which are modified for the attachment of folate. This group was able to attach 12.6 folates to a Generation 2 dendrimer with 16 available attachment sites.[59] Another group has gone one step further and has tested their folate-targeted dendrimers *in vitro*. The dendrimer used was a PAMAM dendrimer of generation 5. They attached folic acid and loaded methotrexate into the dendrimer. The

result of the *in vitro* study was that the targeted delivery improved the cytotoxic response of the cells to methotrexate 100 fold over the free drug.[63]

Although the results for carbohydrate and folate-targeted dendrimers are promising, there are some challenges and disadvantages associated with the use of dendrimers. It has been observed that dendrimers seem to move out of tumor tissue rather quickly, which prevents the drug from concentrating in the tumor.[56] A similar result has been shown in a polyester dendritic system where doxorubicin was covalently bound to the dendrimer. It was found that two of their polyester dendrimer formulations were excreted in 4-5 hours after intravenous injection of mice, while another compound had significant accumulation in the liver. Their longest circulating compound had a half-life of 72 minutes.[1] In order for a macromolecular delivery system to be successful, its circulation time must be long enough so that accumulation in tumor tissue can occur through the EPR effect. The circulation times reported for the polyester dendrimers are considerably shorter than those seen for block copolymer drug systems, which have been reported as high as 98.3 hours.[64] Another disadvantage to using dendrimers is that the size of the system is limited to the size of the interior of the dendrimer, which is approximately 10 nm in diameter.[15] The number of generations that the dendrimer can reach is limited by the degree of crowding at the exterior, where the maximum number of generations can range from 6 to 10 depending on the structure. Drug capacity is therefore limited by steric constraints. Furthermore, the chemistry required to create dendrimers at high generations can be a disadvantage, where the chemistry can often be extensive, costly, and labor-intensive. Last, as seen in the example above, there have been issues concerning the controllability of drug release from dendrimers, and improvements in

dendrimer chemistry and structure must be made in order to create an effective controlled drug release system.

1.2.5 Nanoparticles for Drug Delivery: Block Copolymer Micelles

The last major group of polymers that have been explored as nanoparticle drug delivery systems is block copolymer micelles. Block copolymer micelles are created from copolymers composed of a hydrophilic segment and a hydrophobic segment, as seen in Figure 1-4. When placed in an aqueous environment, micellization occurs where hydrophobic segregation from the environment is the main thermodynamic driving force.[21]

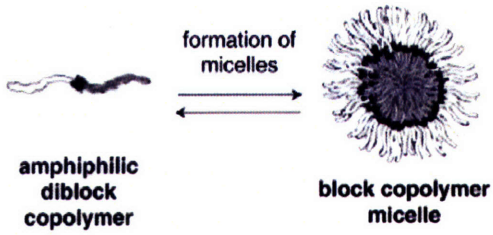

Figure 1-4. The formation of micelles from a diblock copolymer.[55]

The advantages of a block copolymer system is that with the hydrophobic core, the micelles have the ability to solubilize hydrophobic drugs while at the same time have a hydrophilic surface to evade the RES.[4] Micelles that are formed from the block copolymers are also small, thus facilitating evasion from the RES. Additionally, there is a lot of flexibility with a block copolymer system, where modifications in size,

functionality, and stability can be made. Several block copolymer micelle systems have been synthesized and reported such as poly(aspartic acid) and poly(β-benzyl-L-aspartate) as the hydrophobic block and PEG as the hydrophilic block.[21, 65] Other systems include poly(D,L-lactic acid-co-glycolic acid)-PEG,[66] poly(γ-benzyl-L-glutamate)-PEG,[67] and poly(ϵ-caprolactone)-PEG.[68] All of the systems mentioned have used PEG as the hydrophilic exterior in order to create a hydrodynamic barrier against the adsorption of proteins and to evade the RES.

Block copolymer micelle systems have demonstrated to be stable and capable of encapsulating hydrophobic drugs. For example, a poly(ethylene oxide)-poly(aspartic acid) block copolymer with adriamycin, an anticancer drug, conjugated to aspartic acid have been shown to form stable micelles.[69] Another system composed of poly(ethylene glycol) and conjugated doxorubicin-poly(aspartic acid), has been able to encapsulate free doxorubicin (DOX) in particles approximately 40 nm in diameter. These micelles have been tested against tumors inoculated subcutaneously and tumors implanted intravenously in mice. Three out of six mice were cured of mouse colon 26 carcinoma while two out of six mice were cured of human Lu-24 lung cancer. In comparison, free doxorubicin injected into mice was not able to cure any of them. The authors were also able to show that the block copolymer micelle accumulated in the tumor more effectively than free doxorubicin. The results of this study were promising enough to warrant clinical trials in Japan.[64]

In a further step towards creating micelles that can target specific areas of the body, some groups have explored the functionalization of the outer surface of block copolymer micelles. The functional ligands that have been added have included folate,

biotin, monosaccharides, and peptides.[70] Specifically, one group has been able to create galactose-, lactose-, and mannose-installed PEG-Poly(D,L-lactide) block copolymer micelles averaging approximately 100 ligands on the surface. They found that the galactose and lactose functionalized micelles specifically bound to RCA-1 lectin immobilized beads while glucose-PEG-PLA micelles were eluted (RCA-1 lectin is a plant lectin which specifically recognizes β-D-galactose residues). Also, the mannose functionalized micelles specifically bound to concavalin A. Furthermore, they found that there was a "cluster effect" in binding, where multiple sugar residues from one micelle would bind to the beads. A 30-fold concentration of free galactose compared to the micelle-conjugated galactose was required to elute the micelles from the column.[65, 70] Mixed micelles of poly(L-histidine)-PEG and poly(L-lactic acid)-PEG conjugated to folate have been tested *in vitro*, demonstrating that the targeted micelles were more effective against tumor cells than non-targeted micelles.[66, 71]

1.3 Thesis Objectives

Block copolymer micelles have shown to be promising alternatives to liposomes due to its flexibility. However, there is still much left to explore in this area, where many design parameters can be investigated or optimized. For this thesis, a novel linear-dendritic block copolymer has been designed. The linear-dendritic block copolymer is composed of a hydrophobic linear block and a hydrophilic dendritic block, which will self-assemble in aqueous solution into nanoparticles. The proposed drug delivery system hopes to combine the advantages conferred from dendrimers, including its dense surface functionality, with the increased capacity and chemical flexibility of a block copolymer micelle. The system will be similar in size to block copolymer micelles, which are

approximately 20-60 nm. This system will be an improvement over liposome nanoparticles with its smaller size--therefore the particle will have increased circulation times and more facile extravasation into tumors. Also in contrast to liposomes, the proposed system is easily fine-tuned to increase interactions between drug and drug delivery vehicle. Additionally, because it is a polymer system, it will have the ability to include a mechanism that will induce degradation of the nanoparticle system once it is in the endosome. With the addition of the dendritic outer structure, the density of ligand can be explored while maintaining approximately the same particle size. In comparison to dendrimers, the proposed drug delivery vehicle will have one to two orders of magnitude greater functionality with a large aggregation number (PEG-PBLA micelles have shown aggregation numbers ranging from 200-400),[72, 73] while for block copolymer micelles, the functionality of the proposed system will be several times higher depending on the dendron generation. An additional advantage of using the proposed system over dendrimers is that mixed micelles with different ligands could be used to create multi-functional systems or to manipulate the clustering density of ligands on the surface as shown in Figure 1-5.

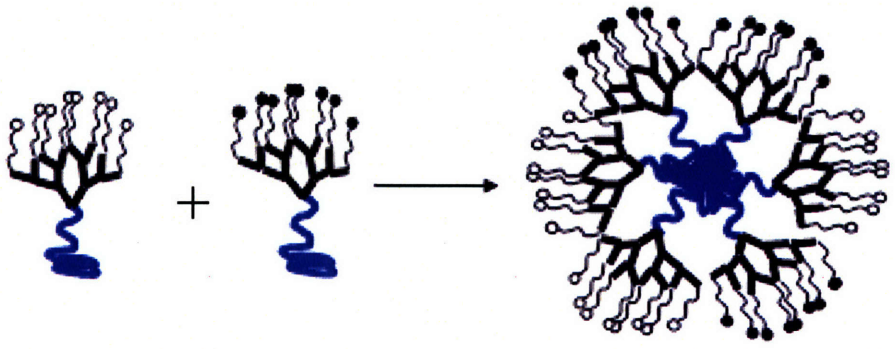

Figure 1-5. Formation of micelles with clustered or multifunctional ligands.

As an improvement over diblock copolymer micelles, the linear-dendritic block copolymers can be stabilized. It has been pointed out that after micelles are injected into the bloodstream, thermodynamic fluctuations could occur causing the breakdown of the micelle (because of the dilution effect leading to concentrations lower than the critical micelle concentration) and the precipitation of hydrophobic drugs.[4] Therefore, the crosslinking of the dendritic micelles will prevent this from occurring. Overall, the design of a new dendritic copolymer micelle will be able to address the issues that previously studied nanoparticle systems have had and hopefully will exceed expectations in performance.

Few linear-dendritic block copolymers have been synthesized and studied for drug delivery.[74] Additionally, those systems that have been explored self-assemble with a hydrophobic dendritic block forming the core and a PEG linear block forming the outer surface of the micelles. In this work, the first objective was to synthesize a linear-dendritic block copolymer with a hydrophilic dendron and a hydrophobic linear block. The second objective was to characterize and obtain a better understanding of the aqueous phase self-assembly behavior of the linear-dendritic block copolymer to ultimately determine its feasibility as a drug delivery vehicle. The third objective was to develop drug delivery approaches that could determine whether the dendritic block could confer advantages to the block copolymer micelles over conventional linear block copolymer micelles. This includes using the linear-dendritic block copolymer micelles in two different applications. The first application explored utilized the linear-dendritic block copolymer micelles as circulating targeted drug delivery vehicles. The other

application studied was to incorporate these linear-dendritic block copolymers into films as potential coatings for biomedical implants.

1.4 Thesis Overview

The remainder of this thesis is divided into 7 additional chapters. Chapter 2 discusses the synthesis of a linear-dendritic block copolymer. The solution-phase characterization of the block copolymer was performed including critical micelle concentration measurements, light scattering measurements, and TEM. Furthermore, encapsulation of a model hydrophobic drug was investigated.

In Chapter 3, results of molecular dynamics simulations of the linear-dendritic block copolymer micelles are detailed. Various micelle configurations are explored based on experimental data obtained through static light scattering experiments used to determine the aggregation number of the micelles. The simulations were performed to get a better understanding of the microstructure of the micelles formed and the thermodynamics of the micelle formation. Furthermore, locus of solubilization of a model hydrophobic drug is studied.

Chapter 4 explores the use of the linear-dendritic block copolymer micelles as circulating colloidal nanoparticles for targeted drug delivery. The linear-dendritic block copolymer was functionalized with a carbohydrate targeting ligand. Its binding behavior and drug delivery efficacy was determined *in vitro*.

Chapter 5 and Chapter 6 put forward methods to improve the linear-dendritic block copolymer micelles for future testing *in vivo*. First, a stabilization technique is explored in Chapter 5 to ensure that during administration into the body, the micelles

would not break apart. In Chapter 6, the synthesis of an improved linear-dendritic block copolymer is detailed, and its solution-phase and encapsulation behavior is investigated.

Chapter 7 discusses the second application for the linear-dendritic block copolymer micelles. The micelles are incorporated into a film created through a layer-by-layer dipping method. The micelles create hydrophobic domains for encapsulation of hydrophobic drugs. The films formed were characterized to ensure that the micelles incorporated were not disrupted. Additionally, *in vitro* testing of the films were done as a proof-of-concept for potential use as an antibacterial film on various biomedical implants.

Last, Chapter 8 includes the overall conclusions to the thesis project and suggests future directions for the project.

1.5 References

1. Padilla De Jesús, O.; Ihre, H.; Gagne, L.; Fréchet, J.; Szoka, F., "Polyester dendritic systems for drug delivery applications: In vitro and in vivo evaluation," *Bioconj. Chem.*, **2002,** 13, 453-561.

2. Allen, T. M.; Hansen, C.; Martin, F.; Redemann, C.; Yau-Young, A., "Liposomes containing synthetic lipid derivatives of poly(ethylene glycol) show prolonged curiculation half-lives in vivo," *Biochim. Biophys. Act.*, **1991,** 1066, 29-36.

3. Klibanov, A. L.; Maruyama, K.; Torchilin, V. P.; Huang, L., "Amphipathic polyethyleneglycols effectively prolong the circulation time of liposomes," *FEBS Lett.*, **1990,** 268, 235-237.

4. Liu, H.; Farrell, S.; Uhrich, K., "Drug release characteristics of unimolecular polymeric micelles," *J. of Controlled Rel.*, **2000,** 68, 167-174.

5. Gabizon, A., "Liposome circulation time and targeting: Implication for cancer chemotherapy," *Adv. Drug Del. Rev.*, **1995,** 16, 285-294.

6. Matsumara, Y.; Maeda, H., "A new concept for macromolecular therapeutics in cancer chemotherapy: Mechanism of tumoritropic accumulation of proteins and the antitumor agent smancs," *Cancer Research*, **1986,** 46, 6387-6392.

7. Lavasanifar, A.; Samuel, J.; Kwon, G., "Poly(ethylene oxide)-*block*-poly(l-amino acid) micelles for drug delivery," *Adv. Drug Delivery Rev.*, **2002,** 54, 169-190.

8. Scholes, P.; Coombes, A.; Davies, M.; Illum, L.; Davis, S., *Controlled drug delivery: Challenges and strategies*. American Chemical Society: Washington, D.C., 1997.

9. Torchilin, V. P., "Multifunctional nanocarriers," *Adv. Drug Del. Rev.*, **2006,** 58, 1532-1555.

10. Kumar, N.; Ravikumar, M.; Domb, A. J., "Biodegradable block copolymers," *Adv. Drug Del. Rev.*, **2001,** 53, 23-44.

11. Moghimi, S. M.; Patel, H. M., "Serum factors that regulate phagocytosis of liposomes by kupffer cells," *Biochem. Soc. Trans.*, **1993,** 21, 128S.

12. Patel, H. M., "Serum opsonins and liposomes: Their interactions and opsonophagocytosis," *Crit. Rev. Ther. Drug Carrier Syst.*, **1992,** 9, 39-90.

13. Nagayasu, A.; Uchiyama, K.; Kiwada, H., "The size of liposomes: A factor which affects their targeting efficiency to tumors and therapeutic activity of liposomal antitumor drugs," *Adv. Drug Del. Rev.*, **1999,** 40, 75-87.

14. El-Sayed, M.; Kiani, M.; Naimark, M.; Hikal, A.; Ghandehari, H., "Extravasation of poly(amidoamine) (pamam) dendrimers across microvacular network endothelium," *Pharm. Res.*, **2001,** 18, (1), 23-28.

15. Florence, A.; Hussain, N., "Transcytosis of nanoparticle and dendrimer delivery systems: Evolving vistas," *Adv. Drug Del. Rev.*, **2001,** 50, S69-S89.

16. Jain, R. K., "Delivery of molecular medicine to solid tumors: Lessons from in vivo imaging of gene expression and function," *J. of Controlled Rel.*, **2001,** 74, 7-25.

17. Reddy, J. A.; Low, P. S., "Folate-mediated targeting of therapeutic and imaging agents to cancers," *Crit. Rev. Ther. Drug Carrier Syst.*, **1998,** 15, 587-627.

18. Lian, T.; Ho, R., "Trends and developments in liposomes drug delivery systems," *J. Of Pharm. Sci.*, **2001,** 90, 667-680.

19. Beezer, A. E.; King, A.; Martin, I.; Mitchel, J.; Twyman, L.; Wain, C., "Dendrimers as potential drug carriers; encapsulation of acidic hydrophobes within water soluble pamam derivatives," *Tetrahedron*, **2003,** 59, 3873-3880.

20. Kojima, C.; Kono, K.; Maruyama, K.; Takagishi, R., "Synthesis of polyamidoamine dendrimers having poly(ethylene glycol) grafts and their ability to encapsulate anticancer drugs," *Bioconj. Chem.*, **2000,** 11, 910-917.

21. Kataoka, K.; Harada, A.; Nagasaki, Y., "Block copolymer micelles for drug delivery: Design, characterization and biological significance," *Adv. Drug Del. Rev.*, **2001,** 47, 113-131.

22. Li, Y.; Pei, Y.; Zhang, X.; Gu, X.; Zhou, Z.; Yuan, W.; Zhou, J.; Zhu, J.; Gao, X., "Pegylated plga nanoparticles as protein carriers: Synthesis, preparation, and biodistribution in rats," *J. Control. Rel.*, **2001,** 71, 203-211.

23. Stolnik, S.; Illum, L.; Davis, S. S., "Long circulating microparticulate drug carriers," *Adv. Drug Del. Rev.*, **1995,** 16, 195-214.

24. Bhadra, D.; Bhadra, S.; Jain, S.; Jain, N. K., "A pegylated dendritic nanoparticulate carrier of fluorouracil," *Int. J. of Pharm.*, **2003,** 257, 111-124.

25. Hofland, H.; Masson, C.; Iginla, S.; Osetinksky, I.; Reddy, J.; Leamon, C.; Scherman, D.; Bessodes, M.; Wils, P., "Folate-targeted gene transfer *in vivo*," *Molecular Therapy*, **2002,** 5, (6), 739-744.

26. Forssen, E.; Willis, M., "Ligand-targeted liposomes," *Adv. Drug Del. Rev.*, **1998,** 29, 249-271.

27. Hatakeyama, H.; Akita, H.; Maruyama, K.; Suhara, T.; Harashima, H., "Factors governing the in vivo tissue uptake of transferrin-coupled polyethylene glycol liposomes in vivo," *Int. J. of Pharm.*, **2004,** 281, 25-33.

28. Ishida, O.; Maruyama, K.; Tanahashi, H.; Iwatsuru, M.; Sasaki, K.; Eriguchi, M.; Yanagie, H., "Liposomes bearing polyethyleneglycol-coupled transferrin with intracellular targeting property to the solid tumors in vivo," *Pharm. Res.*, **2001,** 18, 1042-1048.

29. Lee, Y. C., "Biochemistry of carbohydrate-protein interaction," *FASEB Journal*, **1992,** 6, 3193-3200.

30. Perillo, N. L.; Marcus, M. E.; Baum, L. G., "Galectins: Versatile modulators of cell adhesion, cell proliferation, and cell death," *J. Mol. Med.*, **1998,** 76, 402-412.

31. Park, T. G.; Jeong, J. H.; Kim, S. W., "Current status of polymeric gene delivery systems," *Adv. Drug Del. Rev.*, **2006,** 58, (4), 467-486.

32. Gabor, F.; Bogner, E.; Weissenboeck, A.; Wirth, M., "The lectin-cell interaction and its implications to intestinal lectin-mediated drug delivery," *Adv. Drug Del. Rev.*, **2004,** 56, 459-480.

33. Chiu, M.; Tamura, T.; Wadhwa, M. S.; Rice, K. G., "In vivo targeting functin of n-linked oligosaccharides with terminating galactose and n-acetyl-galactosamine residues," *J. Bio. Chem.*, **1994,** 269, 16195-16202.

34. David, A.; Kopecková, P.; Kopecek, J.; Rubinstein, A., "The role of galactose, lactose, and galactose valency in the biorecognition of n-(2-hydroxypropyl)methacrylamide copolymers by human colon adenocarcinoma cells," *Pharm. Res.*, **2002,** 19, 1114-1122.

35. Omelyanenko, V.; Kopečková, P.; Gentry, C.; Kopeček, J., "Targetable hpma copolymer-adrimycin conjugates. Recognition, internalization, and subcellular fate," *J. Control. Rel.*, **1998,** 53, 25-37.

36. Lu, Y.; Low, P., "Folate-mediated delivery of macromolecular anticancer therapeutic agents," *Adv. Drug Del. Rev.*, **2002,** 54, 675-713.

37. Sudimack, J.; Lee, R., "Targeted drug delivery via the folate receptor," *Adv. Drug Del. Rev.*, **2000,** 41, 147-162.

38. Lee, R.; Wang, S.; Low, P., "Measurement of endosome ph following folate receptor-mediated endocytosis," *Biochim. Biophys. Act.*, **1996,** 1312, 237-242.

39. Hong, S.; Leroueil, P.; Majoros, I.; Orr, B.; Baker, J., Jr.; Holl, M. M., "The binding avidity of a nanoparticle-based multivalent targeted drug delivery platform," *Chem. & Bio.*, **2007,** 14, 107-115.

40. Gabizon, A.; Shmeeda, H.; Horowitz, A.; Zalipsky, S., "Tumor cell targeting of liposome-entrapped drugs with phospholipid-anchored folic acid-peg conjugates," *Adv. Drug Del. Rev.*, In Press.

41. Guo, W.; Lee, T.; Sudimack, J.; Lee, R., "Receptor-specific delivery of liposomes via folate-peg-chol," *J. of Liposome Res.*, **2000,** 10, 179-195.

42. Gabizon, A.; Horowitz, A. T.; Goren, D.; Tzemach, D.; Mandelbaum-Shavit, V.; Qazan, M. M.; Zalipsky, S., "Targeting folate receptor with folate linked to extremities of poly(ethyleneglycol)-grafted liposomes: In vitro studies," *Bioconj. Chem.*, **1999,** 10, 289-298.

43. Allen, T. M.; Ahmad, I.; Lopes de Menezes, D. E.; Moase, E. H., "Immunoliposome-mediated targeting of anti-cancer drugs in vivo," *Biochem. Soc. Trans.*, **1995,** 23, 1073-1079.

44. Fujimori, K.; Covell, D. G.; Fletcher, J. E.; Weinstein, J. N., "A modeling analysis of monoclonal antibody percolation through tumors: A binding-site barrier," *J. Nucl. Med.*, **1990,** 3, 1191-1198.

45. Gabizon, A.; Martin, F., "Polyethylene glycol-coated (pegylated) liposomal doxorubicin. Rationale for use in solid tumours," *Drugs*, **1997,** 54 Suppl 4, 15.

46. Lee, R.; Low, P., "Delivery of liposomes into cultured kb cells via folate receptor-mediated endocytosis," *J. Bio. Chem.*, **1994,** 269, 3198-3204.

47. Park, J. W.; Kirpotin, D. B.; Hong, K.; Shalaby, R.; Shao, R.; Nielsen, U. B.; Marks, J. D.; Papahadjopoulos, D.; Benz, C. C., "Tumor targeting using anti-her2 immunoliposomes," *J. Control. Rel.*, **2001,** 74, 93-113.

48. Kamps, J. A.; Koning, G. A.; Velinova, M. J.; Morsel, H. W.; Wilkens, M.; Gorter, A.; Donga, J.; Scherphof, G. L., "Uptake of long-circulating immunoliposomes, directed against colon adenocarcinoma cells, by liver metasteses of colon cancer," *J. Drug. Target.*, **2000,** 8, 235-245.

49. Barratt, G.; Tenu, J.; Yapo, A.; Petit, J., "Preparation and characterization of liposomes containing mannosylated phospholipids capable of targeting drugs to macrophages," *Biochem. Biophys. Acta.*, **1986,** 862, 152-164.

50. Umezawa, F.; Eto, Y., "Liposome targeting to mouse brain: Mannose as recognition marker," *Biochem. Biophys. Res. Commun.*, **1988,** 153, 1038-1044.

51. Wu, J.; Liu, P.; Zhu, J.-L.; Maddukuri, S.; Zern, M., "Increased liver uptake of liposomes and improved targeting efficacy by labeling with asialofetuin in rodents," *Hepatology*, **1998,** 27, (3), 772-778.

52. Hara, T.; Aramaki, Y.; Takada, S.; Koike, K.; Tsuchiya, S., "Receptor-mediated transfer of psv2cat DNA to a human hepatoblastoma cell line hepg2 using asialofetuin-labeled cationic liposomes," *Gene*, **1995,** 159, (2), 167-174.

53. Lee, R.; Low, P., "Folate-mediated tumor cell targeting of liposome-entrapped doxorubicin in vitro," *Biochim. Biophys. Act.*, **1995,** 1233, 134-144.

54. Pan, X. Q.; Wang, H.; Lee, R., "Antitumor activity of folate receptor-targeted liposomal doxorubicin in a kb oral carcinoma murine xenograft model," *Pharm. Res.*, **2003,** 20, 417-422.

55. Rösler, A.; Vandermeulen, G.; Klok, H., "Advanced drug delivery devices via self-assembly of amphiphilic block copolymers," *Adv. Drug Del. Rev.*, **2001,** 53, 95-108.

56. Henry, C., "Drug delivery," *C&EN*, **2002,** 80, (34), 39.

57. Kawashima, Y., "Nanoparticulate systems for improved drug delivery," *Adv. Drug Del. Rev.*, **2001,** 47, 1-2.

58. Malik, N.; Wiwattanapatapee, R.; Klopsch, R.; Lorenz, K.; Frey, H.; Weener, J. W.; Meijer, E. W.; Paulus, W.; Duncan, R., "Dendrimers: Relationship between structure and biocompatibility in vitro, and preliminary studies on the biodistribution of ^{125}i-labelled polyamidoamine dendrimers in vivo," *J. Control. Rel.*, **2000,** 65, 133-148.

59. Kono, K.; Liu, M.; Fréchet, J., "Design of dendritic macromolecules containing folate or methotrexate residues," *Bioconj. Chem.*, **1999,** 20, 1115-1121.

60. Aoi, K.; Itoh, K.; Okada, M., "Globular carbohydrate macromolecule "sugar balls". 1. Synthesis of novel sugar-persubstituted poly(amido amine) dendrimers," *Macromolecules*, **1995,** 28, 5391-5393.

61. Woller, E.; Cloninger, M., "Mannose functionalization of a sixth generation dendrimer," *Biomacromolecules*, **2001,** 2, 1052-1054.

62. Wolfenden, M.; Cloninger, M., "Carbohydrate-functionalized dendrimers to investigate the predictable tunability of multivalent interactions," *Bioconj Chem*, **2006,** 17, 958-966.

63. Quintana, A.; Raczka, E.; Piehler, L.; Lee, I.; Myc, A.; Majoros, I.; Patri, A.; Thomas, T.; Mulé, J.; Baker, J., Jr., "Design and function of a dendrimer-based therapeutic nanodevice targeted to tumor cells through the folate receptor," *Pharm. Res.*, **2002,** 19, 1310-1316.

64. Nakanishi, T.; Fukushima, S.; Okamoto, K.; Suzuki, M.; Matsumura, Y.; Yokoyama, M.; Okano, T.; Sakurai, Y.; Kataoka, K., "Development of the polymer micelle carrier system for doxorubicin," *J. Control. Rel.*, **2001,** 74, 295-302.

65. Kataoka, K.; Matsumoto, T.; Yokoyama, M.; Okano, T.; Sakurai, Y.; Fukushima, S.; Okamoto, K.; Kwon, G., "Doxorubicin-loaded poly(ethylene glycol)-poly(β-benzyl-l-aspartate) copolymer micelles: Their pharmaceutical characteristics and biological significance," *J. Control. Rel.*, **2000,** 64, 143-153.

66. Yoo, H.; Park, T. G., "Folate receptor targeted biodegradable polymeric doxorubicin micelles," *J. Control. Rel.*, **2004,** 96, 273-283.

67. Nah, J.-W., "Drug-delivery system based on core-shell-type nanoparticles composed of poly(γ-benzyl-l-glutamate) and poly(ethylene oxide)," *J. of App. Poly. Sci.*, **1999,** 75, 1115-1126.

68. Shuai, X.; Ai, H.; Nasongkla, N.; Kim, S.; Gao, J., "Micellar carriers based on block copolymers of poly(ϵ-caprolactone) and poly(ethylene glycol) for doxorubicin delivery," *J. Control. Rel.*, **2004,** 98, 415-426.

69. Yokoyama, M.; Kwon, G.; Okano, T.; Sakurai, Y.; Seto, T.; Kataoka, K., "Preparation of micelle-forming polymer-drug conjugates," *Bioconj. Chem.*, **1992,** 3, 295-301.

70. Nagasaki, Y.; Yasugi, K.; Yamamoto, Y.; Harada, A.; Kataoka, K., "Sugar-installed block copolymer micelles: Their preparation and specific interaction with lectin molecules," *Biomacromolecules*, **2001,** 2, 1067-1070.

71. Lee, E. S.; Na, K.; Bae, Y., "Polymeric micelle for tumor ph and folate-mediated targeting," *J. Control. Rel.*, **2003,** 91, 103-113.

72. Cammas, S.; Kataoka, K., "Functional poly[(ethylene oxide)-co-(β-benzyl-l-aspartate)] polymeric micelles: Block copolymer synthesis and micelles formation," *Macromolecular Chem. and Phys.*, **1995,** 196, (6), 1899-1905.

73. Kwon, G.; Naito, M.; Yokoyama, M.; Okano, T.; Sakurai, Y.; Kataoka, K., "Micelles based on ab block copolymers of poly(ethylene oxide) and poly(β-benzyl-l-aspartate)," *Langmuir*, **1993,** 9, 945-949.

74. Gillies, E.; Fréchet, J., "Ph-responsive copolymer assemblies for controlled release of doxorubicin," *Bioconj Chem*, **2005,** 16, (2), 361-368.

CHAPTER 2: Synthesis and Characterization of Poly(propylene oxide)-*b*-Poly(amidoamine)

2.1 Introduction

Amphiphilic block copolymers have been studied extensively for applications that can exploit their self-assembly behavior in aqueous media. Recently, amphiphilic linear-dendritic block copolymers have emerged as a new class of amphiphilic block copolymers with potential applications ranging from drug delivery and biomaterials to molecular templating.[1-3] The synthetic pathway used to make these block copolymers permits low polydispersity and a great deal of control over molecular architecture. Linear-dendritic block copolymers have been synthesized as both diblock[4-8] and dendritic-linear-dendritic triblock systems.[9-13] Most of the linear-dendritic block copolymers that have been studied are composed of a hydrophilic linear block, usually poly(ethylene oxide) (PEO), attached to a hydrophilic dendritic block or to another dendritic block that is relatively hydrophobic. These systems include a linear PEO block attached to dendritic blocks of either poly(amidoamine) (PAMAM),[14, 15] poly(benzyl ether),[16-19] or poly(α,ε-L-lysine).[4, 20] The amphiphilic systems display interesting solution phase behavior with the ability to form multimolecular micelles that have critical micelle concentrations (CMC) values well below the CMC values of low molecular weight surfactants such as sodium dodecyl sulfate.[19] Several groups have shown that the hydrophobic dendritic block, such as poly(benzyl ether) or poly(α,ε-L-lysine), forms the core of the micelle, which increases in size with higher generations, while the PEO block forms a protective corona around the micelle.[4, 19, 20] Because of the excellent

biocompatibility and stealth properties of PEO, these linear-dendritic block copolymer systems have been proposed for drug delivery and gene therapy applications.[7, 11, 20-23]

Relatively few studies have been performed for linear-dendritic block copolymers with a hydrophobic linear block and a hydrophilic dendritic block. For such systems, the linear block forms the micelle core while the dendrimer block faces the aqueous media. The Meijer group has performed extensive solution phase studies of polystyrene with poly(propylene imine) dendrimers that have demonstrated the control of aggregation morphology by changing the dendrimer generation and pH.[24-27] Synthesis and self-assembly behavior have been studied on more biocompatible systems such as block copolymers of dendritic polyether with poly(N-isopropylacrylamide),[28] dendritic L-lysine attached to poly(lactic acid) modified with cholesterol,[29] and hyperbranched poly(glycerol) (though not dendritic) and poly(propylene oxide) (PPO).[30] These systems formed varying morphologies in solution ranging from micelles to cylinders with low CMCs. To the author's knowledge, extensive characterization studies have not been performed on linear-dendritic or dendritic-linear-dendritic block copolymers containing a hydrophobic linear block for drug delivery.

This chapter will discuss the synthesis of an ABA triblock consisting of PAMAM as the A block and PPO as the B block, with varying generations of PAMAM. The series of polymers created is well-defined due to the monodisperse nature of dendrimer synthesis. The solution-phase behavior of the series of PPO-PAMAM has been studied. Because of its amphiphilic nature, the triblock forms micelles in solution which have been characterized as a function of the PAMAM generation. The drug encapsulation

efficiency and release rate were studied with a model hydrophobic drug to determine the feasibility of the novel polymeric triblock as a drug delivery vehicle.

2.2 Experimental

2.2.1 Materials

Poly(propylene glycol) bis(2-aminopropyl ether) (MW ~4000, Mw/Mn = 1.04), methanol, diethyl ether, pyrene (sublimed, 99%), and 5-chloro-2-(2,4-dichlorophenoxy)phenol (triclosan, ≥97.0% purity) were purchased from Sigma-Aldrich and used as received. Methyl acrylate and ethylenediamine were obtained from Sigma-Aldrich and distilled over calcium hydride before use. MilliQ (18.2 MΩ) water was used in all experiments requiring water.

2.2.2 Synthesis of PPO-PAMAM

Synthesis of PPO-PAMAM Generation 0.5

PPO-[N(^{a}CH$_2$^{b}CH$_2$CO$_2$^{c}CH$_3$)$_2$]$_2$. A 7 g sample of poly(propylene glycol) bis(2-aminopropyl ether) (PPO) was dissolved in methanol and added dropwise to 200 times molar excess of methyl acrylate (32 ml). The reaction mixture was stirred under nitrogen for 3 days at room temperature. Excess methyl acrylate and methanol were removed with a rotary evaporator leaving a viscous oil. The copolymer was redissolved in methanol and removed by rotary evaporation three times thereafter and vacuum-dried overnight (yield = 7.62 g, 100%). ^{1}H NMR ($CDCl_3$): δ_{PPO}(–OCH$_2$CHC**H$_3$**–) = 1.14 (t); δ_{PPO}(–OCH$_2$C**H**CH$_3$–) = 3.40 (m); δ_{PPO}(–OC**H$_2$**CHCH$_3$–) = 3.61 (m); δ_{PAMAM} = 3.66 (s, c); δ_{PAMAM} = 2.77-2.81 (m, a); δ_{PAMAM} = 2.42 (t, b). FTIR peak ν cm^{-1}: 1111, 1741, 2870, 2971.

Synthesis of PPO-PAMAM G1.0

PPO-[N($^{a}CH_2{}^{b}CH_2CO^{c}NH^{d}CH_2{}^{e}CH_2NH_2)_2]_2$. PPO-PAMAM generation 0.5 (7.6 g) was dissolved in methanol and added dropwise into 200 times molar excess ethylenediamine (24 ml). The reaction was stirred under nitrogen for 4 days at room temperature. Ethylenediamine and methanol were removed through rotary evaporation at 45 °C, leaving copolymer that was a viscous oil. To ensure complete evaporation of ethylenediamine, an azeotropic mixture of toluene and methanol was used to dissolve the copolymer and removed through rotary evaporation three times. Afterwards, the copolymer was vacuum-dried overnight (yield = 7.7 g, 100%). ^{1}H NMR ($CDCl_3$): δ_{PPO}(–OCH_2CHCH_3–) = 1.14 (t); δ_{PPO}(–OCH_2CHCH_3–) = 3.40 (m); δ_{PPO}(–OCH_2CHCH_3–) = 3.61 (m); δ_{PAMAM} = 8.01 (m, c); δ_{PAMAM} = 3.25-3.32 (m, d); δ_{PAMAM} = 2.6-3.0 (m, e+a); δ_{PAMAM} = 2.38 (m, b). FTIR peak ν cm^{-1}: 1111, 1557, 1651, 2870, 2971, 3292.

Synthesis of PPO-PAMAM G1.5

PPO-[N($^{a}CH_2{}^{b}CH_2CO^{c}NH^{d}CH_2{}^{e}CH_2N(^{f}CH_2{}^{g}CH_2CO_2{}^{h}CH_3)_2)_2]_2$. PPO-PAMAM generation 1.0 (7.7 g) was dissolved in methanol and added dropwise to methyl acrylate (63 ml). Methyl acrylate was in 400 molar excess over the copolymer. The reaction conditions and purification procedures were similar to the synthesis of generation 0.5 (yield = 8.5 g, 96%). ^{1}H NMR ($CDCl_3$): δ_{PPO}(–OCH_2CHCH_3–) = 1.14 (t); δ_{PPO}(–OCH_2CHCH_3–) = 3.40 (m); δ_{PPO}(–OCH_2CHCH_3–) = 3.61 (m); δ_{PAMAM} = 8.01 (m, c); δ_{PAMAM} = 3.66 (s, h); δ_{PAMAM} = 3.28 (m, d); δ_{PAMAM} = 2.75-3.0 (m, a+f); δ_{PAMAM} = 2.54 (t, e); δ_{PAMAM} = 2.44 (t, g); δ_{PAMAM} = 2.34 (t, b); FTIR peak ν cm^{-1}: 1110, 1539, 1669, 1739, 2870, 2971.

PPO-PAMAM G2.0

PPO-[N($^{a}CH_2$$^{b}CH_2CO^{c}NH^{d}CH_2$$^{e}CH_2N$($^{f}CH_2$$^{g}CH_2CO^{h}NH^{i}CH_2$$^{j}CH_2NH_2$)$_2$)$_2$]$_2$. The synthesis, reaction conditions, and purification procedure was similar to the procedure described for generation 1.0, with 8.5 g of generation 1.5 with 45 ml ethylenediamine. An additional purification step was performed where the polymer dissolved in methanol was run through a sephadex LH-20 column. The methanol in the collected fractions was removed through rotary evaporation (yield = 8.12 g, 89%). ^{1}H NMR ($CDCl_3$): δ_{PPO}(–OCH_2CHCH_3–) = 1.14 (t); δ_{PPO}(–OCH_2CHCH_3–) = 3.40 (m); δ_{PPO}(–OCH_2CHCH_3–) = 3.61 (m); δ_{PAMAM} = 7.66-8.02 (bs, c+h); δ_{PAMAM} = 3.31 (m, i); δ_{PAMAM} = 3.24 (m, d); δ_{PAMAM} = 2.74-2.89 (t, a+f+j); δ_{PAMAM} = 2.54 (t, e); δ_{PAMAM} = 2.38 (t, g); δ_{PAMAM} = 2.32 (m, b); FTIR peak ν cm^{-1}: 1110, 1552, 1647, 2870, 2971, 3275.

PPO-PAMAM G2.5

PPO-[N($^{a}CH_2$$^{b}CH_2CO^{c}NH^{d}CH_2$$^{e}CH_2N$($^{f}CH_2$$^{g}CH_2CO^{h}NH^{i}CH_2$$^{j}CH_2N$ ($^{k}CH_2$$^{l}CH_2CO_2$$^{m}CH_3$)$_2$)$_2$)$_2$]$_2$. The synthesis, reaction conditions, and purification procedure were similar to the procedure described for generation 1.5, with 8.12 g of generation 2.0 copolymer with 113 ml methyl acrylate (yield = 9.6 g, 93%). ^{1}H NMR ($CDCl_3$): δ_{PPO}(–OCH_2CHCH_3–) = 1.14 (t); δ_{PPO}(–OCH_2CHCH_3–) = 3.40 (m); δ_{PPO}(–OCH_2CHCH_3–) = 3.61 (m); δ_{PAMAM} = 7.66-8.02 (bs, c+h); δ_{PAMAM} = 3.67 (s, m); δ_{PAMAM} = 3.28 (m, d+i); δ_{PAMAM} = 2.74-2.83 (m, a+f+k); δ_{PAMAM} = 2.53-2.59 (m, e+j); δ_{PAMAM} = 2.44 (t, l); δ_{PAMAM} = 2.37 (t, b+g); FTIR peak ν cm^{-1}: 1110, 1540, 1665, 1738, 2870, 2971.

PPO-PAMAM G3.0

PPO-[N($^{a}CH_2{}^{b}CH_2CO^{c}NH^{d}CH_2{}^{e}CH_2N($^{f}CH_2{}^{g}CH_2CO^{h}NH^{i}CH_2{}^{j}CH_2N ($^{k}CH_2{}^{l}CH_2CO^{m}NH^{n}CH_2{}^{o}CH_2NH_2)_2)_2)_2]_2$. A 9.6 g sample of PPO-PAMAM generation 2.5 was dissolved in methanol and added dropwise to 63 ml of ethylenediamine. The reaction solution was stirred under nitrogen for 4 days. Ethylenediamine and methanol were removed through rotary evaporation at 45 °C. Further purification involved dissolving the polymer in an azeotropic mixture of methanol and toluene and removal with a rotary evaporator 3 times. The resulting polymer was dissolved in methanol and precipitated in 10 times excess diethyl ether. After decanting, the polymer was vacuum dried (yield = 5.33 g, 54%). ^{1}H NMR ($CDCl_3$): δ_{PPO}(–OCH_2CHCH_3–) = 1.14 (t); δ_{PPO}(–OCH_2CHCH_3–) = 3.40 (m); δ_{PPO}(–OCH_2CHCH_3–) = 3.61 (m); δ_{PAMAM} = 7.73-8.09 (bs, c+h+m); δ_{PAMAM} = 3.23-3.30 (m, d+i+n); δ_{PAMAM} = 2.72-2.84 (m, a+f+k+o); δ_{PAMAM} = 2.53 (m, e+j); δ_{PAMAM} = 2.36 (t, l); δ_{PAMAM} = 2.33 (m, b+g); FTIR peak ν cm^{-1}: 1110, 1553, 1645, 2870, 2971, 3069, 3284.

PPO-PAMAM G3.5

PPO-[N($^{a}CH_2{}^{b}CH_2CO^{c}NH^{d}CH_2{}^{e}CH_2N($^{f}CH_2{}^{g}CH_2CO^{h}NH^{i}CH_2{}^{j}CH_2N ($^{k}CH_2{}^{l}CH_2CO^{m}NH^{n}CH_2{}^{o}CH_2N($^{p}CH_2{}^{q}CH_2CO_2{}^{r}CH_3)_2)_2)_2)_2]_2$. The synthesis, reaction conditions, and purification procedure were similar to the procedure described for generation 1.5, with 3 g of generation 3.0 with 64 ml methyl acrylate (yield = 4.0 g, 95%). ^{1}H NMR ($CDCl_3$): δ_{PPO}(–OCH_2CHCH_3–) = 1.14 (t); δ_{PPO}(–OCH_2CHCH_3–) = 3.40 (m); δ_{PAMAM} = 7.73-8.09 (bs, c+h+m); δ_{PPO}(–OCH_2CHCH_3–) = 3.61 (m); δ_{PAMAM} = 3.67 (s, r); δ_{PAMAM} = 3.28 (m, d+i+n); δ_{PAMAM} = 2.75-2.81 (m, a+f+k+p); δ_{PAMAM} = 2.53-

2.58 (m, e+j+o); δ_{PAMAM} = 2.44 (t, q); δ_{PAMAM} = 2.37 (m, b+g+l); FTIR peak ν cm^{-1}: 1110, 1542, 1652, 1738, 2870, 2971, 3293.

PPO-PAMAM G4.0

PPO-[N($^{a}CH_2{}^{b}CH_2CO^{c}NH^{d}CH_2{}^{e}CH_2N(^{f}CH_2{}^{g}CH_2CO^{h}NH^{i}CH_2{}^{j}CH_2N$

($^{k}CH_2{}^{l}CH_2CO^{m}NH^{n}CH_2{}^{o}CH_2N(^{p}CH_2{}^{q}CH_2CO^{r}NH^{s}CH_2{}^{t}CH_2NH_2)_2)_2)_2)_2]_2$. The synthesis, reaction conditions, and purification procedure were similar to the procedure described for generation 3.0, with 4.0 g of generation 3.5 with 45 ml ethylenediamine (yield = 3.53 g, 85%). ^{1}H NMR ($CDCl_3$): δ_{PPO}(–OCH_2CHCH_3–) = 1.14 (t); δ_{PPO}(–OCH_2CHCH_3–) = 3.40 (m); δ_{PPO}(–OCH_2CHCH_3–) = 3.61 (m); δ_{PAMAM} = 7.63-8.07 (bs, c+h+m+r); δ_{PAMAM} = 3.26 (m, d+i+n+s); δ_{PAMAM} = 2.71-2.82 (m, a+f+k+p+t); δ_{PAMAM} = 2.51 (bs, e+j+o); δ_{PAMAM} = 2.32-2.37 (m, b+g+l+q); FTIR peak ν cm^{-1}: 1110, 1554, 1647, 2870, 2971, 3069, 3279.

PPO-PAMAM G4.5

PPO-[N($^{a}CH_2{}^{b}CH_2CO^{c}NH^{d}CH_2{}^{e}CH_2N(^{f}CH_2{}^{g}CH_2CO^{h}NH^{i}CH_2{}^{j}CH_2N$

($^{k}CH_2{}^{l}CH_2CO^{m}NH^{n}CH_2{}^{o}CH_2N(^{p}CH_2{}^{q}CH_2CO^{r}NH^{s}CH_2{}^{t}CH_2N$

($^{u}CH_2{}^{v}CH_2CO_2{}^{w}CH_3)_2)_2)_2)_2)_2]_2$. Generation 4.0 (1.3 g) was dissolved in methanol and added dropwise to excess methyl acrylate (38 ml). The reaction was stirred under nitrogen for 3 days. Unreacted methyl acrylate and methanol were removed by rotary evaporation. Subsequently, the polymer was redissolved in methanol and removed with rotary evaporation 3 times. The polymer was dissolved in methanol and precipitated in 10 times excess diethyl ether. The ether was decanted and the polymer was dried by vacuum (yield = 1.2 g, 58%). ^{1}H NMR ($CDCl_3$): δ_{PPO}(–OCH_2CHCH_3–) = 1.14 (t);

δ_{PPO}(–OCH_2CHCH_3–) = 3.40 (m); δ_{PPO}(–OCH_2CHCH_3–) = 3.61 (m); δ_{PAMAM} = 7.63-8.07 (bs, c+h+m+r); δ_{PAMAM} = 3.66 (s, w); δ_{PAMAM} = 3.27 (m, d+i+n+s); δ_{PAMAM} = 2.74-2.82 (m, a+f+k+p+u); δ_{PAMAM} = 2.58-2.53 (m, e+j+o+t); δ_{PAMAM} = 2.43 (t, v); δ_{PAMAM} = 2.36 (bs, b+g+l+q); FTIR peak ν cm^{-1}: 1110, 1542, 1647, 1736, 2870, 2971, 3287.

PPO-PAMAM G5.0

PPO-[N($^{a}CH_2^{b}CH_2CO^{c}NH^{d}CH_2^{e}CH_2N(^{f}CH_2^{g}CH_2CO^{h}NH^{i}CH_2^{j}CH_2N$

($^{k}CH_2^{l}CH_2CO^{m}NH^{n}CH_2^{o}CH_2N(^{p}CH_2^{q}CH_2CO^{r}NH^{s}CH_2^{t}CH_2N$

($^{u}CH_2^{v}CH_2CO^{w}NH^{x}CH_2^{y}CH_2NH_2)_2)_2)_2)_2)_2]_2$. The synthesis, reaction conditions, and purification procedure were similar to the procedure described for generation 3.0, with ethylenediamine in excess at a molar ratio of 3200:1 compared to PPO-PAMAM generation 4.5. ^{1}H NMR ($CDCl_3$): δ_{PPO}(–OCH_2CHCH_3–) = 1.14 (t); δ_{PPO}(–OCH_2CHCH_3–) = 3.40 (m); δ_{PPO}(–OCH_2CHCH_3–) = 3.61 (m); δ_{PAMAM} = 8.07-7.97 (bs, c+h+m+r+w); δ_{PAMAM} = 3.27 (m, d+i+n+s+x); δ_{PAMAM} = 2.82-2.74 (m, a+f+k+p+u+y); δ_{PAMAM} = 2.54 (bs, e+j+o+t); δ_{PAMAM} = 2.36 (bs, b+g+l+q+v); FTIR peak *ν* cm^{-1}: 1110, 1552, 1643, 2870, 2971, 3071, 3280.

Synthesis of PPO-PAMAM G5.5

PPO-[N($^{a}CH_2^{b}CH_2CO^{c}NH^{d}CH_2^{e}CH_2N(^{f}CH_2^{g}CH_2CO^{h}NH^{i}CH_2^{j}CH_2N$

($^{k}CH_2^{l}CH_2CO^{m}NH^{n}CH_2^{o}CH_2N(^{p}CH_2^{q}CH_2CO^{r}NH^{s}CH_2^{t}CH_2N$

($^{u}CH_2^{v}CH_2CO^{w}NH^{x}CH_2^{y}CH_2N(^{z}CH_2^{aa}CH_2CO_2^{ab}CH_3)_2)_2)_2)_2)_2)_2]_2$. The synthesis, reaction conditions, and purification procedure were similar to the procedure described for generation 4.5. Methyl acrylate was present 6400 times in molar excess over the copolymer. ^{1}H NMR ($CDCl_3$): δ_{PPO}(–OCH_2CHCH_3–) = 1.14 (t); δ_{PPO}(–OCH_2CHCH_3–)

= 3.40 (m); δ_{PPO}(–OC**H**$_2$CHCH$_3$–) = 3.61 (m); δ_{PAMAM} = 8.07-7.97 (bs, c+h+m+r+w); δ_{PAMAM} = 3.66 (s, ab); δ_{PAMAM} = 3.27 (m, d+i+n+s+x); δ_{PAMAM} = 2.82-2.74 (m, a+f+k+p+u+z); δ_{PAMAM} = 2.59-2.53 (m, e+j+o+t+y); δ_{PAMAM} = 2.43 (t, aa); δ_{PAMAM} = 2.36 (bs, b+g+l+q+v); FTIR peak ν cm^{-1}: 1199, 1544, 1648, 1736, 2840, 2951, 3071, 3291.

Synthesis of PPO-PAMAM G6.0

PPO-[N(^{a}**CH**$_2$^{b}**CH**$_2$**CONH**^{c}**CH**$_2$^{d}**CH**$_2$**N(**^{e}**CH**$_2$^{f}**CH**$_2$**CONH**^{g}**CH**$_2$^{h}**CH**$_2$**N**

(^{i}**CH**$_2$^{j}**CH**$_2$**CONH**^{k}**CH**$_2$^{l}**CH**$_2$**N(**^{m}**CH**$_2$^{n}**CH**$_2$**CONH**^{o}**CH**$_2$^{p}**CH**$_2$**N**

(^{q}**CH**$_2$^{r}**CH**$_2$**CONH**^{s}**CH**$_2$^{t}**CH**$_2$**N(**^{u}**CH**$_2$^{v}**CH**$_2$**CONH**^{w}**CH**$_2$^{x}**CH**$_2$**NH**$_2$**)**$_2$**)**$_2$**)**$_2$**)**$_2$**)**$_2$**]**$_2$**.** The synthesis, reaction conditions, and purification procedure were similar to the procedure described for generation 3.0. Ethylenediamine was present 6400 times in molar excess over the copolymer. ^{1}H NMR (D$_2$O): δ_{PPO}(–OCH$_2$CHC**H**$_3$–) = 1.12 (t); δ_{PPO}(–OCH$_2$C**H**CH$_3$–) = 3.51 (m); δ_{PPO}(–OC**H**$_2$CHCH$_3$–) = 3.66 (m); δ_{PAMAM} = 3.24-3.17 (m, c+g+k+o+s+w); δ_{PAMAM} = 2.78-2.65 (m, a+e+i+m+q+u+x); δ_{PAMAM} = 2.57 (t, d+h+l+p+t); δ_{PAMAM} = 2.36 (t, b+f+j+n+r+v); FTIR peak *ν* cm^{-1}: 1199, 1544 (amide), 1643 (amide), 2840, 2951, 3291.

2.2.3 Characterization of PPO-PAMAM

Each synthesis step was confirmed through FTIR and ^{1}H-NMR. FTIR spectra were recorded on a Nexus 870 FTIR Spectrometer (Thermo Nicolet, Waltham, MA). Samples were solvent cast onto KBr pellets and characterized. ^{1}H-NMR spectra were recorded on a Varian Inova-500 MHz spectrometer. Samples were dissolved in CDCl$_3$ or D$_2$O.

Fluorescence Studies. To determine the CMC of the dendritic block copolymer, pyrene was used as a hydrophobic fluorescent probe.[31, 32] The polymer was suspended in a stock solution containing 10^{-7} M pyrene at concentrations ranging from 10^{-3} M to 10^{-7} M and left overnight in the dark at room temperature to equilibrate. The solutions were analyzed with a FluoroMax-2 Spectrometer (Horiba Jobin Yvon, Longjumeau France) at 25 °C. Emission spectra were recorded over a range of 355 nm to 500 nm with an excitation wavelength of 333 nm, while excitation spectra were recorded from 300 nm to 360 nm with an emission wavelength of 390 nm.

Dynamic Light Scattering. Particle sizes were determined with dynamic light scattering on a Brookhaven Instruments BI-200SM Research Goniometer System. A Coherent Innova 90c (Santa Clara, CA) laser at 514.5 nm was used as the light source. Samples were filtered with a 0.45 μm polytetrafluoroethylene (PTFE) syringe filter (Pall, East Hills, NY) and measured at 25 °C. Measurements were taken at multiple angles from 45 to 135 degrees with 15 degree increments, and autocorrelation functions were recorded at each angle. A fit of the autocorrelation function was made to Equation 2-1 to obtain Γ, the linewidth.[33] Γ was plotted against the square of the scattering vector, q. A linear least-squares fit of the data is used to obtain D_T, the translational diffusion coefficient. Equation 2-3 relates q to the scattering angle, Θ, where n is the refractive index of the solution and λ is the wavelength of the laser. The Stokes-Einstein equation, as shown in Equation 2-4, is used to relate the hydrodynamic diameter, d_h, to D_T for spheres, where k is the Boltzmann constant, T is the temperature, and η is the viscosity of the solution. It was assumed that all solutions were dilute, such that there were no interparticle

interactions and solution properties such as refractive index and viscosity were equivalent to the properties of water at 25 °C.

$$C(\tau) = Ae^{-2\Gamma t} + B \tag{2-1}$$

$$\Gamma = D_T q^2 \tag{2-2}$$

$$q = \frac{4\pi n Sin\left(\frac{\Theta}{2}\right)}{\lambda} \tag{2-3}$$

$$d_h = \frac{kT}{3\pi\eta D_T} \tag{2-4}$$

TEM. To confirm the presence of nanoparticles, polymer samples were visualized with a JEOL 2011 TEM. Carbon coated grids, 400 mesh (Pacific Grid-Tech, Sugar Land, TX), were dipped into dilute aqueous samples of polymer in phosphate buffered water and air-dried overnight.

Drug Loading Studies. An oil/water emulsion technique with a model hydrophobic drug, triclosan, was used for encapsulation with the copolymer. A solution of triclosan in dichloromethane (5 ml, 2 mg/ml) was slowly added to a stirring solution of 1 mg/ml of copolymer in water (10 ml). The solution was vigorously stirred overnight at room temperature. To remove precipitated drug, the solution was centrifuged for 30 minutes at 4500 rpm. The supernatant, which contains the drug solubilized in micelles, was filtered with a 0.45 μm PTFE syringe filter to remove any remaining precipitated drug.

To quantify the amount of drug encapsulated, 1 ml of the supernatant was added to 9 ml of methanol in order to break up the micelles, and the solution was analyzed by

an Agilent 8453 UV-Visible Spectrometer System (Palo Alto, CA). The characteristic absorbance of triclosan at 281 nm was recorded and compared to a calibration curve generated from a 1:9 water:methanol mixture with triclosan concentrations varying from 0-100 μg/ml ($Y = 60.90*X - 1.22$, $r^2 = .9973$). The percent efficiency of encapsulation was calculated with Equation 5 while the weight percent of encapsulated drug was calculated with Equation 6. Due to the 1:1 initial weight ratio of polymer to drug, these two values are equivalent.

$$\%\ \text{drug loading efficiency} = \frac{\text{weight of drug encapsulated}}{\text{total weight of drug introduced}} \times 100 \qquad (2\text{-}5)$$

$$\%\ \text{encapsulation} = \frac{\text{weight of drug encapsulated}}{\text{weight of polymer}} \times 100 \qquad (2\text{-}6)$$

Drug Release Studies. Solutions containing polymer-encapsulated drug were lyophilized and resuspended in either 10 ml of phosphate buffered saline (PBS, pH = 7.4) or acetate buffer (pH = 5.0) and placed into 3500 MWCO dialysis bags (Spectrum Laboratories Inc., Rancho Dominguez, CA). The dialysis bag was placed in 1 liter of buffer at 37 °C, which was changed every two days to maintain sink conditions. Samples were taken out of the dialysis bag at various time intervals and analyzed by UV-vis. The volume of solution in the dialysis bags were measured at each sampling time, so that concentrations measured could be adjusted for volume changes due to osmotic pressure differences and evaporation.

2.3 Results and Discussion

An amphiphilic linear-dendritic triblock copolymer was synthesized and characterized in order to determine its feasibility as a self-assembling drug delivery vehicle with potential targeting applications. The linear-dendritic triblock copolymer is composed of poly(propylene glycol) bis(2-aminopropyl ether) (PPO), which after self-assembly forms the core of the micelle, and hydrophilic poly(amidoamine) (PAMAM), which forms the outer shell of the micelle. The PAMAM presents a dense outer shell of functional groups that can be used for multivalent targeting.

2.3.1 Synthesis of PPO-PAMAM

A series of PPO-PAMAM polymers were synthesized from generation 2.0 (which contains 8 amine ends) through generation 6.0 (containing 128 amine ends). The copolymer was synthesized with a divergent approach starting from PPO with two terminal amines as the core. Sequential steps of Michael addition of the free amine groups with methyl acrylate to create half generations were followed with exhaustive amidation with ethylenediamine to create full generations as shown in Figure 2-1.[14, 15, 34] The amount of excess methyl acrylate and ethylenediamine was increased in proportion to the number of reactive groups available at the ends of the dendrimer. Generally, methyl acrylate and ethylenediamine were used in 50 times excess to the number of reactive sites.

With increasing generations, the bulk morphology of the polymer changed, becoming increasingly solid-like in nature. This is similar to the behavior observed in the synthesis of PEO-PAMAM by Iyer et al.[14] At generation 2, the PPO-PAMAM polymer became tacky. Beginning at generation 3.0 and at every reaction thereafter, the

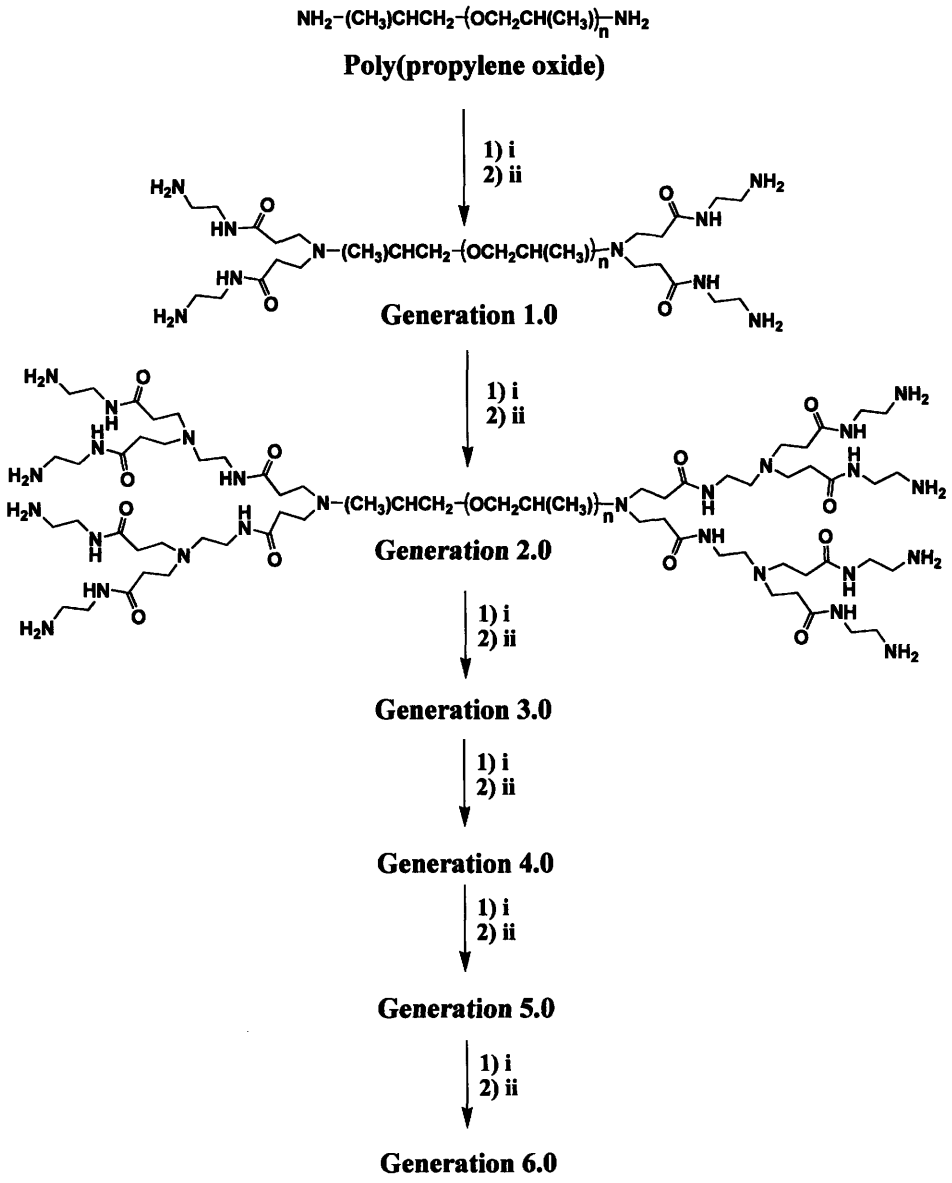

Figure 2-1. Synthesis of PPO-PAMAM by reaction with excess i) methyl acrylate, $CH_2CHCOOCH_3$ and ii) ethylenediamine, $NH_2CH_2CH_2NH_2$.

method used to isolate and purify the product was slightly modified to take advantage of the change in solubility of the copolymer. After the removal of excess reagent and methanol, the polymer was redissolved in methanol and was precipitated in excess ether. The precipitated polymer was vacuum-dried overnight. The synthesis of the triblock copolymers was confirmed through FTIR and ^{1}H-NMR.

2.3.2 Fluorescence Studies

Pyrene was used as a hydrophobic fluorescent probe to determine the critical micelle concentration (CMC) of PPO-PAMAM from generations 2 through 6. Excitation and emission spectra were recorded for each copolymer at varying concentrations. As the concentration of the solution was increased above the CMC, pyrene was found to segregate into the cores of the micelles causing changes in the photophysical properties of pyrene.[31, 32] The vibronic structure of pyrene changes due to its local environment. For example, in the excitation spectrum, a red shift occurs in the system, and the band for pyrene, which is at 335 nm in water, shifts to 340 nm. Ratios of fluorescence intensity from the excitation spectrum at 340 nm to the intensity at 335 nm were plotted against the logarithm of the copolymer as shown in Figure 2-2a. Emission spectra were also obtained, and due to the changes in the local environment of the pyrene above and below the CMC, the magnitude of the peak intensities at 373 nm and 393 nm change. Ratios of fluorescence intensity at 373 nm to 393 nm were taken from emission spectra and plotted as a function of the logarithm of the copolymer concentration in Figure 2-2b. For both plots, lines were fit at low and high concentrations, and the CMC was determined by identifying the point where the two fitted lines intersect. An average of the CMCs obtained from the emission and excitation spectra is reported.

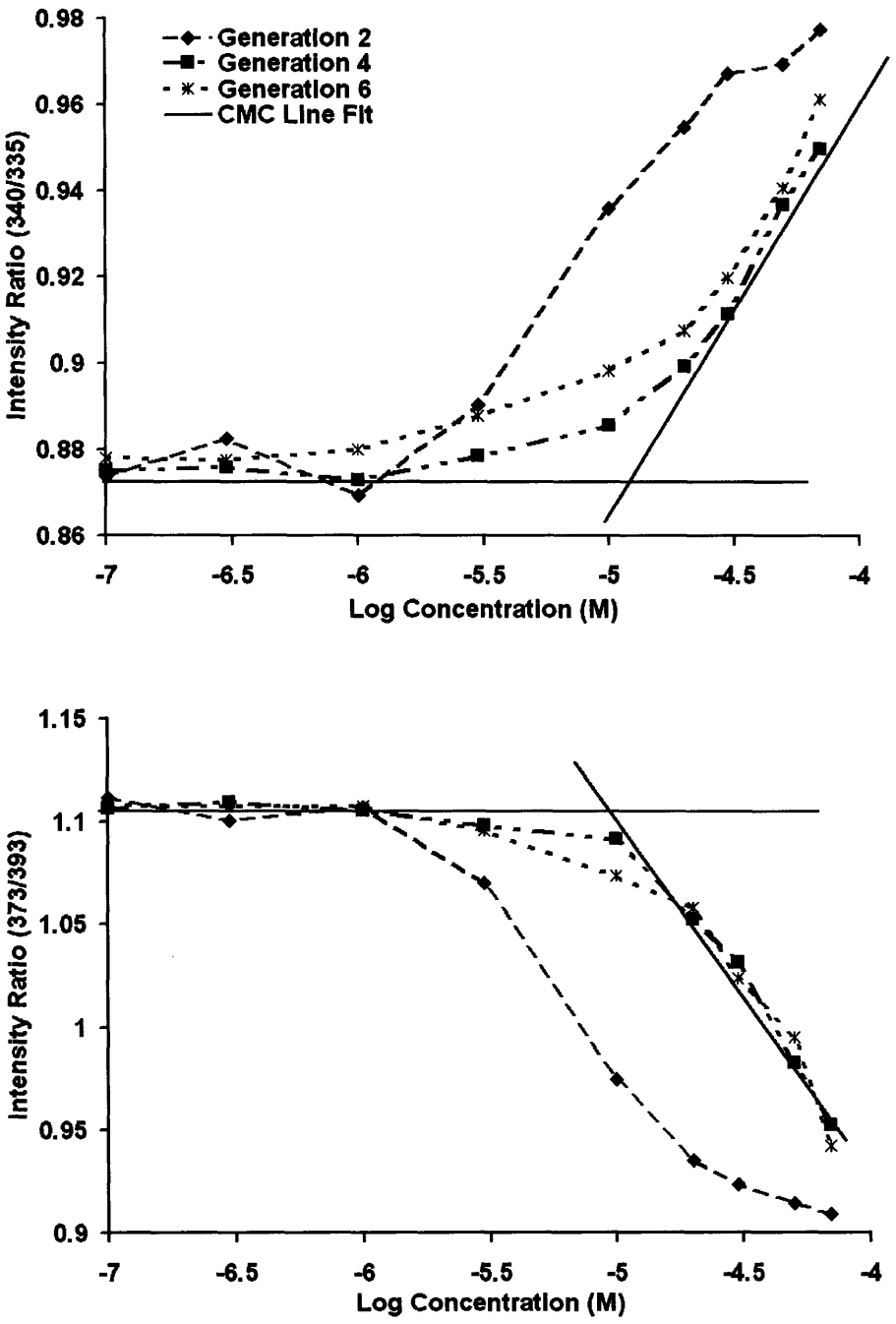

Figure 2-2. a) (top) Ratios of the fluorescence intensity at 340 to 335 nm obtained from the excitation spectra plotted against concentration for PAMAM generations 2, 4, and 6. b) (bottom) Intensity ratios at 273 to 293 nm from emission spectra plotted against concentration. Lines of the intensity ratio versus the concentration are shown to guide the eye. The CMC line fit is shown for generation 4. The point of intersection of the two lines in the CMC fit is given as the CMC value.

The CMC of PPO-PAMAM was measured in deionized water and phosphate buffered saline (PBS) (with an ionic strength of 0.15 M) at approximate pHs of 5.5 and 2.5 to determine the dependence of PAMAM generation, solution pH, and ionic strength on the CMC as shown in Figure 2-3. In one study, PAMAM has been reported to have two pKa values at 3.9 and 6.9 due to the presence of tertiary and primary amines,[35] while another study suggested that the pKa values were approximately 6 and 9.[36] The two different pH values were chosen to determine the effects of protonation of these amines. CMC values of the block copolymer are on the order of 1 μM to 10 μM. This was also confirmed to an order of magnitude through surface tension measurements.

As seen in Figure 2-3, the CMC is a function of PAMAM generation number, ionic strength, and pH. Molecular theory for the formation of micelles can be used to qualitatively describe the trends.[37, 38] Equation 2-7 relates the mole fraction of micelles (X_n) with an aggregation number (n) to the mole fraction of unimers (X_1) in solution and the free energy of micellization (g_{mic}). The mole fraction of micelles in solution is proportional to the CMC.[38]

$$X_n = X_1 \exp(-g_{mic} / kT) \tag{2-7}$$

The term, g_{mic}, is the change in the Gibbs free energy associated with transferring n unimers from the aqueous solution to form a micelle. This free energy can be modeled as the sum of five different free energy terms that take into account all of the free energy changes that occur upon micelle formation. These terms are listed in Equation 2-8.

$$g_{mic} = g_{tr} + g_{int} + g_{pack} + g_{st} + g_{elec} \quad (2\text{-}8)$$

The first three terms, g_{tr}, g_{int}, and g_{pack}, are associated with the hydrophobic block copolymer. The free energy of transfer, g_{tr}, reflects the free energy change associated with transferring the hydrophobic block from the solution to the core of the micelle. The interfacial free energy, g_{int}, takes into account the change in free energy upon formation of the interface between the core and the solution, while g_{pack} involves the free energy change associated with constraining the ends of the linear block (the point of attachment to the hydrophilic block) to lie at the periphery of the core. These three terms could be considered nearly equivalent for the series of block copolymers tested since the PPO hydrophobic linear block is the same size. However, as the PAMAM generation changes in the PPO-PAMAM block copolymers, both g_{st} and g_{elec} are affected. The steric contribution, g_{st}, takes into account the steric interactions between the PAMAM blocks of the unimers. This is a function of the PAMAM block size. The term g_{elec}, the electrostatic free energy, is affected by the degree of charge and location of charge in the PAMAM block.

As the PAMAM generation increases, the CMC was found to generally rise. This can be explained by the growth in the PAMAM block with the increase in generation. As the PAMAM block gets larger, there are higher steric penalties for transferring the large head group into the micelle. Outside of the molecular theory of the formation of micelles, the hydrophilic-lipophilic balance (HLB) also explains the rise in CMC with increasing generation. The weight percent of the hydrophilic portion of the linear-dendritic block copolymer rises with generation (from 23% to 86%), increasing the HLB.

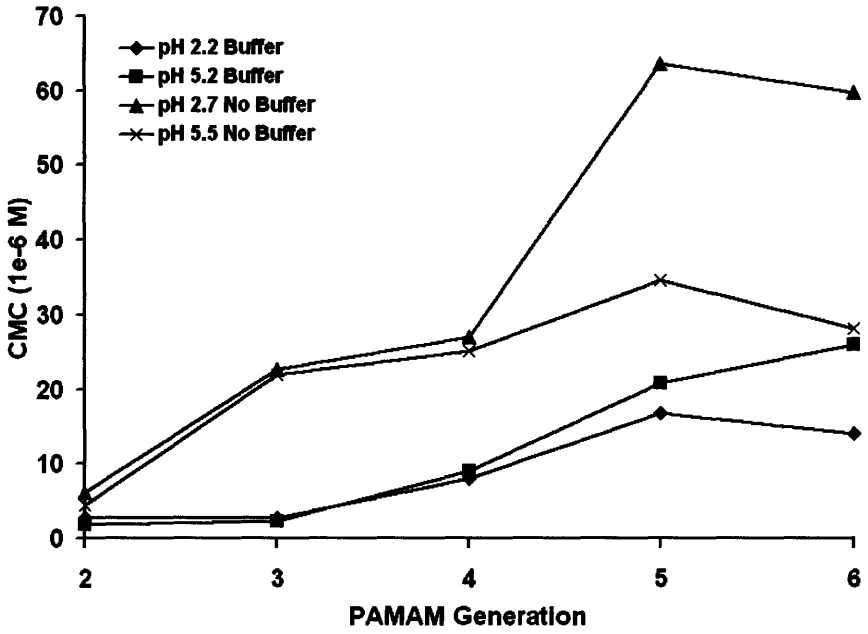

Figure 2-3. CMC of PPO-PAMAM Generations 2 through 6 in low (pH 2.2-2.7) or medium pH (pH 5.2-5.5) with or without buffer. Buffer contains additional NaCl and phosphate salts for a total ionic strength of 0.15 M while unbuffered solutions only have added HCl to reduce the pH to the desired value. Note that the CMC value for the polymer at low ionic strength, pH 5.5 was not significantly different from the CMC in pure deionized water (the deionized water used has a pH of 5.5 due to absorbed carbon dioxide). Lines are shown only as a guide for the eye.

In addition to PAMAM generation dependence, Figure 2-3 indicates that the CMC is dependent on pH at high PAMAM generations and low ionic strengths. From the reported pKa values, it is expected that at pH 2.7, the primary and tertiary amines would be protonated, while at pH 5.5 the primary amines and some tertiary amines would be protonated. For the solutions without buffer, the pH does not affect the CMC from generations 2 through 4. For generations 5 and 6, there is an increase in CMC from pH 5.5 to pH 2.7 that is approximately a 2-fold increase. This result can be explained by the change in the size and increased charge density of the dendrimer head (affecting both g_{st} and g_{elec}). Simulations on the pH effects of dendrimers have shown that the dendrimer radius of gyration (R_g) at low pH, where the tertiary and primary amines are protonated, is larger than the R_g of the dendrimer at neutral or high pH.[39, 40] The protonation of the primary and tertiary amines increase intramolecular repulsion which results in expansion of the PAMAM block. Increased protonation at low pH similarly increases electrostatic repulsion intermolecularly between PAMAM blocks.

The CMC results for the copolymer in buffer were slightly different from copolymer under low ionic strength conditions. For generations 2 through 4, the CMC values are similar in magnitude indicating that pH does not have a significant effect. For CMCs at generations 5 and 6, there are slight differences in CMC with pH. Studies have shown that salt can screen out the effects of low pH,[41] which results in significantly smaller changes in the copolymer CMC as the pH is changed. With ionic shielding, electrostatic repulsion within the PAMAM block is lessened, decreasing the steric effects associated with the expansion of the PAMAM block thus decreasing the headgroup size of the amphiphile. Enhanced water solubility is also anticipated in charged, unshielded

systems. Although there were slight effects of pH at generations 5 and 6 in the buffered solutions, the CMC at higher pH (pH 5.2) was larger than in pH 2.2, which is opposite of what would be expected. These surprising results may be due to specific phosphate and chloride counterion complexation with the PAMAM block affecting its size and shielding more of the electrostatic repulsions. Overall, it was found that pH does not seem to have a large effect on the CMC in buffered salt solutions, but does measurably impact the CMC of the high PAMAM generations at low ionic strength conditions.

In contrast, the effect of ionic strength of CMC is significant over most generations. As anticipated, the CMC is smaller for high ionic strength solutions. Reduction of the CMC is attributed to changes in g_{st} and g_{elec}. Monte Carlo simulations of propyleneimine dendrimers reveal that with increasing ionic strength, the diameter of the dendrimer decreases.[42] With the addition of salt, counterions reduce the electrostatic repulsion within the PAMAM block, resulting in a reduction in PAMAM size. With electrostatic shielding, the electrostatic repulsion of the individual PAMAM blocks with other PAMAM blocks is also reduced, enabling the packing of the dendron-amphiphiles within the micellar aggregates.

2.3.3 Dynamic Light Scattering

PPO-PAMAM generations 2 through 6 suspended in PBS were tested with dynamic light scattering. Similar to the CMC results in buffer, it was found that there was little dependence of the particle diameter on pH due to ionic shielding effects. In contrast, the PAMAM block generation affected the particle diameter as seen in Figure 2-4 with particle sizes ranging from 19 nm down to 9 nm for generation 6.0. As the generation of the PAMAM block increases, the diameter of the particles decreases. With

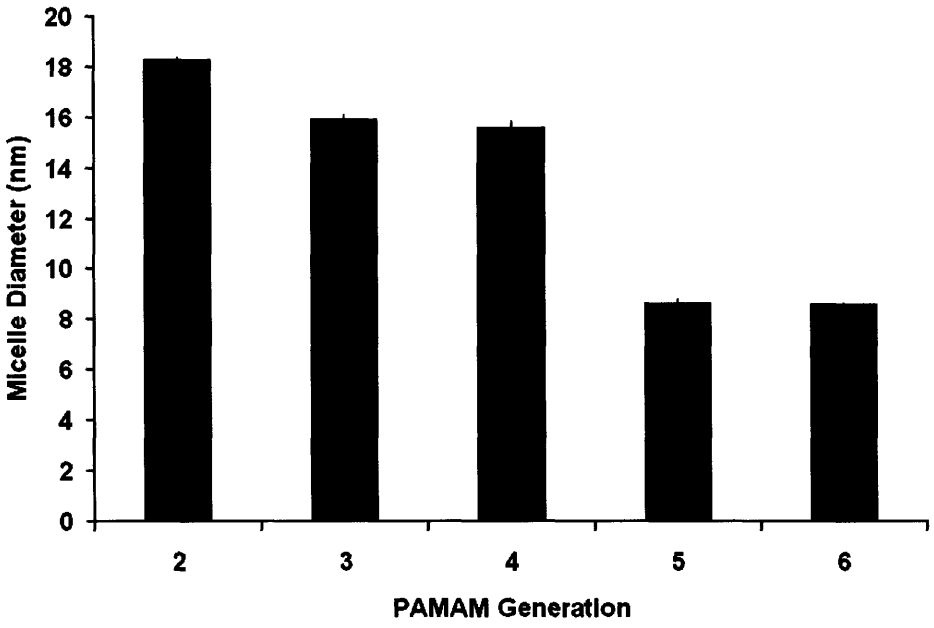

Figure 2-4. Hydrodynamic diameter of PPO-PAMAM micelles as a function of PAMAM generation tested in 0.15 M PBS solution. With increasing generation, the diameter decreases due to the growing PAMAM block which lowers the number of unimers per micelle.

the growth in the head size of the PAMAM block at higher generations, there is increased steric and electrostatic repulsion between the unimers. Therefore, fewer unimers are able to pack into a micelle, and the core is composed of fewer PPO blocks. This results in a reduction of the size of the core and an overall reduction of the micelle size.[43]

2.3.4 TEM

Copolymer samples in PBS visualized with TEM confirm light scattering results. The TEM samples were prepared by dipping the grid into a dilute polymer solution followed by air-drying overnight. Based on TEM observations, the micelles that are formed are relatively monodisperse. TEM results for generation 3.0 are shown in Figure 2-5. Based on TEM, generation 3.0 micelles are approximately 15 nm, similar to the results obtained from dynamic light scattering. TEM results for generations 4.0 through 6.0 were also observed, indicating micelles present in the nanometer range. However, due to the resolution of the TEM and the small size of the micelles, interpretation of the true micelle diameter was difficult to ascertain for all generations. Overall, TEM was able to confirm the formation of micelles for all block copolymer generations.

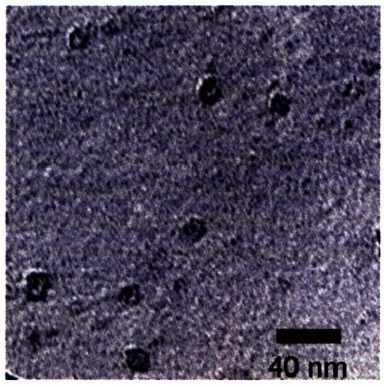

Figure 2-5. TEM micrographs of PPO-PAMAM generation 3.0 micelles air-dried on a 400 mesh carbon grid from phosphate buffered aqueous solutions.

2.3.5 Drug Loading Studies

Triclosan is a bactericide used as a model hydrophobic drug in these studies. It has a log P (octanol-water) of 4.76 and a water solubility of 10^{-2} mg/ml. Triclosan was encapsulated into the PPO-PAMAM micelles from generations 3.0 through 6.0 with the oil/water emulsion technique. The polymers were able to encapsulate from 79% to 86% w/w as shown in Table 2-1. An analysis of variance of the 4 polymer formulations showed no statistically significant difference in the encapsulation efficiency ($n = 3$ for each group, $p = 0.57$). However, the capacity of the micelles grows with increasing generation. Figure 2-6 presents the normalized amount of triclosan encapsulated to the amount of polymer present on a molar basis. There is an increase of this ratio indicating that with the increase in PAMAM generation, each unimer within the micelle can retain more hydrophobic drug.

Dynamic light scattering performed on the drug-loaded samples confirm that at higher generations, more drug is encapsulated in the core. For generation 3.0, the diameter of the particles increased by 5 nm upon drug loading. For generations 4.0 through 6.0, the concentration used for the polymer solutions were very close to the CMC, where there is a mixture of micelles and unimers in solution. The concentration of micelles present in the solution was too low to be detected from dynamic light scattering. Upon the introduction of drug, stable micelles were formed for all generations. For generations 5.0 and 6.0, there was a dramatic increase in the diameter of particles as compared to previous light scattering measurements performed for empty particles (shown in Figure 2-4). The generation 5.0 and 6.0 particles increased from approximately 8 nm to approximately 50 nm. The growth in the diameter can be

Table 2-1. Drug encapsulation characteristics of PPO-PAMAM for generations 3 through 6 and control polymers.

Polymer	% encapsulation (w/w)	Diameter After Drug Loading (nm)
PAMAM-PPO-PAMAM Generation 3.0	80 ± 4	30 ± 1
PAMAM-PPO-PAMAM Generation 4.0	86 ± 11	33 ± 5
PAMAM-PPO-PAMAM Generation 5.0	84 ± 6	57 ± 6
PAMAM-PPO-PAMAM Generation 6.0	79 ± 7	49 ± 3
F127	42 ± 13	--
PAMAM 4.0	5 ± 2	--
PAMAM 6.0	17 ± 6	--

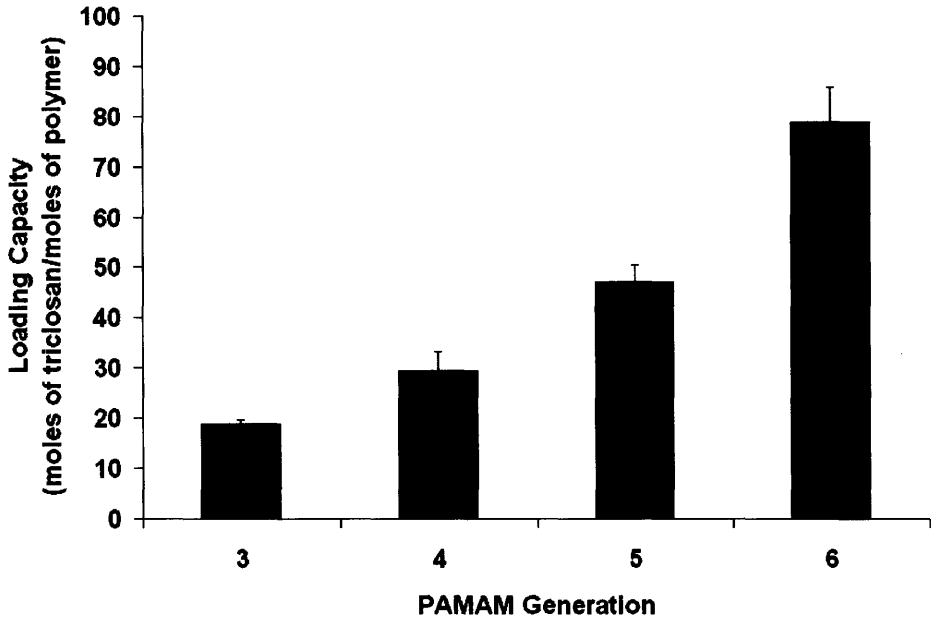

Figure 2-6. Drug encapsulation capacity of PPO-PAMAM generations 3.0 through 6.0. As the generation increases, the amount of triclosan encapsulated to the amount of polymer present increases.

attributed to the expansion of the hydrophobic core as more drug is encapsulated. For generations 5.0 and 6.0, it is possible that the core is composed of solid drug with the PPO core surrounding and stabilizing the solid drug center. If the unimers of the generation 5.0 and 6.0 micelles were to be stretched out, the maximum diameter of the micelle would be approximately 30 nm. The light scattering results indicate particles that are larger than the maximum diameter. Therefore, the presence of a solid drug core would allow the micelle to obtain sizes larger than its theoretical limit. The increased PAMAM head size, arc length, and stiffness of the dendrimer block for generations 5.0 and 6.0 could also contribute to stabilizing this type of structure. With generations 3.0 and 4.0, there is only a slight increase in the core diameter. Either the encapsulated drug is interspersed in the PPO core, or there is a small drug core in the middle of the micelle. It is possible that the formation of a solid drug core could occur if a higher concentration of drug was used during the encapsulation.

As a control, a Pluronic®, F127, and PAMAM dendrimers were processed with the same encapsulation procedure. F127 was chosen as a control because it has been used successfully for drug delivery by other groups.[44, 45] F127 is structurally similar to PPO-PAMAM, as a triblock copolymer with PEO hydrophilic outer blocks and a PPO hydrophobic inner block. The PEO block length is roughly 100, while the PPO block length is approximately 60. Compared to our block copolymer, the PPO block length is similar, and the reported CMC of F127 is also in the micromolar range.[46] Encapsulation of triclosan with F127 was 42% efficient – half the efficiency of the PPO-PAMAM block copolymer at generations 5.0 and 6.0.

Spherical PAMAM dendrimers generation 4.0 and 6.0 (Sigma-Aldrich) were also used as controls. Drug loading with generation 4.0 PAMAM dendrimers showed very little encapsulation, whereas with generation 6.0 PAMAM dendrimers, drug loading efficiency was approximately 17 %w/w. Compared to PAMAM dendrimers, our block copolymer is more efficient at encapsulating hydrophobic drug because the micelles formed from the block copolymer are larger in size and have greater capacity. Additionally, with the incorporation of the PPO hydrophobic block into the linear-dendritic block copolymer, interactions with hydrophobic drugs are more favorable compared to spherical PAMAM dendrimers. Although the encapsulation efficiency of spherical PAMAM generation 6.0 was low, it was not negligible. It is possible that for triblock copolymer generations 5.0 and 6.0 the PAMAM block also contributed to some of the drug loading capacity. It is unknown how compact the PAMAM head group is in the micelle and how well it can retain hydrophobic drug; thus, its independent contribution cannot be determined. It is likely that encapsulation entails sequestration of drug in the PPO core and the interior regions of the PAMAM block, leading to a synergistic effect.

2.3.6 Drug Release Studies

Preliminary drug release studies were performed on PPO-PAMAM generation 3 micelles, since those micelles were the most stable as indicated by the CMC. Drug release was performed in pH 7.4 PBS and pH 5.0 acetate buffer solution to simulate physiological and endosomal conditions in the body, respectively. Figure 2-7 shows an initial burst release over approximately the first day and then slow release afterwards. The logarithmic release profile is indicative of drug diffusing out of the micelles.

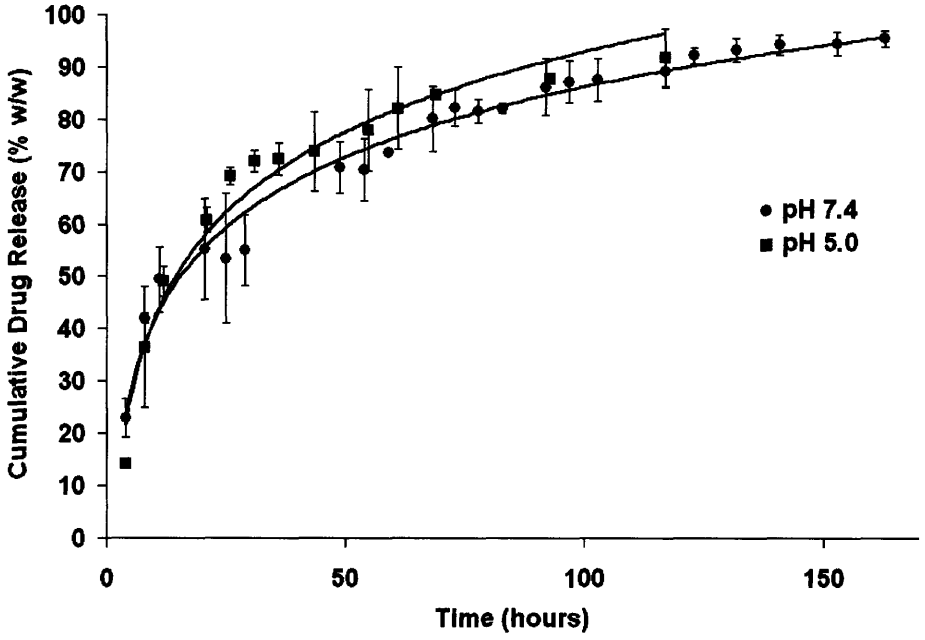

Figure 2-7. Release profile of triclosan from PPO-PAMAM generation 3.0 micelles at pH 7.4 and pH 5.0.

Furthermore, there was no pH dependence on the rate of drug release. This result was expected since for generation 3 the CMC is not pH dependent.

2.4 Conclusions

A novel amphiphilic linear-dendritic block copolymer composed of PAMAM and linear PPO blocks was synthesized up to generation 6.0. The block copolymers form stable micelles in aqueous media with low CMC values, which can be controlled by PAMAM generation, pH, or ionic strength. The ability to control the architecture and properties of the PPO-PAMAM block copolymer makes it possible to create a system that possesses the properties that are desirable for a drug delivery vehicle. The core is biocompatible and has been used in Pluronics® as drug delivery vehicles,[44, 45] and PAMAM is currently being studied as a drug delivery vehicle which can be made biocompatible with simple modifications.[47-49] Because of its unique architecture, the linear-dendritic block copolymer may be useful in targeted drug delivery, due to the dense functionality of the dendrimer block. Targeting ligand can be attached to the periphery of the dendrimer at high density and improve targeting efficiency through increased affinity of multivalent interactions with receptors on the cell surface. In the future, our group plans to study targeted drug delivery through multivalent ligand/receptor interactions. It has been shown that micelles that are formed with and without encapsulated drug are within the size limits that are desired for drug delivery through endocytosis.[50] The PPO-PAMAM block copolymer encapsulates hydrophobic drug at high efficiency and has sustained release of the drug. Although it was shown that at generation 3.0 there was no pH dependence for drug release, it is possible that for triblock copolymers at higher generations such as generation 5.0 or 6.0, there could be

pH dependence. Based on the studies performed, these block copolymers can be a viable new type of drug delivery micelle.

2.5 References

1. Gitsov, I., "Linear-dendritic block copolymers. Synthesis and characterization." In *Advances in dendritic macromolecules*, Newkome, G. R., Ed. Elsevier Science: Amsterdam, 2002; Vol. 5, pp 45-87.

2. Grinstaff, M. W., "Biodendrimers: New polymeric biomaterials for tissue engineering," *Chemistry - A European Journal*, **2002,** 8, (13), 2838-2846.

3. Fréchet, J. M. J., "Dendrimers and other dendritic macromolecules: From building blocks to functional assemblies in nanoscience and nanotechnology," *Journal of Polymer Science Part A: Polymer Chemistry*, **2003,** 41, (23), 3713-3725.

4. Chapman, T.; Hillyer, G.; Mahan, E.; Shaffer, K., "Hydraamphiphiles: Novel linear dendritic block copolymer surfactants," *J. Am. Chem. Soc.*, **1994,** 116, 11195.

5. Gitsov, I.; Ivanova, P. T.; Frechet, J. M. J., "Dendrimers as macroinitiators for anionic ring-opening polymerization. Polymerization of ϵ-caprolactone," *Macromolecular Rapid Communications*, **1994,** 15, (5), 387-93.

6. Leduc, M. R.; Hawker, C. J.; Dao, J.; Frechet, J. M. J., "Dendritic initiators for "living" radical polymerizations: A versatile approach to the synthesis of dendritic-linear block copolymers," *J. Am. Chem. Soc.*, **1996,** 118, (45), 11111-11118.

7. Kim, T.; Jang, H.; Joo, D. K.; Choi, J. S.; Park, J. S., "Synthesis of diblock copolymer, methoxypoly(ethylene glycol)-block-polyamidoamine dendrimer and its generation-dependent self-assembly with plasmid DNA," *Bull. Korean Chem. Soc.*, **2003,** 24, 123-125.

8. Ge, Z.; Luo, S.; Liu, S., "Syntheses and self-assembly of poly(benzyl ether)-*b*-poly(*n*-isopropylacrylamide) dendritic-linear diblock copolymers," *Journal of Polymer Science Part A: Polymer Chemistry*, **2006,** 44, (4), 1357-1371.

9. Gitsov, I.; Wooley, K. L.; Frechet, J. M. J., "Novel polyether copolymers with a linear central unit and dendritic end groups," *Angewandte Chemie*, **1992,** 104, (9), 1282-5 (See also Angew Chem, Int Ed Engl, 1992, 31(9), 1200-2).

10. Gitsov, I.; Frechet, J. M. J., "Novel nanoscopic architectures. Linear-globular aba copolymers with polyether dendrimers as a blocks and polystyrene as b block," *Macromolecules*, **1994,** 27, (25), 7309-15.

11. Choi, J.; Joo, D.; Kim, C.; Kim, K.; Park, J., "Synthesis of barbell-like triblock copolymer, poly(l-lysine) dendrimer-block-poly(ethylene glycol)-block-poly(l-lysine) dendrimer, and its self-assembly with plasmid DNA," *Journal of the American Chemical Society*, **2000,** 122, 474-480.

12. Lambrych, K. R.; Gitsov, I., "Linear-dendritic poly(ester)-*block*-poly(ether)-*block*-poly(ester) aba copolymers constructed by a divergent growth method," *Macromolecules*, **2003,** 36, (4), 1068-1074.

13. Namazi, H.; Adeli, M., "Solution proprieties of dendritic triazine/poly(ethylene glycol)/dendritic triazine block copolymers," *Journal of Polymer Science Part A: Polymer Chemistry*, **2005,** 43, (1), 28-41.

14. Iyer, J.; Fleming, K.; Hammond, P. T., "Synthesis and solution properties of new linear-dendritic diblock copolymers," *Macromolecules*, **1998,** 31, 8757.

15. Iyer, J.; Hammond, P. T., "Langmuir behavior and ultrathin films of new linear-dendritic diblock copolymers," *Langmuir*, **1999,** 15, 1299.

16. Gitsov, I.; Wooley, K.; Hawker, C.; Ivanova, P.; Fréchet, J., "Synthesis and properties of novel linear-dendritic block copolymers. Reactivity of dendritic macromolecules toward linear polymers," *Macromolecules*, **1993,** 26, 5621.

17. Gitsov, I.; Fréchet, J., "Solution and solid-state properties of hybrid linear-dendritic block copolymers," *Macromolecules*, **1993,** 26, 6536.

18. Yu, D.; Vladimirov, N.; Fréchet, J., "Maldi-tof in the characterizations of dendritic-linear block copolymers and stars," *Macromolecules*, **1999,** 32, 5186.

19. Gitsov, I.; Lambrych, K.; Remnant, V.; Pracitto, R., "Micelles with highly branched nanoporous interior: Solution properties and binding capabilities of amphiphilic copolymers with linear dendritic architecture," *J. Polym. Sci.: Part A: Polym Chem.*, **2000,** 38, 2711.

20. Gillies, E.; Jonsson, T.; Fréchet, J., "Stimuli-responsive supramolecular assemblies of linear-dendritic copolymers," *J. Am. Chem. Soc.*, **2004,** 126, 11936.

21. Kim, T.; Seo, H.; Choi, J.; Jang, H.; Baek, J.; Kim, K.; Park, J., "Pamam-peg-pamam: Novel triblock copolymer as a biocompatible and efficient gene delivery carrier," *Biomacromolecules*, **2004,** 5, 2487.

22. Choi, J. S.; Lee, E. J.; Choi, Y. H.; Jeong, Y. J.; Park, J. S., "Poly(ethylene glycol)-block-poly(l-lysine) dendrimer: Novel linear polymer/dendrimer block copolymer forming a spherical water-soluble polyionic complex with DNA," *Bioconjugate Chem.*, **1999,** 10, 62-65.

23. Wood, K.; Little, S.; Langer, R.; Hammond, P., "A family of hierarchically self-assembling linear-dendritic hybrid polymers for highly efficient targeted gene delivery," *Angew. Chem., Int. Ed.*, **2005,** 44, 6704-6708.

24. van Hest, J. C. M.; Delnoye, D. A. P.; Baars, M. W. P. L.; van Genderen, M. H. P.; Meijer, E. W., "Polystyrene-dendrimer amphiphilic block copolymers with a generation-dependent aggregation," *Science*, **1995,** 268, 1592-1595.

25. van Hest, J.; Baars, W.; Elissen-Román, C.; van Genderen, M.; Meijer, W., "Acid-functionalized amphiphiles derived from polystyrene-poly(propylene imine) dendrimers, with a ph-dependent aggregation," *Macromolecules*, **1995,** 28, 6689.

26. van hest, J. C. M.; Delnoye, D. A. P.; Baars, M. W. P. L.; Elissen-Roman, C.; van Genderen, M. H. P.; Meijer, E. W., "Polystyrene-poly(propylene imine) dendrimers: Synthesis, characterization, and association behavior of a new class of amphiphiles," *Chemistry--A European Journal*, **1996,** 2, (12), 1616-1626.

27. Roman, C.; Fischer, H. R.; Meijer, E. W., "Microphase separation of diblock copolymers consisting of polystyrene and acid-functionalized poly(propylene imine) dendrimers," *Macromolecules*, **1999,** 32, (17), 5525-5531.

28. Zhu, L.; Zhu, G.; Li, M.; Wang, E.; Zhu, R.; Qi, X., "Thermosensitive aggregates self-assembled by an asymmetric block copolymer of dendritic polyether and poly(n-isopropylacrylamide)," *Euro. Poly. J.*, **2002,** 38, 2503-2506.

29. Klok, H.-A.; Hwang, J. J.; Hartgerink, J. D.; Stupp, S. I., "Self-assembling biomaterials: L-lysine-dendron-substituted cholesteryl-(l-lactic acid).Hivin.N," *Macromolecules*, **2002,** 35, (16), 6101-6111.

30. Istratov, V.; Kautz, H.; Kim, Y.; Schubert, R.; Frey, H., "Linear-dendritic nonionic poly(propylene oxide)-polyglycerol surfactants," *Tetrahedron*, **2003,** 59, 4017.

31. Kalyanasundaram, K.; Thomas, J., "Environmental effects on vibronic band intensities in pyrene monomer fluorescence and their application in studies of micellar systems," *J. Am. Chem. Soc.*, **1977,** 99, 2039.

32. Kwon, G.; Naito, M.; Yokoyama, M.; Okano, T.; Sakurai, Y.; Kataoka, K., "Micelles based on ab block copolymers of poly(ethylene oxide) and poly(β-benzyl l-aspartate)," *Langmuir*, **1993,** 9, 945.

33. Tscharnuter, W., *Photon correlation spectroscopy in particle sizing*. John Wiley & Sons Ltd: Chichester, 2000; p 5469-5485.

34. Tomalia, D.; Baker, H.; Dewald, J.; Hall, M.; Kallos, G.; Martin, S.; Roeck, J.; Ryder, J.; Smith, P., "Dendritic macromolecules: Synthesis of starburst dendrimers," *Macromolecules*, **1986,** 19, 2466-2468.

35. Tomalia, D.; Naylor, A.; Goddard, W., "Starburst cascade polymers: Molecular-level control of size, shape, surface chemistry, topology, and flexibility from atoms to macroscopic matter," *Angew. Chem. Int. Ed. Engl.*, **1990,** 29, 138-175.

36. Cakara, D.; Kleimann, J.; Borkovec, M., "Microscopic protonation equilibria of poly(amidoamine) dendrimers from macroscopic titrations," *Macromolecules*, **2003,** 36, (4201-4207).

37. Nagarajan, R., "Molecular theory for mixed micelles," *Langmuir*, **1985,** 1, 331.

38. Shiloach, A.; Blankschtein, D., "Measurement and prediction of ionic/nonionic mixed micelle formation and growth," *Langmuir*, **1998,** 14, 7166.

39. Lee, I.; Athey, B.; Wetzel, A.; Meixner, W.; Baker, J., Jr., "Structural molecular dynamics studies on polyamidoamine dendrimers for a therapeutic application: Effects of ph and generation," *Macromolecules*, **2002,** 35, 4510.

40. Maiti, P.; Çağin, T.; Lin, S.; Goddard, W., III, "Effect of solvent and ph on the structure of pamam dendrimers," *Macromolecules*, **2005,** 38, 979.

41. Ramzi, A.; Scherrenberg, R.; Joosten, J.; Lemstra, P.; Mortensen, K., "Structure-property relations in dendritic polyelectrolyte solutions at different ionic strength," *Macromolecules*, **2002,** 35, 827.

42. Welch, P.; Muthukumar, M., "Tuning the density profile of dendritic polyelectrolytes," *Macromolecules*, **1998,** 31, 5892.

43. Israelachvili, J. N., *Intermolecular and surface forces*. 2nd ed.; Academic Press: New York, 1991.

44. Kabanov, A.; Batrakova, E.; Alakhov, V., "Pluronic® block copolymers for overcoming drug resistance in cancer," *Advanced Drug Delivery Reviews*, **2002,** 54, 759-779.

45. Kabanov, A.; Batrakova, E.; Alakhov, V., "Pluronic® block copolymers as novel polymer therapeutics for drug and gene delivery," *Journal of Controlled Release*, **2002,** 82, 189-212.

46. Kozlov, M. Y.; Melik-Nubarov, N. S.; Batrakova, E. V.; Kabanov, A. V., "Relationship between pluronic block copolymer structure, critical micellization concentration and partitioning coefficients of low molecular mass solutes," *Macromolecules*, **2000,** 33, 3305–3313.

47. Malik, N.; Wiwattanapatapee, R.; Klopsch, R.; Lorenz, K.; Frey, H.; W., W. J.; Meijer, E. W.; Paulus, W.; Duncan, R., "Dendrimers: Relationship between structure and biocompatibility in vitro, and preliminary studies on the biodistribution of 125i-labelled polyamidoamine dendrimers in vivo," *Journal of controlled release*, **2000,** 65, 133-148.

48. Jevprasesphant, R.; Penny, J.; Attwood, D.; McKeown, N.; D'Emanuele, A., "Engineering of dendrimer surfaces to enhance transepithelial transport and reduce cytotoxicity," *Pharmaceutical Research*, **2003,** 20, 1543-1550.

49. Roberts, J. C.; Bhalgat, M. K.; Zera, R. T., "Preliminary biological evaluation of polyamidoamine (pamam) starburst dendrimers," *J. Biomed. Mater. Res.*, **1996,** 30, 53-65.

50. Rejman, J.; Oberle, V.; Zuhorn, I.; Hoekstra, D., "Size-dependent internalization of particles via the pathways of clathrin- and caveolae-mediated endocytosis," *Biochem. J.*, **2004,** 377, 159.

CHAPTER 3: Experiments and Molecular Dynamics Simulations of PPO-PAMAM Linear-Dendritic Block Copolymer Unimers and Micelles

3.1 Introduction

Linear-dendritic block copolymers are a new class of block copolymers that have recently shown to have potential as biomaterials for tissue engineering,[1] gene therapy delivery vehicles,[2] and drug delivery vehicles.[3, 4] When used for drug delivery, linear-dendritic block copolymers are designed to be amphiphilic so that self-assembly into colloidal particles (often times micelles) occurs, creating a hydrophobic compartment in the micellar interior for drug encapsulation. Several groups have synthesized linear-dendritic block copolymers with a hydrophilic linear block and a hydrophobic dendritic block.[3, 4] These block copolymers self-assemble with the dendritic block forming the core. It is hypothesized that with the dendrimer forming the core, more hydrophobic drug could be encapsulated due to the free volume created by the aggregated dendrimer blocks. Recently, we reported the synthesis of a linear-dendritic block copolymer with a hydrophilic dendritic block and hydrophobic linear block, so that in aqueous solution the linear block forms the core while the dendrimer block forms the corona of the micelle.[5] A potential advantage of our approach is that with the dendritic block located in the corona region of the micelles, targeting ligand that can bind to receptors multivalently can be presented for targeted drug delivery. In a previous study, we also found that the dendritic block of the self-assembled micelles resulted in increased encapsulation of a model hydrophobic drug, triclosan. The encapsulation efficiency for linear-dendritic block copolymers composed of poly(amidoamine) (PAMAM) and poly(propyleneoxide)

(PPO) was approximately 82%. In comparison, the encapsulation efficiency for a pluronic, F127, which has a similar PPO block length and similar CMC characteristics to PPO-PAMAM had an encapsulation efficiency of 42%.

While our experimental results indicate that PPO-PAMAM linear-dendritic block copolymer micelles have interesting and unexpected drug encapsulation properties and show promise as drug-delivery vehicles, little is understood about the structure and dynamics of these micelles (or even, more generally, for any linear-dendritic block copolymer micelle) and the relationship between these characteristics and the micelles' ability to deliver drug.

In order to understand structural characteristics of self-assembled dendritic micelles, we have performed experiments to determine the aggregation number of these micelles in aqueous solution, and performed atomistic molecular dynamics simulations to determine the equilibrated structures of PPO-PAMAM block copolymer micelles with the experimentally measured aggregation numbers. With these simulations, we are able to better understand the structure and solubilization behavior of these drug delivery vehicles, which may enable us to better design these block copolymers for drug delivery. There have been numerous molecular dynamics studies on PAMAM dendrimers examining PAMAM structure at various generations,[6-8] different solvation states,[9-11] and several ionically charged states.[7, 10, 12, 13] There have also been a few coarse-grain molecular dynamics studies on the formation of linear block copolymer micelles.[14-16] However, there is only one cited instance of molecular dynamics simulations of a Fréchet-type linear-dendritic block copolymer unimer in various solvents.[6] The block copolymer was composed of linear poly(ethylene glycol) (PEG) and poly(benzyl ether)

dendron. Therefore, although prior simulations have provided further insight into the behavior of linear-dendritic block copolymer unimers, molecular dynamics simulations of linear-dendritic block copolymer micelles have never been reported. In this work in collaboration with Brian Stephenson of the Blankschtein group, these simulations are conducted for the first time.

3.2 Experimental Section

3.2.1 Materials

Poly(propylene glycol) bis(2-aminopropyl ether) (MW ~4000, Mw/Mn = 1.04), methanol, diethyl ether, and pyrene (sublimed, 99%), were purchased from Sigma-Aldrich and used as received. Methyl acrylate and ethylenediamine were obtained from Sigma-Aldrich and distilled over calcium hydride before use. MilliQ (18.2 MΩ) water was used in all experiments requiring water.

3.2.2 Synthesis of PPO-PAMAM

The amphiphilic ABA linear-dendritic block copolymer was previously synthesized.[5] Briefly, the synthesis begins with poly(propylene glycol) bis(2-aminopropyl ether) (PPO). The poly(amidoamine) (PAMAM) blocks are synthesized from the amine ends of the PPO with alternating reaction steps of the first reaction, Michael addition with methyl acrylate, and the second reaction, exhaustive amidation with ethylenediamine. Generations 4.0 through 6.0 PPO-PAMAM were synthesized. The synthesis of the block copolymer was confirmed through ^{1}H-NMR and FTIR.

3.2.3 Aggregation Number Determination

For aqueous solutions of PPO-PAMAM generations 4.0 through 6.0, a BI-DNDC differential refractometer (Brookhaven Instruments) was used to determine the specific refractive index, *dn/dc*, where *n* is the solvent refractive index and *c* is the concentration of the polymer in solution. Polymer solutions ranging from 1 mg/ml to 10 mg/ml were measured at 25 °C and 535 nm. Static light scattering was performed on a Brookhaven Instruments BI-200SM Research Goniometer System. A Coherent Innova 90c (Santa Clara, CA) laser at 514.5 nm was used as the light source. Static light scattering is used to measure the angular dependence of the excess time-averaged scattered intensity known as the excess Rayleigh ratio, $R_{vv}(q)$. The Rayleigh ratio at dilute solution can be related to the weight-average molecular weight, M_w, radius of gyration, R_g, and the second virial coefficient, A_2, in the following equation:

$$\frac{Hc}{R_{vv}(q)} \approx \frac{1}{M_w}\left(1+\frac{\langle R_g^2\rangle}{3}q^2\right)+2A_2c \qquad (3\text{-}1)$$

where $H = 4\pi^2 n_{st}^2 (dn/dc)^2 / N_A\lambda^4$, $q = 4\pi n\lambda^4 \sin(\theta/2)$, n_{st} is the refractive index of toluene, N_A is Avogadro's number, λ is the wavelength of the laser, and θ is the scattering angle.[17] Samples ranging from 1 to 10 mg/ml were measured at 10 degree increments from 40 to 140 degrees at 25 °C. Zimm plots were generated. To determine the M_w of the aggregates, $R_{vv}(q)$, was extrapolated to zero scattering angle and zero polymer concentration. The y-axis intercept was used to calculate the M_w. A_2 and R_g are also determined from the Zimm plot. As the scattering angle approaches zero, the slope is equal to $2A_2c$, while at zero polymer concentration, the slope equals $16\pi^2 n^2 R_g^2/(3M_w)$.[17]

3.2.4 Simulation Methodology and Parameters

All simulations were conducted using a 2006 developers' version of the GROMACS software package.[18, 19] Each dendrimer and the hydrophobic solute triclosan were simulated using the GROMACS forcefield, in which all atoms are simulated at an atomistic level except hydrogens bound to carbon atoms.[20] The GROMACS force field is expected to be well-parameterized for the chemical structures present in each dendrimer and triclosan, and has been applied by other researchers in simulating PAMAM dendrimers with an ethylenediamine core and amine terminal ends.[9] Water was simulated explicitly using the simple extended point-charge model (SPC/E).[21] The amines in each dendrimer were simulated as being unprotonated, a charge state corresponding to an alkali solution (pH > 10). Using Gaussian '98, atomic charges were assigned to each dendrimer molecule and triclosan using values predicted with the Hartree-Fock method and the 6-31G(d) basis set.[22]

van der Waals interactions were modeled using a cutoff distance of 9 Å, and Coulombic interactions were evaluated using a cutoff distance of 14 Å. A long-range dispersion correction was applied to more accurately estimate the energy and pressure of the system. In modeling short-ranged nonbonded interactions, a neighbor list of 9.0 Å was maintained and updated every 10 simulation timesteps. Each simulation was carried out using fixed bond lengths, which allowed the simulation timestep to be increased to 3 fs. Bond lengths were constrained using the SHAKE algorithm.[23]

Simulations were conducted in the NPT (constant number of particles, constant pressure, and constant temperature) ensemble. In each simulation, the cell temperature was maintained at 298.15 K using a Berendsen temperature coupling algorithm, which

mimics weak coupling to an external heat bath with first-order kinetics.[19] A Berendsen pressure coupling algorithm was applied to maintain each simulation cell at the specified pressure of 1.0 bar.[19]

To minimize the number of solvent molecules that must be included in each simulation cell, each simulation was conducted in a rhombic dodecahedron simulation cell. The volume of this geometry is 0.71 times that of a cubic simulation cell providing the same separation distance between a solute and its periodic image. Details for each simulation are given in Table 3-1.

3.2.5 System Preparation and Equilibration

Generations 4, 5, and 6 linear-dendritic block copolymers were simulated in both unimeric and micellar states. In a separate simulation, ten molecules of the solute triclosan were added to a generation 4 micelle to investigate the locus of its solubilization. Initial energy minimization and simulation of both block copolymer unimers and micelles were conducted in vacuum, but with the application of a dielectic constant of 4.0 in order to roughly approximate the electrostatic shielding effects of water.[24] Each unimer or micelle was annealed at very high temperature and gradually cooled to room temperature. Each system was then simulated at room temperature (298.15 K) for the vacuo simulation time listed in Table 3-1. Initial simulation in vacuum was conducted to permit rough equilibration of unimer/micelle structure with a minimum of computational expense and was useful in this study because of the large size of each linear-dendritic block copolymer system.

Next, explicit water molecules were added to each simulation cell. The number of water molecules added is listed in Table 3-1. The number of added water molecules

was sufficient that the distance between the wall of each simulation cell and the closest dendrimer atom was 1 nm in each direction. After placing each unimer or micelle in the solvent box, an energy minimization was performed to remove close contacts. Next, simulation in water was performed at 298.15 K for the water simulation time listed in Table 3-1.

The equilibration of each system was monitored by evaluating the system potential energy and the unimer or micelle radius of gyration. The potential energy of each system appeared to stabilize within the first nanosecond of simulation in water. However, changes in the radius of gyration occurred over much longer timescales. The extent to which each system had equilibrated was quantified using the autocorrelation function of the radius of gyration, $C_{Rg}(t)$, which is evaluated using the following equation:

$$C_{R_g}(t) = \frac{\left\langle \left(R_g(t) - \langle R_g \rangle\right)\left(R_g(0) - \langle R_g \rangle\right)\right\rangle}{\left\langle R_g^{\,2}\right\rangle - \langle R_g \rangle^2} \tag{3-2}$$

Figure 3-1 shows the autocorrelation profiles for PPO-PAMAM generations 4, 5, and 6 block copolymer unimers (Figures A, B, and C, respectively) and micelles (Figures A', B', and C', respectively). Each autocorrelation profile drops to zero in less than the total simulation time. We have used each autocorrelation profile for R_g to compute a relaxation time, defined as the time at which $C_{Rg}(t) = 1/e$. Each relaxation time is listed in Table 3-1, and it ranges in time from 0.68 ns (generation 5 micelle) to 7.6 ns (generation 4 micelle). We note that each relaxation time is significantly shorter than the total simulation time, ranging from 4% of the total simulation time for the generation 5

Table 3-1. Simulation condition parameters for unimers and micelles of PPO-PAMAM generations 4 through 6.

Simulation Name	Unimer PAMAM Generation	Surface Group No.	No. Dendrimer Atoms	No. Water Molecules	Total No. Atoms Simulated	Simulation Time in Vacuo/Water (ns)	Relaxation Times τ_{Rg} (ns)
ppog4uni	4	32	865	4,836	15,373	5.0/20.0	2.40
ppog5uni	5	64	1,505	18,353	56,564	5.0/8.8	1.28
ppog6uni	6	128	2,785	28,959	89,662	5.0/10.0	0.44
Simulation Name	**Micelle PAMAM Generation**	**Surface Group No.**	**No. Dendrimer Atoms**	**No. Water Molecules**	**Total No. Atoms**	**Simulation Time in Vacuo/Water (ns)**	**Relaxation Times τ_{Rg} (ns)**
ppog4mic	4	32	865*8 = 6,920	32,438	104,234	20.0/53.2	7.6
ppog4drug	4	32	865*8 = 6,920	29,107	94,421	20.0/49.5	--
ppog5mic	5	64	1,505*6 = 9,030	37,781	122,373	20.0/17.1	0.68
ppog6mic	6	128	2,785*6 = 16,710	53,322	176,676	40.0/14.5	1.92

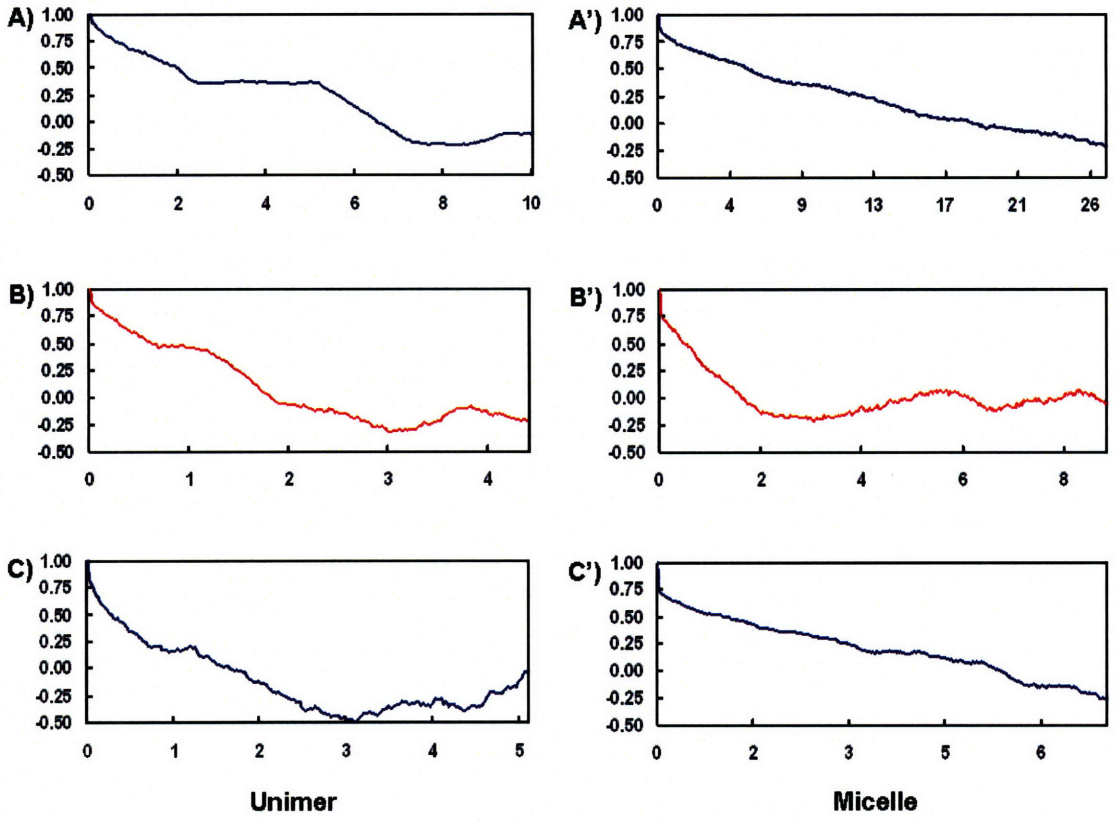

Figure 3-1. Autocorrelation profiles for unimers of PPO-PAMAM generations 4, 5, and 6 (A, B, C, respectively) and for micelles of PPO-PAMAM generations 4, 5, and 6 (A, B, C, respectively). The y-axis is a dimensionless number while the x-axis is time (ns). The relaxation time, τ_{Rg}, is determined from these autocorrelation profiles.

micelle to 15% of the total simulation time for the generation 4 micelle.

3.3 Results and Discussion

A linear-dendritic block copolymer composed of a linear hydrophobic PPO block and two outer PAMAM dendritic blocks was previously synthesized and characterized to determine its viability as a drug delivery vehicle (shown in Figure 3-2). Interesting properties were displayed in these studies including decreasing R_h with an increase in the PAMAM generation and high drug loading capacity of triclosan due to the addition of the PAMAM dendritic block. Further studies were needed to elucidate what was observed. Additional experiments were conducted to determine the micelle aggregation number, which would help to explain the micelle size trend. Furthermore, the results of these experiments were the basis for subsequent molecular dynamics simulations of micelles in order to determine micelle structure and the location of drug solubilization within the micelles in the hopes that such understanding will guide future efforts towards developing increasingly effective drug delivery vehicles.

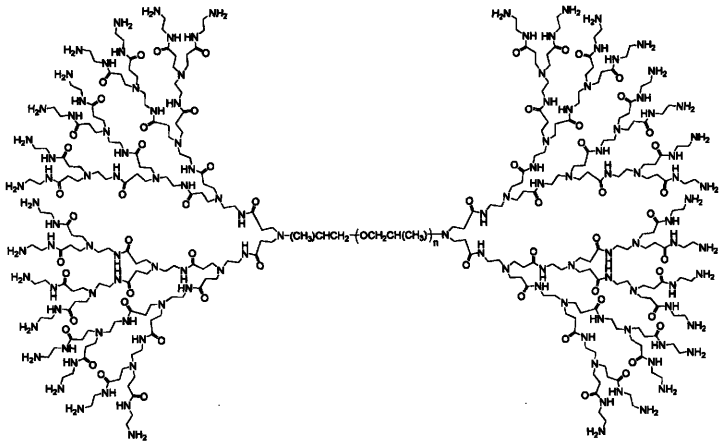

Figure 3-2. Chemical structure of generation 4.0 PPO-PAMAM.

3.3.1 Micelle Aggregation Number

The aggregation number of PPO-PAMAM micelles generations 4, 5, and 6 were determined with static light scattering and a Zimm plot analysis. That data is summarized in Table 3-2 and the Zimm plots are shown in Figure 3-3. The aggregation numbers ranged from 8 to 6, where generally with increasing generation there was a decrease in aggregation number. The trend observed closely follows the reduction in the hydrodynamic radius previously reported with increasing PAMAM generation.[5] With less unimers in each micelle, the size of the micelle would decrease.

Table 3-2. Zimm plot results of PPO-PAMAM generations 4, 5, and 6 micelles in DI water.

PPO-PAMAM Generation	dn/dc (ml/g)	A_2 ($cm^3 \cdot mol/g^2$)	Average Micelle Mw (g/mol)	Aggregation Number	R_h (nm)
4	1.26E-01	-1.68E-04	7.94E+04 ± 0.98E+04	8 ± 1	8 ± 0.2
5	1.39E-01	2.55E-04	9.14E+04 ± 5.8E+04	6 ± 3.6	4.5 ± 0.1
6	-9.81E-02	1.09E-04	1.41E+05 ± 0.2E+04	6 ± 1	4.5 ± 0.1

The A_2 values obtained from the Zimm plots indicate how well the solvent solvates the polymer molecules. A_2 is negative for generation 4 while it is positive for generations 5 and 6. This trend is corroborated in the CMC of these linear-dendritic block copolymers, where as the PAMAM generation increases the CMC increases due to the rise in the overall hydrophilicity of the polymer. It was previously observed that the CMC increased dramatically from generation 4 to 5 while it slightly decreased from generation 5 to 6.[5] The same trend is seen with A_2.

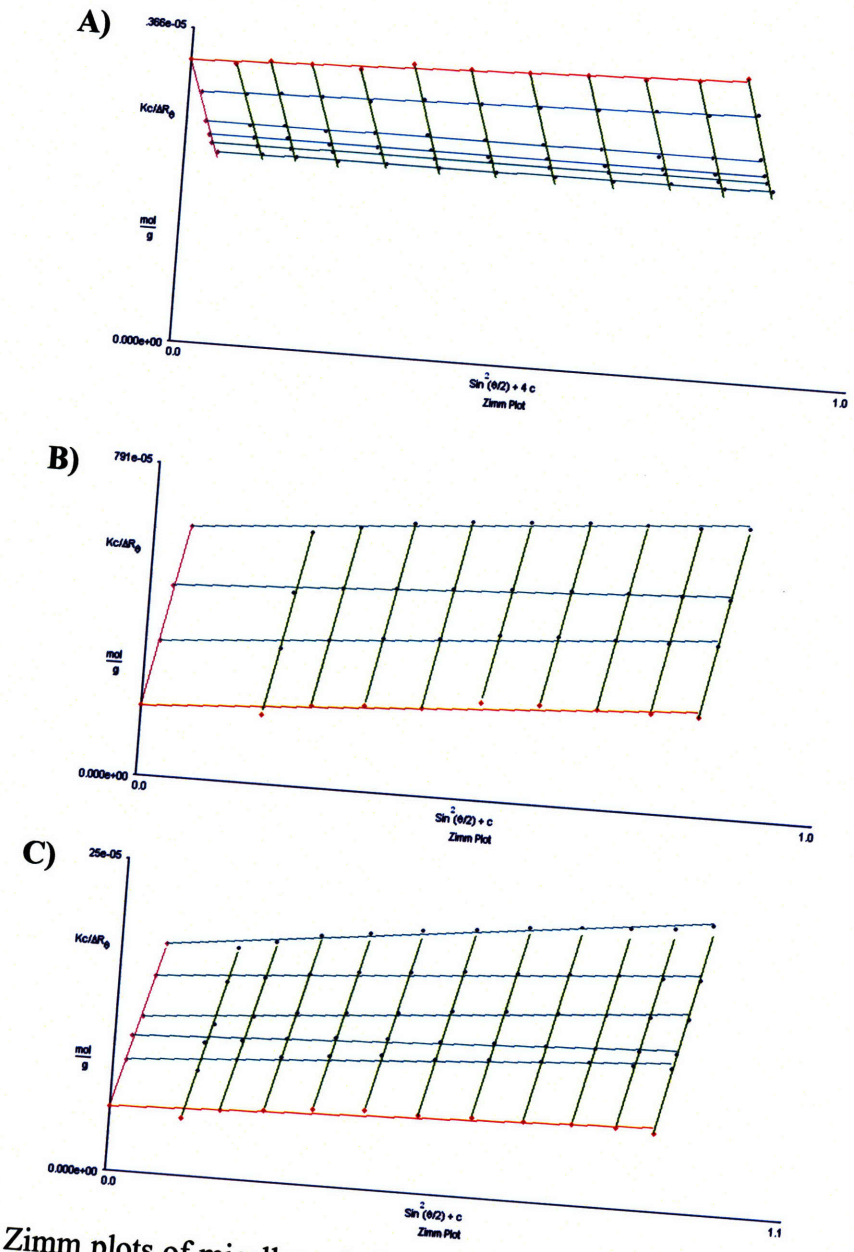

Figure 3-3. Zimm plots of micellar solutions of PPO-PAMAM generations 4.0 (A), 5.0 (B), and 6.0 (C).

The R_g values of the micelles in solution could not be determined accurately with Zimm plots. As seen in Figure 3-3, the extrapolation to zero concentration does not fit well with the actual data, since there is curvature at low and high angles. Furthermore, it has been noted that static light scattering is not able to determine the R_g of particles with R_g values smaller than 10 nm.[17]

3.3.2 Computer Simulation: Asphericity

Snapshots of the post-equilibration configurations of each simulated unimer and micelle are shown in Figure 3-4. For clarity, water molecules are not shown. Hydrogen atoms are depicted in white, carbon atoms cyan, nitrogen atoms blue, and oxygen atoms red. As can be observed in the snapshots, in general, the micelles are less spherical and more irregular in shape than the unimers.

In order to provide a quantitative measure of the asphericity of the simulated unimers and micelles, we have computed the moment of inertia tensor. The average values of the three principal moments of inertia I_z, I_y, and I_x, where I_z, I_y, and I_x are the eigenvalues of the moment of inertia tensor in descending order, are given in Table 3-3 along with the time period used to generate the average results. Each time period selected for averaging should be representative of the characteristics of the micelle after reaching an equilibrium shape and size, and was chosen based on the radius of gyration data shown in Figure 3-5. The average aspect ratios I_z/I_x and I_z/I_y, and the relative shape anisotropy κ^2, which is equal to 1 for a linear set of atoms and 0 for shapes with high 3D symmetry, are also reported in the table. The relative shape anisotropy is computed using the following formula:

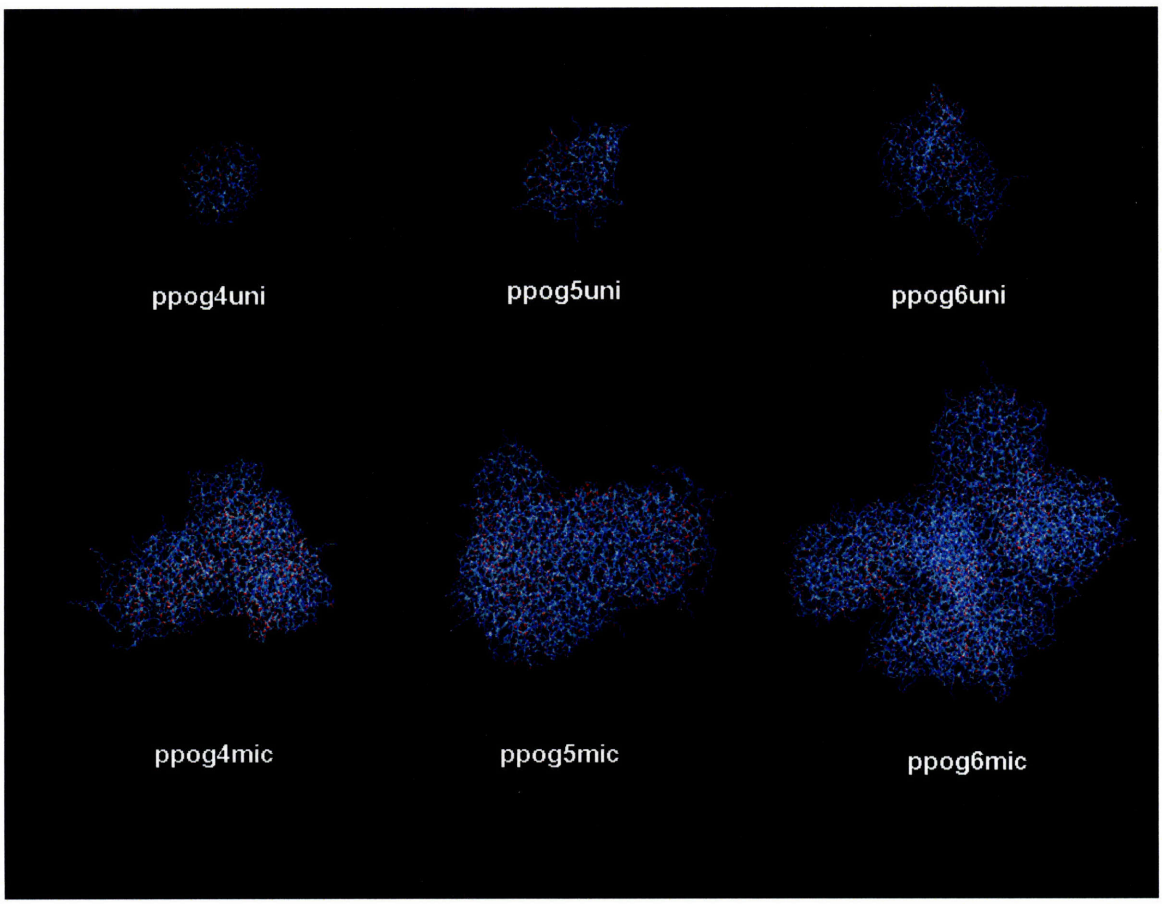

Figure 3-4. Snapshots of PPO-PAMAM unimers and micelles post-equilibration. Hydrogen atoms are depicted in white, carbon atoms cyan, nitrogen atoms blue, and oxygen atoms red.

$$\kappa^2 = 1 - \frac{3\langle I_2 \rangle}{\langle I_1^2 \rangle} \tag{3-3}$$

where I_1 and I_2 are the first and second invariants of the radius of gyration tensor: $I_1 = I_x + I_y + I_z$, $I_2 = I_x I_y + I_y I_z + I_x I_z$.

The aspect ratio I_z/I_x ranges between 1.52 and 2.26, while the ratio I_z/I_y ranges between 1.04 and 1.49. Both aspect ratios deviate significantly from 1.0 in most cases for both unimers and micelles, indicating that the equilibrated configuration of the simulated unimers and micelles are not very spherical. The relative shape anisotropy, κ^2, ranges from 0.02 for the generation 5 unimer to 0.05 for the generations 4 and 5 micelles. Although these values are relatively close to 0, which indicates a structure with high 3D symmetry, they are significantly larger than values of κ^2 reported by other researchers quantifying the shape anisotropy of PAMAM dendrimers in aqueous solution (ranging between 0.015 for a generation 1 dendrimer and 0.005 for a generation 5 dendrimer),[9] indicating that the unimers and micelles considered in this study have a much higher degree of shape anisotropy than simple dendrimers.

3.3.3 Computer Simulation: Radius of Gyration

The mass-weighted radius of gyration was computed for each unimer and micelle over the course of simulation. Each radius of gyration was computed as follows:

$$R_g = \frac{\sum_i (r_i - r_{COM})^2 m_i}{\sum_i m_i} \tag{3-4}$$

Table 3-3. Moments of inertia values for PPO-PAMAM unimers and micelles.

Simulation Name	Time Range for Averaging (ns)	I_x (a.m.u. nm^2)	I_Y (a.m.u. nm^2)	I_Z (a.m.u. nm^2)	I_z/I_x	I_z/I_y	κ^2
ppog4uni	10-20	12198.0	11764.1	8034.2	1.52	1.04	0.03
ppog5uni	5-8.8	54734.8	36691.2	34827.5	1.57	1.49	0.02
ppog6uni	5-10	130100.4	110381.8	62032.2	2.10	1.18	0.03
ppog4mic	35-50	538095.4	458526.8	252791.2	2.13	1.17	0.05
ppog5mic	5-17	710767.1	609167.8	314532.9	2.26	1.17	0.05
ppog6mic	3-14.5	1870012	1596542	1053896	1.77	1.17	0.03

where r_i is the location of atom i, r_{COM} is the location of the center of mass of the unimer/micelle, and m_i is the mass of atom i.

Figure 3-5 shows the radius of gyration profiles for PPO-PAMAM generations 4, 5, and 6 unimers in water (figures A, B, and C, respectively) and micelles (figures A', B', and C', respectively) as a function of simulation time. The starting point for each profile is the ending radius of gyration of the unimer/micelle after simulation in vacuo. Although the magnitude of the radius of gyration values reported for each unimer and micelle are different, to facilitate comparison of the results, the range of R_g values reported on the y-axis is the same (0.2 nm) for each plot. Each unimer and micelle shows change in the radius of gyration after the addition of explicit solvent molecules to the simulation cell. Two of the micelles (generations 4 and 6) show gradual increases in R_g over long periods of time, but in both cases the rate of change in R_g slowed significantly by the end of the simulation. As reflected in the relaxation times reported in Table 3-1, the timescale associated with stabilization of R_g is larger for the generation 4 micelle than for the unimer, smaller for the generation 5 micelle than for the generation 5 unimer, and larger for the generation 6 micelle than for the unimer. The radius of gyration values recorded for each unimer and micelle appear to have roughly stabilized by the end of the simulation time and to be fluctuating about an equilibrium value.

Table 3-4 summarizes the R_g values obtained from the simulations performed. The unimer R_g values are in the same range that has been observed through simulations and experimentation of PAMAM dendrimers (note that the PAMAM generation notation is different between this paper and the references).[8, 25] Comparing the lowest generation block copolymer (generation 4), the R_g value is very similar to the corresponding

PAMAM dendrimer, indicating that the PPO block does not add much to the size of the block copolymer unimer.[8] However, as the PAMAM generation increases, the R_g values increase as well due to the rise in the molecular weight of the PAMAM block. The rate of increase is faster than what is observed with the PAMAM dendrimers, where generation 6 is approximately 2-4 nm larger than the corresponding dendrimer.[8] Most likely for the block copolymer, the PPO block which separates the PAMAM dendrons allows the PAMAM to spread out to a greater extent. In comparison, PAMAM dendrimers are constrained due to crowding at the exterior, which limits their outgrowth.

For PPO-PAMAM micelles, the simulations revealed that the R_g increased with increasing generation. Assuming that the micelles formed are similar in structure to each other, the R_g/R_h ratio is constant. For a hard sphere, $R_g/R_h = 0.77$, and for a linear coil, $R_g/R_h = 1.8$.[17] Assuming a hard sphere, the theoretical R_g is presented in Table 3-4. The calculated R_g data has the reverse trend observed from the simulations and is larger than the simulated R_g data. The discrepancy could be explained due to how the R_h was calculated from the Stokes-Einstein equation assuming a spherical particle. As discussed in the previous section, the micelles were not particularly spherical in nature. It has been observed that dendrimers are considered to be prolate ellipsoids.[26] All of the micelles simulated were quite anisotropic which would result in large R_h measurements.[27] This in turn would produce larger R_g calculations in comparison to the simulated results.

Generally, the R_g values obtained from the simulations and the R_g values calculated from the experimental R_h values were of the same order of magnitude. However, the differences in the values observed could also be explained through the difference in the ionization state of the micelles. In the simulations, the micelles were not

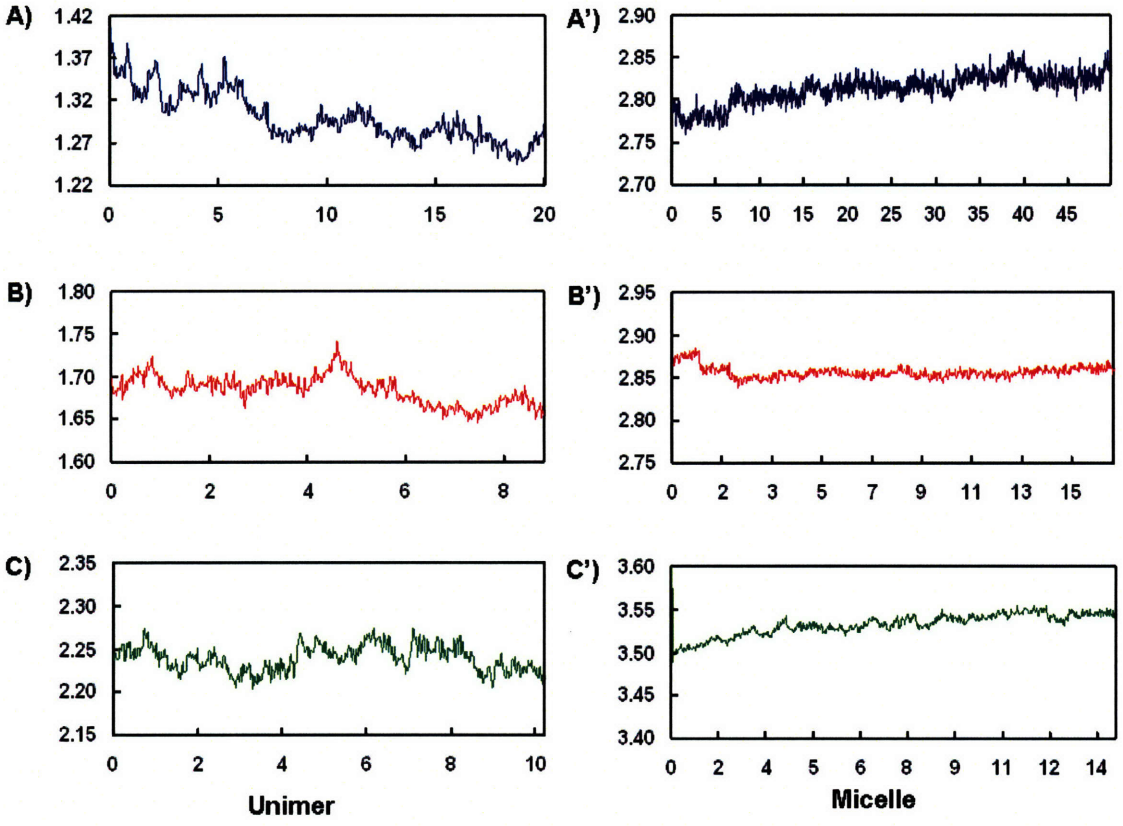

Figure 3-5. The time evolution of Rg for generations 4, 5, and 6 PPO-PAMAM unimers (A, B, and C, respectively) and micelles (A', B', and C', respectively). The y-axis is Rg (nm) while the x-axis is time (ns).

Table 3-4. Rg values obtained from simulation and calculated through experimental data for PPO-PAMAM unimers and micelles.

Simulation Name	Simulation R_g (nm)	R_h (nm)	Calculated R_g (nm) (hard sphere)
ppog4uni	1.28 ± 0.02	--	--
ppog5uni	1.67 ± 0.01	--	--
ppog6uni	2.24 ± 0.01	--	--
ppog4mic	2.83 ± 0.01	8 ± 0.2	6.2
ppog5mic	2.86 ± 0.01	4.5 ± 0.1	3.5
ppog6mic	3.54 ± 0.01	4.5 ± 0.1	3.5

charged, while the experimental data is for micelles in a partially charged environment. The radius of gyration expected for a partially protonated unimer or micelle would be expected to be larger than the values recorded here, because electrostatic repulsions among similarly charged nitrogen groups would be expected to cause swelling in aqueous solution.

3.3.4 Computer Simulation: Monomer Density Distribution

To quantify the time-averaged structure of the simulated micelles, the radial density profile of PAMAM monomers was computed with respect to the micelle center of mass. The radial density profile was evaluated by counting the number of atoms within a spherical shell between r and $r + \Delta r$, where r is the distance from the micelle center of mass and dividing by the volume of the spherical shell. The value of Δr used was 0.1 nm, a value which is large enough to provide good statistics on the density values except at small values of r (less than 0.5 nm[9]), where the volume of the spherical shell becomes quite small and results in the density profile data becoming very noisy. The relationship between the total number of atoms between the micelle center of mass and the value of r is given by the following expression:

$$N(r) = 4\pi \int_0^r r^2 \rho(r) dr \tag{3-5}$$

Values of $\rho(r)$ were computed for PPO-PAMAM generation 4, 5, and 6 micelles using simulation data taken from 35-50 ns, 5-17 ns, and 3-14.5 ns, respectively (the same time frames used in computing the asphericity data given in Table 3-3). Figure 3-6 shows $\rho(r)$ as a function of r for the different micelles.

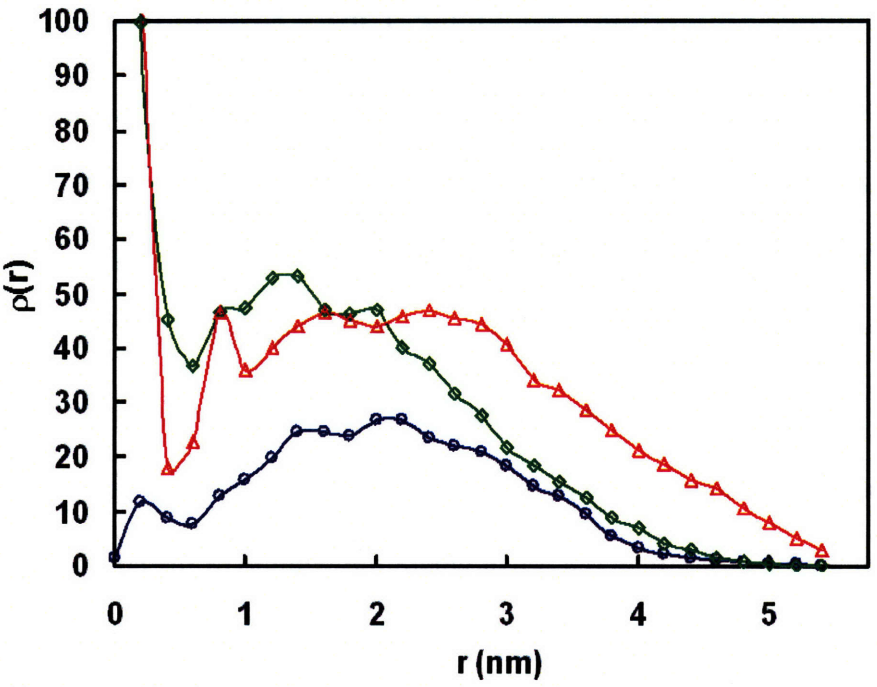

Figure 3-6. PAMAM monomer radial density distribution of PPO-PAMAM micelles generations 4 (blue circles), 5 (green diamonds), and 6 (red triangles).

Before r becomes sufficiently small that the density profiles become unreliably noisy, each of the $\rho(r)$ profiles appears to trend slightly downward as r decreases below 1 nm. This decrease in density is consistent with the visual observation that the hydrophobic PPO units tended to localize near the center of each micelle, displacing PAMAM dendrimers. It is interesting to note that for each of the three generations the decrease in $\rho(r)$ as r increases is slow and fairly linear. The rate at which $\rho(r)$ decreases is distinctly slower than that observed by other researchers simulating dendrimers of similar generation,[8-10] and reflects the fact that each of the dendritic micelles simulated here are more irregular in shape than unimolecular PAMAM generation 4, 5, or 6 dendritic molecules.

3.3.5 Computer Simulation: Terminal Group Distribution

Values of $\rho(r)$ for the terminal amine groups in each dendritic micelle were computed for generations 4, 5, and 6 (once again using simulation data taken from 35-50 ns, 5-17 ns, and 3-14.5 ns, respectively). Profiles of $\rho(r)$ as a function of r are shown in Figure 3-7. The location of terminal amine groups is important in the context of targeted drug delivery, because targeting ligands are typically attached to terminal amine groups. Furthermore, the extent to which terminal amine groups localize near the surface of the micelle or in the interior of the micelle is important in understanding the composition of the micelle/water interface.

At values of r less than 0.5, $\rho(r)$ data becomes unreliably noisy. At values of r greater than 0.5, values of $\rho(r)$ for generation 4 are observed to be relatively level with no general upwards or downwards trend up until about 3 nm. At this point $\rho(r)$ begins to decrease, and reaches zero at approximately 5 nm. The density data shows that rather

than being localized only near the exterior of the micelle, terminal amine groups are dispersed fairly evenly throughout the micelle interior, indicating that back-folding of terminal amine groups is prevalent through the dendritic micelle. Such back-folding is also observed in single dendrimer molecules[9] The $\rho(r)$ profiles for generation 5 and 6 show greater variation at small values of r, but once again the concentration of terminal amine groups in both micelles is found to be quite high within the interior of the micelle.

3.3.6 Computer Simulation: Dendrimer/Water Interface

In drug delivery applications, the structure and composition of the micelle/water interface plays an important role in determining the manner in which the dendrimer will interact with cells and deliver drugs within the body. The density profiles discussed in the previous two sections indicate that, due to the high degree of back-folding observed within dendrimer unimers, both primary and terminal amine groups are present at the micelle/water interface. Figure 3-8 plots the density of atoms comprising each micelle (the solid line) and water atoms as a function of distance from the micelle center of mass for the PPO-PAMAM generations 4, 5, and 6 systems.

For values of $r > 0.5$ nm, where the $\rho(r)$ profiles are reliable, the atom density of water does not drop to zero within the interior of the generations 4 and 6 micelles, while it does drop to essentially zero in the interior of the generation 5 micelle. Researchers simulating dendrimer molecules have observed that the density of water does drop to zero near the center of dendrimer molecules, even at low generation numbers, a finding which stands in contrast to the results for generations 4 and 6 micelles observed here.[9, 10] Although the interior of the PPO-PAMAM generations 4, 5, and 6 micelles simulated in this article are expected to be more hydrophobic on average than the interior of a simple

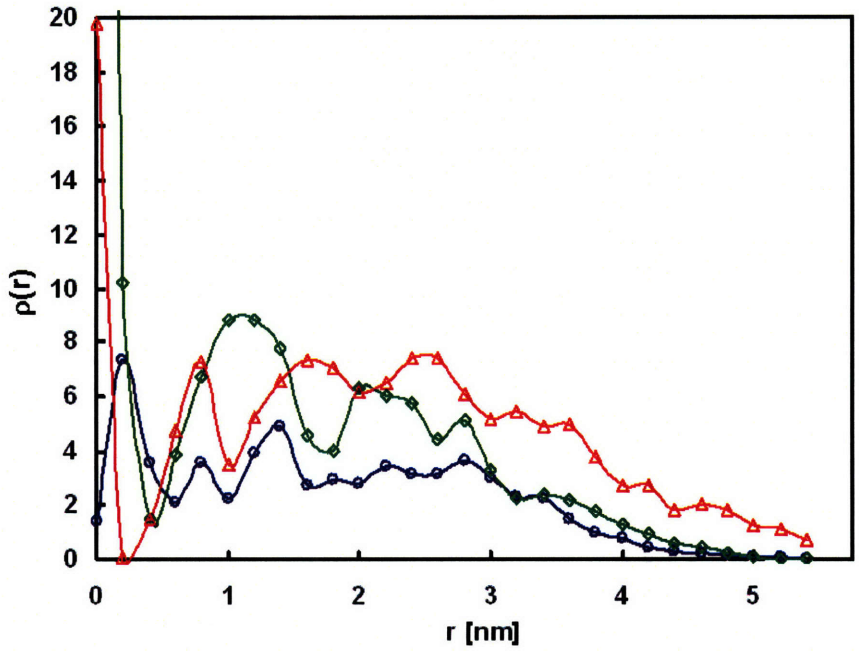

Figure 3-7. The radial density distribution of the terminal groups. Generation 4 is shown as blue circles, generation 5 as green diamonds, and generation 6 as red triangles.

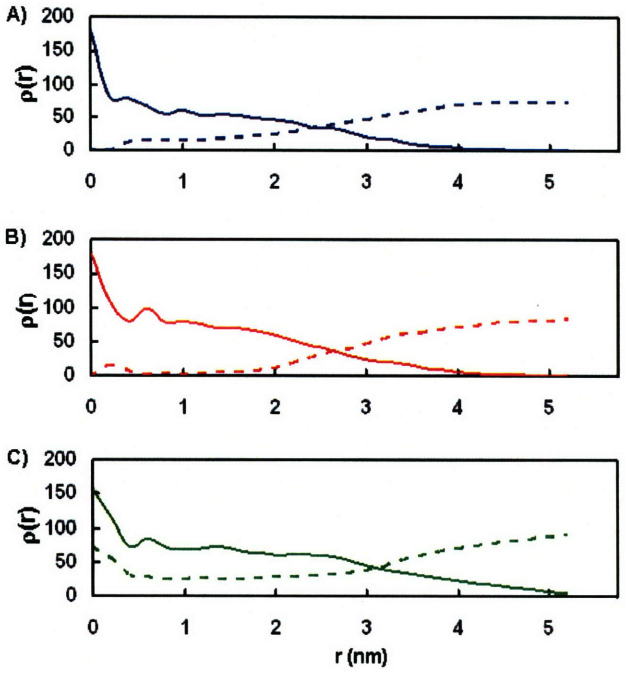

Figure 3-8. The density of atoms comprising each micelle (the solid line) and water atoms as a function of distance from the micelle center of mass for the PPO-PAMAM generation 4 system (A), generation 5 system (B), and generation 6 system (C).

dendrimer molecule because of the hydrophobicity of the PPO groups connecting each PAMAM head, the shape of the micelles simulated in this article are much more irregular and less spherical than that observed for simple dendrimers (see Section 3.3.2). The $\rho(r)$ profiles for water for generations 4 and 6 micelles are likely due to the observed asphericity of the dendritic micelles. These results should not be taken to conclude that water is adjacent to the hydrophobic PPO groups within the micelle core; however, due to the irregular geometry of the micelle, water penetrates more closely to the micelle core than is typically observed for surfactant micelles.

3.3.7 Computer Simulation: Locus of Hydrophobic Drug Solubilization

In Figure 3-9, density profiles are shown for PPO-PAMAM generation 4 dendrimer atoms, the atoms in 10 triclosan molecules, and water atoms. The $\rho(r)$ profile for triclosan has been scaled by the ratio of the total number of dendrimer atoms to the total number of triclosan atoms (=38.44) to amplify the triclosan density profile and make it more easily visible. The density profile appears to lie relatively evenly between the dendrimer and water molecules. The post-equilibration locus of solubilization is similar to the location where the triclosan was originally introduced during construction of the generation 4/triclosan/water micellar system (at the micelle/water interface). None of the 10 triclosan molecules initially placed at the micelle/water interface diffused out into aqueous solution, instead preferring to reside near the interface and remain in contact with the more hydrophobic environment provided by the dendritic micelle. As discussed in Section 3.2.4, 49.5 ns of equilibration of the ppog4drug system was conducted. However, it is not clear whether this level of simulation was sufficient to permit diffusion

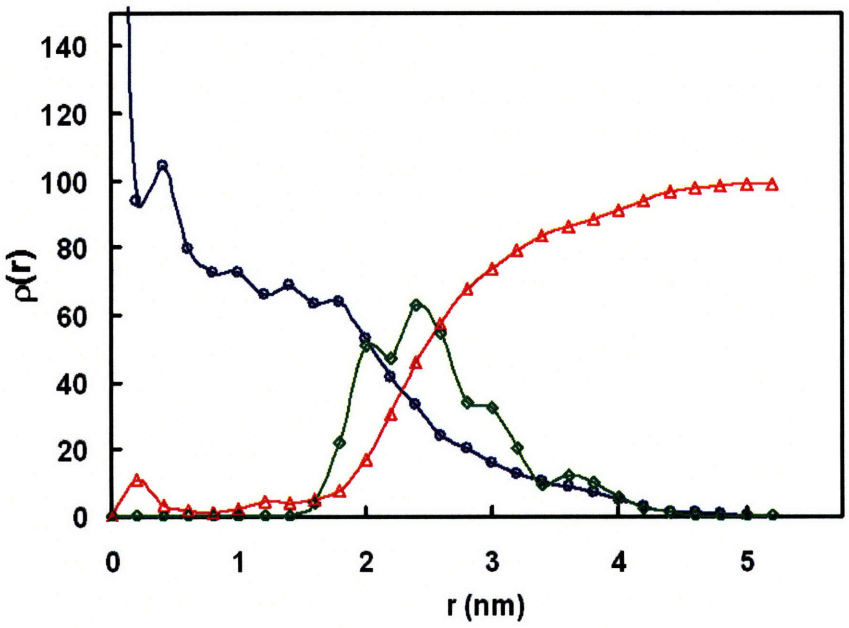

Figure 3-9. Radial distribution density profiles are shown for PPO-PAMAM dendrimer atoms (blue circles), the atoms in 10 triclosan molecules (green diamonds), and water atoms (red triangles).

of triclosan molecules to their thermodynamically preferred location within the micelle because significant diffusion from their initial position was not observed. Simulation of triclosan starting from different initial locations within each micelle is required to conclusively identify the preferred locus of solubilization of triclosan in PPO-PAMAM generation 4 micelles.

3.3.8 Computer Simulation: Solvent Accessible Surface Area

We have calculated the solvent accessible surface area (SASA) using the double cubic lattice method as implemented in GROMACS.[20] A probe sphere of radius 0.14 nm was used to compute the total (all atoms), hydrophobic (carbon and hydrogen bonded to carbon), and hydrophilic (oxygen, hydrogen bonded to oxygen, nitrogen, and hydrogen bonded to nitrogen) solvent accessible regions at each simulation time.[28-30] SASA values were computed for PPO-PAMAM generations 4, 5, and 6 micelles using simulation data taken from 35-50 ns, 5-17 ns, and 3-14.5 ns, respectively. Average hydrophobic, hydrophilic, and total SASA values are reported in Table 3-5, and the errors reported in the table are the standard deviation associated with each SASA value. Hydrophobic SASA values are much smaller than hydrophilic SASA values, indicating that the surface of each dendritic micelle is largely hydrophilic.

We have computed SASA using spheres of radius 0.14, 0.2, 0.3, 0.4, 0.5, 0.6, 0.7, 0.8, and 0.9 nm using the same simulation data used to generate Table 3-5 in order to determine the dependence of SASA on probe sphere radius. Results for the square root of the total solvent accessible surface area are shown in Figure 3-10 as a function of the probe sphere radius for PPO-PAMAM generations 4, 5, and 6 micelles. Each $SASA^{1/2}$ profile initially decreases as the probe radius increases. However, as the probe radius

increases further this trend slows and is eventually reversed. At sufficiently large values of the probe radius, $SASA^{1/2}$ begins to increase linearly with the probe radius. $SASA^{1/2}$ decreases with probe radius when the initial probe radius is smaller than the size of the largest internal voids present in a micelle. When the probe radius is larger than the largest internal voids, $SASA^{1/2}$ increases linearly with the probe radius. Evaluation of the radius at which each system begins to show a linear increase in $SASA^{1/2}$ with the probe radius allows us to determine that the largest voids in the generation 4, 5, and 6 micelle systems are approximately 0.35 nm, 0.4 nm, and 0.6 nm, respectively. It is interesting to note that the size of the largest void increases with the generation number of the molecules comprising the micelle. This observation is in agreement with visual observation of the equilibrated PPO-PAMAM generations 4, 5, and 6 micellar systems. As shown in Figure 3-4, the irregularity of the micelle surface appears to increase as the generation number increases (compare, in particular the irregularity of the generation 6 micelle's surface with that of generation 4 and 5). The effect of generation number on the morphology of the self-assembled micelles observed here could be related to drug delivery performance where the diffusion of drug through the micelle could be altered. Additionally, the morphology of the outer surface of the micelles could affect how targeting ligands are clustered on the surface and affect the binding characteristics of the drug delivery vehicle.

Table 3-5. Average SASA values for PPO-PAMAM generations 4, 5, and 6 micelles.

System	Hydrophobic SASA (nm^2)	Hydrophilic SASA (nm^2)	Total SASA (nm^2)
ppog4mic	53.4 ± 0.3	265.4 ± 1.9	318.8 ± 2.5
ppog5mic	32.5 ± 0.3	273.0 ± 2.2	305.4 ± 2.4
ppog6mic	41.5 ± 0.4	464.6 ± 0.5	506.1 ± 0.5

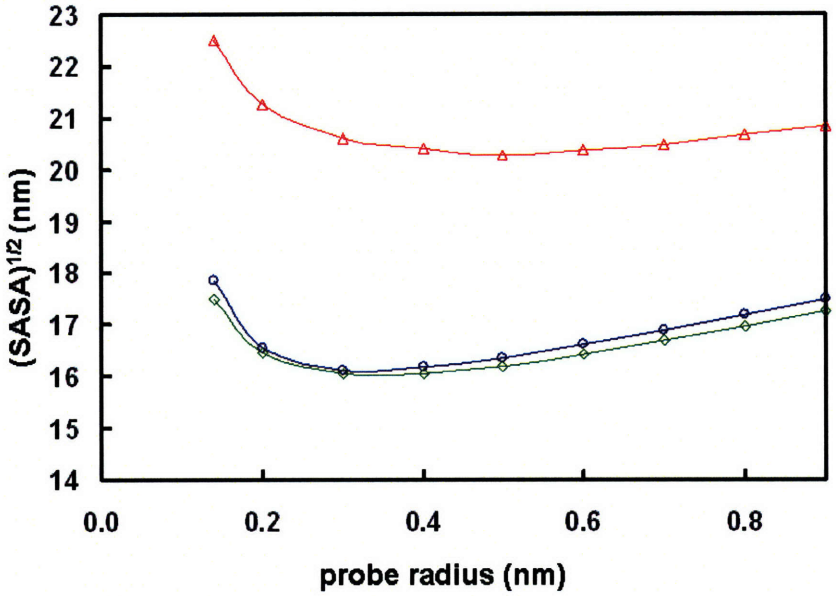

Figure 3-10. The square root of the total solvent accessible surface area, $SASA^{1/2}$, as a function of the probe sphere radius for PPO-PAMAM micelles generation 4 (blue circles), generation 5 (green diamonds), and generation 6 (red triangles).

3.4 Conclusion

An amphiphilic linear-dendritic block copolymer system which displayed interesting aqueous self-assembly behavior and high drug loading capacity was simulated using the GROMACS software package in order to gain detailed information about the structure of the micelles formed. Static light scattering experiments were used to explain the trends in R_h values as a function of dendrimer generation previously observed experimentally. Experimentally determined aggregation numbers were used to set up simulations of a PPO-PAMAM generation 4 micelle (containing eight unimers), a generation 5 micelle (containing six unimers), and a generation 6 micelle (containing six unimers).

In some respects, the micelles were found to have structural characteristics similar to PAMAM dendrimers. R_g values of the linear-dendritic block copolymer unimers were found to be of the same order of magnitude as the corresponding dendrimer, and back-folding of the PAMAM terminal amines was seen.[8, 10] However, in contrast to dendrimers, the micelles were quite a bit more irregular in shape and showed much more asphericity than dendrimers with even a low number of generations.[9] Simulations that were also performed to determine where triclosan, a model hydrophobic drug, would localize to in the block copolymer micelles showed the drug localizing in both the PAMAM and PPO block and not diffusing out into the aqueous environment. Previous experimental data confirms that triclosan can be encapsulated in PPO-PAMAM block copolymer micelles as well as PAMAM dendrimers.[5] Evaluation of the post-equilibration solvent accessible surface areas (SASAs) of each simulated micelle using spheres of different probe radii permitted determination of the largest voids in the

generation 4, 5, and 6 micelle systems. This could affect drug delivery performance by altering the diffusion of drug and water in and out of the micelles. Additionally, the spacing for drug delivery targeting would differ due to the different pore sizes.

The simulations performed provide a great deal of insight into the microstructure of linear-dendritic block copolymer micelles than was previously available and the manner in which these micelles encapsulate hydrophobic drugs for drug delivery. This data is potentially useful for further design and improvement of the system. For example, simulations could be used to predict the micelle equilibrium size as a function of the block length, or it could be used to design drug delivery vehicles with the correct targeting ligand spacing. Additionally, more information about the affinity of a drug to a particular hydrophobic polymer could be gleaned from simulations. With the work presented here, insight into the structural details of linear-dendritic block copolymer micelles was gained and can be used to develop more efficient drug delivery systems.

3.5 References

1. Grinstaff, M. W., "Biodendrimers: New polymeric biomaterials for tissue engineering," *Chemistry - A European Journal*, **2002,** 8, (13), 2838-2846.

2. Kim, T.; Seo, H.; Choi, J.; Jang, H.; Baek, J.; Kim, K.; Park, J., "Pamam-peg-pamam: Novel triblock copolymer as a biocompatible and efficient gene delivery carrier," *Biomacromolecules*, **2004,** 5, 2487.

3. Ihre, H. R.; Padilla De Jesús, O.; Szoka, F. C., Jr.; Fréchet, J., "Polyester dendritic systems for drug delivery applications: Design, synthesis, and characterization," *Bioconjugate Chem.*, **2001,** 13, 443-452.

4. Gillies, E.; Jonsson, T.; Fréchet, J., "Stimuli-responsive supramolecular assemblies of linear-dendritic copolymers," *J. Am. Chem. Soc.*, **2004,** 126, 11936.

5. Nguyen, P. M.; Hammond, P., "Amphiphilic linear-dendritic triblock copolymers composed of poly(amidoamine) and poly(propylene oxide) and their micellar-phase and encapsulation properties," *Langmuir*, **2006,** 22, (18), 7825-7832.

6. Çağin, T.; Wang, G.; Martin, R.; Breen, N.; Goddard, W. A., "Molecular modelling of dendrimers for nanoscale applications," *Nanotechnology*, **2000,** 11, 77-84.

7. Lee, I.; Athey, B.; Wetzel, A. W.; Meixner, W.; Baker, J. R. J., "Structural molecular dynamics studies of polyamidoamine dendrimers for a therapeutic application: Effects of ph and generation," *Macromolecules*, **2002,** 35, 4510-4520.

8. Maiti, P.; Çağin, T.; Want, G.; Goddard, W. A., "Structure of pamam dendrimers: Generations 1 through 11," *Macromolecules*, **2004,** 38, 6236-6254.

9. Han, M.; Chen, P.; Yang, X., "Molecular dynamics simulation of pamam dendrimer in aqueous solution," *Polymer*, **2005,** 46, 3481-3488.

10. Maiti, P.; Çağin, T.; Lin, S.; Goddard, W., III, "Effect of solvent and ph on the structure of pamam dendrimers," *Macromolecules*, **2005,** 38, 979.

11. Lee, H.; Baker, J. R. J.; Larson, R. G., "Molecular dynamics studies of the size, shape, and internal structure of 0% and 90% acetylated fifth-generation polyamidoamine dendrimers in water and methanol," *J. Phys. Chem. B*, **2006,** 110, 4014-4019.

12. Lyulin, S. V.; Darinskii, A. A.; Lyulin, A. V.; Michels, M. A. J., "Computer simulation of the dynamics of neutral and charged dendrimers," *Macromolecules*, **2004,** 37, 4676-4685.

13. Terao, T.; Nakayama, T., "Molecular dynamics study of dendrimers: Structure and effective interaction," *Macromolecules*, **2004,** 37, 4686-4694.

14. Srinivas, G.; Discher, D. E.; Klein, M. L., "Self-assembly and properties of diblock copolymers by coarse-grain molecular dynamics," *Nature Materials*, **2004,** 3, 638-644.

15. Srinivas, G.; Shelley, J. C.; Nielsen, S. O.; Discher, D. E.; Klein, M. L., "Simulation of diblock copolymer self-assembly, using a coarse-grain model," *J. Phys. Chem. B*, **2004,** 108, 8153-8160.

16. Milchev, A.; Bhattacharya, A.; Binder, K., "Formation of block copolymer micelles in solution: A monte carlo study of chain length dependence," *Macromolecules*, **2001,** 34, 1881-1893.

17. Liu, T.; Chu, B., "Light-scattering by proteins." In *Encyclopedia of surface and colloid science*, Hubbard, A. T., Ed. Marcel Dekker, Inc.: New York, 2002; pp 3023-3043.

18. Berendsen, H. J. C.; van der Spoel, D.; van Drunen, R., "Gromacs: A message-passing parallel molecular dynamics implementation," *Computational Physics Communications*, **1995,** 91, 43-56.

19. Lindahl, E.; Hess, B.; van der Spoel, D., "Gromacs 3.0: A package for molecular simulation and trajectory analysis," *Journal of Molecular Modeling*, **2001,** 7, 306-317.

20. van der Spoel, D.; Lindahl, E.; Hess, B.; van Buuren, A. R.; Apol, E.; Meulenhoff, P. J.; Tieleman, D. P.; Sijbers, A. L. T. M.; Feenstra, K. A.; van Drunen, R.; Berendsen, H. J. C., *Gromacs user manual version 3.2.* www.gromacs.org: 2004.

21. Berendsen, H. J. C.; Grigera, J. R.; Straatsma, T. P., "The missing term in effective pair potentials," *Journal of Phys. Chem.*, **1987,** 91, 6269-6271.

22. Foresman, J.; Frisch, A., *Exploring chemistry with electronic structure methods.* Gaussian, Inc.: Pittsburgh, Pennsylvania, 1996.

23. van Gunsteren, W. F.; Berendsen, H. J. C., "A leap-frog algorithm for stochastic dynamics," *Journal of Computation Chemistry*, **1997,** 18, 1463-1472.

24. *Materials studio help manual*, Accelrys.

25. Mansfield, M. L.; Jeong, M., "Simulation of lattice dendrimers by a monte carlo technique with detailed balance," *Macromolecules*, **2002,** 35, 9794-9798.

26. Freire, J. J., "Conformational properties of branched polymers: Theory and simulations," *Advances in Polymer Science*, **1999,** 143.

27. Eimer, W.; Niermann, M.; Eppe, M. A.; Jockusch, B. M., "Molecular shape of vinculin in aqueous solution," *J. Mol. Biol.*, **1993,** 229, 146-152.

28. Hermann, R. B., "Theory of hydrophobic bonding. Ii. The correlation of hydrocarbon solubility in water with solvent cavity surface area," *Journal of Phys. Chem.*, **1972,** 76, 2754-2759.

29. Levy, R. M.; Zhang, L. Y.; Gallicchio, E.; Felts, A. K., "On the nonpolar hydration free energy of proteins: Surface area and continuum solvent models for the solute-solvent interaction energy," *J. Am. Chem. Soc.*, **2003,** 125, 9523-9530.

30. Reynolds, J. A.; Gilbert, D. B.; Tanford, C., "Empirical correlation between hydrophobic free energy and aqueous cavity surface area," *Proceedings of the National Academy of Sciences*, **1974,** 71, 2925-2927.

CHAPTER 4: PPO-PAMAM *IN-VITRO* TESTING

4.1 Introduction

Nanoparticle drug carriers can accumulate in targeted drug delivery areas that display vascular permeability.[1] For example, extravasation of polymeric nanoparticles into solid tumors occurs through a phenomenon called the enhanced permeability and retention effect (EPR).[2, 3] Recently, it has been shown that micellar particles can accumulate in arteries that had sustained injury from angioplasty or stenting[4] or in areas of a myocardial infarction.[5] Another region of polymeric micelle accumulation that has been studied is at choroidal neovascularization sites in rat eyes.[1, 6]

In order to further enhance targeting to the desired treatment sites, targeting ligand can be attached to the outer surface of the polymeric nanoparticles. The ligand used is often paired to a cell surface receptor that is only expressed or overly expressed in the cells of interest. Therefore, utilizing targeting ligand can contribute to drug retention through internalization of particles by receptor-mediated endocytosis. Ligands such as folate,[7-9] RGD,[10, 11] and transferrin[12] have been used with polymer nanoparticles and liposomes.

Linear-dendritic block copolymers have previously been shown to be viable drug delivery vehicles.[13] Amphiphilic linear-dendritic block copolymers may have an advantage as a targeted drug delivery vehicle over conventional linear block copolymers due to the dense functional groups presented on the surface of the hydrophilic dendritic blocks forming the corona of the micelle. There are many multivalent targeting systems within the body that require dense clustering of functional groups. For example,

carbohydrate/lectin systems have been demonstrated to be multivalent systems.[14, 15] Dendrimers conjugated to carbohydrates, such as mannose or lactose, have been shown to have multivalent binding affinity with lectins.[16-18] Block copolymer micelles[19-21] have been functionalized with galactose, and their binding affinity to RCA-1 lectin have been studied. Studies with liposomes have been the most developed, where testing of galactose-functionalized liposomes *in vitro* and *in vivo* have been done indicating enhanced uptake by hepatic cells.[22]

To the author's knowledge, linear-dendritic block copolymer micelles have not yet been functionalized with targeting ligand for cell-specific drug delivery. There have been initial *in vitro* tests with amphiphilic linear-dendritic block copolymers composed of a hydrophilic linear block and a hydrophobic dendritic block indicating comparable drug efficacy as bare doxorubicin.[23] However, the self-assembly behavior of the Fréchet-type linear-dendritic block copolymers uses the dendritic block as the hydrophobic core. In contrast, the proposed linear-dendritic block copolymer system is composed of a hydrophobic linear block and a hydrophilic dendritic block. This linear-dendritic block copolymer self-assembles with the linear hydrophobic block forming the core and the dendritic block forming the corona of the micelles formed. Here we can take advantage of the dense functional groups presented on the outer surface of the micelles for multivalent targeting.

In this chapter, experiments performed to determine the viability of linear-dendritic block copolymer micelles as a targeted drug delivery vehicle will be presented. The experiments include the synthesis of a targeted linear-dendritic block copolymer and

in vitro experiments determining the binding efficiency and drug delivery efficacy of these novel linear-dendritic block copolymer micelles.

4.2 Experimental

4.2.1 Materials

Chemicals including methanol, dimethylformamide (DMF), dimethylsulfoxide (DMSO), triethylamine (TEA), N,N-diisopropylethylamine, 1-Amino-1-deoxy-β-D-galactose (galactosylamine), phosphate buffered saline (PBS) and asialofetuin (ASF) were acquired from Sigma Aldrich and used as received. BOP, HBTU, HOBT, doxorubicin, and 3-(4,5-dimethylthiazol-2-yl)-2,5-diphenyltetrazolium bromide (MTT) were obtained from EMD biosciences. Dialysis bags were purchased from Spectrum Laboratories. Alexa Fluor® 488 carboxylic acid, succinimidyl ester was obtained from Invitrogen. Water used in any experiments was from a MilliQ water purification system.

4.2.2 Synthesis of Galactose Functionalized PPO-PAMAM

Deprotection of PPO-PAMAM X.5 Generation. Generally, half generations of PPO-PAMAM terminated with methyl ester groups were deprotected by base hydrolysis. For example, PPO-PAMAM G3.5 (1.39 g, 0.2 mmol) was dissolved in 5 ml of methanol. 1.3 ml of 5 M aqueous NaOH was added dropwise to the stirring solution. The reaction was monitored by FTIR. After completion, the solvent was removed by rotary evaporation and dialyzed for 24 hours (3500 MWCO). The dialyzed solution was lyophilized until dry (yield 63%).

PPO-PAMAM-COOH G2.5. ^{1}H NMR (D_6-DMSO): δ_{PPO}(–OCH_2CHCH_3–) = 1.14 (t); δ_{PPO}(–OCH_2CHCH_3–) = 3.40 (m); δ_{PPO}(–OCH_2CHCH_3–) = 3.61 (m); δ_{PAMAM} (–CONH–)

= 7.66-8.02 (bs); δ_{PAMAM} (–C**H**$_2$CH$_2$N–) = 3.28 (m); δ_{PAMAM} (–C**H**$_2$CH$_2$CO–) = 2.74-2.83 (m); δ_{PAMAM} (–CH$_2$C**H**$_2$N–) = 2.53-2.59 (m); δ_{PAMAM} (–CH$_2$C**H**$_2$CO–) = 2.37-2.44 (t); FTIR peak ν cm^{-1}: 1110, 1540, 1665.

PPO-PAMAM-COOH G3.5. ^{1}H NMR (D$_6$-DMSO): δ_{PPO}(–OCH$_2$CHC**H**$_3$–) = 1.14 (t); δ_{PPO}(–OCH$_2$C**H**CH$_3$–) = 3.40 (m); δ_{PPO}(–OC**H**$_2$CHCH$_3$–) = 3.61 (m); δ_{PAMAM} (–CON**H**–) = 7.73-8.09 (bs); δ_{PAMAM} (–C**H**$_2$CH$_2$N–) = 3.28 (m); δ_{PAMAM}(–C**H**$_2$CH$_2$CO–) = 2.75-2.81 (m); δ_{PAMAM} (–CH$_2$C**H**$_2$N–) = 2.53-2.58 (m); δ_{PAMAM} (–CH$_2$C**H**$_2$CO–) = 2.37-2.44 (m); FTIR peak ν cm^{-1}: 1110, 1542, 1652.

PPO-PAMAM-COOH G4.5. ^{1}H NMR (D$_6$-DMSO): δ_{PPO}(–OCH$_2$CHC**H**$_3$–) = 1.14 (t); δ_{PPO}(–OCH$_2$C**H**CH$_3$–) = 3.40 (m); δ_{PPO}(–OC**H**$_2$CHCH$_3$–) = 3.61 (m); δ_{PAMAM} (–CON**H**–) = 7.63-8.07 (bs); δ_{PAMAM} (–C**H**$_2$CH$_2$N–) = 3.27 (m); δ_{PAMAM} (–C**H**$_2$CH$_2$CO–) = 2.74-2.82 (m); δ_{PAMAM} (–CH$_2$C**H**$_2$N–) = 2.53-2.58 (m); δ_{PAMAM} (–CH$_2$C**H**$_2$CO–) = 2.36-2.43 (m); FTIR peak ν cm^{-1}: 1110, 1542, 1647.

Synthesis of PPO-PAMAM-Galactose. As an example, PPO-PAMAM-COOH G3.5 (0.5 g) was dried by azeotropic distillation with toluene using the rotary evaporator at 45 °C. The polymer was dissolved in 20 ml of anhydrous DMSO. One molar equivalent of DIPEA was added (0.24 g). Next, HOBT (1.16 g) and BOP (3.78 g) was added. The solution was stirred for 5 minutes, and then 0.92 g galactosylamine was put into the solution. After 2 days, water was mixed into the reaction to make approximately a 10% DMSO solution. The solution was centrifuged for 10 minutes at 4000 rpm to collect the

by-product precipitate. The solution was decanted and dialyzed (3500 MWCO) for 24 hours at room temperature. The dialyzed solution was lyophilized until dry (yield 59%).

PPO-PAMAM-COOH G2.5. ^{1}H NMR (D_6-DMSO): δ_{PPO}(–OCH_2CHCH_3–) = 1.14 (t); δ_{PPO}(–OCH_2CHCH_3–) = 3.40 (m); δ_{PPO}(–OCH_2CHCH_3–) = 3.61 (m); δ_{PAMAM} (–CONH–) = 7.66-8.02 (bs); δ_{PAMAM} (–CH_2CH_2N–) = 3.28 (m); δ_{PAMAM} (–CH_2CH_2CO–) = 2.74-2.83 (m); δ_{PAMAM} (–CH_2CH_2N–) = 2.53-2.59 (m); δ_{PAMAM} (–CH_2CH_2CO–) = 2.37-2.44 (m); δ_{Gal} = 3.8-4.0 (m).

PPO-PAMAM-COOH G3.5. ^{1}H NMR (D_6-DMSO): δ_{PPO}(–OCH_2CHCH_3–) = 1.14 (t); δ_{PPO}(–OCH_2CHCH_3–) = 3.40 (m); δ_{PPO}(–OCH_2CHCH_3–) = 3.61 (m); δ_{PAMAM} (–CONH–) = 7.73-8.09 (bs); δ_{PAMAM} (–CH_2CH_2N–) = 3.28 (m); δ_{PAMAM}(–CH_2CH_2CO–) = 2.75-2.81 (m); δ_{PAMAM} (–CH_2CH_2N–) = 2.53-2.58 (m); δ_{PAMAM} (–CH_2CH_2CO–) = 2.37-2.44 (m); δ_{Gal} = 3.8-4.0 (m).

PPO-PAMAM-COOH G4.5. ^{1}H NMR (D_6-DMSO): δ_{PPO}(–OCH_2CHCH_3–) = 1.14 (t); δ_{PPO}(–OCH_2CHCH_3–) = 3.40 (m); δ_{PPO}(–OCH_2CHCH_3–) = 3.61 (m); δ_{PAMAM} (–CONH–) = 7.63-8.07 (bs); δ_{PAMAM} (–CH_2CH_2N–) = 3.27 (m); δ_{PAMAM} (–CH_2CH_2CO–) = 2.74-2.82 (m); δ_{PAMAM} (–CH_2CH_2N–) = 2.53-2.58 (m); δ_{PAMAM} (–CH_2CH_2CO–) = 2.36-2.43 (m); δ_{Gal} = 3.8-4.0 (m).

4.2.3 Polymer Characterization

^{1}H NMR was used to characterize each polymer. ^{1}H-NMR spectra were recorded on a Varian Inova-500 MHz spectrometer. Samples were dissolved in deuterated DMSO. FTIR spectra were recorded on a Nexus 870 FTIR Spectrometer (Thermo Nicolet,

Waltham, MA). Samples were solvent cast onto polyethylene IR cards. MALDI-TOF was performed by the MIT CCR Biopolymers Laboratory on an Applied Biosystems Model Voyager DE-STR instrument. The samples were dissolved in 20 μl of a 1:1 mixture of methanol:acetonitrile and 0.1% trifluoroacetic acid. 1 μl of the solution was mixed with 10 μl of a 2,5 dihydroxybenzoic acid matrix solution and analyzed.

4.2.4 *In Vitro* Testing

Drug Loading. PPO-PAMAM block copolymers were dissolved into DI water at a concentration of 5 mg/ml. The pH of the solution was adjusted to 7.4 by addition of either dilute HCl or dilute NaOH. 1 mg of doxorubicin·HCl was dissolved in 1 ml of chloroform and 3 equivalents of triethylamine. The doxorubicin solution was added dropwise to the stirred polymer solution and left open overnight in the dark. After the chloroform evaporated, the solution was centrifuged at 4000 rpm for 10 minutes to remove insoluble doxorubicin. The solution was filtered through a 0.20 μm polytetrafluoroethylene filter, and then using a centriprep centrifugal filter (Ultracel-YM 3, Millipore), ultrafiltration was performed in triplicate. The concentration of doxorubicin in water was quantified by UV-vis (Agilent 8453 UV-Visible Spectrometer System, Palo Alto, CA) by measuring the absorbance at 495 nm and compared to a standard curve (concentration (μg/ml) = $76.728*ABS_{495}-4.9553$).

Drug Release. 5 ml of drug-loaded micelles in PBS were placed in dialysis bags (3500 MWCO) and put into a reservoir of PBS heated at 37 °C. A sample of the retentate was measured by UV-vis at various time points at 495 nm. The PBS reservoir was replaced every few days.

Cell Culture. Hepatocellular carcinoma cells (Hep G2, ATCC HB-8065) were maintained in Dulbecco's Modified Eagle Medium containing high glucose, 25 mM HEPES, but no phenol red (DMEM, Invitrogen) supplemented with 10% fetal bovine serum, 0.2 units/ml penicillin, and 100 μg/ml streptomycin. The cells were kept in an incubator at 37 °C in a 5% CO_2 atmosphere. The media was changed every two days. When the cells were confluent, trypsin-EDTA was added to the flask. After 15-30 seconds, the trypsin-EDTA was removed, and the flask was incubated at 37 °C for 10 minutes. The cells were subcultivated at a 1:6 ratio. Primary rat hepatocytes were obtained from the Griffith Lab and seeded onto 6-well plates ($0.4x10^6$ cells/well, BD Falcon) with serum-free hepatocyte growth media. The 6-well plates were first prepared by incubating PBS solutions of 30 μg/ml rat-tail collagen type I (BD Biosciences) for 1 hour at room temperature in each well. The cells were incubated for 3-4 hours at 37 °C in a 5% CO_2 atmosphere before use.

Binding Inhibition. ASF was modified with a reactive fluorescent tag, Alexa Fluor 488 succinimidyl ester. 7 mg of ASF was dissolved in 2 ml of water, and then 0.5 ml of 1 M sodium bicarbonate solution was added to attain a solution with a pH of 8. 50 μl of a 10 mg/ml solution of Alexa Fluor 488 succinimidyl ester in DMSO was added to the ASF solution and stirred at room temperature for 4 hours in the dark. The Alexa Fluor modified ASF (ASF-AF488) was purified by dialysis at 4 °C for 2 days. Varying concentrations of galactose-modified PPO-PAMAM or soluble ASF dissolved in DPBS was introduced into 6-well plates of primary rat hepatocytes. 5 μl of ASF-AF488 was introduced for every 1 ml of media. The solutions were incubated with the cells for 30 minutes. Afterwards, the cells were washed with PBS two times and then fixed with 2%

paraformaldehyde in PBS at 4 °C overnight. The cells were then washed with PBS 3 times and then incubated with 1 mL/well of PBS. To stain the nucleus, 2 μl of Hoescht 33342 (2 mM solution in water) was added to each well and incubated at room temperature for 15 minutes. Afterwards, the cells were washed with PBS 3 times. The cells were visualized with a fluorescent inverted microscope (Zeiss Axiovert 200) using FITC and DAPI filters.

Cytoxocity Testing. Hep G2 cells were detached from the flask with trypsin-EDTA and seeded into 96-well plates (BD Falcon) at 10,000 cells/well. The cells were incubated overnight at 37 °C in a 5% CO_2 atmosphere. The media was aspirated and incubated in 100 μl of polymer dissolved in complete media for 24 to 48 hours. Afterwards, the media was removed and replaced with 100 μl of complete media. 10 μl of MTT (5 mg/ml in PBS) was added to each well. The cells were incubated for 4 hours at 37 °C, and then 50 μl of an extraction solution (20% sodium dodecyl sulfate in 1:1 DMF/Water pH 4.7, adjusted with 0.5 N HCl/40% acetic acid) was added. The plates were left overnight at 37 °C. A BioTek Powerwave microplate plate reader was used to get the absorbance at 570 nm.

4.3 Results and Discussion

Linear-dendritic block copolymer micelles are promising polymeric nanoparticles for drug delivery.[13, 23] Linear-dendritic block copolymer micelles with the dendritic block forming the interface between the core and the aqueous environment may offer an advantage over linear block copolymers due to the presentation of dense functional groups on the surface of the nanoparticles. A representation of PPO-PAMAM generation

4.0 was developed in Materials Studio, which was equilibrated in an environment with a dielectric constant of 4.0 to simulate water (Figure 4-1). As seen in Figure 4-1, the length scales of the PAMAM dendritic ends are approximately 1-3 nm apart. Multivalent binding systems that have been previously studied exhibiting binding on similar length scales are lectins. For example, asialoglycoprotein receptors bind to galactose in a trivalent fashion with a triangular binding configuration that is approximately 2 nm apart.[15] Therefore to determine whether PPO-PAMAM has the ability to bind multivalently for targeted drug delivery, the system chosen for testing was the asialoglycoprotein receptor and galactose as the binding ligand.

4.3.1 Synthesis of Galactose Functionalized PPO-PAMAM

In order to conjugate galactose to the dendritic ends of the linear-dendritic block copolymer, half generations of PPO-PAMAM were used (Figure 4-2). The PPO-PAMAM was synthesized as previously described in Chapter 2. The PPO-PAMAM half generations, terminating in methyl ester groups, were deprotected in basic methanol. The reaction was monitored by FTIR observing the disappearance of the ester peak at approximately 1740 cm^{-1} as shown in Figure 4-3.

An amine derivative of D-galactose, galactosylamine, was attached to the dendritic ends of the PPO-PAMAM block copolymers utilizing conventional amidation chemistry. Due to the disparate solubility of each block, the best solvent to use was DMSO. The coupling agents used were either BOP or HBTU with HOBT. These

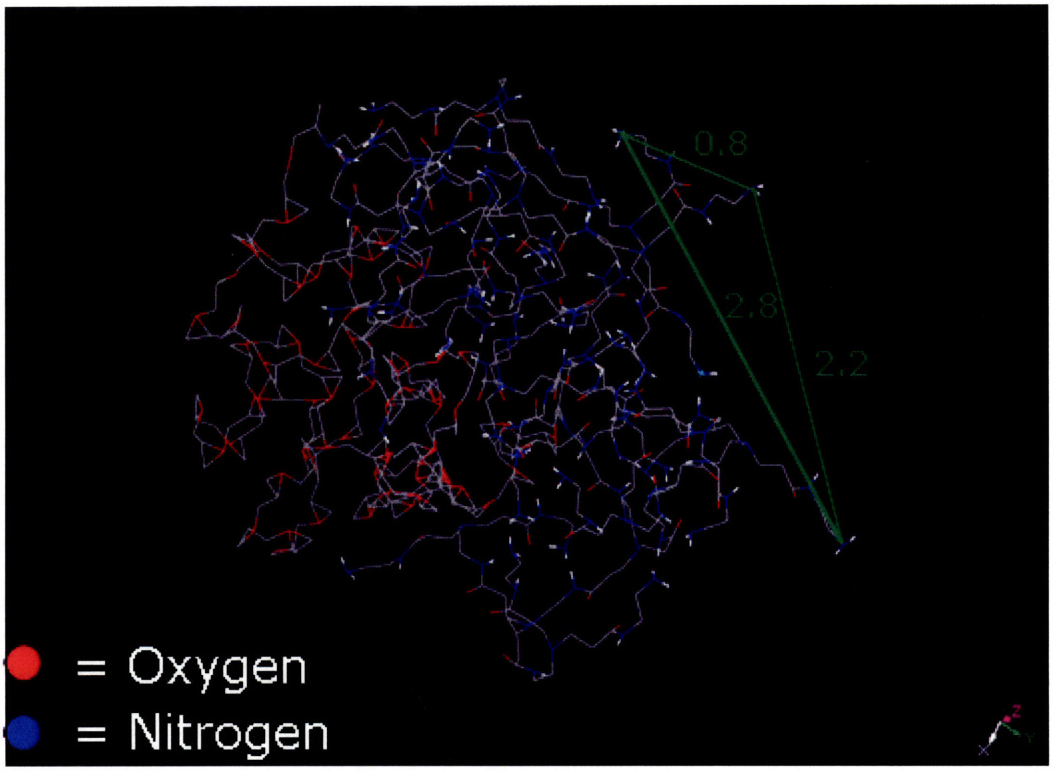

Figure 4-1. Model of PPO-PAMAM generation 4.0 generated in Materials Studio and equilibrated by molecular dynamics in GROMACS.

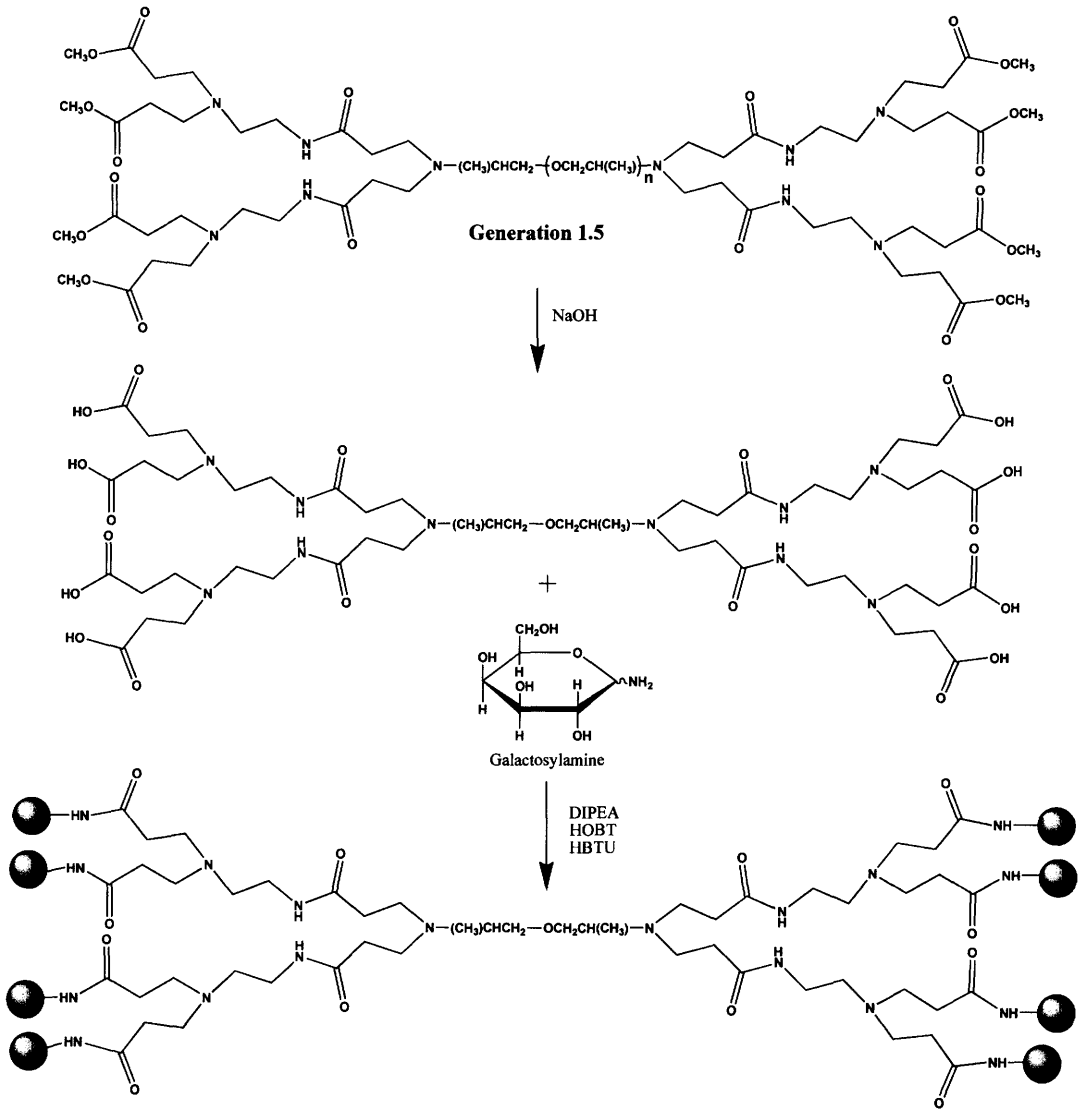

Figure 4-2. Synthesis of PPO-PAMAM-Galactose from a half-generation PPO-PAMAM deprotected through base hydrolysis. Galactose is added through traditional amidation chemistry.

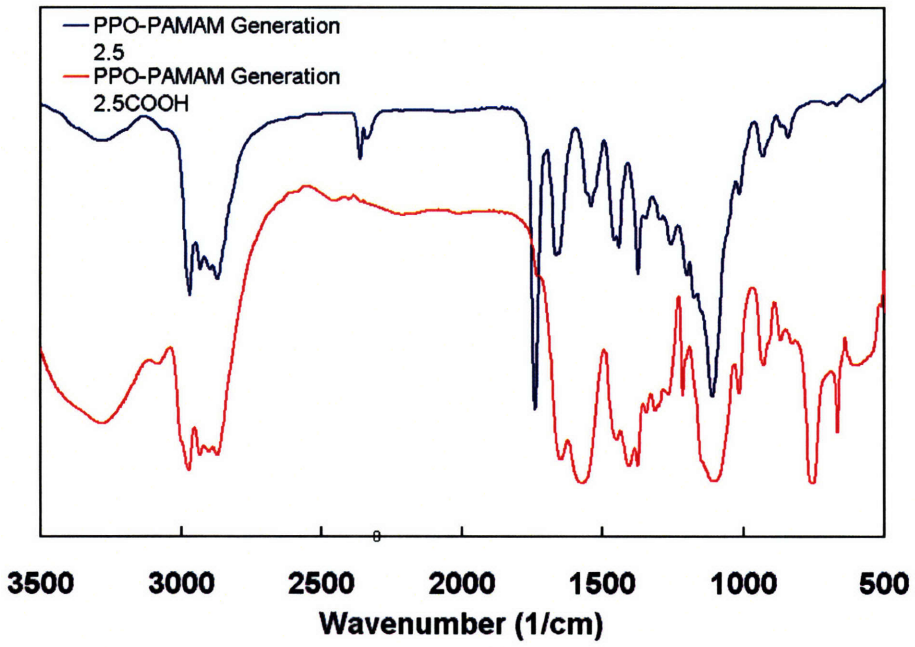

Figure 4-3. FTIR of PPO-PAMAM generation 2.5 before and after methyl ester deprotection. The disappearance of the 1740 cm^{-1} indicates the deprotection of the methyl ester group.

coupling reagents were used in approximately 5 times excess of the reactive groups to ensure completion of coupling. Additionally, the reactions were run for 2 to 4 days.

Reactions with PPO-PAMAM generations 2.5, 3.5, and 4.5 were performed. The reaction products were analyzed with ^{1}H-NMR and MALDI-TOF. ^{1}H-NMR indicates the presence of the galactosylamine after purification. MALDI-TOF was used to determine the molecular weight of the polymer before and after the reaction. The amount of galactosylamine was calculated based on the gain in mass. As seen in Table 4-1, the percent functionalization ranged from 27% to 60%. It is possible that the percent functionalization could be increased by reacting the galactose functionalized polymer again, or it is possible that the functionalization with galactose plateaus due to steric hindrance and crowding at the periphery of the dendrimer. Testing was performed on polymers 2, 4 and 5 listed in Table 4-1.

4.3.2 *In Vitro* Testing

An initial test to gauge the targeting potential of the galactose-functionalized polymers was performed with primary rat hepatocytes. Asialofetuin, a protein with 14 galactose and 2 N-acetyl-galactosamine,[24] was first modified with a fluorescent molecule (Alexa Fluor 488 succinimidyl ester). When the fluorescent ASF (ASF-AF488) is incubated with the primary rat hepatocytes, the ASF-AF488 binds multivalently to the asialoglycoprotein receptors on the surface of the hepatocytes and is taken up into the cells by receptor-mediated endocytosis. This can be seen by the bright spots, presumably endosomes, as shown in Figure 4-4A. When ASF-AF488 is incubated with excess soluble ASF, which would block the binding of fluorescent ASF, there is no uptake and no punctuated bright spots present in the cells (Figure 4-4B). There is only nonspecific

Table 4-1. Percent galactose functionalization of various generations of PPO-PAMAM.

Polymer	Generation	–COOH MW (g/mol)	–Galactose MW (g/mol)	% Functionalized (# attached/# available)
1	Gen 2.5	7001	8318	46 (7.4/16)
2	Gen 2.5	7001	9070	60 (9.6/16)
3	Gen 3.5	9338	11224	27 (8.7/32)
4	Gen 3.5	9338	12557	56 (18/32)
5	Gen 4.5	15173	18921	33 (21/64)
6	Gen 4.5	15173	21617	56 (36/64)

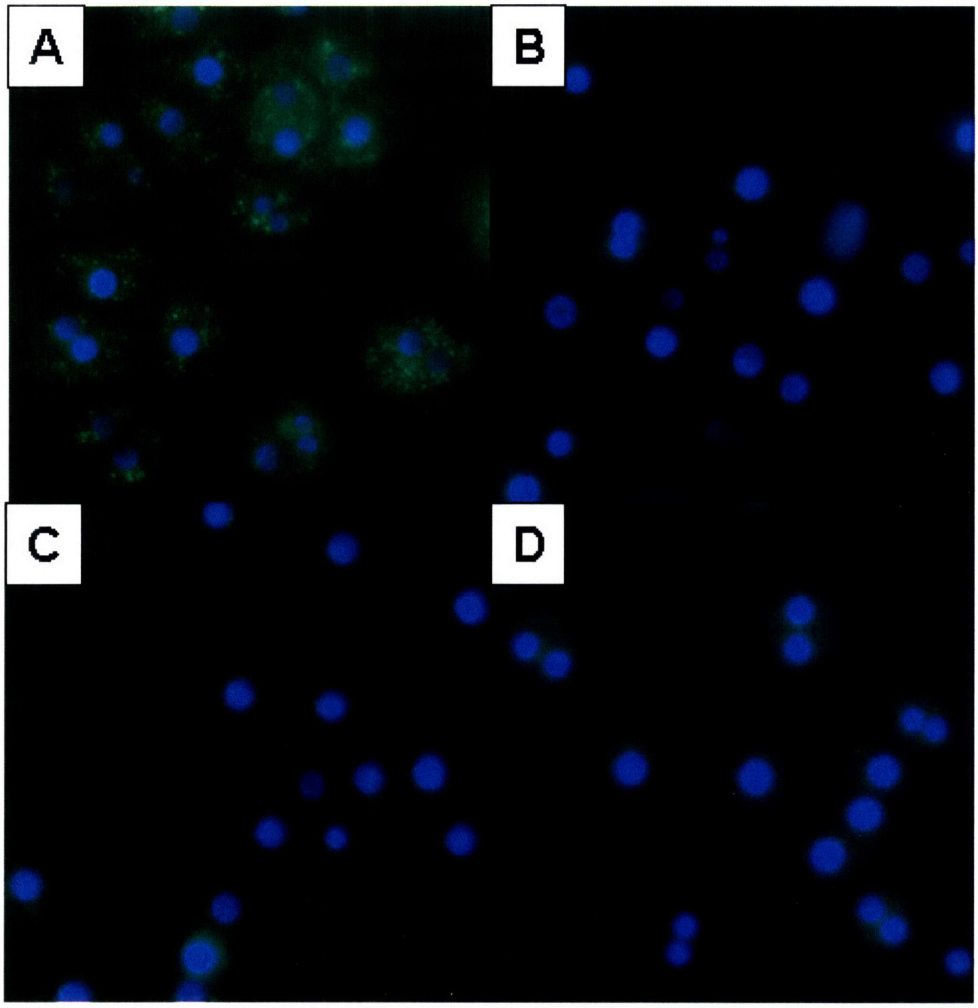

Figure 4-4. A) Primary rat hepatocytes incubated with ASF-AF488 (25 ug/ml). B) Primary rat hepatocytes incubated with ASF-AF488 (25 ug/ml) and excess ASF (1 mg/ml). C) Primary rat hepatocytes incubated with ASF-AF488 (25 ug/ml) and excess PPO-PAMAM-Gal gen. 3.5 (0.5 mg/ml). D) Primary rat hepatocytes incubated with ASF-AF488 (25 ug/ml) and excess PPO-PAMAM-Gal gen. 4.5 (0.5 mg/ml). For treatment A, there is uptake of ASF-AF488 through receptor-mediated endocytosis. For treatments B, C, and D, very little fluorescence indicates that uptake of ASF-AF488 was blocked by excess reagent.

binding (Figures 4-4C and 4-4D). When ASF-AF488 is incubated with galactose-modified PPO-PAMAM generations 3.5 and 4.5, there is also only nonspecific binding. Thus, the galactose-modified PPO-PAMAM binds to the asialoglycoprotein receptor and prevents uptake of ASF-AF488.

Cytotoxicity testing was used to determine the useable polymer concentrations for all *in vitro* testing. Hep G2 cells were incubated with polymers varying in concentration and compared to cells with no treatment to determine the IC_{50}, which is defined as the concentration at which 50% of the cells are still viable. MTT tests indicate that all of the polymers tested, PPO-PAMAM-COOH and PPO-PAMAM terminating in galactose, except for PPO-PAMAM-Galactose G2.5 had IC_{50} values greater than 10 mg/ml (Table 4-2). Ideally, the working concentration of the polymer should be lower than the IC_{50} and higher than the CMC to ensure micelles are still present. Concentrations of 5 mg/ml of polymer were chosen for subsequent tests since it is below the IC_{50} and well above the CMC.

For targeting efficacy studies, doxorubicin was chosen as the model drug due to its absorbance at 495 nm, its fluorescence properties, and its hydrophobicity. An oil/water emulsion technique was used for the encapsulation of doxorubicin into PPO-PAMAM micelles.[25] The doxorubicin was prepared by dissolving it in chloroform and 3 molar excess amounts of triethylamine. The triethylamine is present to ensure deprotonation of the amine group of the doxorubicin, which converts the doxorubicin to a hydrophobic state. The doxorubicin solution was added dropwise to an aqueous solution of preformed PPO-PAMAM micelles. The emulsion is stirred overnight in the dark, and the chloroform is removed through evaporation. The amount of doxorubicin

encapsulated is quantified by UV-vis and compared against a standard curve created in the same solvent. The amount of doxorubicin encapsulated for all generations ranged from 10-30 μg/ml.

Drug release studies of doxorubicin from PPO-PAMAM generation 4.0 micelles were conducted. The release studies were done in PBS at 37 °C. As seen in Figure 4-5, drug release is quite fast, with a half-life of approximately 1 hour. Ideally, drug release should last over a period of at least a day, since the half life of micelles or other colloidal particles circulating in the body has been observed as high as 98 hours.[25, 26] However, for the purposes of later studies, the release times are long enough to ensure that during the duration of *in vitro* targeting efficiency studies most of the drug being delivered is still in the micelles.

In vitro experiments to determine targeting efficiency were performed with PPO-PAMAM generations 3.5 and 4.5 (polymers 4 and 5 from Table 4-1). PPO-PAMAM generation 2.5 modified with galactose was too toxic to be used. PPO-PAMAM generations 3.5 and 4.5 either terminating in carboxylic acid or galactose were used to encapsulate doxorubicin. These micellar solutions were diluted with Opti-MEM media modified with 2 mM Ca^{2+} to obtain doxorubicin concentrations ranging from 10 μg/ml to 0.01 μg/ml. The micellar solutions encapsulating doxorubicin, bare doxorubicin as a positive control, and only Opti-MEM were incubated with Hep G2 cells in 96 well plates for 1 hour. Afterwards, the solutions were removed and replaced with complete media. The cells were incubated for 48 hours. Cytotoxicity due to the doxorubicin delivered was determined by MTT testing.

Table 4-2. IC_{50} and CMC values for various generations of PPO-PAMAM modified with galactose and unmodified.

Polymer	IC_{50} (mg/ml)	CMC (mg/ml)
PPO-PAMAM Gen 2.5-COOH	>10	0.07
PPO-PAMAM Gen 2.5-Galactose	0.4	0.09
PPO-PAMAM Gen 3.5-COOH	>10	0.09
PPO-PAMAM Gen 3.5-Galactose	8	0.11
PPO-PAMAM Gen 4.5-COOH	>10	0.34
PPO-PAMAM Gen 4.5-Galactose	>10	0.34

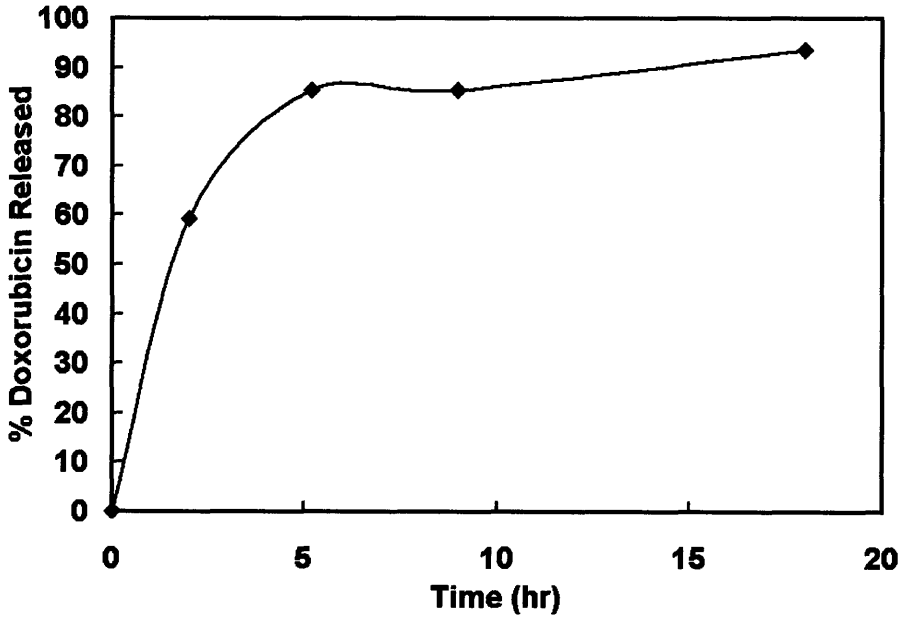

Figure 4-5. Drug release of doxorubicin from PPO-PAMAM generation 4.0 micelles in PBS at 37 °C.

Figure 4-6 is an example of the results of the targeting efficacy studies. The cell viability as compared to the negative control was plotted against the doxorubicin concentration. The IC_{50} values were determined from these plots. Figure 4-7 summarizes the results obtained for PPO-PAMAM generations 3.5 and 4.5 in comparison to bare doxorubicin. The IC_{50} of doxorubicin was 4.2 ± 2 μg/ml. For PPO-PAMAM generations 3.5 and 4.5 terminated with carboxylic acid, the IC_{50} values were not significantly different from bare doxorubicin ($p = 0.15$). For PPO-PAMAM generation 3.5 and 4.5 with galactose groups present, the IC_{50} was lower than the non-functionalized PPO-PAMAM micelles ($p << 0.05$ for both generations 3.5 and 4.5). This indicates that the addition of targeting ligand increases the uptake of doxorubicin into the HepG2 cells. For targeted generation 3.5 micelles, there was no significant decrease in cytotoxicity in comparison to bare doxorubicin ($p = 0.45$). In contrast, for PPO-PAMAM generation 4.5 modified with galactose, the IC_{50} was significantly smaller than bare doxorubicin ($p = 0.03$). It is possible that targeting with generation 4.5 micelles are much more efficient than using generation 3.5 micelles due to several factors. With generation 4.5 PPO-PAMAM's larger dendrimer head group, the end groups can sample a larger configuration space that can bind to the asialoglycoprotein receptor. Although PPO-PAMAM generations 3.5 and 4.5 had the same number of galactose attached to the dendritic block, generation 4.5 performed much better. It is possible that for generation 3.5, the density of galactose was too high, where binding to the asialoglycoprotein receptor was sterically hindered. In contrast, the generation 4.5 dendron was bigger and had a lower density of galactose, which created a more ideal configuration of galactose that would match the asialoglycoprotein binding sites. The improvement in the targeted

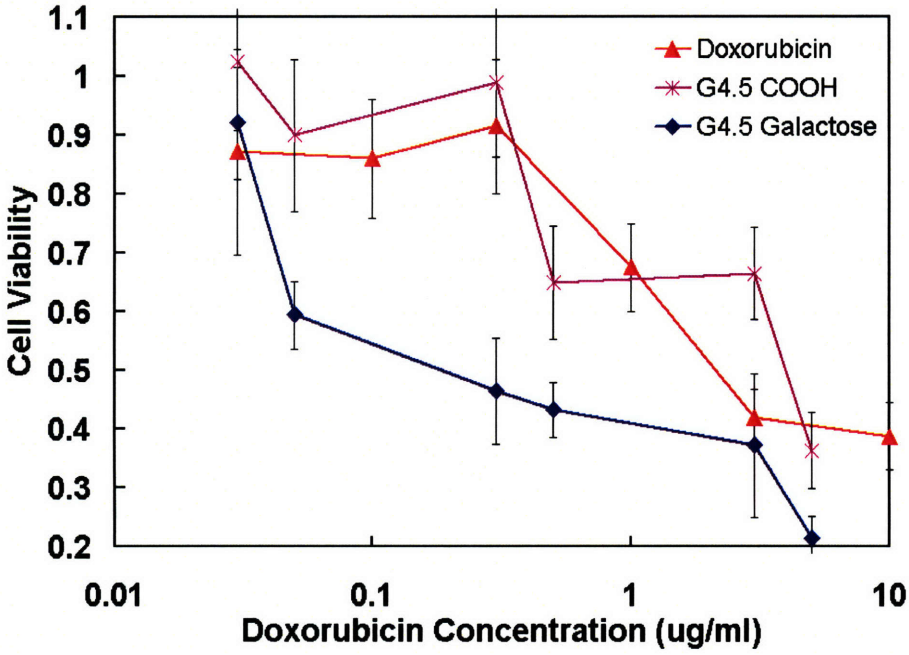

Figure 4-6. Cell viability as a function of doxorubicin concentrations via different drug delivery modalities.

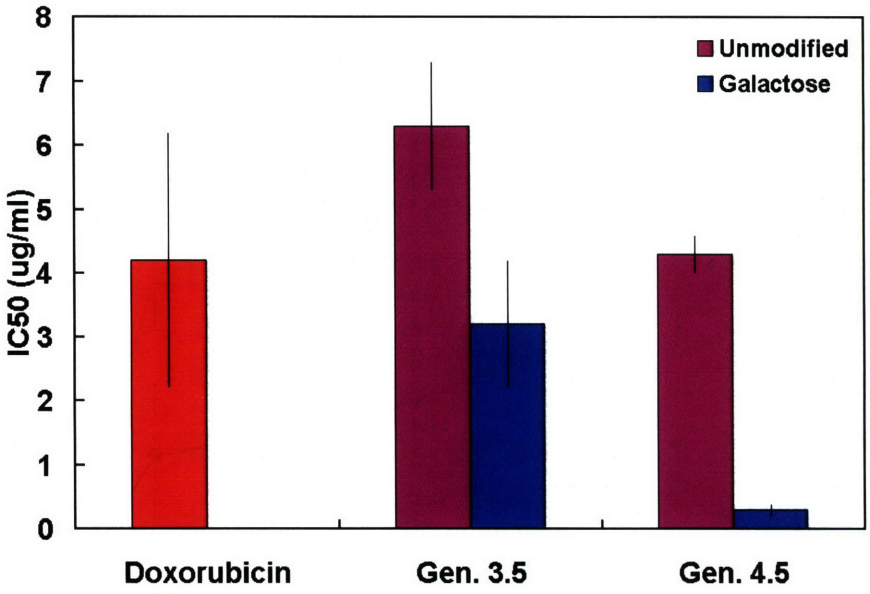

Figure 4-7. IC_{50} values of doxorubicin for either bare doxorubicin delivery or doxorubicin delivery via unmodified or galactose-functionalized micelles.

generation 4.5 polymer compared to the control polymer is approximately 15-fold. In comparison, other groups have seen improvements approximately 4 to 5 times better with galactose functionalized linear polymers over non-targeted treatments.[27, 28]

To ensure the results from the drug targeting efficacy experiments were due to specific interactions, inhibition tests were performed. Similar to the primary hepatocyte tests, varying concentrations of PPO-PAMAM generation 4.5 modified with galactose encapsulating doxorubicin were incubated with increasing amounts of asialofetuin. As shown in Figure 4-8, as the amount of asialofetuin increases, the IC_{50} of the drug delivery vehicle also increases. This indicates that the asialofetuin is blocking the binding and delivery of the galactose-modified PPO-PAMAM micelles.

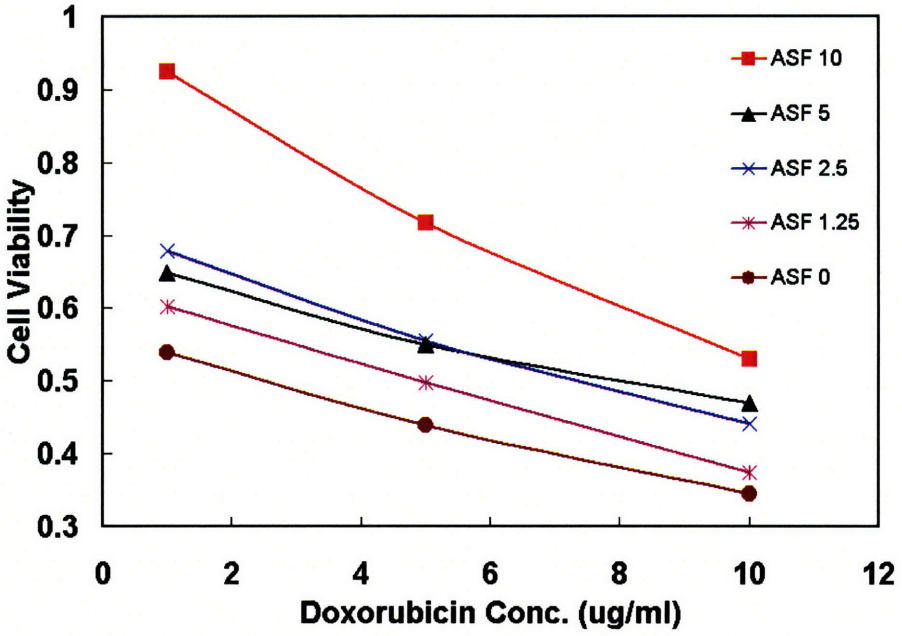

Figure 4-8. Inhibition of PPO-PAMAM generation 4.5 galactose modified micelles containing doxorubicin with various concentrations of ASF.

4.4 Conclusions

Linear-dendritic block copolymer micelles have promise as a novel method to incorporate multivalent targeting for drug delivery applications. Here we have shown that micelles composed of linear-dendritic block copolymers are the proper size to bind multivalently to lectins. Testing with primary rat hepatocytes and hepatocellular carcinoma cells have demonstrated that galactose-functionalized PPO-PAMAM micelles can bind to the asialoglycoprotein receptor specifically. Furthermore, these targeted micelles can effectively deliver drug to the cells of interest. An application that was explored in this work was delivering these micelles to cancer cells. Micelles are particularly suited for delivery to solid tumors due to the EPR effect. Their size allows for higher retention within the tumors, and with the addition of targeting ligand, retention within the tumors and delivery into cells can be more effective. Therefore, large improvements could be realized with targeted drug delivery vehicles that can bind in a multivalent fashion.

4.5 References

1. Nishiyama, N.; Kataoka, K., "Current state, achievements, and future prospects of polymeric micelles as nanocarriers for drug and gene delivery," *Pharmacology & Therapeutics*, **2006,** 112, 630-648.

2. Matsumura, Y.; Maeda, H., "A new concept for macromolecular therapeutics in cancer chemotherapy: Mechanism of tumoritropic accumulation of proteins and the antitumor agent smancs," *Cancer Res*, **1986,** 46, 6387-6392.

3. Maeda, H., "Smancs and polymer-conjugated macromolecular drugs: Advantages in cancer chemotherapy," *Adv Drug Deliv Rev*, **2001,** 46, 169-185.

4. Uwatoku, T.; Shimokawa, H.; Abe, K.; Matsumoto, Y.; Hattori, T.; Oi, K.; Matsuda, T.; Kataoka, K.; Takeshita, A., "Application of nanoparticle technology for the prevention of restenosis after balloon injury in rats," *Circ Res*, **2003,** 92, e62-e69.

5. Lukyanov, A.; Hartner, W. C.; Torchilin, V. P., "Increased accumulation of peg-pe micelles in the area of experimental myocardial infarction in rabbits.," *J. Control Release*, **2004,** 4, 187-193.

6. Ideta, R.; Tasaka, F.; Jang, W.-D.; Nishiyama, N.; Zhang, G.-D.; Harada, A.; Yanagi, Y.; Yasuhiro, T.; Takuzo, A.; Kataoka, K., "Nanotechnology-based photodynamic therapy for neovascular disease using a supramolecular nanocarrier loaded with a dendritic photosensitizer," *Nano Lett*, **2005,** 5, 2426-2431.

7. Bae, Y.; Jang, W.-D.; Nishiyama, N.; Fukushima, S.; Kataoka, K., "Multifunctional polymeric micelles with folate-mediated cancer cell targeting and ph-triggered drug releasing properties for active intracellular drug delivery," *Mol Biosyst*, **2005,** 1, 242-250.

8. Lee, R. J.; Low, P. S., "Delivery of liposomes into cultured kb cells via folate receptor-mediated endocytosis," *J. Bio. Chem.*, **1994,** 269, (5), 3198-3204.

9. Lee, R. J.; Low, P. S., "Folate-targeted liposomes for drug delivery," *J. of Liposome Research*, **1997,** 7, (4), 455-466.

10. Nasongkla, N.; Shuai, X.; Ai, H.; Weinberg, B.; Pink, J.; Boothman, D.; Gao, J., "Bioorganic chemistry: Crgd-functionalized polymer micelles for targeted doxorubicin delivery," *Angewandte Chemie, Int. Ed.*, **2004,** 43, (46), 6323-6327.

11. Xiao-Bing, X.; Abdullah, M.; Hasan, U.; Afsaneh, L., "Conjugation of arginine-glycine-aspartic acid peptides to poly(ethylene oxide)-b-poly(epsilon-caprolactone) micelles for enhanced intracellular drug delivery to metastatic tumor cells," *Biomacromolecules*, **2007,** 8, (3), 874-884.

12. Eavarone, D. A.; Yu, X.; Bellamkonda, R. V., "Targeted drug delivery to c6 glioma by transferrin-coupled liposomes," *J. Biomed. Mat. Res.*, **2000,** 51, (1), 10-14.

13. Nguyen, P. M.; Hammond, P., "Amphiphilic linear-dendritic triblock copolymers composed of poly(amidoamine) and poly(propylene oxide) and their micellar-phase and encapsulation properties," *Langmuir*, **2006,** 22, (18), 7825-7832.

14. Lundquist, J.; Toone, E., "The cluster glycoside effect," *Chem. Rev.*, **2002,** 102, 555-578.

15. Lee, Y. C., "Biochemistry of carbohydrate-protein interaction," *FASEB Journal*, **1992,** 6, 3193-3200.

16. Aoi, K.; Itoh, K.; Okada, M., "Globular carbohydrate macromolecule "sugar balls". 1. Synthesis of novel sugar-persubstituted poly(amido amine) dendrimers," *Macromolecules*, **1995,** 28, 5391-5393.

17. Woller, E.; Cloninger, M., "Mannose functionalization of a sixth generation dendrimer," *Biomacromolecules*, **2001,** 2, 1052-1054.

18. Wolfenden, M.; Cloninger, M., "Carbohydrate-functionalized dendrimers to investigate the predictable tunability of multivalent interactions," *Bioconj Chem*, **2006,** 17, 958-966.

19. Yasugi, K.; Nakamura, T.; Nagasaki, Y.; Kato, M.; Kataoka, K., "Sugar-installed polymer micelles: Synthesis and micellization of poly(ethylene glycol)-poly(d,l-lactide) block copolymers having sugar groups at the peg chain end," *Macromolecules*, **1999,** 32, 8024-8032.

20. Jule, E.; Nagasaki, Y.; Kataoka, K., "Surface plasmon resonance study on the interaction between lactose-installed poly(ethylene glycol)-poly(d,l-lactide) block copolymer micelles and lectins immobilized on a gold surface," *Langmuir*, **2002,** 18, 10334-10339.

21. Bes, L.; Angot, S.; Limer, A.; Haddleton, D., "Sugar-coated amphiphilic block copolymer micelles from living radical polymerization: Recognition of immobilized lectins," *Macromolecules*, **2003,** 36, 2493-2499.

22. Managit, C.; Kawakami, S.; Yamashita, F.; Hashida, M., "Effect of galactose density on asialoglycoprotein receptor-mediated uptake of galactosylated liposomes," *J. Pharm. Sci.*, **2005,** 94, (10), 2266-2275.

23. Gillies, E.; Fréchet, J., "Ph-responsive copolymer assemblies for controlled release of doxorubicin," *Bioconj Chem*, **2005,** 16, (2), 361-368.

24. Green, E. D.; Adelt, G.; Baenziger, J., "The asparagine-linked oligosaccharides on bovine fetuin. Structural analysis of n-glycanase-released oligosaccharides by 500-megahertz ^{1}h nmr spectroscopy.," *J. Bio. Chem.*, **1988,** 263, (34), 18253-18268.

25. Kataoka, K.; Matsumoto, T.; Yokoyama, M.; Okano, T.; Sakurai, Y.; Fukushima, S.; Okamoto, K.; Kown, G., "Doxorubicin-loaded poly(ethylene glycol)-poly(β-benzyl-$_{L}$-aspartate) copolymer micelles: Their pharmaceutical characteristics and biological significance," *J. Control Release*, **2000,** 64, (1-3), 143-153.

26. Nakanishi, T.; Fukushima, S.; Okamoto, K.; Suzuki, M.; Matsumura, Y.; Yokoyama, M.; Okano, T.; Sakurai, Y.; Kataoka, K., "Development of the polymer micelle carrier system for doxorubicin," *J. Control. Rel.*, **2001,** 74, 295-302.

27. David, A.; Kopečková, P.; Minko, T.; Rubinstein, A.; Kopeček, J., "Design of a multivalent galactoside ligand for selective targeting of hpma copolymer-doxorubicin conjugates to human colon cancer cells," *European J. of Cancer*, **2004,** 40, 148-157.

28. Zaman, N.; Tan, F.; Joshi, S.; Ying, J., "Targeted stimuli-responsive dextran conjugates for doxorubicin delivery to hepatocytes," **2005.**

CHAPTER 5: Stabilization of PPO-PAMAM Micelles

5.1 Introduction

Colloidal drug delivery vehicles must be stable in solution for intravenous use *in vivo*. It is possible for thermodynamically self-assembled structures, such as micelles or vesicles, with high critical micelle concentrations (CMC) to break apart once introduced into the bloodstream since dilution occurs and the concentration of the polymer falls below the CMC. This results in dose dumping, in which high concentrations of drug, which could be potentially toxic, are released prematurely.[1]

The most commonly used strategy to stabilize micelles is through crosslinking the colloidal particle unimers to each other. Several crosslinking strategies have been previously developed, including crosslinking the core of the micelle or crosslinking the corona of the micelles. In order to crosslink the core, there are two different schemes. The first strategy involves introducing a polymerizable group at the end of the hydrophobic block. For example, the Kataoka group synthesizes poly(lactic acid)-*b*-poly(ethyleneglycol) (PLA-PEG) block copolymers with a methacryloyl group at the end of the PLA block. The polymerization is initiated with UV irradiation.[2, 3] The other method is to incorporate crosslinkable groups along the backbone of the hydrophobic block such as poly(ethyleneoxide)-*b*-poly(butadiene)[4] and poly(2-cinnamoylethyl methacrylate)-*b*-poly(acrylic acid).[5] The only drawback to this approach is that the free volume in the core for hydrophobic drug encapsulation is reduced after crosslinking.

The other approach for directly crosslinking micelles is by crosslinking the blocks forming the corona of the micelle. The Wooley group was the first to introduce shell

crosslinked knedels. The corona of the micelles composed of poly(acrylic acid)-b-poly(styrene) are crosslinked by introducing ethylene diamine.[6-8]

Much research has been performed on stabilizing micelles with available functional groups. However, relatively few stabilization studies have been done with block copolymers that do not have any functional groups. Three alternative strategies have been explored for stabilizing pluronic systems: 1) stabilizing through direct crosslinking of the core 2) stabilizing by introducing hydrophobic additives and 3) stabilizing by physical entrapment. Direct stabilization of a pluronic was performed by introducing a hydrophobic initiator, benzoyl peroxide into the micelle cores.[9] It was found that the free volume was dramatically reduced for drug loading. Experiments using a hydrophobic additive, vegetable oil, showed increased stability of micelles below the published CMC.[9] The most developed method of stabilizing pluronic micelles is through physical entrapment. Hydrophobic acrylamide[9-11] or acrylate[12] reactive monomers are introduced into the core of the pluronic micelles by forming an emulsion. The monomers are subsequently polymerized with either a heat-activated or UV-activated initiator forming entangled polymer chains around the core of the micelle. Stability tests, either using fluorescent probes or sonication, have shown this method to work. However, *in vitro* testing of these systems has not been thoroughly performed. There has been brief work exploring doxorubicin release through insonation, but very little drug was released.[11]

In this chapter we present a method to stabilize PPO-PAMAM micelles through physical entrapment of the core with hydrophobic polymer. The stabilization is performed through a UV-initiated emulsion polymerization, and the micelles are

characterized after stabilization. The drug encapsulation and drug release behavior of these micelles are explored. Additionally, the cytotoxicity of these stabilized micelles is examined to determine whether this type of stabilization technique is viable to create long-lasting circulating nanoparticles for drug delivery.

5.2 Experimental

5.2.1 Materials

Ethyl methacrylate, benzyl methacrylate, 1,3-butanediol dimethacrylate, 2,2 diethoxyacetophenone, 1,6-diphenyl-1,3,5-hexatriene (DPH), and phosphate buffered saline (PBS) were obtained from Sigma-Aldrich and used as purchased. Water used in all experiments is 18.2 Ω MQ water.

5.2.2 Stabilization of Generation 4.5 PPO-PAMAM-COOH Micelles

Generation 4.5 PPO-PAMAM-COOH (5.0 mg/ml) was dissolved in water, which had been purged with nitrogen for 1 hour, and the pH was adjusted to 7.4 with NaOH. A dichloromethane solution containing mixtures of ethyl methacrylate, benzyl methacrylate, 1,3-butanediol dimethacrylate and 2,2 diethoxyacetophenone (1 ml) was added to the aqueous solution to create an oil/water emulsion. The emulsion was stirred vigorously overnight in a nitrogen environment in the dark to ensure the evaporation of the dichloromethane. The solutions were placed in 6-well plates (BD Falcon) and stirred while being exposed to UV light from a Blak-Ray UV lamp (Model B-100AP) for 2 hours. The solutions were lyophilized for later use.

5.2.3 Characterization of Stabilized Gen. 4.5 PPO-PAMAM-COOH Micelles

Dynamic Light Scattering. Stabilized PPO-PAMAM micelles were dissolved in either water or methanol (5 mg/ml). The solutions were filtered with 0.2 μm PTFE filters. Dynamic light scattering was performed with a Brookhaven Instruments BI-200SM Research Goniometer System. A Coherent Innova 90c (Santa Clara, CA) laser at 514.5 nm was used as the light source. The samples were measured at 90° and a quadratic cumulants analysis was used.

Fluorescence Studies. DPH dissolved in tetrahydrofuran was added to scintillation vials. The tetrahydrofuran was evaporated leaving behind 2 μg of DPH. Aqueous solutions of stabilized and non-stabilized PPO-PAMAM micelles at varying concentrations were incubated with the DPH and stirred overnight. The solutions were analyzed with a FluoroMax-2 Spectrometer (Horiba Jobin Yvon, Longjumeau France) at 25 °C. Emission spectra were recorded over a range of 300 nm to 600 nm with an excitation wavelength of 360 nm. The fluorescence intensity at 430 nm was used.

Drug Encapsulation. A solution of doxorubicin in 1 ml chloroform (1 mg/ml) and 3 molar equivalents of triethylamine were added dropwise to a vigorously stirred aqueous solution of 5 mg/ml stabilized PPO-PAMAM micelles. The solution was left open to air overnight in the dark. To remove unencapsulated doxorubicin, the solution was centrifuged at 4500 rpm for 10 minutes, and the supernatant was filtered with a 0.2 μm PTFE filter. The amount of doxorubicin encapsulated was determined with UV-vis (Agilent 8453 UV-Visible Spectrometer System, Palo Alto, CA) by measuring the

absorbance at 495 nm and compared to a standard curve (Concentration (μg/ml) = 76.728*ABS_{495}-4.9553).

Drug Release. Stabilized PPO-PAMAM micelles (5 mg/ml) encapsulating doxorubicin in PBS was placed into a dialysis bag (3500 MWCO, Spectrum Laboratories). The dialysis bag was put into 1 L of PBS at 37 °C. Some of the micelle solution was removed to measure the absorbance at 495 nm by UV-vis, and then placed back into the dialysis bag. Measurements were taken at various time points.

Cell Culture. Hepatocellular carcinoma cells (Hep G2, ATCC HB-8065) were maintained in Dulbecco's Modified Eagle Medium containing high glucose, 25 mM HEPES, but no phenol red (DMEM, Invitrogen) supplemented with 10% fetal bovine serum, 0.2 units/ml penicillin, and 100 μg/ml streptomycin. The cells were kept in an incubator at 37 °C in a 5% CO_2 atmosphere. The media was changed every two days. When the cells were confluent, trypsin-EDTA was added to the flask. After 15-30 seconds, the trypsin-EDTA was removed, and the flask was incubated at 37 °C for 10 minutes. The cells were subcultivated at a 1:6 ratio.

Cytotoxicity Experiments. Hep G2 cells were seeded into 96 well plates (BD Falcon) at a concentration of 10,000 cells/well. Varying concentrations of stabilized PPO-PAMAM micelles were incubated with the cells for 48 hours in triplicate. After 48 hours, the solution was removed, and 100 μl of complete media was added. 10 μl of MTT (5 mg/ml in PBS) was added to each well. The cells were incubated for 4 hours at 37 °C, and then 50 μl of an extraction solution (20% sodium dodecyl sulfate in 1:1 DMF/Water pH 4.7, adjusted with 0.5 N HCl/40% acetic acid) was added. The plates were left overnight at

room temperature. A BioTek Powerwave microplate reader was used to get the absorbance at 570 nm.

5.3 Results and Discussion

The linear-dendritic block copolymer composed of PPO-PAMAM forms micelles in aqueous solution with a CMC of approximately 10^{-5} M.[13] It is possible that when these micelles are injected into the blood stream, dose dumping could occur (see Figure 5-1). Therefore, a stabilization technique was explored for PPO-PAMAM-COOH Generation 4.5 micelles. The stabilization was performed by first introducing hydrophobic reactive monomers into the core of the micelles. The monomers were polymerized creating interpenetrating polymers that would entrap the hydrophobic PPO linear blocks together.

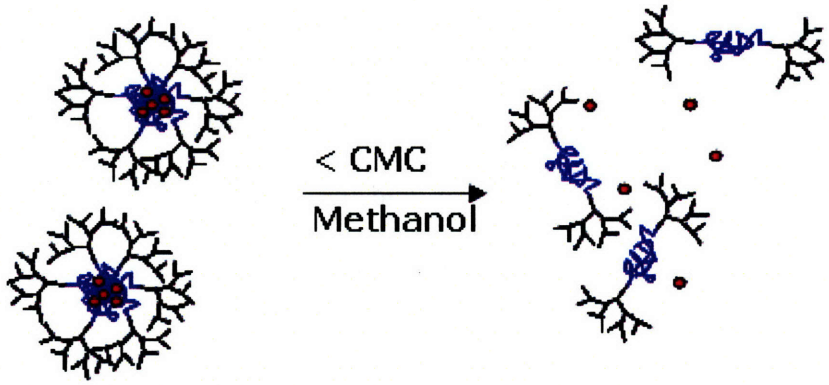

Figure 5-1. Amphiphilic linear-dendritic block copolymer micelles may break apart upon dilution at concentrations below the CMC or in solvents that solubilize both polymeric blocks.

5.3.1 Stabilization of Generation 4.5 PPO-PAMAM-COOH Micelles

The stabilization of PPO-PAMAM-COOH Generation 4.5 micelles were performed with an emulsion polymerization. Three reactive monomers, ethyl

methacrylate, benzyl methacrylate, and 1,3-butanediol dimethacrylate, were solubilized in dichloromethane and introduced into the core of the PPO-PAMAM micelles (Figure 5-2). The monomers were chosen because of their hydrophobicity, reactivity, and non-cytotoxicity.[14] Ethyl methacrylate has been used in tissue engineering applications previously.[15] Benzyl methacrylate was chosen because it had been shown previously that doxorubicin is encapsulated better in the presence of benzyl groups due to pi bond interactions between the drug and the polymer.[16] A biodegradable crosslinker was used, 1,3-butanediol dimethacrylate, to ensure that the methacrylate polymer would degrade to sizes amenable for removal by the kidneys.

The polymerization was initiated by UV-light. A hydrophobic photoinitiator, 2,2 diethoxyacetophenone, was introduced into the core of the micelles, and the emulsion solution was exposed to UV-light while being stirred. The reaction was allowed to proceed until completion and there was no discernible methacrylate odor. Furthermore, the micelles were dialyzed to remove unreacted monomer.

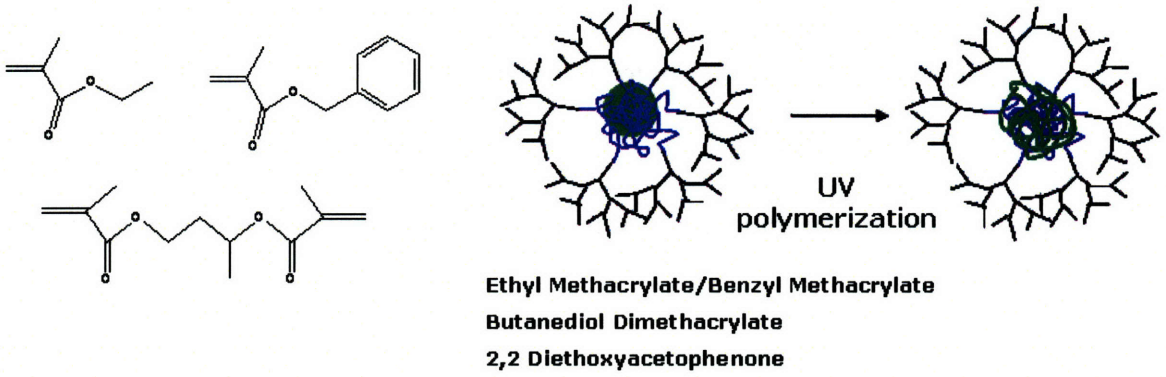

Figure 5-2. Methacrylate monomers are solubilized in the core of PPO-PAMAM micelles through an emulsion. The monomers are polymerized with a UV-initiated polymerization reaction, which forms polymers that interpenetrate the PPO core.

The emulsion polymerizations were performed with either varying ratios of ethyl methacrylate:benzyl methacrylate, methacrylate monomer:PPO-PAMAM polymer, and crosslinker:methacrylate monomer. The initiator:methacrylate monomer ratio was kept constant (see Tables 5-1 and 5-2).

5.3.2 Characterization of Stabilized Generation 4.0 PPO-PAMAM Micelles

In order to determine whether the micelles were stabilized after the emulsion polymerization, dynamic light scattering was performed on the samples (formulation B and C from Table 5-1). The stabilized micelles were measured either in water or in methanol at 2 mg/ml. Generally, for both formulations in water, the hydrodynamic diameter, D_h, was 22 nm. In contrast, the presence of micelles in methanol indicates that the nanoparticles were stabilized. In methanol, unstabilized PPO-PAMAM micelles would not form since both blocks are soluble in methanol, while stabilized micelles maintained their structure. From DLS, the stabilized micelles had a D_h of 11 nm in size. Both components of the PPO-PAMAM block copolymer are soluble in methanol, which would induce swelling of the micelles. However, from the results, the micelles collapsed. It is possible that the collapsed micelles were caused by the insolubility of the methacrylate polymer in methanol.

In addition to dynamic light scattering, fluorescence was used to gauge the stability of the stabilized micelles. Varying concentrations of aqueous solutions containing PPO-PAMAM micelles either unstabilized or stabilized were incubated with 1,6-diphenyl-1,3,5-hexatriene (DPH). DPH is only fluorescent in hydrophobic environments, and it can be detected at 430 nm. As seen in Figure 5-3, at below 1 mg/ml, the unstabilized solution has a fluorescence intensity equal to the intensity of DPH in

water, indicating that no stable micelles are being formed. In contrast, for the crosslinked micelles, the DPH fluorescence emission intensity is well above the background level of water at concentrations as low as 0.1 mg/ml. This suggests micelles are still formed at concentrations below the CMC. Furthermore, the DPH fluorescence intensity of the crosslinked micelles is higher at equivalent concentrations in comparison to the uncrosslinked micelles indicating that the crosslinked micelles are also much more hydrophobic.

Once determining that the emulsion polymerization worked to stabilize the micelles, drug encapsulation was performed to explore how the methacrylate polymer composition and concentration would affect the affinity of doxorubicin to the core. As shown in Tables 5-1 and 5-2, the amount of doxorubicin encapsulated ranged from 10 to 20 μg/ml. The amount of doxorubicin encapsulated by nonstabilized micelles was approximately 6 μg/ml. Generally, there did not seem to be an improvement in doxorubicin encapsulation. However, it was observed that during the filtration step to remove precipitated doxorubicin, there was quite a bit of polymer being removed from the solution. During the encapsulation, the polymer had precipitated out along with the drug due to increased hydrophobicity, which reduces the encapsulation efficiency. To reduce aggregation, the amount of doxorubicin was decreased, as seen in Table 5-1. The encapsulation efficiency increased for those formulations, but the doxorubicin concentration encapsulated remained within the same range. Furthermore, in Table 5-1, the amount of methacrylate monomer was reduced with each subsequent test, which resulted in an increase in the amount of doxorubicin encapsulated. This is due to less hydrophobic aggregation of the particles.

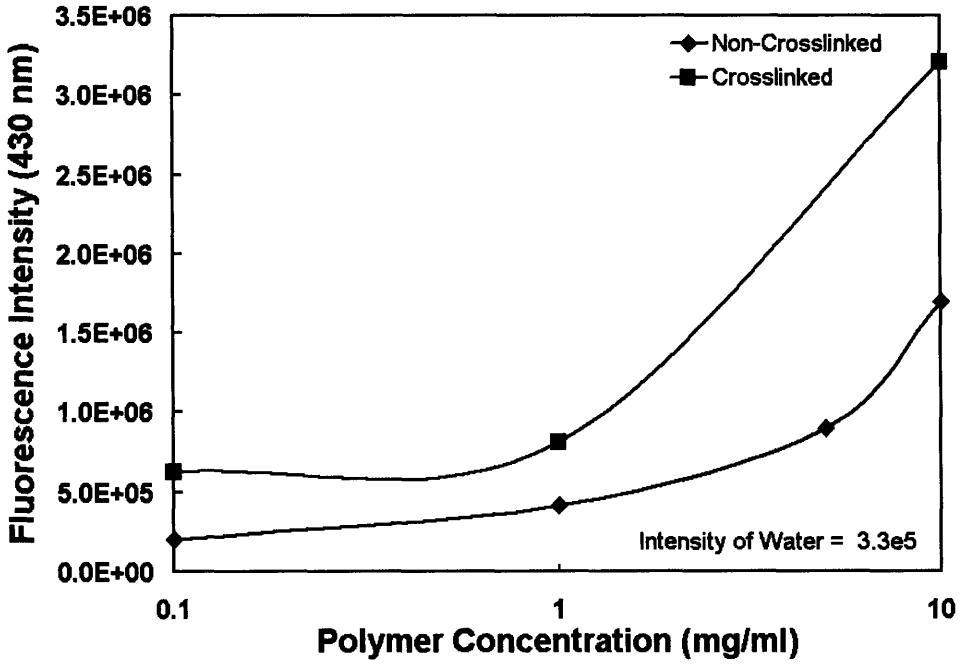

Figure 5-3. Fluorescence measurements of DPH incubated with either uncrosslinked or crosslinked PPO-PAMAM micelles.

From Table 5-2, there did not seem to be a trend in the encapsulation efficiency versus the composition and the amount of the methacrylate monomer. The formulations that encapsulated the most doxorubicin (formulations 1, 4, and 8), either were composed of 100% ethyl methacrylate, or 75% benzyl methacrylate. Generally, greater amounts of crosslinker increased encapsulation efficiency. The differences between the amount of doxorubicin are most likely not significant, and the largest factor to consider is the amount of doxorubicin added for encapsulation and aggregation of the particles during encapsulation.

A drug release study of doxorubicin from the crosslinked micelles was performed at physiological conditions, in PBS buffer and at 37 °C. The formulation used for the drug release profile was formulation B from Table 5-2. As seen from Figure 5-4, drug release is much slower with crosslinked micelles. The drug release profile is more relevant for clinical applications in comparison to the non-crosslinked micelles. The slower drug release is most likely due to the increased hydrophobicity of the core. It is also possible that increased affinity of doxorubicin to benzyl methacrylate could also have slowed down the drug release.

Cytotoxicity testing of the crosslinked micelles was also performed. Various concentrations of the crosslinked micelles (formulation B) were incubated with HepG2 cells for 48 hours. As seen in Figure 5-5, the IC_{50} is 2.2 mg/ml, which is lower than the IC_{50} of uncrosslinked micelles of >10 mg/ml. The addition of the methacrylate monomers contributed to the increased cytotoxicity of the crosslinked micelles. However, due to improved stability of the micelles, it is possible to use lower

Table 5-1. Formulation of methacrylate monomers by varying the monomer concentration.

Formulation	EMA:BMA	Monomer:Polymer	Crosslinker:Monomer	Initiator:Monomer	Conc. Doxorubicin Encapsulated (ug/ml)	Encapsulation Efficiency (%)
Control	--	--	--	--	6	14.7
A	75:25	1:10	1:10	1:100	12	29.0
B	75:25	1:20	1:10	1:100	14	36.1
C	75:25	1:40	1:10	1:100	16	39.7

Table 5-2. Various formulations of methacrylate monomers.

Formulation	EMA:BMA	Monomer:Polymer	Crosslinker:Monomer	Initiator:Monomer	Conc. Doxorubicin Encapsulated (ug/ml)	Encapsulation Efficiency (%)
1	100:0	1:20	2:10	1:100	18	14.5
2	75:25	1:20	2:10	1:100	14	11.0
3	50:50	1:20	2:10	1:100	n/a	n/a
4	25:75	1:20	2:10	1:100	20	15.7
5	0:100	1:20	2:10	1:100	10	8.1
6	50:50	1:20	1:10	1:100	13	10.4
7	50:50	1:20	5:10	1:100	14	11.4
8	25:75	1:20	5:10	1:100	18	14.0

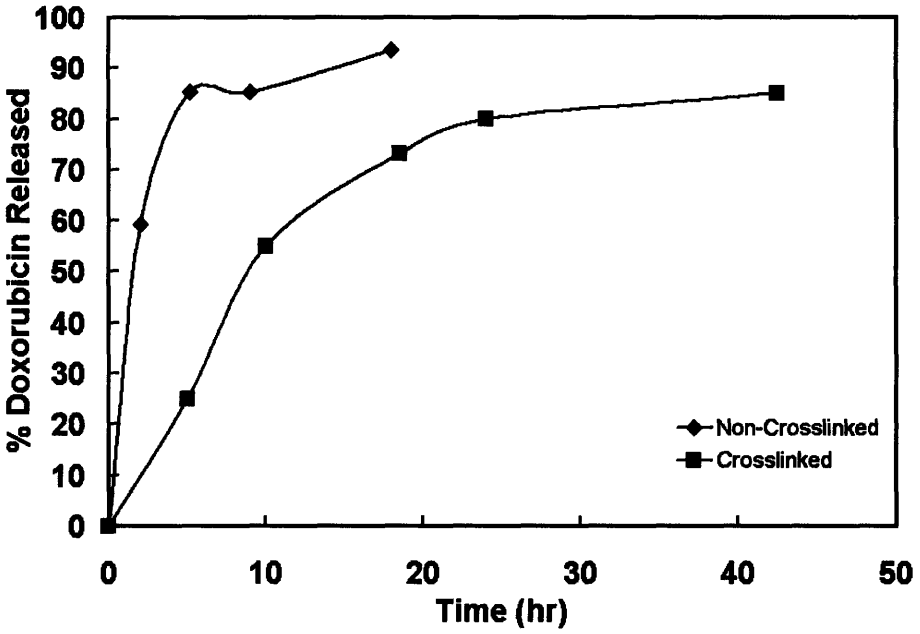

Figure 5-4. Drug release of doxorubicin from crosslinked and uncrosslinked micelles in PBS at 37 °C.

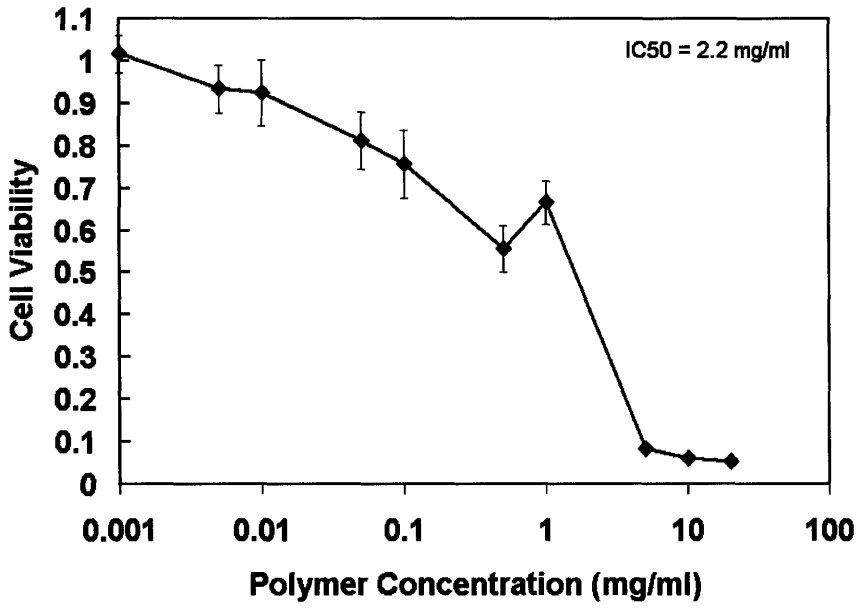

Figure 5-5. Cytotoxocity of crosslinked PPO-PAMAM micelles with HepG2 cells.

concentrations of polymer, although the limit would be around 0.1 mg/ml to 1 mg/ml as determined by Figure 5-3. At these concentrations, the cell viability is only 60 to 70%, which is not high enough to ensure biocompatibility.

5.4 Conclusions

For efficient drug drug delivery into the bloodstream, self-assembled micelles must be stable and retain drug within the core before reaching the target site. Here we have explored one method to stabilize PPO-PAMAM micelles through physical entanglement of the core with hydrophobic poly(methacrylate)-type polymers. The UV-initiated emulsion polymerization was performed on Generation 4.5 PPO-PAMAM-COOH micelles. From dynamic light scattering and fluorescence measurements, it was confirmed that the micelles were stabilized. It was also found that these micelles encapsulated drug at higher amounts than unstabilized micelles. Furthermore, due to increased hydrophobicity of the core and affinity of the drug to the core, drug release of doxorubicin was considerably slowed. However, the increased hydrophobicity of the micelles also increased the cytotoxicity of the micelles. In order to continue on with this stabilization process, less cytotoxic monomers must be used. For example, either the monomer composition could be entirely composed of methyl methacrylate or ethyl methacrylate, or a different system entirely could be used, such as acrylamide systems. The parameter space for these types of model systems need to be explored, but overall, the stabilization process looks promising if cytotoxicity can be reduced.

5.5 References

1. Lavasanifar, A.; Samuel, J.; Kwon, G., "Poly(ethylene oxide)-*block*-poly(l-amino acid) micelles for drug delivery," *Adv. Drug Delivery Rev.*, **2002,** 54, 169-190.

2. Iijima, M.; Nagasaki, Y.; Okada, Y.; Kato, M.; Kataoka, K., "Core-polymerized reactive micelles from heterotelechelic amphiphilic block copolymers," *Macromolecules*, **1999,** 32, 1140-1146.

3. Kim, J.-H.; Emoto, K.; Iijima, M.; Nagasaki, Y.; Aoyagi, T.; Okano, T.; Sakurai, Y.; Kataoka, K., "Core-stabilized polymeric micelle as potential drug carrier: Increased solubilization of taxol," *Polym. Adv. Technol.*, **1999,** 10, 647-664.

4. Won, Y.-Y.; Davis, H. T.; Bates, F. S., "Giant wormlike rubber micelles," *Science*, **1999,** 283, 960-963.

5. Henselwood, F.; Liu, G., "Water-soluble nanospheres of poly(2-cinnamoylethyl methacrylate)-*block*-poly(acrylic acid)," *Macromolecules*, **1997,** 30, 488-493.

6. Thurmond, K. B.; Kowalewski, T.; Wooley, K. L., "Water-soluble knedle-like structures: The preparation of shell-cross-linked small particles," *J. Am. Chem. Soc.*, **1996,** 118, 7239-7240.

7. Murthy, K. S.; Ma, Q.; Clark, C. G.; Remsen, E. E.; Wooley, K. L., "Fundamental design aspects of amphiphilic shell-crosslinked nanoparticles for controlled release applications," *Chem. Commun.*, **2001**, (8), 773-774.

8. Huang, H.; Remsen, E. E.; Kowalewski, T.; Wooley, K. L., "Nanocages derived from shell cross-linked micelle templates," *J. Am. Chem. Soc.*, **1999,** 121, 3805-3806.

9. Rapoport, N., "Stabilization and activation of pluronic micelles for tumor-targeted drug delivery," *Colloids and Surfaces B*, **1999,** 16, 93-111.

10. Pruitt, J. D.; Husseini, G.; Rapoport, N.; Pitt, W. G., "Stabilization of pluronic p-105 micelles with an interpenetrating network of *n-n*-diethylacrylamide," *Macromolecules*, **2000,** 33, 9306-9309.

11. Husseini, G.; Christensen, D. A.; Rapoport, N.; Pitt, W. G., "Ultrasonic release of doxorubicin from pluoronic p105 micelles stabilized with an interpenetrating network of *n-n*-diethylacrylamide," *Journal of Controlled Release*, **2002,** 83, 303-305.

12. Petrov, P.; Bozukov, M.; Tsvetanov, C. B., "Innovative approach for stabilizing poly(ethylene oxide)-b-poly(propylene oxide)-b-poly(ethylene oxide) micelles by forming nano-sized networks in the micelle," *Journal of Materials Chemistry*, **2005,** 15, 1481-1486.

13. Nguyen, P. M.; Hammond, P., "Amphiphilic linear-dendritic triblock copolymers composed of poly(amidoamine) and poly(propylene oxide) and their micellar-phase and encapsulation properties," *Langmuir*, **2006,** 22, (18), 7825-7832.

14. Yoshii, E., "Cytotoxic effects of acrylates and methacrylates: Relationship of monomer structures and cytotoxicity," *Journal of Biomedical Materials Research*, **1998,** 37, (4), 517-524.

15. Revell, P. A.; Braden, M.; Freeman, M. A. R., "Review of the biological response to a novel bone cement containing poly(ethyl methacrylate) and *n*-butyl methacrylate," *Biomaterials*, **1998,** 19, 1579-1586.

16. Kataoka, K.; Matsumoto, T.; Yokoyama, M.; Okano, T.; Sakurai, Y.; Fukushima, S.; Okamoto, K.; Kwon, G., "Doxorubicin-loaded poly(ethylene glycol)-poly(beta-benzyl-l-aspartate) copolymer micelles: Their pharmaceutical characteristics and biological significance," *J. Control Release*, **2000,** 64, (1-3), 143-153.

CHAPTER 6: Synthesis and Characterization of Poly(β-Benzyl-L-Aspartate)-b-Polyester Dendron

6.1 Introduction

Poly(ethylene glycol) (PEG) is the most commonly used polymer to attach to drugs,[1] the surface of liposomes,[2-4] or block copolymer micelles[5-7] to allow these drug delivery vehicles to circulate for longer amounts of time within the body. PEG creates a hydrodynamic barrier that prevents proteins from sticking to the surface (opsonization) of these drug delivery vehicles and their removal through phagocytosis.

Recently, in the Hammond group, a novel linear-dendritic block copolymer was developed with PEG attached to the outer surface of the dendron block.[8, 9] This block copolymer is comprised of a linear hydrophobic polypeptide block of ω-η-dodecyl-L-glutamate and a hydrophobic polyester dendritic block. The addition of the PEG groups creates an amphiphilic polymer. The design of this linear-dendritic block copolymer is quite tunable and flexible, where the alkane side groups on the polypeptide block can be changed to either introduce polymerizable groups or other groups to increase hydrophobicity or chemical affinity to certain drugs. Encapsulation of the block copolymer with triclosan showed high loading efficiency. However, attempts at loading more relevant drugs, such as doxorubicin were not successful.

Here in this chapter, a modification of the linear-dendritic block copolymer that was developed is presented, which allows for greater affinity to doxorubicin. Furthermore, the solution phase behavior of this block copolymer was examined to determine its feasibility as a drug delivery vehicle.

6.2 Experimental

6.2.1 Materials

All chemicals including p-toluenesulfonic acid, 4-di(methylamino)pyridine (DMAP), dimethoxypropane, 2,2-bis(hydroxymethyl)propionic acid (DMPA), N,N-diisopropylcarbodiimide (DIPC), N-hydroxysuccinimide (NHS), and 1,1'-carbonyldiimidazole (CDI) were obtained from either Sigma-Aldrich or VWR and were used as purchased. Some solvents, such as dichloromethane and tetrahydrofuran, when indicated by the word "dry" were obtained from a solvent still and were HPLC grade. MilliQ (18.2 MΩ) water was used in all experiments requiring water

6.2.2 Synthesis

DPTS.[10] 60 g (0.315 mol) of p-toluenesulfonic acid monohydrate was dried by azeotropic distillation (130-150°C) in a toluene solution (300ml) by using a Dean-Stark trap setup. The distillation was run for approximately 3-5 hours. 40 g of 4-(dimethylamino)pyridine (0.327 mol) was dissolved in warm dry toluene. The DMAP solution was added to the p-toluenesulfonic acid monohydrate solution and stirred until the solution reached room temperature. The crude solid was collected by suction filtration. The product was recrystallized in 1200 ml of dichloroethane.

Isopropylidene-2-2-bis(methoxy)propionic Acid. 60 g (0.447 mol) of DMPA, 82.5ml (0.671 mol) of dimethoxypropane, and 4.37 g (0.023 mol) of p-toluenesulfonic acid monohydrate were dissolved in approximately 250 ml of acetone. The mixture was stirred for 6 hours and then 6.0 ml of ammonium hydroxide was added to neutralize the solution. The solvent was removed by rotary evaporation at room temperature. The

crude product was dissolved in 800 ml of dichloromethane, and an extraction was performed with water saturated with NaCl (100 ml, 3 times). The dichloromethane was dried over magnesium sulfate. The magnesium sulfate was filtered through vacuum filtration. The solvent was removed by rotary evaporation and vacuum dried overnight to give white crystals (yield: 74%). ^{1}H NMR ($CDCl_3$): δ1.19 (s, 3H, -CH_3), δ1.43 (s, 3H, -CH_3), δ1.47 (s, 3H, -CH_3), δ3.71 (d, 2H, -CH_2O), δ4.18 (d, 2H, -CH_2O).

Benzyl-2-2-bis(methylol)propionate. 18.0 g of DMPA (0.134 mol) and 8.60 g (0.153 mol) of potassium hydroxide were dissolved into 100 ml of DMF. The reaction was stirred for 1 hour at 100 °C, and then 27.6 g (0.161 mol) of benzyl bromide was added. After 15 hr, the DMF was evaporated off by rotary evaporation at 80 °C. The residue was dissolved in 400ml of dichloromethane, and then washed with 100 ml water saturated with NaCl 3 times. The solvent was then dried over magnesium sulfate. The magnesium sulfate was removed through vacuum filtration. The solvent was removed by rotary evaporation at room temperature. The crude product was dissolved in approximately 30 ml dichloromethane and precipitated in 700 ml of hexane. After the precipitated solution was stored overnight at -40 °C, the solvent was decanted. The remaining solid was collected and vacuum dried overnight (yield: 88.2%). ^{1}H NMR ($CDCl_3$): δ1.08 (s, 3H, -CH_3), δ3.75 (d, 2H, -CH_2O), δ3.92 (d, 2H, -CH_2O), δ5.20 (s, 2H, -CH_2Ar), δ7.35 (m, 5H, -ArH).

B4 Dendron Generation 2. 10.0 g (0.0446 mol) of benzyl-2-2-bis(methylol)propionate, 16.3 g (0.0935 mol) of isopropylidene-2-2-bis(methoxy)propionic acid, and 5.25 g (0.0178 mol)of DPTS were dissolved in approximately 120.0 ml of dry dichloromethane

over nitrogen. The solution was stirred for 10 minutes, and then 15.6 ml (0.1 mol) of DIPC was added into the reaction flask dropwise. The reaction was stirred overnight. After stirring overnight, the solution was vacuum filtered to remove the precipitate. The solvent was removed by rotary evaporation leaving thick oil. The crude product was purified by column chromatography using silica gel and 1:1 ethyl acetate:hexane eluant. The product was collected and dried by rotary evaporation and then vacuum dried (yield: 84.4%). ^{1}H NMR ($CDCl_3$): δ1.09 (s, 6H, -CH_3), δ1.30 (s, 3H, -CH_3), δ1.34 (s, 6H, -CH_3), δ1.41 (s, 6H, -CH_3), δ3.58 (d, 4H, -CH_2O), δ4.10 (d, 4H, -CH_2O), δ4.34 (s, 4H, -CH_2O), δ5.16 (s, 2H, -CH_2Ar), δ7.26-7.35 (m, 5H, -ArH). TLC (silica): R_f = 0.56 (1:1 ethyl acetate:hexane).

B4-COOH Dendron Generation 2. 9.0 g of B4 was dissolved in 100 ml of ethyl acetate, and then 0.90 g of Pd/C catalyst was added to the reaction vessel. The solution was placed under 15-20 psi of hydrogen gas and shaken for 8-10 hours. The solution was vacuum filtered to remove the catalyst. The solvent was removed by rotary evaporation leaving an oily product (yield: 96.5%). ^{1}H NMR ($CDCl_3$): δ1.15 (s, 6H, -CH_3), δ1.32 (s, 3H, -CH_3), δ1.36 (s, 6H, -CH_3), δ1.42 (s, 6H, -CH_3), δ3.63 (d, 4H, -CH_2O), δ4.16 (d, 4H, -CH_2O), δ4.34 (s, 4H, -CH_2O).

B4-OH Dendron Generation 2. B4 (5.34 g, 9.95 mmol) was dissolved in 75 ml of methanol. Approximately 1.4 teaspoons of Dowex H^+ catalyst was added to the reaction vessel. After 3 hours stirring at room temperature, the Dowex H^+ was removed by vacuum filtration. The solvent was removed through rotary evaporation. The crude product was dissolved in 150 ml of ethyl acetate. An extraction was performed on the

solution with saturated salt water (70 ml, 3 times). The organic solution was dried over magnesium sulfate. The magnesium sulfate was filtered off, and the solvent was removed by rotary evaporation. The product was vacuum dried overnight producing white crystals (yield: 77.3%). ^{1}H NMR ($CDCl_3$): δ1.09 (s, 6H, -CH_3), δ1.30 (s, 3H, -CH_3), δ3.58 (d, 4H, -CH_2O), δ4.10 (d, 4H, -CH_2O), δ4.34 (s, 4H, -CH_2O), δ5.16 (s, 2H, -CH_2Ar), δ7.26-7.35 (m, 5H, -ArH).

B16 Dendron Generation 4. 12.0 g of B4-COOH (0.0269 mol), 3 g of B4-OH (6.57 mmol), and 2.7 g of DPTS (9.17 mmol) were dissolved in approximately 150 ml of dry dichloromethane. The clear solution was stirred under nitrogen for 10 minutes, and then 5.3 ml of DIPC (0.034 mol) was added dropwise. The reaction was stirred overnight. After stirring overnight, the solution was vacuum filtered to remove the precipitate. The solvent was removed by rotary evaporation at room temperature, leaving a thick oil. The crude mixture was purified with a silica gel column running an 8:2 mixture of ethyl acetate:hexane. The appropriate fractions were collected, and the solvent was removed by rotary evaporation and vacuum dried overnight (yield: 60.3%). ^{1}H NMR ($CDCl_3$): δ1.12 (s, 24H, -CH_3), δ1.18 (s, 6H, -CH_3), δ1.27 (s, 12H, -CH_3), δ1.30 (s, 3H, -CH_3), δ1.35 (s, 24H, -CH_3), δ1.41 (s, 24H, -CH_3), δ3.62 (d, 16H, -CH_2O), δ4.13-4.16 (m, 16H, -CH_2O), δ4.19-4.30 (m, 28H, -CH_2O), δ5.16 (s, 2H, -CH_2Ar), δ7.39-7.59 (m, 5H, -ArH). TLC (silica): R_f = 0.65 (8:2 ethyl acetate:hexane).

B16-COOH Dendron Generation 4. B16 dendron (13.0 g, 5.99 mmol) was dissolved in 100 ml of ethyl acetate. 1.30 g of Pd/C catalyst was added to the reaction flask. The solution was hydrogenated under 15 PSI of hydrogen gas and shaken for 8-10 hours. The

Pd/C catalyst was removed by vacuum filtration. The solvent was removed by rotary evaporation and dried overnight under high vacuum (yield: 93.6%). ^{1}H NMR ($CDCl_3$): δ1.12 (s, 24H, -CH_3), δ1.18 (s, 6H, -CH_3), δ1.27 (s, 12H, -CH_3), δ1.30 (s, 3H, -CH_3), δ1.35 (s, 24H, -CH_3), δ1.41 (s, 24H, -CH_3), δ3.62 (d, 16H, -CH_2O), δ4.13-4.16 (m, 16H, -CH_2O), δ4.19-4.30 (m, 28H, -CH_2O).

B16-NH_2 Dendron Generation 4. Dissolve 12.0 g of B16-COOH (5.77 mmol) and 1.89 g of CDI in 150ml of dry THF and stir under nitrogen gas for 4 hours. After stirring for 4 hours, add 3.07 ml of diaminopropane (0.0364 mol) into the reaction vessel as quickly as possible. The reaction was stirred for 1 day. The precipitate was removed by vacuum filtration, and the solvent was removed by rotary evaporation. The crude product was dissolved in approximately 500 ml of dichloromethane. The solution was washed first with water saturated with sodium bicarbonate (100 ml) and then with 100 ml of saturated salt water (3 times). The solvent was dried over magnesium sulfate removed through rotary evaporation. The crude product was purified with silica gel column chromatography using 9:1 CH_2Cl_2:MeOH. The solvent was removed through rotary evaporation and vacuum dried overnight (yield: 12.9%). ^{1}H NMR ($CDCl_3$): δ1.12 (s, 24H, -CH_3), δ1.27 (s, 21H, -CH_3), δ1.35 (s, 24H, -CH_3), δ1.41 (s, 24H, -CH_3), δ1.84 (m, 2H, -CH_2-), δ2.98 (m, 2H, -CH_2N-), δ3.42 (m, 2H, -CONCH_2-), δ3.62 (d, 16H, -CH_2O), δ4.14 (d, 16H, -CH_2O), δ4.25-4.35 (m, 28H, -CH_2O). TLC (silica): R_f = 0.4 (9:1 CH_2Cl_2:MeOH).

β-Benzyl-L-Aspartate N-Carboxyanhydride (BLANCA). B-benzyl-L-aspartate (3 g, 0.0134 mol) was dissolved in 30 ml of dry tetrahydrofuran. 1.40 g (4.69 mmol) of

triphosgene was added to the solution. The solution was stirred at 50 °C. After approximately half an hour, the solution was clear. The solution was stirred for a total of 3-4 hours, and then precipitated into 10 times excess hexane. The white precipitate was collected by vacuum filtration and vacuum dried for approximately 5 hours (yield: 85%, m.p. = 125-127 °C). ^{1}H NMR ($CDCl_3$): δ2.84 (d, 1H, -$COCH_2$-), δ3.08 (d, 1H, -$COCH_2$-), δ4.59 (m, 1H, -CHNH-), δ5.19 (s, 2H, -CH_2Ar), δ7.34-7.41 (m, 5H, -ArH). FTIR (cm^{-1}): 1736 (-COOBn), 1789 (-COO-), 1857 (-COO-).

Poly(β-Benzyl-L-Aspartate)-B16 (PBLA-B16). 2.45 g (9.84 mmol) of BLANCA was dissolved in 30 ml of dry dichloromethane, while in a separate reaction flask, 1.6 g (0.76 mmol) of B16-NH_2 was dissolved in 20 ml of dry dichloromethane. The B16-NH_2 solution was added to the BLANCA solution, and then 5 ml of DMF was added. The reaction was stirred at 40 °C and monitored until the anhydride peaks (1790 and 1820 cm^{-1}) disappeared. Most of the solvent was removed through rotary evaporation and then precipitated in 10 times excess diethyl ether. The precipitate, white powder, was collected through vacuum filtration and vacuum dried overnight (yield: 67%). ^{1}H NMR ($CDCl_3$): δ1.12 (m, 24H, -CH_3), δ1.25 (m, 21H, -CH_3), δ1.33 (s, 24H, -CH_3), δ1.39 (s, 24H, -CH_3), δ2.67-3.06 (bs, -$COCH_2$-), δ3.60 (d, 16H, -CH_2O), δ4.13 (d, 16H, -CH_2O), δ4.24-4.32 (m, 28H, -CH_2O), δ4.56 (m, -CHNH-), δ5.03 (bs, -CH_2Ar), δ7.22 (bs, -ArH. FTIR (cm^{-1}): 1539 (-CONH-), 1671 (-CONH-), 1737 (-COOR-).

Poly(β-Benzyl-L-Aspartate)-B16-OH (PBLA-B16-OH). 1.6 g of B16-PBLA was first dissolved in 100 ml of THF, and then methanol was added. 3 g of Dowex H^+ was added to the stirred solution. The reaction was run under argon for up to 48 hours. The reaction

was monitored by NMR. After completion, the Dowex was removed by gravity filtration. The solvent was removed by rotary evaporation and then redissolved in chloroform. An extraction was performed with saturated salt water (2 times). The organic phase was dried over magnesium sulfate and run through gravity filtration. The solvent was removed by rotary evaporation. ^{1}H NMR ($CDCl_3$): δ1.12 (m, 24H, -CH_3), δ1.25 (m, 21H, -CH_3), δ2.67-3.06 (bs, -$COCH_2$-), δ3.60 (d, 16H, -CH_2O), δ4.13 (d, 16H, -CH_2O), δ4.24-4.32 (m, 28H, -CH_2O), δ4.56 (m, -CHNH-), δ5.03 (bs, -CH_2Ar), δ7.22 (bs, -ArH).

Poly(β-Benzyl-L-Aspartate)-B16-PEG (PBLA-B16-PEG). Poly(ethylene glycol) bis(carboxymethyl) ether (10.92 g, 18.2 mmol) was dried through an azeotropic distillation with toluene via rotary evaporation. PBLA-B16-OH (2.1g, 0.38 mmol) was first dissolved in 20 ml of dry THF and then 120 ml of dry DCM was added. The dissolved solution was added to the round bottom flask containing the dried PEG, and the whole solution was stirred. 2.82 ml of DIPC (18.2 mmol) and 1.32 g (4.6 mmol) of DPTS was added. The reaction took place for 3 days at room temperature. Afterwards, insoluble precipitate was removed through gravity filtration. The organic solvent was removed by rotary evaporation, and then DI water was added to the polymer. The polymer was dialyzed for 1 day (MWCO 15k) at 4 °C, and then the solution was concentrated by ultrafiltration with a centriprep centrifugal filter (Ultracel-YM 10, Millipore). The polymer was lyophilized. Last, the polymer was dissolved in DCM and precipitated in ethyl ether. ^{1}H NMR ($CDCl_3$): δ1.12 (m, -CH_3), δ1.25 (m, -CH_3, -CH_2), δ2.67-3.06 (bs, -$COCH_2$-), δ3.65 (m, -CH_2), δ4.13 (m, -CH_2), δ4.32 (m, -CH_2O), δ4.56 (m, -CHNH-), δ5.03 (bs, -CH_2Ar), δ7.22 (bs, -ArH).

Poly(β-Benzyl-L-Aspartate)-B16-PEG-NHS (PBLA-B16-PEG-NHS). PBLA-B16-PEG (0.3 g, 6.6 μmol) was dissolved in dichloromethane (10 ml), and DIPC (0.048 ml, 0.48 mmol) and NHS (0.055 g, 0.48 mmol) were added to the stirred solution. The reaction took place for 2 days at room temperature. The solution was precipitated with ethyl ether, and the polymer was collected by centrifugation. ^{1}H NMR ($CDCl_3$): δ1.12 (m, $-CH_3$), δ1.25 (m, $-CH_3$, $-CH_2$), δ2.67-3.06 (bs, $-COCH_2-$), δ2.83 (m, $-CH_2$), δ3.65 (m, $-CH_2$), δ4.13 (m, $-CH_2$), δ4.32 (m, $-CH_2O$), δ4.56 (m, -CHNH-), δ5.03 (bs, $-CH_2Ar$), δ7.22 (bs, -ArH).

Poly(β-Benzyl-L-Aspartate)-B16-PEG-Galactose (PBLA-B16-PEG-Gal). PBLA-B16-PEG-NHS (0.2 g) was dissolved in DMSO (5 ml) and 3 times molar excess of galactosylamine was added. The reaction took place for 2 days. Afterwards, the reaction solution was diluted 10 fold with DI water and dialyzed (MWCO 3500) for 1 day at 4 °C. The solution was concentrated by ultrafiltration with a centriprep centrifugal filter (Ultracel-YM 10, Millipore) and lyophilized. ^{1}H NMR ($CDCl_3$): δ1.12 (m, $-CH_3$), δ1.25 (m, $-CH_3$, $-CH_2$), δ2.67-3.06 (bs, $-COCH_2-$), δ3.65 (m, $-CH_2$), δ3.8-δ4.0 (m, $-CH_2$), δ4.13 (m, $-CH_2$), δ4.32 (m, $-CH_2O$), δ4.56 (m, -CHNH-), δ5.03 (bs, $-CH_2Ar$), δ7.22 (bs, -ArH).

6.2.3 Polymer Characterization

During the synthesis, all of the polymers were characterized with ^{1}H NMR, which was performed on a 500 Mhz Varian Inova spectrometer. FTIR was done on a Nexus 870 FTIR Spectrometer (Thermo Nicolet, Waltham, MA). Samples were solvent cast onto KBr disks.

Fluorescence Studies. To determine the CMC of the PEG-modified linear-dendritic block copolymer, a hydrophobic fluorescent probe, pyrene, was used.[11, 12] The polymer was suspended in a stock solution containing 10^{-7} M pyrene at concentrations ranging from 1 mg/ml to 10^{-7} mg/ml and left overnight in the dark at room temperature to equilibrate. The solutions were analyzed with a FluoroMax-2 Spectrometer (Horiba Jobin Yvon, Longjumeau France) at 25 °C. Emission spectra were recorded over a range of 355 nm to 500 nm with an excitation wavelength of 333 nm, while excitation spectra were recorded from 300 nm to 360 nm with an emission wavelength of 390 nm.

Dynamic Light Scattering. Particle sizes were determined with dynamic light scattering on a Brookhaven Instruments BI-200SM Research Goniometer System. A Coherent Innova 90c (Santa Clara, CA) laser at 514.5 nm was used as the light source. Samples were at 0.5 mg/ml and were filtered with a 0.45 μm polytetrafluoroethylene (PTFE) syringe filter (Pall, East Hills, NY) and measured at 25 °C. Measurements were taken at multiple angles from 45 to 135 degrees with 15 degree increments, and autocorrelation functions were recorded at each angle. A fit of the autocorrelation function was made to Equation 6-1 to obtain Γ, the linewidth.[13] Γ was plotted against the square of the scattering vector, q. A linear least-squares fit of the data is used to obtain D_T, the translational diffusion coefficient. Equation 6-3 relates q to the scattering angle, Θ, where n is the refractive index of the solution and λ is the wavelength of the laser. The Stokes-Einstein equation, as shown in Equation 6-4, is used to relate the hydrodynamic diameter, d_h, to D_T for spheres, where k is the Boltzmann constant, T is the temperature, and η is the viscosity of the solution. It was assumed that all solutions were dilute, such

that there were no interparticle interactions and solution properties such as refractive index and viscosity were equivalent to the properties of water at 25 °C.

$$C(\tau) = Ae^{-2\Gamma t} + B \tag{6-1}$$

$$\Gamma = D_T q^2 \tag{6-2}$$

$$q = \frac{4\pi n Sin\left(\frac{\Theta}{2}\right)}{\lambda} \tag{6-3}$$

$$d_h = \frac{kT}{3\pi\eta D_T} \tag{6-4}$$

6.2.4 *In Vitro* Testing

Drug Loading Studies. An oil/water emulsion technique with a model hydrophobic drug, doxorubicin, was used for encapsulation with the copolymer. A solution of doxorubicin in chloroform (0.5 ml, 1 mg/ml) and 3 molar excess of triethylamine was slowly added to a stirring solution of 0.5 mg/ml of copolymer in water (5 ml). The solution was vigorously stirred overnight at room temperature. To remove precipitated drug, the solution was centrifuged for 10 minutes at 4500 rpm. The supernatant, which contains the drug solubilized in micelles, was filtered with a 0.20 μm PTFE syringe filter to remove insoluble doxorubicin. To remove soluble doxorubicin, the aqueous solution was purified through ultrafiltration using a centriprep centrifugal filter (Ultracel-YM 10, Millipore). Ultrafiltration was performed in triplicate. The concentration of doxorubicin in water was quantified by UV-vis (Agilent 8453 UV-Visible Spectrometer System, Palo Alto, CA) by measuring the absorbance at 495 nm and compared to a standard curve

(concentration (μg/ml) = 76.728*ABS_{495}-4.9553). The percent efficiency of encapsulation was calculated with Equation 6-5 while the weight percent of encapsulated drug was calculated with Equation 6-6.

$$\%\ \text{drug loading efficiency} = \frac{\text{weight of drug encapsulated}}{\text{total weight of drug introduced}} \times 100 \qquad (6\text{-}5)$$

$$\%\ \text{encapsulation} = \frac{\text{weight of drug encapsulated}}{\text{weight of polymer}} \times 100 \qquad (6\text{-}6)$$

Drug Release Studies. The micellar solution encapsulating doxorubicin was lyophilized and resuspended in phosphate buffered saline (PBS, pH = 7.4) and placed into 3500 MWCO dialysis bags (Spectrum Laboratories Inc., Rancho Dominguez, CA). The dialysis bag was placed in 1 liter of buffer at 37 °C, which was changed every two days to maintain sink conditions. Samples were taken out of the dialysis bag at various time intervals and analyzed by UV-vis. The volume of solution in the dialysis bags were measured at each sampling time, so that concentrations measured could be adjusted for volume changes due to osmotic pressure differences and evaporation.

Cell Culture. Hepatocellular carcinoma cells (Hep G2, ATCC HB-8065) were maintained in Dulbecco's Modified Eagle Medium containing high glucose, 25 mM HEPES, but no phenol red (DMEM, Invitrogen) supplemented with 10% fetal bovine serum, 0.2 units/ml penicillin, and 100 μg/ml streptomycin. The cells were kept in an incubator at 37 °C in a 5% CO_2 atmosphere. The media was changed every two days.

When the cells were confluent, trypsin-EDTA was added to the flask. After 15-30 seconds, the trypsin-EDTA was removed, and the flask was incubated at 37 °C for 10 minutes. The cells were subcultivated at a 1:6 ratio.

Cytoxocity Testing. Hep G2 cells were detached from the flask with trypsin-EDTA and seeded into 96-well plates (BD Falcon) at 10,000 cells/well. The cells were incubated overnight at 37 °C in a 5% CO_2 atmosphere. The media was aspirated and incubated in 100 µl of polymer dissolved in complete media for 24 to 48 hours. Afterwards, the media was removed and replaced with 100 µl of complete media. 10 µl of MTT (5 mg/ml in PBS) was added to each well. The cells were incubated for 4 hours at 37 °C, and then 50 µl of an extraction solution (20% sodium dodecyl sulfate in 1:1 DMF/Water pH 4.7, adjusted with 0.5 N HCl/40% acetic acid) was added. The plates were left overnight at 37 °C. A BioTek Powerwave microplate plate reader was used to get the absorbance at 570 nm.

6.3 Results and Discussion

A variation of a linear-dendritic block copolymer was synthesized based on previous work done in the Hammond group.[8, 9] The linear-dendritic block copolymer is composed of a linear hydrophobic block of poly(β-benzyl-L-aspartate) (PBLA), which was chosen to interact better to the encapsulated drug, doxorubicin.[14] It is thought that the aromatic groups in the PBLA would be able to interact with doxorubicin through pi-stacking interactions.[5, 15] The dendritic block is composed of a polyester dendron that is biodegradable. The addition of the PEG groups on the outer periphery of the polyester dendron transforms the block copolymer into an amphiphilic polymer. The addition of

the PEG group allows for the self-assembled nanoparticles to avoid being taken up by the reticuloendothelial system and allow for longer circulation times within the body.[16, 17]

6.3.1 Synthesis of PBLA-B16-PEG-Gal

The linear-dendritic block copolymer was synthesized first with the synthesis of the polyester dendron block through a convergent synthetic method.[18] The dendron block was then used to initiate the polymerization of the poly(amino acid) block through a pseudo-living polymerization reaction as shown in Figure 6-1.[19] The degree of polymerization was typically chosen from 10-15 monomeric units. Afterwards, the PEG groups were added to the outer dendritic block through an esterification reaction. The amount of PEG used was 3 molar excess of the reactive groups present in the dendron to ensure that the PEG attached would not react at both ends and crosslink the dendrons. The PEG groups had a degree of polymerization of approximately 10-15 units. It has been shown that densely packed PEG groups can create an effective hydrodynamic barrier against proteins.[20] Due to the hydrophobicity of the PBLA-B16-PEG polymer, any reactions in aqueous solution would be difficult. Therefore, the PBLA-B16-PEG polymer was activated first with NHS in dichloromethane, and then galactosylamine was added to the activated polymer in DMSO to be conjugated to the linear-dendritic block copolymer (Figure 6-2). The synthesis was confirmed through ^{1}H-NMR and FTIR.

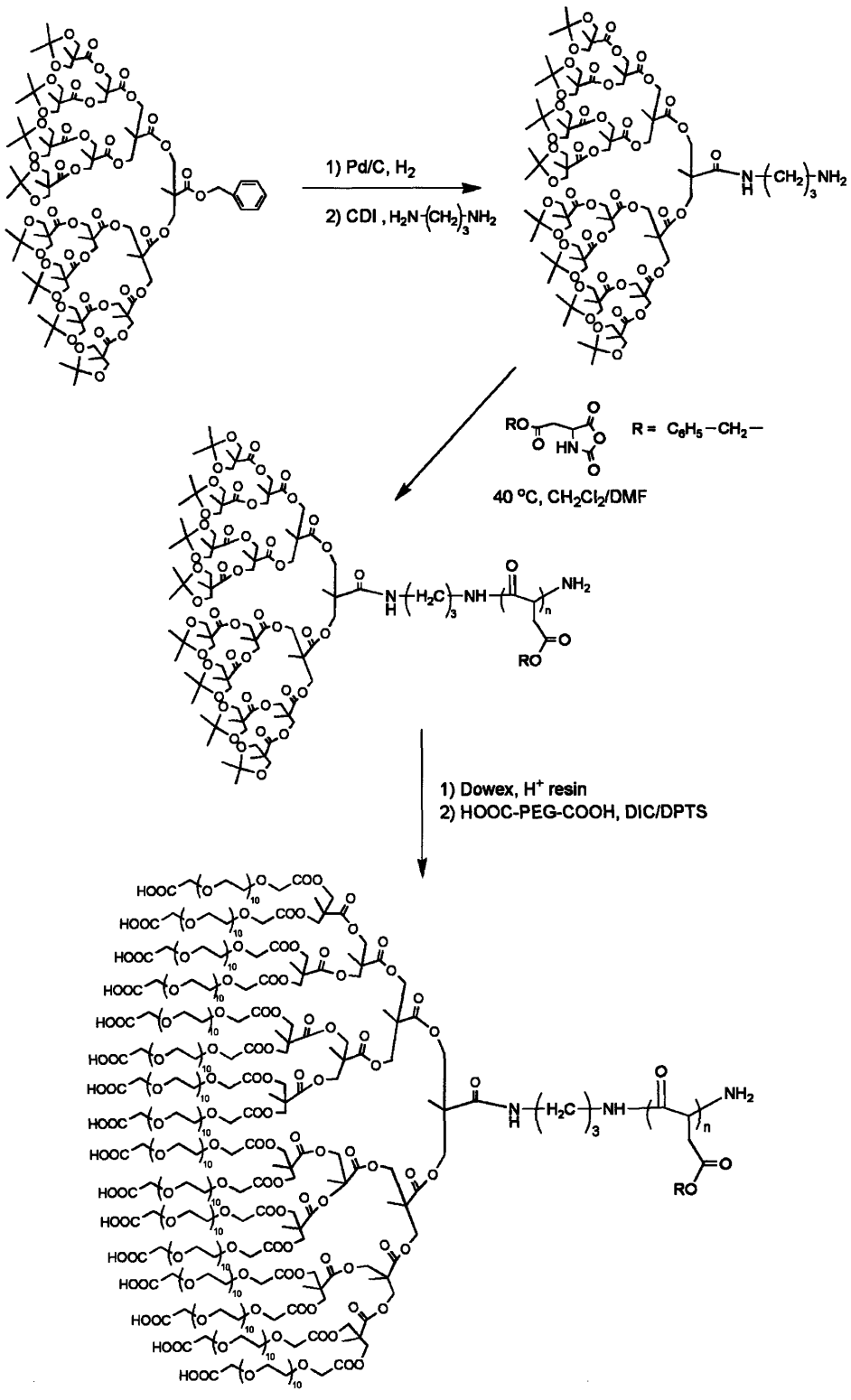

Figure 6-1. Synthesis of PBLA-B16-PEG composed of a hydrophobic linear block of poly(β-benzyl-L-aspartate), a polyester dendron, and PEG on the outer periphery of the dendron.

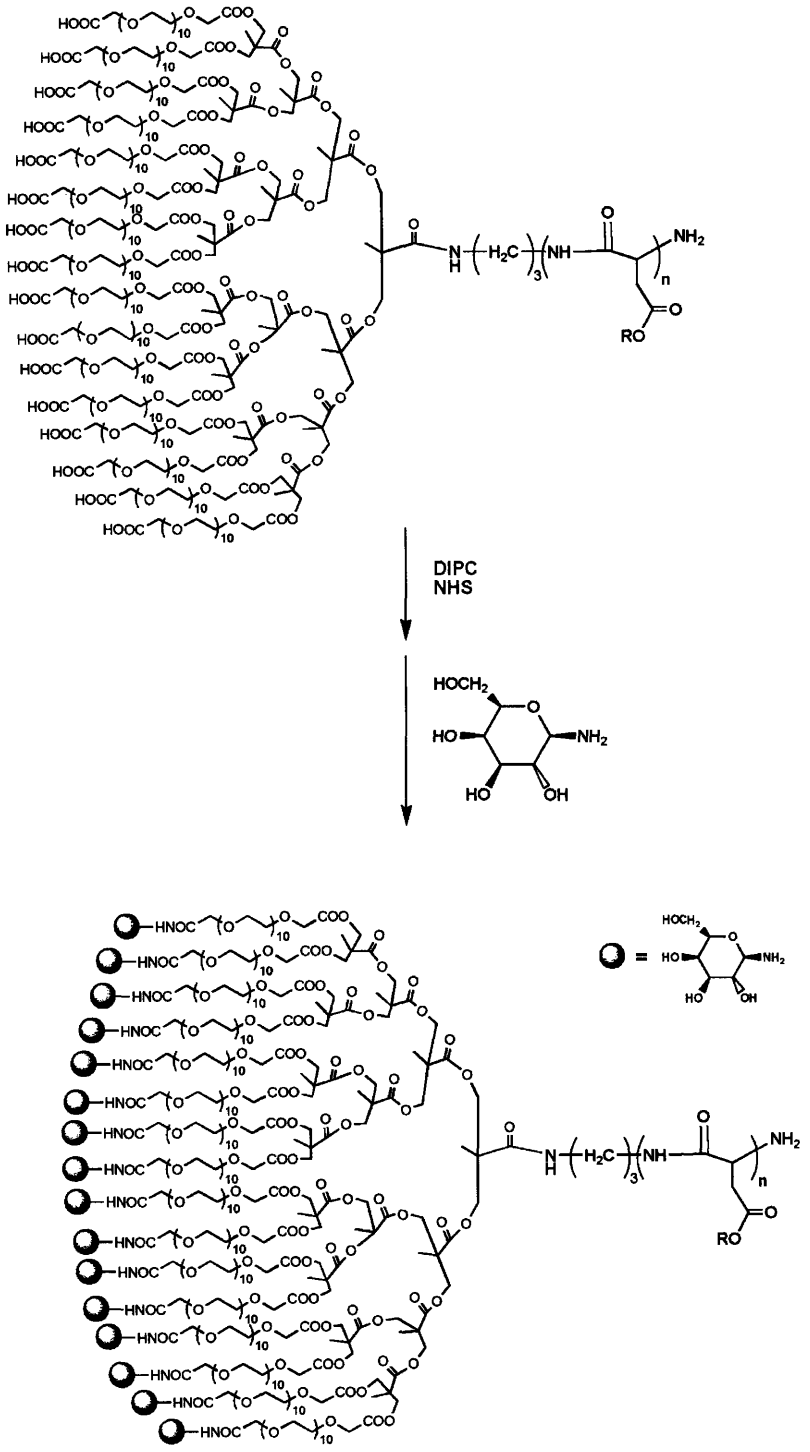

Figure 6-2. Functionalization of PBLA-B16-PEG with galactosylamine. First, the PEG group was activated with NHS, and then the polymer was further reacted with galactosylamine.

6.3.2 Characterization of PBLA-B16-PEG

To ensure that the block copolymers that were synthesized were amphiphilic and would self-assemble in aqueous solution, the critical micelle concentration (CMC) of PBLA-B16-PEG was determined through a pyrene fluorescence method. Constant concentrations of pyrene were incubated with varying concentrations of polymer in DI water. The ratio of the emission intensities at 373 and 393 nm were plotted as a function of the polymer concentration to determine the CMC as shown in Figure 6-3. It was determined that the CMC was 3.6e-8 M (5.5e-4 mg/ml), which is orders of magnitude lower than the CMC found from pluronics[21] and from the CMC of PPO-PAMAM linear-dendritic block copolymers.[22] This indicates that these linear-dendritic block copolymers would be more stable when introduced into the body for *in vivo* applications. In addition to the extremely low CMC values found, the crystallinity and the low T_g of the PBLA blocks thermodynamically slow down the disintegration of the micelles formed upon dilution in the body.[12, 23]

To further probe the self-assembly behavior of PBLA-B16-PEG, dynamic light scattering was used. Aqueous solutions of PBLA-B16-PEG were measured, and it was found that the average hydrodynamic diameter of the aggregates formed were 70 ± 6 nm. The correlation function of the samples displayed only one decay time, indicating that the samples were monodisperse.[13] The hydrodynamic diameter indicates the presence of micellar structures that may not necessarily be spherical in nature, but more cylindrical. To produce smaller structures that are spherical, either the size of the linear block would have to be reduced, or the size of the PEG groups would have to be increased according to the Israelachvili model.[24]

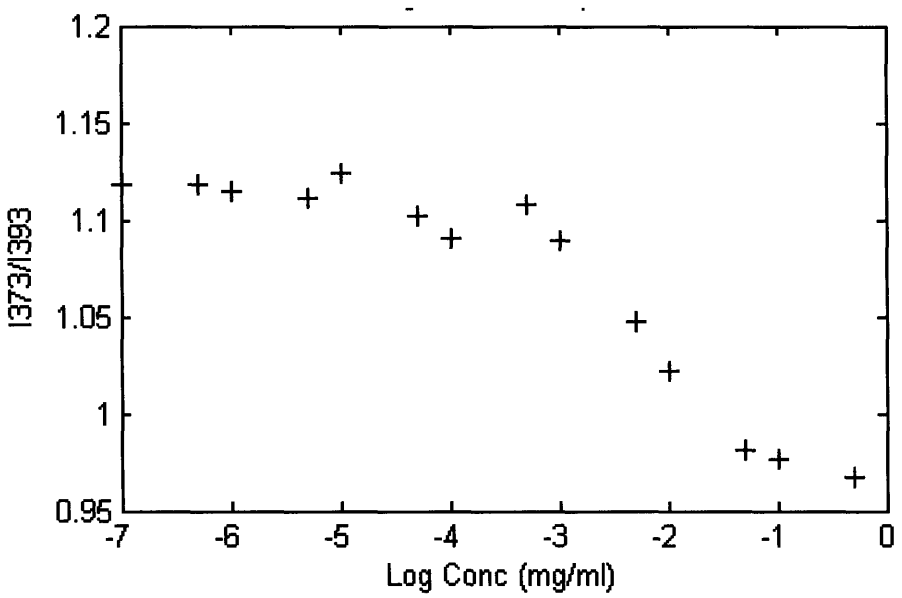

Figure 6-3. Ratio of the emission intensity of pyrene at 373 nm and 393 nm at various concentrations of PBLA-B16-PEG. The CMC is determined as 3.6e-8 M (5.5e-4 mg/ml).

6.3.3 *In Vitro* Testing

Doxorubicin was loaded into PBLA-B16-PEG micelles through an oil/water emulsion technique. Due to the increased hydrophobicity of the polymer, the polymer concentration and the amount of doxorubicin added was critical to ensure that the polymer and drug would not aggregate. Aggregation and precipitation would reduce the loading efficiency. It was determined that the loading efficiency was 36 ± 6% with a loading capacity of 6 w/w%. In comparison the PBLA-PEG block copolymers, the loading capacity of the linear-dendritic block copolymers was lower. The PBLA-PEG block copolymers had a loading efficiency ranging from 39-43 w/w% and a loading capacity of 12-22 w/w%.[25] The difference could be due to the purification procedure, where the linear-dendritic block copolymers were filtered before ultrafiltration. During filtration, polymeric aggregates containing doxorubicin were removed, which would lower the drug loading capacity value. Additionally, the presence of aggregates in the solution could potentially stabilize the formulation, creating less destabilization and drug release during the ultrafiltration step.

A drug release study on the linear-dendritic block copolymer micelles encapsulating doxorubicin was performed. The test was done in a sink of PBS at 37 °C to simulate physiological conditions. As seen in Figure 7-4, there were two phases of drug release, with an initial burst and then delayed drug release which was more linear in nature. The $t_{1/2}$ of release was approximately 15 hours, which indicates that these nanoparticles interact with doxorubicin better than PPO-PAMAM micelles either through greater hydrophobic interaction or chemical affinity between the aromatic rings present in

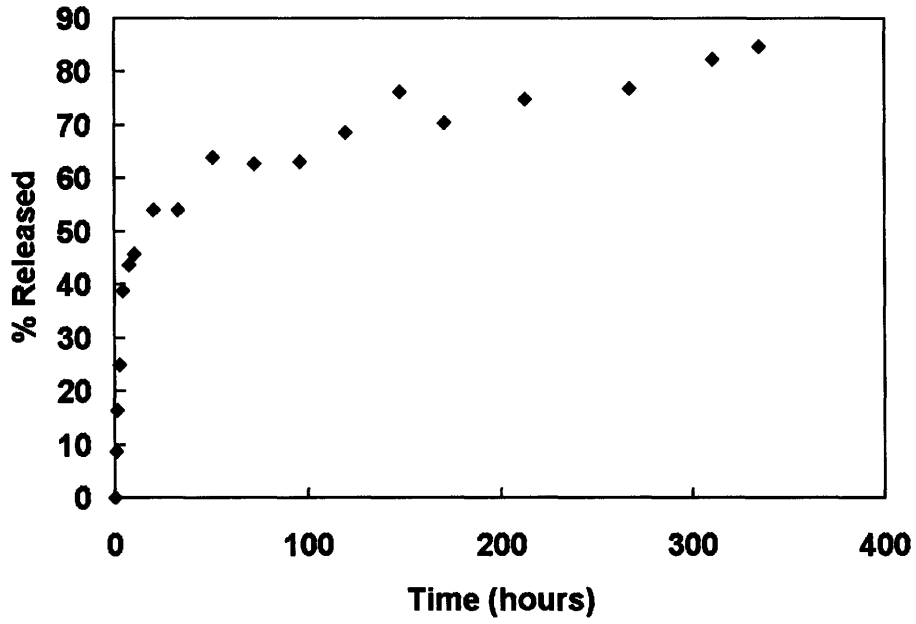

Figure 6-4. Release profile of doxorubicin from PBLA-B16-PEG micelles in PBS at 37 °C.

the drug and polymer structure. Furthermore, the overall release of the drug was sustained for a period of weeks, which is relevant for clinical applications.

PBLA-B16-PEG was tested for cytotoxicity on HepG2 cells. Figure 6-5 indicates that the polymer is not toxic for a large range of concentrations, up to the solubility limit of the polymer in PBS. Most likely, the presence of the PEG groups makes the polymers less toxic.

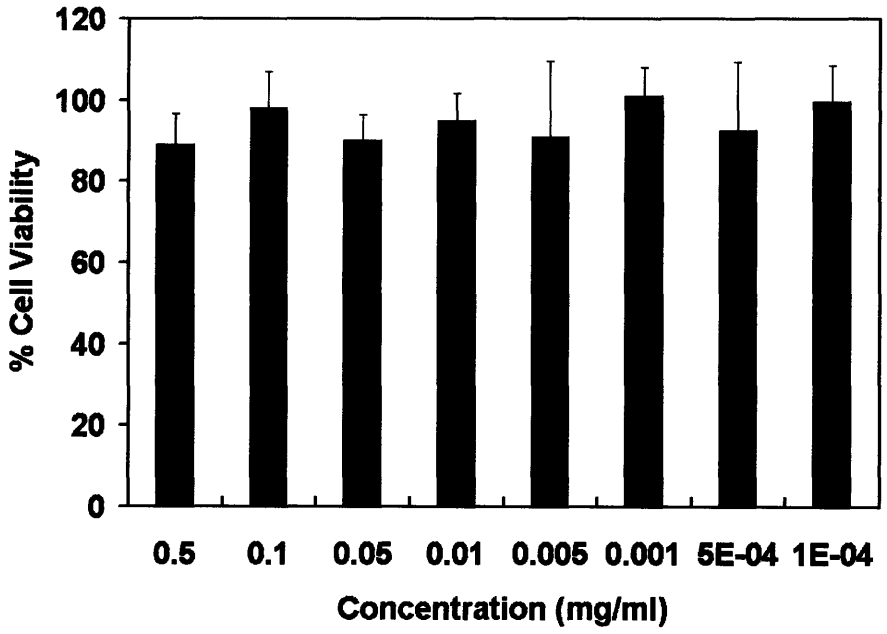

Figure 6-5. Cytotoxicity of PBLA-B16-PEG on HepG2 hepatocellular carcinoma cells. The polymer is non-toxic over a large concentration range.

6.4 Conclusions

A linear-dendritic block copolymer, PBLA-B16-PEG, has been synthesized and characterized. This block copolymer composed of a linear hydrophobic polyaspartate-based polypeptide, a polyester dendron, and PEG groups forms stable micelles in solution. The CMC is in the 10^{-8} M region. Furthermore, the hydrophobic block has a

low T_g. Therefore, when administered into the body, the block copolymer micelles would be less apt to break apart, and the kinetics of the micelle destabilization would also be slow. The block copolymer also exhibited good *in vitro* properties, with its ability to encapsulate doxorubicin and had an extended release profile. Moreover, the polymer was not toxic, and would be degradable at the ester bonds through hydrolysis and at the amide bonds through enzyme-catalyzed hydrolysis. The block copolymer was also functionalized with a targeting ligand, galactose. The reactivity of the block copolymer allows for functionalization with other targeting ligands as well. This linear-dendritic block copolymer offers a lot of flexibility in tuning the polymer for a specific drug delivery purpose. Additionally, with the presence of the PEG groups on the outer periphery of the nanoparticles formed, the block copolymer micelles would be able to circulate in the body for longer amounts of time, to allow for accumulation at solid tumor sites through the EPR effect and also through receptor binding. The linear-dendritic block copolymer synthesized has a lot of promise as a targeted drug delivery vehicle, especially in the area of multivalent targeting.

6.5 References

1. Greenwald, R. B.; Choe, Y. H.; McGuire, J.; Conover, C. D., "Effective drug delivery by pegylated drug conjugates," *Adv. Drug Del. Rev.*, **2003,** 55, 217-250.

2. Allen, T.; Hansen, C.; Martin, F.; Redemann, C.; Yau-Young, A., "Liposomes containing synthetic lipid derivatives of poly(ethylene glycol) show prolongs circulation half-lives *in vivo*," *Biochim. Biophys. Acta*, **1991,** 1066, 29-36.

3. Klibanov, A. L.; Maruyama, K.; Torchilin, V. P.; Huang, L., "Amphipathic polyethyleneglycols effectively prolong the circulation time of liposomes," *FEBS Lett.*, **1990,** 268, 235-237.

4. Gabizon, A., "Stealth liposomes and tumor targeting: One step further in the quest for the magic bullet," *Clinical Cancer Res.*, **2001,** 7, (2), 223-225.

5. Nakanishi, T.; Fukushima, S.; Okamoto, M.; Suzuki, M.; Matsumura, Y.; Yokoyama, M.; Okano, T.; Sakurai, Y.; Kataoka, K., "Development of the polymer micelle carrier system for doxorubicin," *J. Controlled Release*, **2001,** 74, 295-302.

6. Shuai, X.; Ai, H.; Nasongkla, N.; Kim, S.; Gao, J., "Micellar carriers based on block copolymers of poly(ϵ-caprolactone) and poly(ethylene glycol) for doxorubicin delivery," *J. Controlled Release*, **2004,** 98, 415-426.

7. Lo, C.-L.; Huang, C.-K.; Lin, K.-M.; Hsiue, G.-H., "Mixed micelles formed from graft and diblock copolymers for application in intracellular drug delivery," *Biomaterials*, **2007,** 28, 1225-1235.

8. Tian, L.; Hammond, P. T., "Comb-dendritic block copolymers as tree-shaped macromolecular amphiphiles for nanoparticle self-assembly," *Chem. Mater.*, **2006,** 18, (17), 3976-3984.

9. Tian, L.; Nguyen, P.; Hammond, P. T., "Vesicular self-assembly of comb-dendritic block copolymers," *Chem. Commun.*, **2006,** 33, 3489-3491.

10. Moore, J. S.; Stupp, S. I., "Room temperature polyesterification," *Macromolecules*, **1990,** 23, 65-70.

11. Kalyanasundaram, K.; Thomas, J., "Environmental effects on vibronic band intensities in pyrene monomer fluorescence and their application in studies of micellar systems," *J. Am. Chem. Soc.*, **1977,** 99, 2039.

12. Kataoka, K.; Kwon, G.; Yokoyama, M.; Okano, T.; Sakurai, Y., "Block copolymers as vehicles for drug delivery," *J. Controlled Release*, **1993,** 24, 119-132.

13. Tscharnuter, W., *Photon correlation spectroscopy in particle sizing*. John Wiley & Sons Ltd: Chichester, 2000; p 5469-5485.

14. Kataoka, K.; Matsumoto, T.; Yokoyama, M.; Okano, T.; Sakurai, Y.; Fukushima, S.; Okamoto, K.; Kwon, G., "Doxorubicin-loaded poly(ethylene glycol)-poly(beta-benzyl-l-aspartate) copolymer micelles: Their pharmaceutical characteristics and biological significance," *J. Control Release*, **2000,** 64, (1-3), 143-153.

15. Fukushima, S.; Machida, M.; Akutsu, T.; Shimizu, K.; Tanaka, S.; Okamoto, K.; Mashiba, H.; Yokoyama, M.; Okano, T.; Sakurai, Y.; Kataoka, K., "Roles of adriamycin and adriamycin dimer in antitumor activity of the polymeric micelle carrier system," *Coll and Surfaces B: Biointerfaces*, **1999,** 16, (227-236).

16. Woodle, M. C.; Lasic, D. D., "Sterically stabilized liposomes," *Biochim. Biophys. Acta*, **1992,** 1113, 171-199.

17. Lasic, D. D.; Martin, F.; Gabizon, A.; Huang, S. K.; Papahadjopoulos, D., "Sterically stabilized liposomes: A hypothesis on the molecular origin of the extended circulation times.," *Biochim. Biophys. Acta*, **1991,** 1070, 187-192.

18. Ihre, H.; Hult, A.; Fréchet, J. M. J.; Gitsov, I., "Double-stage convergent approach for the synthesis of functionalized dendritic aliphatic polyesters based on 2,2-bis(hydroxymethyl)propionic acid," *Macromolecules*, **1998,** 31, 4061-4068.

19. Odian, G., *Principles of polymerization*. 4th ed.; Wiley-Interscience: Hoboken, 2004; p 578-580.

20. Unsworth, L. D.; Sheardown, H.; Brash, J. L., "Polyethylene oxide surfaces of variable chain density by chemisorption of peo-thiol on gold: Adsorption of proteins from plasma studied by radiolabelling and immunoblotting," *Biomaterials*, **2005,** 26, 5927-5933.

21. Kozlov, M. Y.; Melik-Nubarov, N. S.; Batrakova, E. V.; Kabanov, A. V., "Relationship between pluronic block copolymer structure, critical micellization concentration and partitioning coefficients of low molecular mass solutes," *Macromolecules*, **2000,** 33, 3305–3313.

22. Nguyen, P. M.; Hammond, P., "Amphiphilic linear-dendritic triblock copolymers composed of poly(amidoamine) and poly(propylene oxide) and their micellar-phase and encapsulation properties," *Langmuir*, **2006,** 22, (18), 7825-7832.

23. Kwon, G.; Naito, M.; Kataoka, K.; Yokoyama, M.; Sakurai, Y.; Okano, T., "Block copolymer micelles as vehicles for hydrophobic drugs," *Coll and Surfaces B: Biointerfaces*, **1994,** 2, 429-434.

24. Israelachvili, J. N., *Intermolecular and surface forces*. 2nd ed.; Academic Press: New York, 1991.

25. Kwon, G.; Naito, M.; Yokoyama, M.; Okano, T.; Sakurai, Y.; Kataoka, K., "Block copolymer micelles for drug delivery: Loading and release of doxorubicin," *J. Controlled Release*, **1997,** 48, 195-201.

CHAPTER 7: Incorporation of PPO-PAMAM Linear-Dendritic Block Copolymer Micelles Into Extended Release Antibacterial Layer-by-Layer Films

7.1 Introduction

The layer-by-layer (LbL) method of assembling thin films has drawn a great deal of attention because of its versatility[1] and potential use in many applications, including cell patterning,[2] controlled drug release,[3] and biosensors.[4] In this chapter we demonstrate the use of charged linear-dendritic block copolymer micelles as a building block for LbL films, providing a matrix for the incorporation of hydrophobic drug into ionically crosslinked LbL assemblies at high concentrations. The micelles remain intact within the LbL films, providing hydrophobic microenvironments. Drug release lasts over a clinically relevant period of weeks in an active form, which has previously not been demonstrated with hydrophobically encapsulated molecules in LbL films.

LbL films are easily fabricated by exposing charged substrates sequentially to baths of oppositely charged polyions; in some cases, hydrogen bonding acceptors and donors are also used.[5] The films are able to conformally coat substrates of nearly any geometry, making them useful as coatings for medical devices such as implants or stents. Several common strategies for using LbL films for drug delivery have been demonstrated. The first general area involves coating microparticles with an LbL film. The film can act as a diffusion barrier when coating a hydrophobic drug microparticle,[3] or hollow LbL microcapsules can be fabricated and loaded with water-soluble drug.[6, 7] These types of LbL systems rely on diffusion of the drug through the LbL layer, which is often only slowed down by a matter of hours. An alternative approach is to integrate the

drug directly into the thin films during the fabrication process. For example, our group has previously shown that LbL films composed of drug and a degradable polymer, can be used to release the drug gradually as the film comes apart.[8, 9] The drawback to using the drug as one of the building blocks of the film is that it has only included drugs which are polyionic and water soluble. This method excludes drugs without the necessary functionality and water solubility, such as small, hydrophobic molecules. A solution to this limitation has been offered by the use of prodrugs to integrate hydrophobic molecules into the LbL assembly.[10] However there are also limitations with this approach. Drugs with no functional groups may not be used, and for drugs with multiple functional groups, the synthesis of the prodrug would require many steps. Another method to incorporate hydrophobic drugs is to use porous multilayers to take up hydrophobic molecules and then release them in aqueous solution.[11] A disadvantage of this approach is that it requires the use of organic solvents to dissolve the drug, which may still be present in the films and cause toxicity. Furthermore, the amount of drug loaded may be limited by diffusion and poor interaction and wetting of the multilayer with the organic solvent. Interactions between the drug and the multilayer, such as electrostatics or other secondary forces may also prevent the drug from being released.

Our approach to incorporating drug molecules that would otherwise exhibit poor integration into LbL films is to use amphiphilic block copolymers. This method is more universal than other previous approaches because amphiphilic block copolymers, which self-assemble in solution, can be designed to solubilize and encapsulate any hydrophobic molecule within the hydrophobic core of the self-assembled structure. Encapsulation can be achieved at high concentrations. Incorporation into micelles provides an environment

isolated from the rest of the film, which protects the drug from adversely interacting with other components of the LbL structure. The only requirement is that the hydrophilic block be polyionic; thus, this approach is quite flexible and can be adapted to include a number of biocompatible materials. The hydrophobic block can be tuned to interact with the encapsulated hydrophobic drug for greater encapsulation efficiency and for adjustment of release times. The amount of drug in the film can be adjusted either by the amount of drug encapsulated by the block copolymer micelles or by altering how many bilayers of polymer are deposited.

Other groups have explored incorporating charged micelles into LbL assemblies. Some of these micelles need to be stabilized through crosslinking prior to assembling in a LbL film,[12, 13] while others are directly incorporated into the film with no modification.[14-16] There are limitations to these films, as the release times of representative hydrophobic molecules in all of these systems were quite short, on the order of several minutes for 10 to 16 bilayer films.[14, 16]

This early progress, though encouraging, did not indicate a route toward greater control of the drug release profile or delivery times. This study is the first to investigate LbL/micelle thin films as a viable sustained release drug delivery device. We have integrated linear-dendritic block copolymer micelles encapsulating a hydrophobic antibacterial drug into LbL films. Dendritic polymers have recently been shown to have potential for use as biomaterials and as drug delivery agents.[17-19] Our group has recently synthesized a linear-dendritic block copolymer,[20] using hydrophilic poly(amidoamine) (PAMAM) dendritic blocks, and a hydrophobic poly(propylene oxide) (PPO) linear block. The copolymer assembles in water such that the linear block forms the

hydrophobic interior of the micelle, with the positively charged dendrons on the exterior. It has been shown that the polymers form micelles in solution and have a significantly higher encapsulation capacity for a model hydrophobic bactericide, triclosan, over pluronic micelles.[20] These micelles incorporated into the LbL films have a long release time, and the drug released is still active, providing the possibility for the film to be utilized as an antibacterial coating for implants.

7.2 Experimental

7.2.1 Materials

Poly(acrylic acid) (PAA) (M_w ~ 90,000, 25% aqueous solution) was obtained from Polysciences. Pyrene (sublimed, 99%) and 5-chloro-2-(2,4-dichlorophenoxy)phenol (triclosan, ≥97.0% purity) were purchased from Sigma-Aldrich and used as received. Quartz slides were obtained from Chemglass and silicon was purchased from Silicon Quest International.

7.2.2 Synthesis of PPO-PAMAM

The synthesis and complete characterization of the amphiphilic ABA linear-dendritic block copolymers have been previously published.[20] Briefly, the synthesis begins with poly(propylene glycol) bis(2-aminopropyl ether) (α,ω-amino-PPO). The poly(amidoamine) (PAMAM) blocks are synthesized from the amine ends of the PPO with alternating reaction steps of 1) Michael addition with methyl acrylate, and 2) exhaustive amidation with ethylenediamine. Generation 4.0 PPO-PAMAM block copolymers with 16 amine ends present on each dendritic block were synthesized. The synthesis of the block copolymer was confirmed through ^{1}H-NMR and FTIR.

Drug Loading. An oil/water emulsion technique was utilized to load a model hydrophobic drug, triclosan, into preformed PPO-PAMAM micelles. Triclosan, dissolved in dichloromethane, was added dropwise to an aqueous solution of PPO-PAMAM. The emulsion was vigorously stirred and left open overnight for the dichloromethane to evaporate. The final concentrations of the PPO-PAMAM and triclosan in aqueous solution were 19 mg/ml and 5 mg/ml, respectively. The solution obtained was centrifuged at 4500 rpm for 10 minutes. Any undissolved triclosan was removed with a 0.45 μm PTFE syringe filter. To quantify the amount of drug in solution for subsequent studies, the solution was analyzed by an Agilent 8453 UV-Visible Spectrometer System (Palo Alto, CA). The characteristic absorbance of triclosan was measured at 281 nm. For concentrated solutions of triclosan encapsulated by PPO-PAMAM micelles, the solution was diluted with methanol in a 1:9 ratio. A calibration curve applicable in the 0-100 μg/ml range for triclosan in 1:9 water:methanol mixtures was used to determine the concentration ($Y = 60.90*X - 1.22$, $r^2 = .9973$).

7.2.3 LbL Film Formation

LbL films were assembled with a modified programmable Carl Zeiss HMS slide stainer. The films were constructed on quartz or silicon substrates approximately 1 cm by 2 cm in size. The substrate was dipped into a PPO-PAMAM aqueous solution (1.9 mg/ml, with or without drug encapsulated) adjusted to pH 5.5 with dilute HCl for 10 minutes and then subsequently rinsed off in three water baths for 0.5, 1.0, and 1.0 minutes, respectively. Next, the substrate was dipped into an aqueous solution of PAA adjusted to pH 5.0 with dilute HCl (20 mM based on repeat unit) for 10 minutes. The substrate was rinsed off in three water baths for 0.5, 1.0, and 1.0 minutes, respectively.

The dipping process was repeated until the number of layer pairs desired was achieved. For LbL films containing pyrene, PPO-PAMAM micellar aqueous solutions were incubated with 10^{-7} M pyrene overnight before being used for film formation.

7.2.4 LbL Film Characterization

Film thickness was measured with a Tencor P-10 Surface Profilometer. For film fluorescence studies, the LbL films were formed on a quartz substrate, and a FluoroMax-2 Spectrometer (Horiba Jobin Yvon) was used to obtain emission spectra. The emission spectra were recorded over a range of 355 nm to 500 nm with an excitation wavelength of 333 nm. For detection of triclosan deposited in the LbL films on a quartz substrate, an Agilent 8453 UV-Visible Spectrometer System was used.

Grazing Incidence Small Angle X-ray Scattering (GISAXS). LbL films of PAA and PPO-PAMAM with or without triclosan on silicon substrates were examined with GISAXS performed at the G1 beamline at the Cornell High Energy Synchotron Source (CHESS). The wavelength of the incident beam was 1.239Å, the sample to detector distance was 1122 mm, and a 2-D area detector was used for data collection.[21]

Thermogravimetric Analyzer (TGA). LbL films were deposited onto polypropylene substrates. Films composed of PAA and PPO-PAMAM with or without triclosan were fabricated up to 150 layer pairs. The films were peeled from the substrate and tested on a TA Instruments Q50 Thermogravimetric Analyzer. The films were equilibrated at 120 °C for 15 minutes before the temperature was ramped up at a rate of 5 °C per minute up to 600 °C.

Elemental Analysis. LbL films were prepared in the same fashion as the films used for TGA analysis. The analysis was performed by Atlantic Microlab, Inc (Norcross, GA).

7.2.5 *In Vitro* Testing

Drug Release Studies. LbL films on silicon substrates composed of PAA and PPO-PAMAM encapsulating triclosan were placed into vials of phosphate buffered saline (PBS) at pH 7.4 and 37 °C. To maintain sink conditions, the films were moved to fresh vials of PBS at appropriate time points. The PBS solutions were analyzed with UV-vis. A calibration curve of triclosan in PBS from 0-9 μg/ml was used to calculate the concentration of the solution and the amount of triclosan released ($Y = 105.76*X - 0.0599$, $R^2 = .99$).

Kirby Bauer Test. A standard Kirby Bauer test was performed using *Staphylococcus Aureus* (*S. Aureus*).[22] Cation-adjusted Mueller Hinton broth was inoculated with *S. Aureus* and cultured overnight. The culture was diluted to a concentration where with UV-vis, the O.D. was 0.1 at 600 nm. The culture was then grown for an additional 4 hours, and then plated onto agar plates containing cation-adjusted Mueller Hinton broth. LbL films of PAA and PPO-PAMAM with or without triclosan on 3 mm by 3 mm silicon substrates were placed onto the plate. The plates were incubated at 37 °C overnight. A zone of inhibition (ZOI) was measured for each sample and was calculated as:

$$ZOI = \frac{Outer\ Diameter\ of\ Inhibition - Diameter\ of\ Substrate}{2} \qquad (7\text{-}1)$$

7.3 Results and Discussion

LbL films containing amphiphilic linear-dendritic block copolymers encapsulating a hydrophobic bactericide were produced as a potential drug delivery coating (see Figure 7-1). The LbL films produced are comprised of poly(acrylic acid) (PAA) and PPO-PAMAM block copolymer micelles. The linear-dendritic block copolymer is composed of a hydrophobic block of poly(propylene oxide) (PPO) flanked by two hydrophilic dendritic poly(amidoamine) (PAMAM) blocks (Figure 7-2). Generation 4.0 PPO-PAMAM linear-dendritic block copolymers, with 16 primary amine ends on each block, were used to form charged micelles in aqueous solution with the PPO block forming the core and the PAMAM block forming the corona of the micelle. Non-cytotoxic materials were intentionally chosen for these LbL systems; PAA and PPO are biocompatible, while PAMAM is non-cytotoxic when the primary amines are complexed.[23-25] For these studies, the micelles were used to encapsulate a hydrophobic bactericide, triclosan. Triclosan has a log P_{OW} (octanol-water) of 4.76 and a water solubility of 10^{-2} mg/ml. As shown in a previous paper, the loading efficiency of triclosan into PPO-PAMAM micelles is significantly high (86 w/w%) compared to the loading efficiency of F127 (42 w/w%), a pluronic with similar PPO block length and CMC value.[20] Loaded micelles were approximately 30 nm in diameter, as determined by dynamic light scattering. It is hypothesized that the architecture of the linear-dendritic block copolymer aids in increasing the loading capacity.

7.3.1 Formation and Characterization of Micelle-Containing LbL Films

The LbL films were formed through an alternating dipping process in which the positively charged micelles acted as the counter-polyelectrolyte to PAA in the

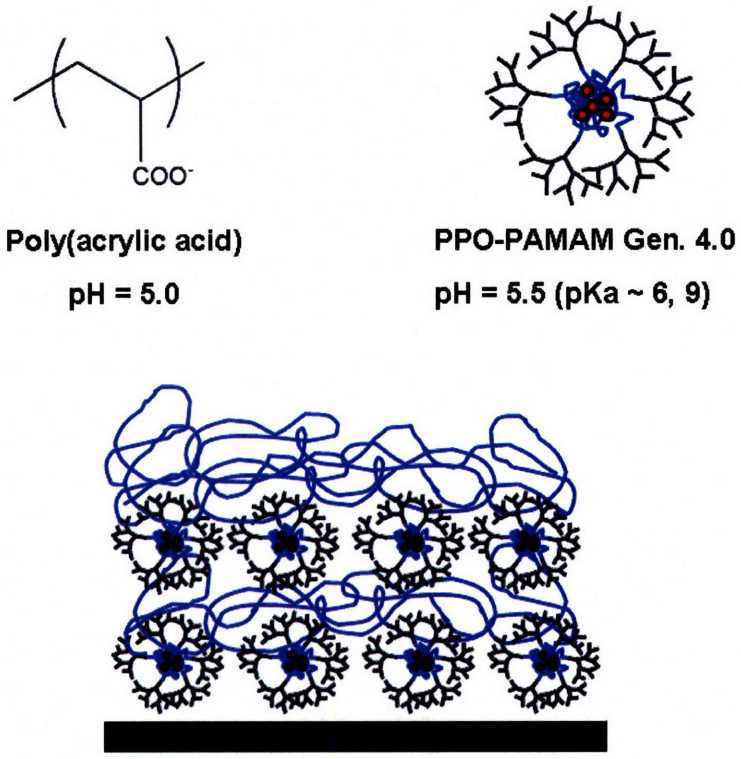

Figure 7-1. Schematic illustrating the formation of LbL films with positively charged PPO-PAMAM micelles encapsulating either hydrophobic drug or pyrene and negatively charged PAA.

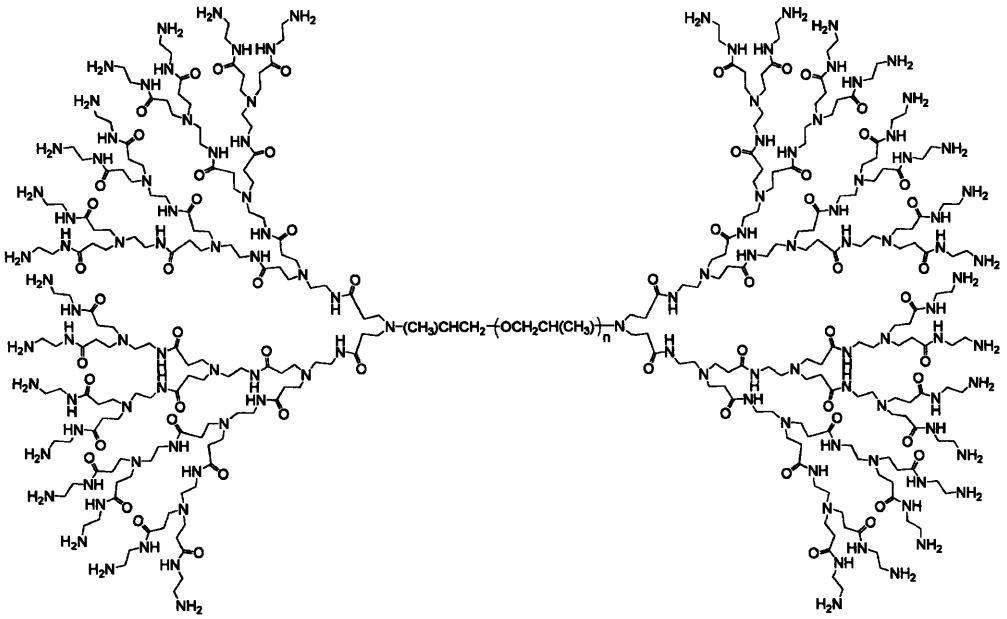

Figure 7-2. Chemical structure of PPO-PAMAM generation 4.0.

assembly procedure.

The films were fabricated on either quartz or silicon surfaces, with the positively charged micelles acted as the counter-polyelectrolyte to PAA in the assembly procedure. The films were fabricated on either quartz or silicon surfaces, with the positively charged PPO-PAMAM micelles deposited first from an aqueous solution. The solution containing PPO-PAMAM micelles encapsulating triclosan was adjusted to a pH of 5.5 to ensure that the primary amines and the tertiary amines on the PAMAM dendrimer were protonated. The concentration of polymer was at 1.9 mg/ml, which is well above the critical micelle concentration of approximately 10^{-5} M, and the concentration of drug in solution was 0.5 mg/ml. After several rinse steps, the film was exposed to negatively charged poly(acrylic acid) (PAA). The concentration of the PAA solution was 20 mM based on the repeat unit, with a pH of 5 to yield a partially charged polymer. The dipping process was repeated multiple times until the desired film thickness was achieved (Figure 7-1). Films were formed in a linear fashion from 4 bilayers up to 25 bilayers (Figure 7-3). On average, a bilayer was approximately 108 nm thick. Previous experiments from dynamic light scattering had determined the hydrodynamic diameter of generation 4.0 PPO-PAMAM micelles as 17 nm in pH 5.5 water. Assuming a perfectly spherical micelle, the radius of gyration is calculated as 5.7 nm. TEM measurements indicated micelle size to be approximately the same order of magnitude.[20] The large bilayer thickness suggests that either PAA is heavily deposited into the film, multiple layers of micelles are added to the film, or both. It should be noted that similar large bilayer thicknesses are observed for other polyamine/polyacid films when the pH values are close to the pKa of the polyions. Examples include assembly of poly(allylamine

hydrochoride) (PAH) and PAA, and linear polyethyleneimine (LPEI) and PAA. The pKa of PAA is approximately 5.5 to 6.5.[26] The pKa's of the tertiary and primary amines in PAMAM have been observed as 3.9 and 6.9, respectively, by one group,[27] and approximately 6 and 9, respectively, by another group.[28] The construction of films from partially charged weak polyelectrolytes tend to lead to polymer chains with thick, loopy conformations within the multilayer. Additional polymer-polymer interactions such as hydrogen bonding can also yield thicker films.

Film growth was also corroborated by measuring the UV-vis absorbance of the triclosan incorporated into the film via the micelles as a function of the number of bilayers in the film. As shown in Figure 7-4, triclosan was integrated into the films linearly up to 25 bilayers.

To ensure the triclosan remained in the micelles during the LbL dipping process, an indirect assessment was done by measurement of pyrene fluorescence in the films. The use of pyrene fluorescence can confirm the presence of hydrophobic encapsulating domains within the film. PPO-PAMAM micelles were equilibrated in an aqueous solution with 10^{-7} M pyrene. The LbL films were fabricated with the PPO-PAMAM micelles encapsulating pyrene on quartz substrates. The fluorescence emission spectra of the films were measured, and the maximum emission at 393 nm was recorded. Similar to the thickness and UV-vis measurements, there was a linear relationship between the number of bilayers in the film and the fluorescence emission of the pyrene in the film (Figure 7-5). Additionally, examining the vibronic band intensities of the fluorescence emission spectrum can elucidate the nature of the pyrene environment.[29] The ratio of the

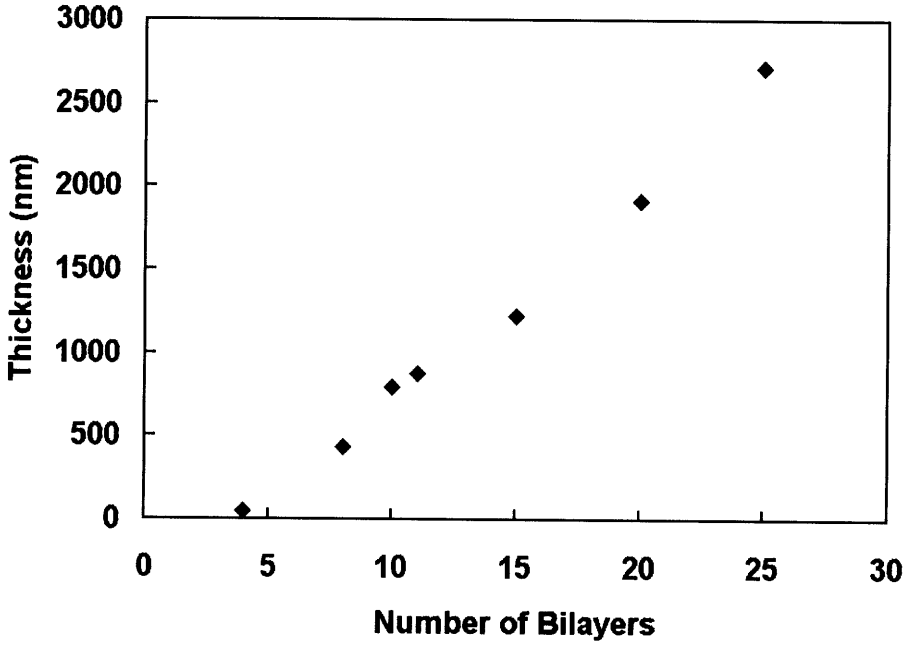

Figure 7-3. Growth curve of PAA and PPO-PAMAM encapsulating triclosan indicating linear growth from 4 to 25 bilayers.

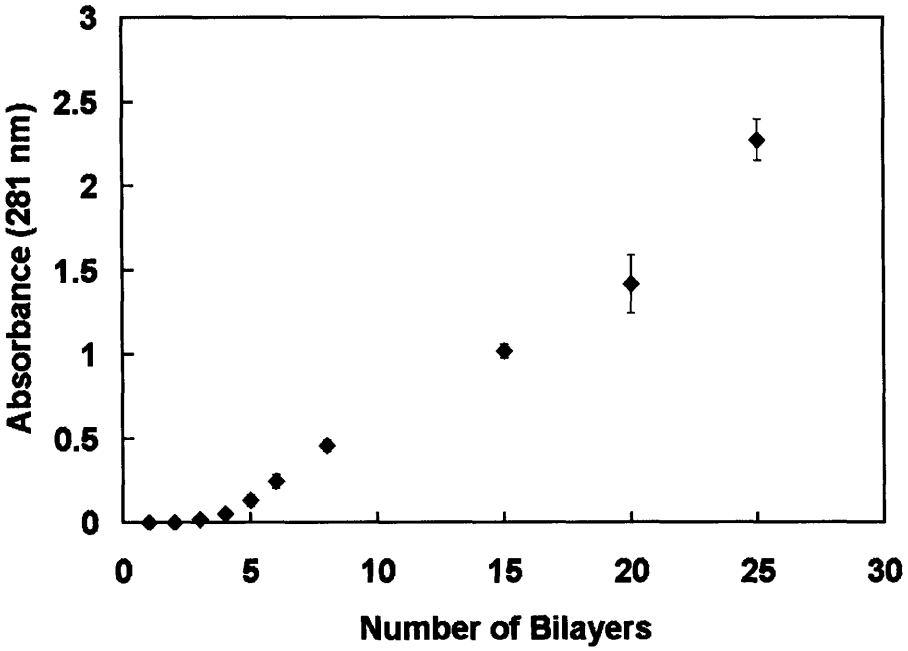

Figure 7-4. UV-vis measurements of triclosan at a characteristic wavelength of 281 nm at varying number of bilayers in a PPO-PAMAM·triclosan/PAA LbL film showing linear incorporation of triclosan into the film.

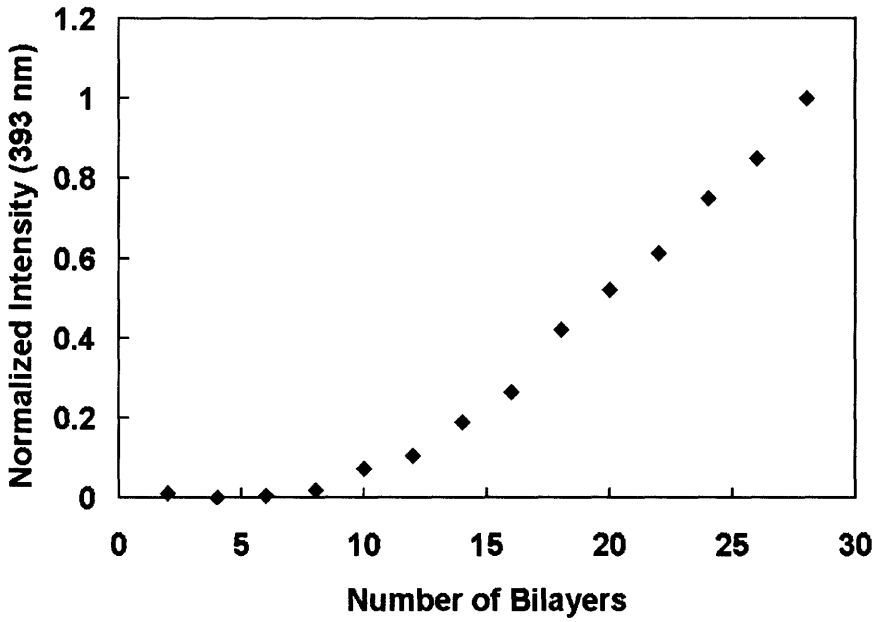

Figure 7-5. Fluorescence measurements of PPO-PAMAM·pyrene/PAA LbL films as a function of the number of bilayers in the film.

emission intensity at 383 nm to 373 nm (I_3/I_1) is indicative of the type of solvent-solute interactions of pyrene and its environment; this ratio is higher in more hydrophobic environments. In LbL films of PPO-PAMAM and PAA, the I_3/I_1 ratio of pyrene was 0.91, while the I_3/I_1 ratio of pyrene in an aqueous PPO-PAMAM solution above the critical micelle concentration was 0.85. In contrast, the I_3/I_1 ratio for pyrene in aqueous solutions of PPO-PAMAM below the CMC was 0.73. The I_3/I_1 ratio indicates that pyrene is in a hydrophobic environment that is at least as hydrophobic as the original micelles in solution. Furthermore, films fabricated from aqueous solutions of linear poly(ethyleneimine) (LPEI) with 10^{-7} M pyrene and solutions of PAA revealed no integration of pyrene into the film, indicating that hydrophobic domains are needed for pyrene incorporation (Figure 7-6).

To further confirm the presence of micelles in the LbL films, GISAXS was performed on LbL films composed of PPO-PAMAM and PAA. The films contained either empty micelles or micelles encapsulating triclosan. GISAXS allows for the investigation of periodic structure within a thin film with respect to orientation. The off-specular scattering can be analyzed for incidence angles close to the critical angle of total external reflection of the composite, allowing for both lateral structure within the film and structure normal to the substrate to be investigated.[30] From the GISAXS data, as shown in Figure 7-7, it was established that there was regular spacing of 10.5 nm and 11.7 nm in the plane parallel to the substrate for the films with no drug and with drug, respectively. Additionally, for the film containing drug, scattering in the angstrom length scales indicate the presence of triclosan, which has crystallized within the micelles. As reported in earlier work, the triclosan loading is unusually large in the linear-dendritic

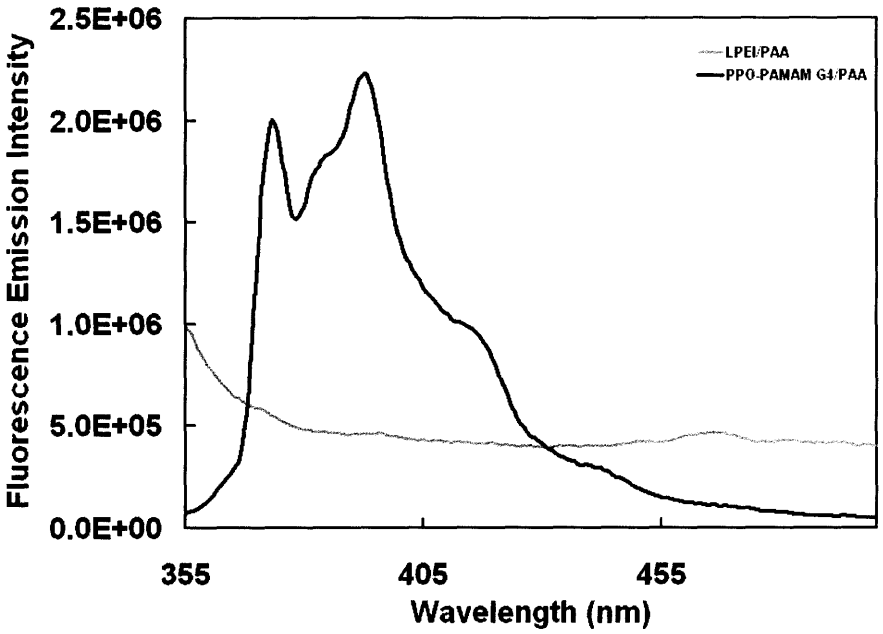

Figure 7-6. Pyrene emission spectra of LPEI/PAA films and PPO-PAMAM G4/PAA films.

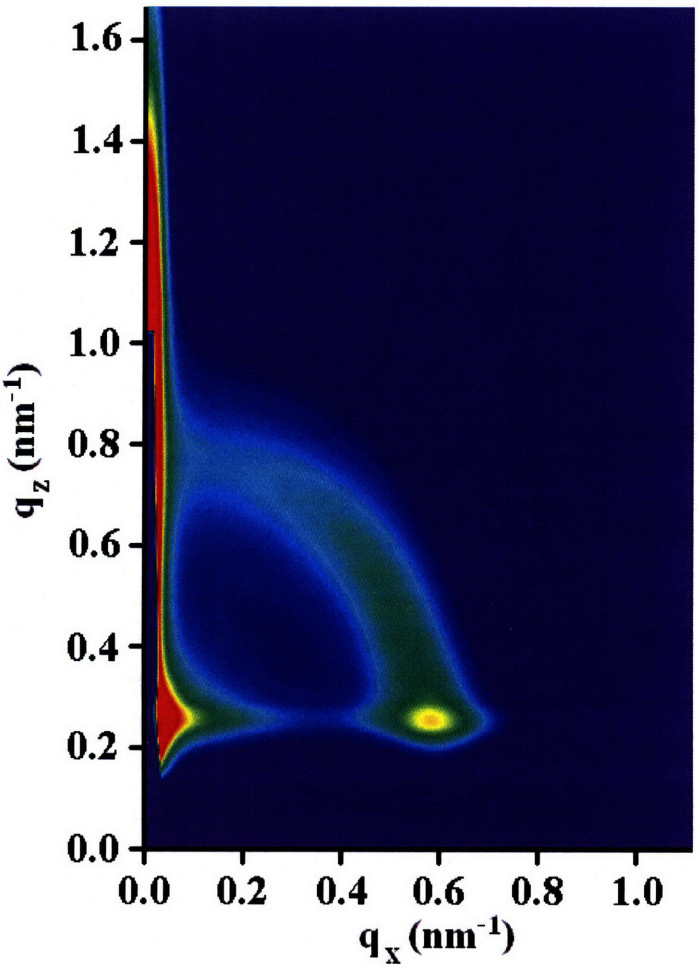

Figure 7-7. GISAXS scattering data of a 10 bilayer LbL film composed of PPO-PAMAM micelles and PAA. Scattering reveals there is regular spacing of 10.5 nm spacing in the direction parallel to the substrate. There is some evidence of scattering in the plane perpendicular to the substrate but is inconclusive.

block copolymer micelles, yielding stabilized nanoparticles containing bulk drug within the core of the micelle. There is also evidence of regular spacing on the nanometer length scale of the same order of magnitude in the direction normal to the substrate, which would correspond to the spacing of the micelles in the y-plane direction. However, the scattering is less intense and inconclusive due to interference of the beam stop and specular reflectance. The spacing in the LbL films revealed by GISAXS is of the same order of magnitude as the size of the micelles determined in aqueous solution, based on the calculated radius of gyration of 5.7 nm.

To ensure that the spacing determined from GISAXS was caused by regularly spaced micelles, the volume fraction of each film component was calculated. The volume fraction calculations were based on weight fractions assuming a density of 1 g/ml. Elemental analysis was performed on LbL films of PAA and PPO-PAMAM. The volume percent which is equivalent to weight percent due to the density assumption was 51% for PAA and 49% for PPO-PAMAM in the film. These numbers closely match the theoretical calculations for a configuration of 10 nm micelles closely packed to each other in a layer as indicated by GISAXS (Figure 7-8). This configuration yields 48 (v/v)% of PAA and 52 (v/v)% of PPO-PAMAM. The differences calculated from elemental analysis and the theoretical LbL structure can most likely be attributed to the density assumption.

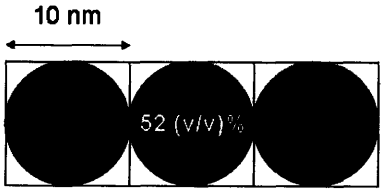

Figure 7-8. Illustration of the possible configuration of PPO-PAMAM polymer micelles within the LbL film with the spacing determined by GISAXS of 10 nm.

Elemental analysis and TGA were also employed to determine the composition of LbL films containing PAA and PPO-PAMAM micelles encapsulating triclosan. The weight percent of each component was calculated by comparing the TGA data of the LbL films to TGA data of bulk PAA, generation 4.0 PPO-PAMAM, and triclosan. There are variations in the data between the two techniques because there is a larger error when estimating film composition with TGA due to overlapping decomposition peaks of some of the components. As seen in Table 7-1, the PPO-PAMAM content, ranging from 52-57%, increased in comparison to films with no triclosan which had a PPO-PAMAM content of 49%. The increase is most likely due to the increased hydrophobicity of the PPO-PAMAM micelles encapsulating triclosan, which contributes to the driving force for inclusion in the film. The weight percent of triclosan to PPO-PAMAM polymer in solution was 26 (w/w)%. In comparison, in the film, the weight percent of triclosan to PPO-PAMAM was 35%, calculated from both TGA and elemental analysis data. The amount of drug loaded into the micelles before the dipping process was low in comparison to the optimal loading capacity previously determined of 86%.[20] Because the micelles are not at their equilibrium loading capacity, the micelles incorporated into the film are able to take up any free triclosan available in the PPO-PAMAM·triclosan micellar dipping bath.

7.3.2 Drug Release and Efficacy

Drug release experiments were performed on the LbL film to determine the length scales of drug release. LbL films (10 bilayers) on silicon substrates were placed in 0.1 M PBS solutions at 37 °C. Sink conditions were maintained by changing the solutions before the concentration of triclosan in the PBS was too high. As demonstrated in Figure

7-9, the half-life of triclosan release was approximately 77 hours, with release lasting up to 20 days.

Table 7-1. Composition of PAA and PPO-PAMAM with or without triclosan LbL films as determined by two different methods.

Film Component	PPO-PAMAM/PAA	PPO-PAMAM·Triclosan/PAA	
	Elemental Analysis	TGA	Elemental Analysis
PAA (wt %)	51	22	30
PPO-PAMAM G4 (wt %)	49	57	52
Triclosan (wt %)	--	20	18

According to the drug release profile, the mechanism of release from the film is through diffusion. FTIR of a PPO-PAMAM/PAA film constructed with no drug and a PPO-PAMAM·triclosan/PAA film after release show that the PPO-PAMAM remains in the film as shown in Figure 7-10. The amide groups in the PAMAM block at 1650 and 1570 cm^{-1} are present after drug release. Furthermore, the relative intensities of these peaks to the other peaks in the spectra are similar in magnitude. GISAXS further indicates that the same spacing is maintained after drug release. Thus, with the film remaining intact during the drug release process, the mechanism of diffusion release is confirmed.

A Kirby Bauer assay was completed to determine the efficacy of the released triclosan (Figure 7-11). LbL films (10 bilayers) of PAA and PPO-PAMAM with and without triclosan on silicon substrates were tested against *Staphylococcus Aureus*. As the

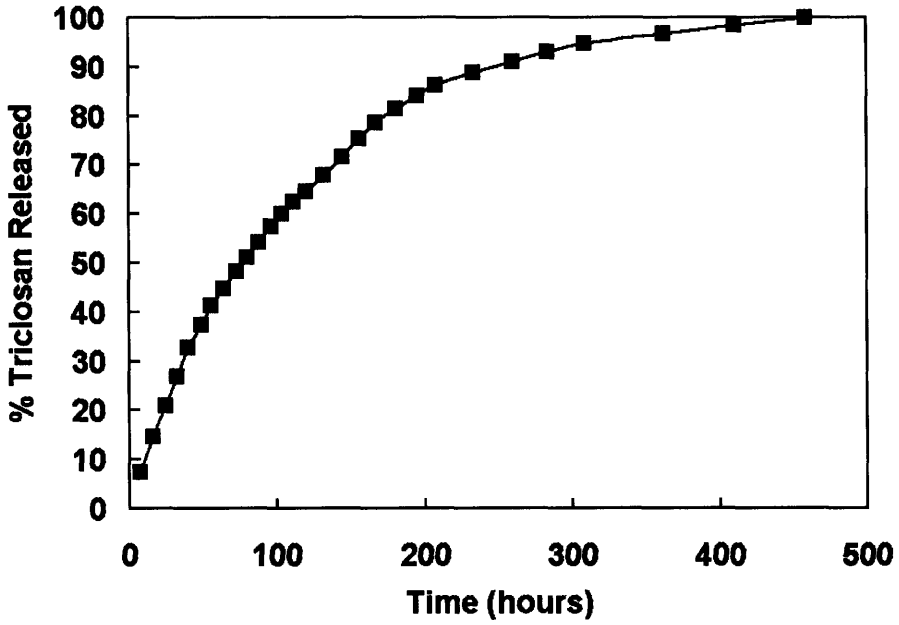

Figure 7-9. Drug release profile of triclosan in an LbL film composed of PPO-PAMAM·triclosan/PAA. The release was performed at 37 °C in 0.1 M PBS.

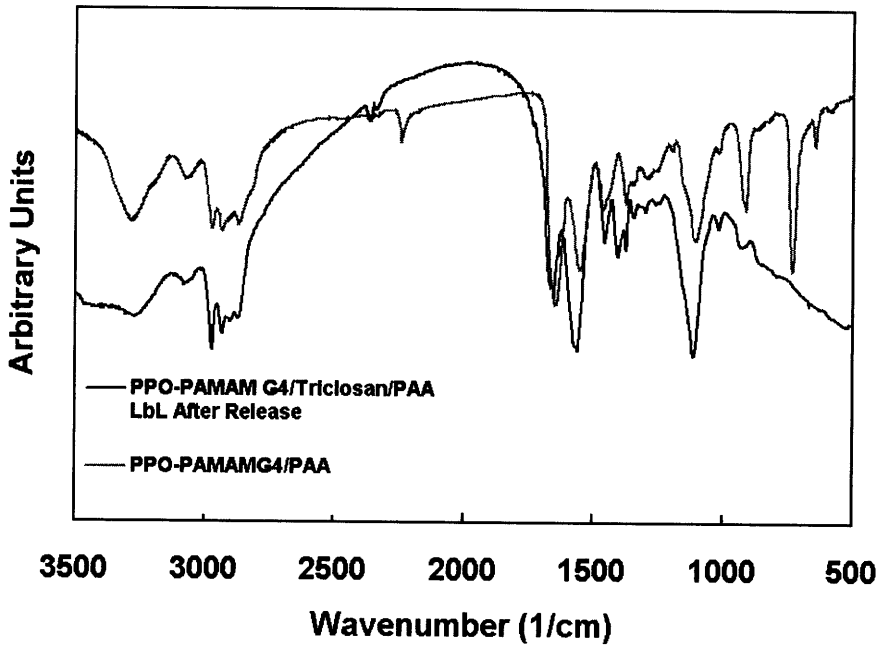

Figure 7-10. FTIR spectra of PPO-PAMAM/PAA films after triclosan release or PPO-PAMAM/PAA films fabricated with no drug.

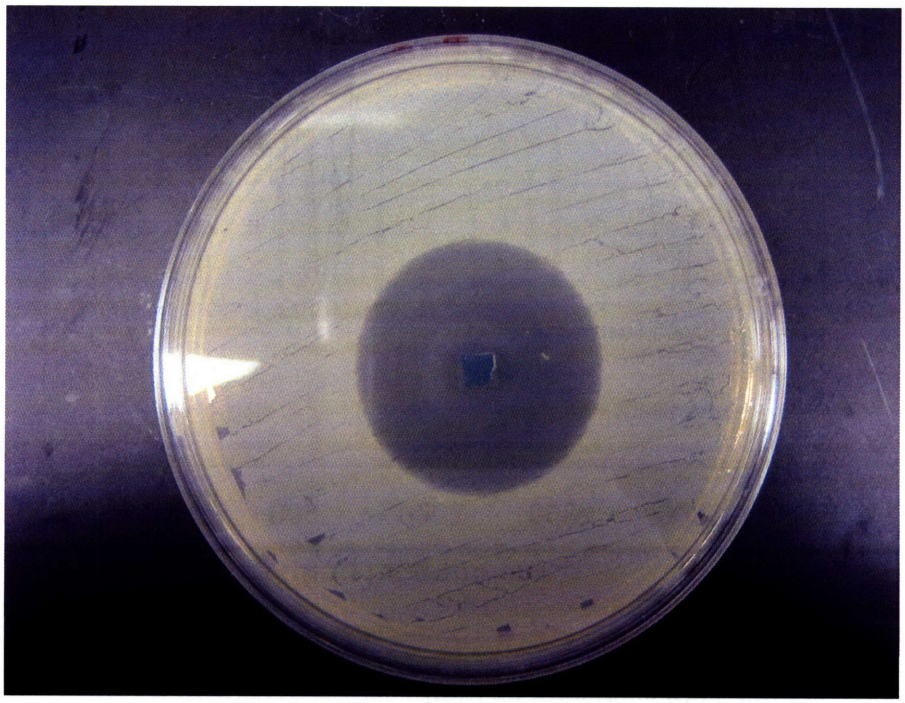

Figure 7-11. Agar plate of *S. Aureus* growth inhibited by release of triclosan from a 10 bilayer LbL film of PPO-PAMAM micelles encapsulating triclosan and PAA.

films are incubated with the bacterial agar plates, the drug diffuses out and leaves a circular area free of bacteria called the zone of inhibition (ZOI). The ZOI for the film containing drug was 14.6±0.3 mm while there was no ZOI of the film without drug.

7.4 Conclusions

An LbL film was fabricated incorporating micelles composed of a novel amphiphilic linear-dendritic block copolymer. When compared to charged linear-linear block copolymer micelles introduced into LbL films, as shown in other groups' past studies[14, 16, 31], drug encapsulation and release is superior in the case of PPO-PAMAM micelles encapsulating triclosan due to the linear-dendritic architecture.[20] The formation of the PPO-PAMAM·triclosan/PAA film was shown to be linear after the initial first 4 bilayers. GISAXS and film composition measurements confirmed the presence of micelles within the multilayer films. Additionally, *in vitro* tests indicated that the films created are functional. Drug release studies show that there is prolonged release of drug from the film over a period of several weeks. Due to the versatility of the LbL method, the drug release time can be addressed by either changing the amount of drug encapsulated within the micelles or by changing the number of times the substrate is dipped into the electrolyte solutions, thereby controlling the total amount of drug within the film. Kirby Bauer tests demonstrate that the drug released retains activity. The results presented demonstrate the applicability of obtaining hydrophobic domains within an LbL film by incorporating charged micelles in order to deliver hydrophobic drugs. This could potentially be applied as a film coating to biomedical devices such as stents, catheters, and other biomedical implants.

7.5 References

1. Decher, G., "Fuzzy nanoassemblies: Toward layered polymeric multicomposites," *Science*, **1997,** 277, (5330), 1232-1237.

2. Berg, M. C.; Yang, S. Y.; Hammond, P. T.; Rubner, M. F., "Controlling mammalian cell interactions on patterned polyelectrolyte multilayer surfaces," *Langmuir*, **2004,** 20, (4), 1362-1368.

3. Caruso, F.; Yang, W.; Trau, D.; Renneberg, R., "Microencapsulation of uncharged low molecular weight organic materials by polyelectrolyte multilayer self-assembly," *Langmuir*, **2000,** 16, (23), 8932-8936.

4. Decher, G.; Lehr, B.; Lowack, K.; Lvov, Y.; Schmitt, J., "New nanocomposite films for biosensors: Layer-by-layer adsorbed films of polyelectrolytes, proteins of DNA," *Biosensors & Bioelectronics*, **1994,** 9, (9/10), 677-684.

5. Stockton, W. B.; Rubner, M. F., "Molecular-level processing of conjugated polymers. 4. Layer-by-layer manipulation of polyaniline via hydrogen-bonding interactions," *Macromolecules*, **1997,** 30, (9), 2717-2725.

6. Shchukin, D. G.; Patel, A. A.; Sukhorukov, G. B.; Lvov, Y., "Nanoassembly of biodegradable microcapsules for DNA encasing," *J. Am. Chem. Soc.*, **2004,** 126, 3374-3375.

7. Dejugnat, C.; Halozan, D.; Sukhorukov, G. B., "Defined picogram dose inclusion and release of macromolecules using polyelectrolyte microcapsules," *Macromolecular Rapid Communications*, **2005,** 26, (12), 961-967.

8. Vázquez, E.; Dewitt, D. M.; Hammond, P. T.; Lynn, D. M., "Construction of hydrolytically-degradable thin films via layer-by-layer deposition of degradable polyelectrolytes," *J. Am. Chem. Soc.*, **2002,** 124, 13992-13993.

9. Wood, K. C.; Boedicker, J. Q.; Lynn, D. M.; Hammon, P. T., "Tunable drug release from hydrolytically degradable layer-by-layer thin films," *Langmuir*, **2005,** 21, (4), 1603-1609.

10. Thierry, B.; Kujawa, P.; Tkaczyk, C.; Winnik, F. M.; Bilodeau, L.; Tabrizian, M., "Delivery platform for hydrophobic drugs: Prodrug approach combined with self-assembled multilayers," *Journal of the American Chemical Society*, **2005,** 127, (6), 1626-1627.

11. Berg, M. C.; Zhai, L.; Cohen, R. E.; Rubner, M. F., "Controlled drug release from porous polyelectrolyte multilayers," *Biomacromolecules*, **2006,** 7, (1), 357-364.

12. Emoto, K.; Iijima, M.; Nagasaki, Y.; Kataoka, K., "Functionality of polymeric micelle hydrogels with organized three-dimensional architecture surfaces," *J. Am. Chem. Soc.*, **2000,** 122, 2653-2654.

13. Emoto, K.; Nagasaki, Y.; Kataoka, K., "A core-shell structured hydrogel thin layer on surfaces by lamination of a poly(ethylene glycol)-*b*-poly(d,l-lactide) micelle and polyallylamine," *Langmuir*, **2000,** 16, 5738-5742.

14. Ma, N.; Zhang, H.; Song, B.; Wang, Z.; Zhang, X., "Polymer micelles as building blocks for layer-by-layer assembly: An approach for incorporation and controlled release of water-insoluble dyes," *Chemistry of Materials*, **2005,** 17, (20), 5065-5069.

15. Ma, N.; Wang, Y.; Wang, Z.; Zhang, X., "Polymer micelles as building blocks for the incorporation of azobenzene: Enhancing the photochromic properties in layer-by-layer films," *Langmuir*, **2006,** 22, (8), 3906-3909.

16. Qi, B.; Tong, X.; Zhao, Y., "Layer-by-layer assembly of two different polymer micelles with polycation and polyanion coronas," *Macromolecules*, **2006,** 39, (17), 5714-5719.

17. Grinstaff, M. W., "Biodendrimers: New polymeric biomaterials for tissue engineering," *Chemistry - A European Journal*, **2002,** 8, (13), 2838-2846.

18. Ihre, H. R.; Padilla De Jesús, O.; Szoka, F. C., Jr.; Fréchet, J., "Polyester dendritic systems for drug delivery applications: Design, synthesis, and characterization," *Bioconjugate Chem.*, **2001,** 13, 443-452.

19. Gillies, E.; Jonsson, T.; Fréchet, J., "Stimuli-responsive supramolecular assemblies of linear-dendritic copolymers," *J. Am. Chem. Soc.*, **2004,** 126, 11936.

20. Nguyen, P. M.; Hammond, P., "Amphiphilic linear-dendritic triblock copolymers composed of poly(amidoamine) and poly(propylene oxide) and their micellar-phase and encapsulation properties," *Langmuir*, **2006,** 22, (18), 7825-7832.

21. Smilgies, D.-M.; Busch, P.; Papadakis, C. M.; Posselt, D., "Characterization of polymer thin films with small-angle x-ray scattering undering grazing incidence (gisaxs)," *Synchotron Radiation News*, **2002,** (15), 35.

22. Bauer, A. W.; Kirby, W. M. M.; Sherris, J. C.; Turck, M., "Antibiotic susceptibility testing by a standardized single disc method," *Am. J. Clin. Pathol.*, **1966,** 45, 493-496.

23. Roberts, J. C.; Bhalgat, M. K.; Zera, R. T., "Preliminary biological evaluation of polyamidoamine (pamam) starburst dendrimers," *J. Biomed. Mater. Res.*, **1996,** 30, 53-65.

24. Malik, N.; Wiwattanapatapee, R.; Klopsch, R.; Lorenz, K.; Frey, H.; W., W. J.; Meijer, E. W.; Paulus, W.; Duncan, R., "Dendrimers: Relationship between structure and biocompatibility in vitro, and preliminary studies on the biodistribution of 125i-labelled polyamidoamine dendrimers in vivo," *Journal of controlled release*, **2000,** 65, 133-148.

25. Jevprasesphant, R.; Penny, J.; Jalal, R.; Attwood, D.; McKeown, N. B.; D'Emanuele, A., "The influence of surface modification on the cytotoxicity of pamam dendrimers," *International journal of pharmaceutics*, **2003,** 252, (1-2), 263-266.

26. Choi, J.; Rubner, M. F., "Influence of the degree of ionization on weak polyelectrolyte multilayer assembly," *Macromolecules*, **2005,** 38, 116-124.

27. Tomalia, D.; Naylor, A.; Goddard, W., "Starburst cascade polymers: Molecular-level control of size, shape, surface chemistry, topology, and flexibility from atoms to macroscopic matter," *Angew. Chem. Int. Ed. Engl.*, **1990,** 29, 138-175.

28. Cakara, D.; Kleimann, J.; Borkovec, M., "Microscopic protonation equilibria of poly(amidoamine) dendrimers from macroscopic titrations," *Macromolecules*, **2003,** 36, (4201-4207).

29. Kalyanasundaram, K.; Thomas, J., "Environmental effects on vibronic band intensities in pyrene monomer fluorescence and their application in studies of micellar systems," *J. Am. Chem. Soc.*, **1977,** 99, 2039.

30. Busch, P.; Rauscher, M.; Smilgies, D.-M.; Posselt, D.; Papadakis, C. M., "Grazing-incidence small-angle x-ray scattering from thin polymer films with lamellar

structures - the scattering cross section in the distorted-wave born approximation," *J. Appl. Cryst.*, **2006,** 39, 433-442.

31. Cho, J.; Hong, J.; Char, K.; Caruso, F., "Nanoporous block copolymer micelle/micelle multilayer films with dual optical properties," *Journal of the American Chemical Society*, **2006,** 128, (30), 9935-9942.

CHAPTER 8: Conclusions and Future Work

The main objective of this thesis was to develop a novel amphiphilic linear-dendritic block copolymer and explore its potential use as a drug delivery vehicle. Previous work with linear-dendritic block copolymers developed polymers with hydrophobic dendritic blocks that would form the core.[1, 2] A feature unique to this polymer system is the formation of micelles with the linear hydrophobic block forming the core and the dendritic block facing the aqueous solution presenting dense functional groups on the surface of the self-assembled micelles. The work detailed in this thesis is summarized in the next section, going over the characterization of the polymer in an aqueous environment and describing two potential applications where the linear-dendritic architecture is used advantageously for drug delivery.

8.1 Thesis Summary

In Chapter 2, the synthesis and characterization of an amphiphilic linear-dendritic block copolymer is described. The linear-dendritic block copolymer synthesized is similar in structure to a pluronic, with a hydrophobic middle block composed of PPO joined to outer hydrophilic dendritic blocks composed of PAMAM. A series of the PPO-PAMAM block copolymers was synthesized with PAMAM generations varying from 1 through 6. To understand the linear-dendritic block copolymers' self-assembly behavior in aqueous solution, the CMC was studied as a function of PAMAM generation, solution pH, and the ionic strength. The generation of the PAMAM block was important to study to determine the magnitude of the driving force for the self-assembly of the polymers and whether the nanoparticles formed were stable enough for future use *in vivo*. The CMC as

a function of pH and ionic strength were studied to understand the behavior of the block copolymer in subsequent processing conditions and *in vitro* assay conditions, where the block copolymers would experience a drop in pH moving from the environment of the cell culture media to the environment of endosomes formed from receptor-mediated endocytosis. The particle sizes of the self-assembled block copolymer nanoparticles were also examined with dynamic light scattering and TEM. From these studies, it was found that the nanoparticles formed were in the correct size range for systemic drug delivery applications. Next, as an initial study, a model hydrophobic drug, triclosan, was used for encapsulation by the PPO-PAMAM block copolymers. It was found that with the presence of the PAMAM dendritic blocks, the encapsulation efficiency and the loading capacity of triclosan was significantly higher compared to a pluronic counterpart. This indicates that there are some synergies that are gained by introducing the dendritic block, perhaps due to either triclosan being encapsulated in the PAMAM block or due to the architecture of the linear-dendritic block copolymer. The results from Chapter 2 indicate that the linear-dendritic block copolymers synthesized have solution-phase characteristics that are within the design parameters for use as a circulating drug delivery nanoparticle and have a lot of potential promise in that area.

Due to the interesting behavior found from the experiments detailed in Chapter 2, Chapter 3 discusses molecular dynamics simulations of PPO-PAMAM unimers and micelles to gain a better understanding of their atomistic details. Static light scattering was performed to determine the aggregation number of the micelles, which was then used to set up the micelle simulations. The results from the simulations indicated that the unimers and micelles formed had high asphericity, and due to the asphericity, some water

was observed in the core of these micelles. Furthermore, the amine terminal ends were found to have some backfolding into the interior regions of the dendritic block, which had previously been observed with simulations of full dendrimers. Last, from the simulation that included triclosan in a micelle, it was found that triclosan did not localize exclusively to the core but was present in the core and dendritic regions, which could explain the high encapsulation data previously observed.

With the greater knowledge of the linear-dendritic block copolymers synthesized, further studies to assess the potential benefits of utilizing the block copolymer nanoparticles as systemic drug delivery vehicles were undertaken in Chapter 4. To take advantage of the dense functional groups presented by the dendritic blocks on the outer surface of the micelles, galactose was chosen as a targeting ligand due to its multivalent binding behavior to the asialoglycoprotein receptor. Galactose was conjugated to PPO-PAMAM of varying generations. Cytotoxicity studies indicated that the polymers synthesized were not toxic and the concentrations that could be used for further testing was well above the CMC. *In vitro* studies showed that the galactose-modified polymer could bind to its corresponding receptor, the asialoglycoprotein receptor, and deliver drugs to cells in a specific manner. The drug delivery efficiency improved drastically with the addition of the galactose targeting ligand, ranging from a 2-15 fold decrease in the IC_{50} over unmodified block copolymer micelle carriers. In comparison, linear polymers such as HPMA, with galactose conjugated to its side chains only experienced a 4-5 fold improvement.[3,4] The *in vitro* studies detailed in this chapter show that there is a lot of promise in utilizing these linear-dendritic block copolymers as multivalent drug delivery carriers. Due to the length-scales of the dendrimer blocks, multivalent drug

delivery is particularly suited for carbohydrate-lectin systems. A multitude of diseases could be treated by taking advantage of the multivalent binding between carbohydrates and lectins, such as colon and hepatic cancers,[5, 6] and hepatic inflammation.[7]

With the positive *in vitro* results obtained in Chapter 4, improvements to the linear-dendritic block copolymer system was presented in Chapters 5 and 6 that could be implemented to increase the success of these systems when tested *in vivo*. Chapter 5 details a method to stabilize PPO-PAMAM micelles. The micelles were stabilized through the physical entrapment of the core. Hydrophobic reactive methacrylate monomers were introduced into the core of the PPO-PAMAM micelles through an emulsion, and the monomers were polymerized with a UV-activated photoinitiator. Fluorescence studies and dynamic light scattering revealed that the micelles were stabilized at concentrations below the CMC and also in a solubilizing solvent condition. Additionally, the monomers introduced into the micelle core led to higher drug encapsulation and slower drug release. Although the results showed an improvement in the drug delivery properties of the micelles, cytotoxicity tests revealed that the introduction of the methacrylate monomers increased the cytotoxicity of the polymer. In order to decrease the cytotoxicity, other reactive monomers would have to be explored. Stabilizing the PPO-PAMAM micelles through physical entrapment yielded positive improvements in the drug delivery characteristics of the micelles; however, some changes would have to be made to decrease the cytotoxicity.

In Chapter 6, the synthesis and characterization of a new linear-dendritic block copolymer was introduced. The chemical structure of the linear-dendritic block copolymer is modified from what had been previously synthesized in the Hammond

group.[8, 9] This linear-dendritic block copolymer is composed of linear poly(β-benzyl-L-aspartate) (PBLA) and a polyester dendron. The PBLA block was introduced to have greater affinity with the drug of interest, doxorubicin. Drug encapsulation studies showed high encapsulation efficiency, and drug release from the nanoparticles formed was slow and prolonged. Overall, the new block copolymers had an extremely low CMC, which would reduce the need for further particle stabilization, and they self-assembled in aqueous solution into micellar nanoparticles. The linear-dendritic block copolymers synthesized also had PEG attached to the outer dendritic block. PEG was not attached to the PPO-PAMAM block copolymers, since it was thought that the addition would increase the polymers' CMCs and would make it impractical for *in vivo* use. With this new linear-dendritic block copolymer design, even with the addition of PEG, the CMC is still very low. The PEG is necessary to prolong the circulation of the nanoparticles in the body by avoiding removal by the RES. Therefore, this new linear-dendritic block copolymer has a lot of potential to be a successful targeted colloidal drug delivery vehicle *in vivo*.

In Chapter 7, a different drug delivery application was explored for the PPO-PAMAM micelles. In this application, the dendritic block is used as a densely charged polyelectrolyte in the formation of a conformal coating created by the layer-by-layer dipping process. The incorporation of linear-dendritic block copolymer micelles into an LbL film was a general method offered to introduce hydrophobic domains into a hydrophilic film for hydrophobic drug delivery. Through profilometry and fluorescence studies, it was shown that the linear-dendritic block copolymer micelles formed films with a counter-polyelectrolyte in a controlled and linear fashion. GISAXS and elemental

analysis data confirmed that the linear-dendritic block copolymer micelles remained in the film as micelles. Additionally, due to the exceptional loading capacity of triclosan in PPO-PAMAM micelles, the LbL films created were unique in comparison to other LbL films that had explored the use of block copolymer micelles. The amount of drug loaded into the films was quite high, and the drug release out of the film was on the order of weeks. Other groups had seen complete release of a model hydrophobic molecule in a matter of minutes.[10, 11] Overall, the general approach that was suggested in this chapter for incorporating hydrophobic domains into LbL films was shown to be a controllable and a predictable method. Furthermore, the outstanding system that was fabricated which could potentially be used as an antibacterial coating on biomedical implants gave greater proof that this general method is a viable technique for hydrophobic drug delivery in LbL films.

8.2 Future Work

In this section, future research directions related to studying and improving the linear-dendritic block copolymer systems previously synthesized are discussed. Improvements for the linear-dendritic block copolymer micelles used as both circulating targeted colloidal drug delivery vehicles and as hydrophobic nanocontainers in a polymer film coating are explored.

8.2.1 Improvements to the PPO-PAMAM System

One of the main issues encountered with the linear-dendritic PPO-PAMAM system was that the system could possibly not be stable enough to maintain its structure when administered systemically. In order to improve this aspect, either the hydrophobic

block must be more insoluble or a method to crosslink the copolymer unimers has to be determined. In order to increase the hydrophobicity of the block copolymer, a longer PPO block could be used to decrease the HLB balance. Theoretically, the PPO block could be synthesized to an unlimited molecular weight. However, for biological applications, the PPO block would have to be limited to the size that could be removed through kidney filtration since PPO can not be broken down degradatively. This size has been cited as approximately 42-50 kDa for water-soluble polymers.[12]

A method to stabilize the PPO-PAMAM micelles was suggested in Chapter 5 which involved physical entrapment of the PPO-PAMAM micelle core. However, direct covalent bonding of the block copolymer backbone would be more desirable. Since PPO does not have any reactive groups present, a scheme that would enable covalent bonding would be to introduce another polymer block with reactive side chains. This could be difficult to do since these side chains would have to be protected while the PAMAM reactions are carried out to create the dendrimer. Furthermore, the protecting group would have to be orthogonal to the methyl ester group, should the PAMAM synthesis end in a half generation. Additionally, the reactive group on the side chains revealed after deprotection should not be able to crosslink with the amines present on the PAMAM dendrimer. A potential polymer block that could be introduced is polycysteine (Figure 8-1). The amine on the PPO block could be used to initiate an N-carboxyanhydride (NCA) ring opening polymerization, which reforms an amine at the terminus of the block. With this, the PAMAM reactions could be carried forward as done previously with amine-terminated PPO. With the introduction of the cysteine block, the block copolymer micelles formed could be crosslinked in the shell region through oxidation of the thiol

groups present on cysteine, or a dithiol linker could be introduced to ensure crosslinking between unimers.

With the introduction of crosslinked disulfide bonds, the PPO-PAMAM system would be more stable as micelles and would be biologically responsive. The primary reducing agent for disulfide bonds in mammalian cells is glutathione. Glutathione is abundant in the cell (in the millimolar range) while it is scarce in the blood plasma (in the micromolar range).[13, 14] Therefore, the disulfide bonds could be used so that the drug delivery vehicles would only destabilize and release drug in the cell, making the system more specific and safer.

8.2.2 Improvements to the PBLA-B16-PEG System

The PBLA-B16-PEG linear-dendritic block copolymer has many of the desirable attributes needed for circulating drug delivery nanoparticles. Furthermore, the design of the linear-dendritic block copolymer allows for great flexibility. For example, the benzyl side group on the polyaspartate block could be changed to include polymerizable vinyl groups to further stabilize the micelles. However, with this strategy, crosslinking the hydrophobic blocks would reduce the free volume in the core for encapsulation of hydrophobic drugs. Here, a similar solution proposed in section 8.2.1 could be utilized where an additional block could be introduced. The addition of another functional polymer block would be even simpler with the use of another NCA-activated amino acid, allowing for a one-pot reaction. For example, the B16 dendron could be used to initiate the middle poly(amino acid) block, and once that reaction is complete, the NCA for the terminal block could be added as shown in Figure 8-2.

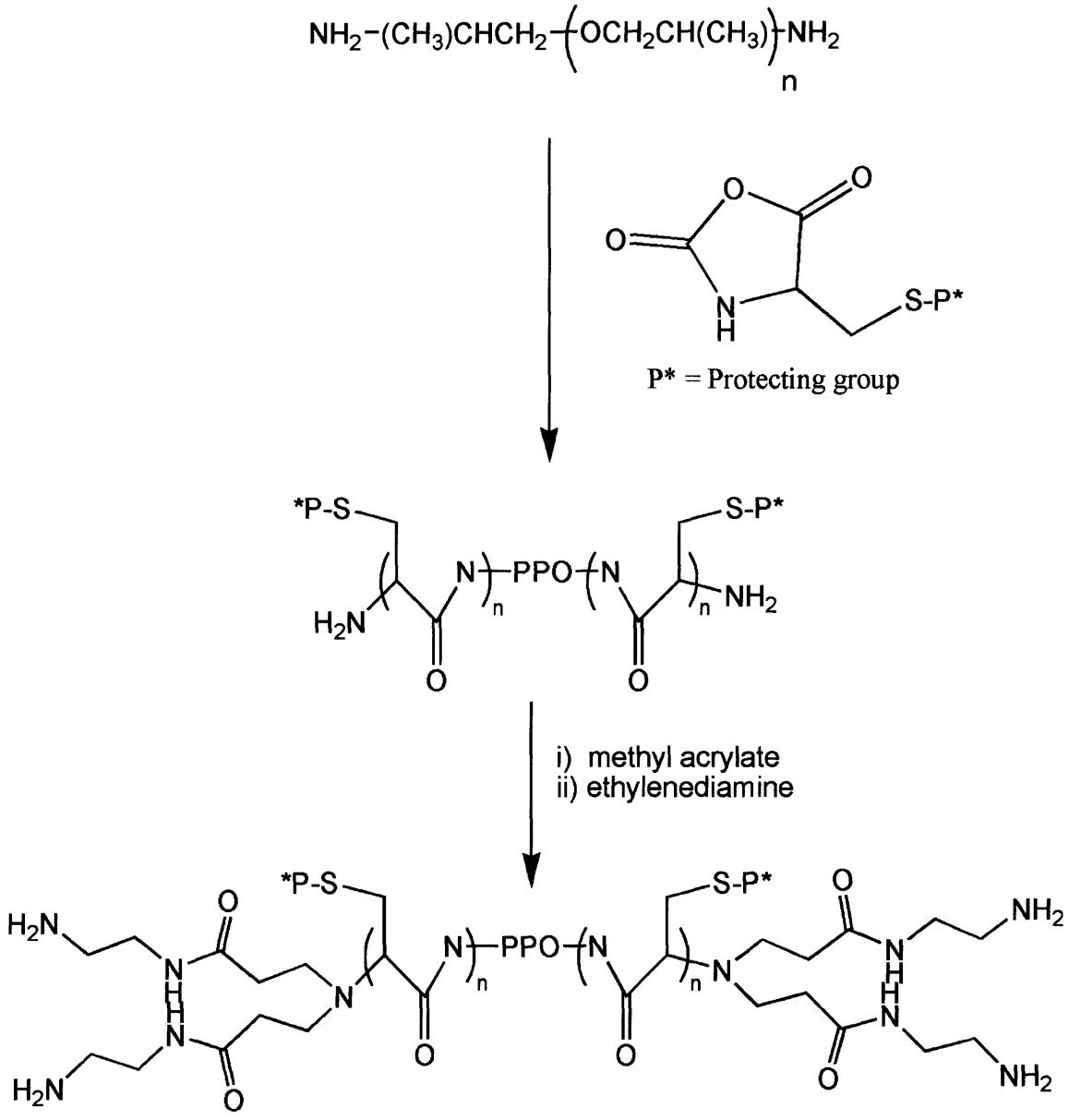

PPO-PolyCys-PAMAM Generation 1.0

Figure 8-1. Synthetic scheme to create a triblock copolymer of PPO, polycysteine, and PAMAM, where the polycysteine block adds a smart response component to the drug delivery vehicle.

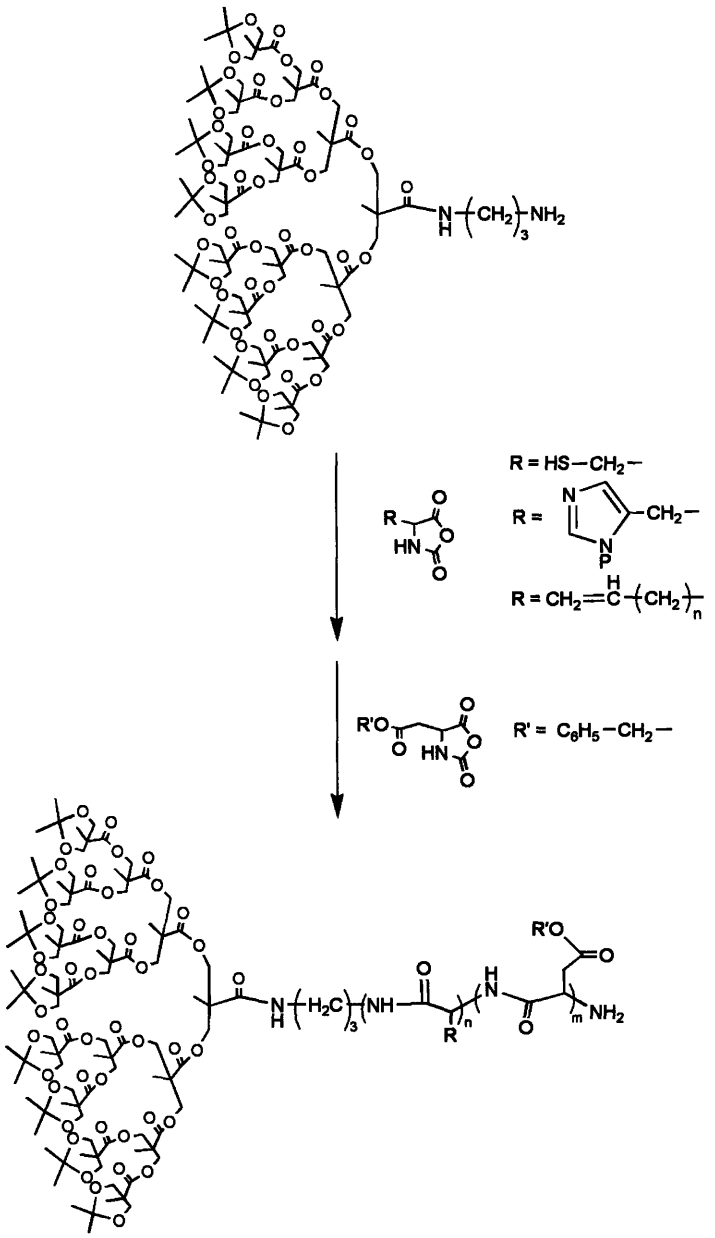

Figure 8-2. Synthetic scheme for the synthesis of a triblock linear-dendritic block copolymer with a polyester dendron, a linear PBLA end block, and a poly(amino acid) middle block that could be used as either a proton sponge, biologically responsive crosslinking system, or a covalently crosslinking system.

With the formation of the triblock copolymer, many different functionalities could be introduced. A feature that is lacking in the linear-dendritic block copolymer is a stimulus-response mechanism where the drug release profile could be tuned. A method that has been suggested in section 8.2.1 is to create a polycysteine middle block. Another stimulus that is important in cancer therapies is pH. It has been found that tumors have a lower pH than physiological pH ranging from 5.7 to 7.8.[15, 16] Moreover, for targeted drug delivery vehicles, a pH responsive system is desirable. When targeted drug delivery vehicles are taken up by cells through receptor-mediated endocytosis, vesicles called endosomes form. The pH in endosomes is reduced by the protons that are pumped in. In order to ensure complete drug release, a system created to destabilize and release drug at low pH values is needed. The incorporation of polyhistidine into micelles as a way to tune the response pH has been studied previously.[17, 18] It is hypothesized that histidine can disrupt endosomes through the proton sponge effect due to the buffering capacity of the imidazole groups present.[19] The pKa of the histidine side chain is approximately 6.0 as measured by various methods.[20] Therefore, histidine can absorb extra protons in the endosome and act as a proton sponge. Additionally, histidine has been found to be fusogenic as well, which could lead to the disruption the endosome membrane and the release of its contents.[17] The introduction of the polyhistidine block would add multiple benefits for the drug delivery vehicle by creating a stimulus-responsive system and allowing for greater release of drugs from the endosomal compartment.

8.2.3 Multivalent Targeting

In addition to the galactose-functionalized system that was studied, another multivalent system that could be explored is the folate-folate receptor system. This

system is especially amenable for systemic targeted drug delivery. The folate receptor is overexpressed in cancer cells and is clustered in lipid rafts for subsequent receptor-mediated endocytosis.[21] It has been found that folate receptors are clustered in microdomains about 70 nm in size containing approximately 50 folate receptors.[22] The density of the folate receptors in the microdomain suggests that the receptors are spaced apart in the nanometer length scale which would match the size of the drug delivery vehicles that have been tested previously. This has been confirmed with folate-targeted dendrimers, and multivalent interactions to the receptor have been observed.[23] Approximately 3-4 folates were needed to achieve maximal binding.

The use of folate conjugated to the B16-PBLA-PEG linear-dendritic block copolymer could yield a powerful multivalently targeting drug delivery system. The synthesis of the block copolymer would only have to be slightly modified from the synthesis of B16-PBLA-PEG-Gal (Figure 7-2). The γ-carboxyl group of folate would have to be modified to be an amine before reacting it with B16-PBLA-PEG-NHS as shown in Figures 8-3 and 8-4.

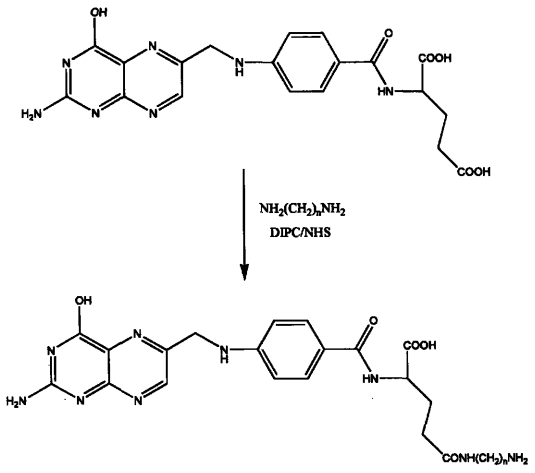

Figure 8-3. Activation of folate through conventional carbodiimide chemistry.

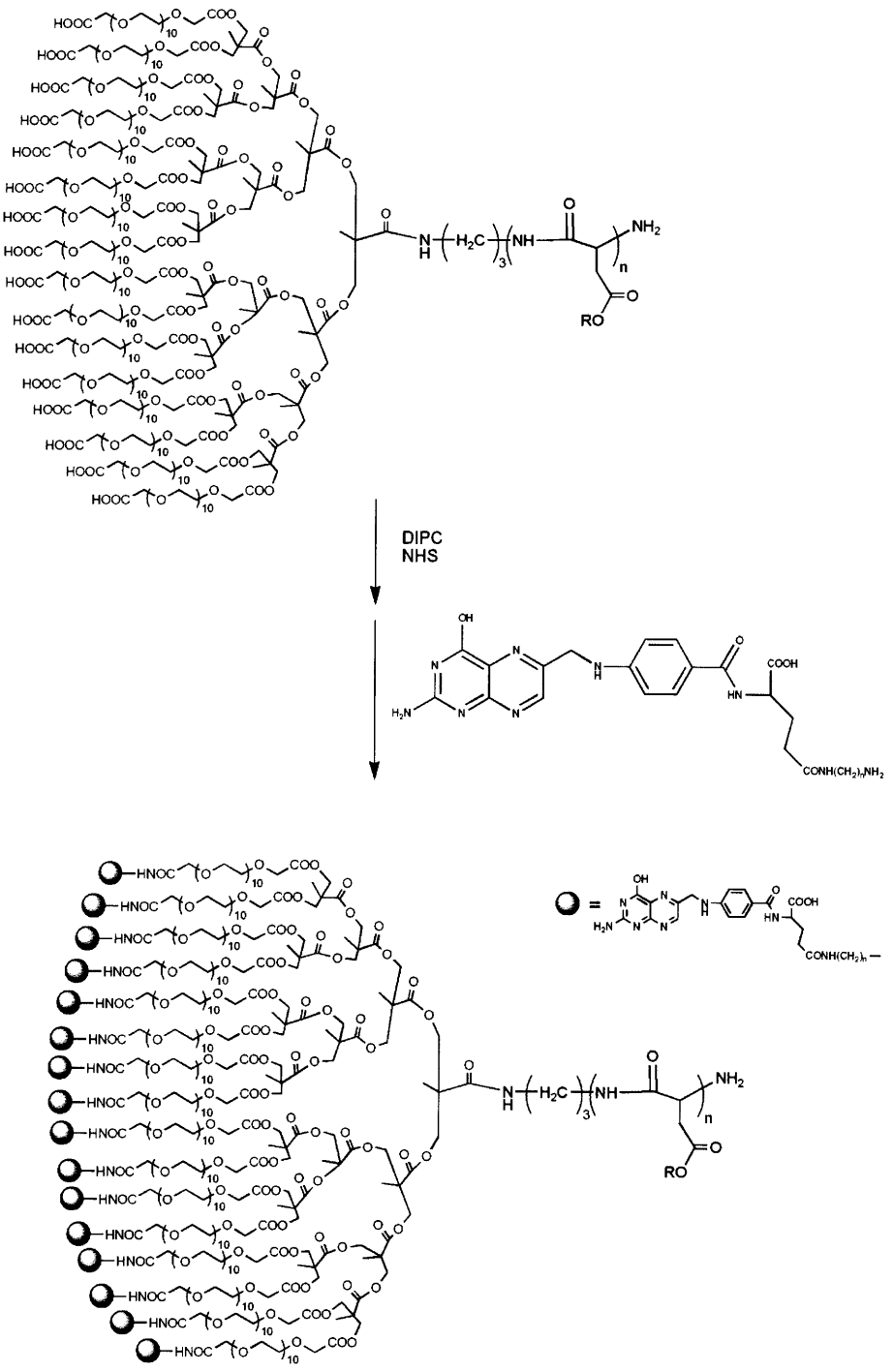

Figure 8-4. Synthetic scheme to introduce folate targeting ligand to the dendritic ends of the linear-dendritic block copolymer.

With the two multivalent systems that have been proposed, galactose and folate, a great deal is still needed to be explored. First, a more thorough study on the effects of dendrimer generation and ligand density has to be undertaken. Previous studies with dendrimers have shown that that there is an optimal density for the targeting ligand.[23, 24] With a self-assembled system, the trends observed may be more interesting. If the ligand density and generation are varied, this may cause variations in the size of the particles formed and different aggregation numbers of unimers in the nanoparticles. An additional variable that needs to be studied is the PEG length. The PEG length influences the multivalent binding behavior as well as the stability of the particles circulating *in vivo*. An optimal PEG length should be determined to balance the destabilizing effect of an increase in the CMC with increasing PEG length and increased RES removal with decreasing PEG length.

8.2.4 PPO-PAMAM Micelles in LbL Films

PPO-PAMAM micelles were successfully incorporated into LbL films for hydrophobic drug delivery. From the drug release profiles, the mechanism of release was diffusion-controlled. Ideally, the drug release profile should be tunable. Further experiments would have to be performed to determine how the drug release profile is altered by varying the initial drug concentration encapsulated and the number of multilayers fabricated. Most likely, the release curve should be similar, although the length scales would be altered. A scheme to change the shape of the release curve is to include degradable polyeletrolytes into the LbL film. Previous work in the Hammond lab has demonstrated linear drug release profiles with a degradable polymer called Poly1.[25, 26] Films containing tetralayers of PPO-PAMAM/PAA/Poly1/PAA have previously been

constructed. However, these films expelled most of the drug content and most likely a high concentration of PPO-PAMAM within the first 30 minutes of a drug release experiment. This may be due to the disruption of the micelles by Poly1. Poly1 has hydrophobic domains that may interact with PPO-PAMAM. Additionally, it was hypothesized that interdiffusion may play a role. Movement of LPEI through an LbL film was observed,[27] and this may be occurring with PPO-PAMAM. Further exploration of the fabrication conditions may lead to a more stable film. Possible factors that could be tested include a different degradable polymer. Perhaps a polymer that is less hydrophobic could be utilized. Another idea to explore is to vary the tetralayer structure. For example, a film composed of $[PPO\text{-}PAMAM/PAA]_n$/[Poly1/PAA], where n is 2 or higher, may reduce the amount of interaction between PPO and Poly1. Another possible way to reduce interdiffusion issues is to lightly crosslink the PPO-PAMAM/PAA bilayers during the formation of the film.

By introducing a degradable polymer into the LbL film, the release rate of the hydrophobic drug can be controlled in a more precise manner. Additionally, this may be a way to gradually introduce circulating nanoparticles into the surrounding area. Ideally, these nanoparticles would also be stabilized to ensure that they don't break apart due to dilution effects. This application may be useful as a stent coating. Currently, stents are being used to deliver hydrophobic drugs to the placement site. Additionally, there is lot of injury induced in these areas, and previous studies have shown that nanoparticles accumulate in arteries that have experienced balloon injury.[28, 29] This may also be applicable for treatment of ophthalmic neovascular diseases, where it has been reported that micelles accumulate in the choroidal neovascularization sites in rat eyes.[30] This

delivery approach is promising for localized delivery and dispersion of drugs into the affected area.

8.3 Concluding Remarks

This thesis demonstrated that linear-dendritic block copolymer micelles is a viable drug delivery vehicle that could either be used as a circulating targeted nanoparticle or as a nanoparticle embedded into a drug delivery film. It is hoped that the research presented here contributed to the collective knowledge of the self-assembly behavior of these novel amphiphilic linear-dendritic block copolymers and is a foundation for the further acquisition of fundamental knowledge regarding multivalent binding behavior and drug delivery. Additionally, it is hoped that the systems developed in this thesis provide a foundation for the advancement in the design of drug delivery vehicles leading to the creation of an optimized platform that is ultimately used to treat and cure important diseases.

8.4 References

1. Gillies, E.; Jonsson, T.; Fréchet, J., "Stimuli-responsive supramolecular assemblies of linear-dendritic copolymers," *J. Am. Chem. Soc.*, **2004,** 126, 11936.

2. Gitsov, I.; Lambrych, K.; Remnant, V.; Pracitto, R., "Micelles with highly branched nanoporous interior: Solution properties and binding capabilities of amphiphilic copolymers with linear dendritic architecture," *J. Polym. Sci.: Part A: Polym Chem.*, **2000,** 38, 2711.

3. David, A.; Kopečková, P.; Minko, T.; Rubinstein, A.; Kopeček, J., "Design of a multivalent galactoside ligand for selective targeting of hpma copolymer-doxorubicin conjugates to human colon cancer cells," *European J. of Cancer*, **2004,** 40, 148-157.

4. Zaman, N.; Tan, F.; Joshi, S.; Ying, J., "Targeted stimuli-responsive dextran conjugates for doxorubicin delivery to hepatocytes," **2005.**

5. Hashida, M.; Hirabayashi, H.; Nishikawa, M.; Takakura, Y., "Targeted delivery of drugs and proteins to the liver via receptor-mediated endocytosis," *J. Controlled Rel.*, **1997,** 46, 129-137.

6. Perillo, N. L.; Marcus, M. E.; Baum, L. G., "Galectins: Versatile modulators of cell adhesion, cell proliferation, and cell death," *J. Mol. Med.*, **1998,** 76, 402-412.

7. Lotersztajn, S.; Julien, B.; Teixeira-Clerc, F.; Grenard, P.; Mallat, A., "Hepatic fibrosis: Molecular mechanisms and drug targets," *Annu. Rev. Pharmacol. Toxicol.*, **2005,** 45, 605-628.

8. Tian, L.; Hammond, P. T., "Comb-dendritic block copolymers as tree-shaped macromolecular amphiphiles for nanoparticle self-assembly," *Chem. Mater.*, **2006,** 18, (17), 3976-3984.

9. Tian, L.; Nguyen, P.; Hammond, P. T., "Vesicular self-assembly of comb-dendritic block copolymers," *Chem. Commun.*, **2006,** 33, 3489-3491.

10. Ma, N.; Zhang, H.; Song, B.; Wang, Z.; Zhang, X., "Polymer micelles as building blocks for layer-by-layer assembly: An approach for incorporation and controlled release of water-insoluble dyes," *Chemistry of Materials*, **2005,** 17, (20), 5065-5069.

11. Qi, B.; Tong, X.; Zhao, Y., "Layer-by-layer assembly of two different polymer micelles with polycation and polyanion coronas," *Macromolecules*, **2006,** 39, (17), 5714-5719.

12. Seymour, L. W.; Duncan, R.; Strohalm, J.; Kopeček, J., "Effect of molecular weight (mw) of n-(2-hydroxypropyl)methacrylamide copolymers on body distribution and rate of excretion after subcutaneous, intraperitoneal, and intravenous administration to rats," *J. Biomed. Mater. Res.*, **1987,** 21, 1341-1358.

13. Kakizawa, Y.; Harada, A.; Kataoka, K., "Glutathione-sensitive stabilization of block copolymer micelles composed of antisense DNA and thiolated poly(ethylene glycol)-block-poly(l-lysine): A potential carrier for systemic delivery of antisense DNA," *Biomacromolecules*, **2001,** 2, 487-491.

14. Bickel, U.; Yoshikawa, T.; Pardridge, W., "Delivery of peptides and proteins through the brain-blood barrier," *Adv. Drug Del. Rev.*, **2001,** 46, 247-279.

15. Engin, K.; Leeper, D. B.; Cater, J. R.; Thistlethwaite, A. J.; Tupchong, L.; McFarlane, J. D., "Extracellular ph distribution in human tumors," *Int. J. Hypertherm.*, **1995,** 11, 211-216.

16. Stubbs, M.; Mcsheehy, R. M. J.; Griffiths, J. R.; Bashford, L., "Causes and consequences of tumour acidity and implications for treatment," *Opinion*, **2000,** 6, 15-19.

17. Lee, E.; Shin, H. J.; Na, K.; Bae, Y., "Poly(l-histidine)-peg block copolymer micelles and ph-induced destabilization," *J. Controlled Rel.*, **2003,** 90, 363-374.

18. Lee, E.; Na, K.; Bae, Y., "Polymeric micelle for tumor ph and folate-mediated targeting," *J. Controlled Rel.*, **2003,** 91, 103-113.

19. Pichon, C.; Goncalves, C.; Midoux, P., "Histidine-rich peptides and polymers for nucleic acid delivery," *Adv. Drug Del. Rev.*, **2001,** 53, 75-94.

20. Krężel, A.; Bal, W., "A formula for correlating pk_a values determined in d_2o and h_2o," *J. of Inorg. Biochem.*, **2004,** 98, 161-166.

21. Sabharanjak, S.; Sharma, P.; Parton, R. G.; Mayor, S., "Gpi-anchored proteins are delivered to recycling endosomes via a distinct cdc42-regulated, clathrin-independent pinocytic pathway," *Dev. Cell Bio.*, **2002,** 2, 411-423.

22. Mayor, S.; Varma, R., "Gpi-anchored proteins are organized in submicron domains at the cell surface," *Nature*, **1998,** 394, 798-801.

23. Hong, S.; Leroueil, P.; Majoros, I.; Orr, B.; Baker, J., Jr.; Holl, M. M., "The binding avidity of a nanoparticle-based multivalent targeted drug delivery platform," *Chem. & Bio.*, **2007,** 14, 107-115.

24. Wolfenden, M.; Cloninger, M., "Carbohydrate-functionalized dendrimers to investigate the predictable tunability of multivalent interactions," *Bioconj Chem*, **2006,** 17, 958-966.

25. Vázquez, E.; Dewitt, D. M.; Hammond, P. T.; Lynn, D. M., "Construction of hydrolytically-degradable thin films via layer-by-layer deposition of degradable polyelectrolytes," *J. Am. Chem. Soc.*, **2002,** 124, 13992-13993.

26. Wood, K. C.; Boedicker, J. Q.; Lynn, D. M.; Hammon, P. T., "Tunable drug release from hydrolytically degradable layer-by-layer thin films," *Langmuir*, **2005,** 21, (4), 1603-1609.

27. Zacharia, N. S.; DeLongchamp, D. M.; Modestino, M.; Hammon, P. T., "Controlling diffusion and exchange in layer-by-layer assemblies," *Macromolecules*, **2007,** 40, (5), 1598-1603.

28. Uwatoku, T.; Shimokawa, H.; Abe, K.; Matsumoto, Y.; Hattori, T.; Oi, K.; Matsuda, T.; Kataoka, K.; Takeshita, A., "Application of nanoparticle technology for the prevention of restenosis after balloon injury in rats," *Circ Res*, **2003,** 92, e62-e69.

29. Nishiyama, N.; Kataoka, K., "Current state, achievements, and future prospects of polymeric micelles as nanocarriers for drug and gene delivery," *Pharm. & Thera.*, **2006,** 112, 630-648.

30. Ideta, R.; Tasaka, F.; Jang, W.-D.; Nishiyama, N.; Zhang, G.-D.; Harada, A.; Yanagi, Y.; Tamaki, Y.; Aida, T.; Kataoka, K., "Nanotechnology-based photodynamic therapy for neovascular disease using a supramolecular nanocarrier loaded with a dendritic photosensitizer," *Nano Lett.*, **2005,** 5, 2426-2431.